Millennial-Scale Changes of Intermediate Water Ventilation, Productivity and Nutrient Supply in the Okhotsk Sea and Subarctic North Pacific During the Last 18,000 Years

Dissertation

zur Erlangung des Doktorgrades der Naturwissenschaften

am Fachbereich Geowissenschaften

der Universität Bremen

vorgelegt von

Lester Lembke-Jene

Bremerhaven, Juni 2013

Gutachter:

Prof. Dr. Ralf Tiedemann

Prof. Dr. Heiko Pälike

Erklärung

Hiermit versichere ich, daß ich

1. diese Arbeit ohne unerlaubte fremde Hilfe angefertigt habe,

2. keine anderen als die von mir angegebenen Quellen und Hilfsmittel benutzt habe,

3. die den benutzten Werken wörtlich oder inhaltlich entnommenen Stellen als solche kenntlich gemacht habe.

Weiterhin versichere ich, dass der Inhalt dieses Dokuments weder in dieser, noch in veränderter Form einer anderen Stelle im Rahmen eines Prüfungsverfahrens vorgelegen hat, veröffentlicht wurde oder zur Veröffentlichung eingereicht worden ist. Diese Arbeit ist unter Einhaltung der Regeln guter wissenschaftlicher Praxis der Deutschen Forschungs-gemeinschaft entstanden.

Bremen, den 03. Juni 2013

Lester Lembke-Jene

Anschrift:

Am Teich 4

24534 Neumünster

To my parents

Dorette and Walter

and my grandmother

Dora Schulz

Acknowledgements

I want to thank the people who supported me during my time in Kiel and Bremerhaven in the realization of this dissertation.

I owe many profound and deep thanks to Ralf Tiedemann, who gave me the opportunity to carry out this dissertation project; I also thank him for all his support, his supervision and encouragement with many fruitful and stimulating discussions.

I also wholeheartedly and sincerely thank Dirk Nürnberg for co-supervising this thesis, providing great scientific support despite busy schedules and valuable contributions in discussions and during supervision.

My additional thanks go to Heiko Pälike for taking over the role as second thesis reviewer and helpful comments.

For the preparations of large amounts of samples I sincerely thank Antonia Dix, Nicole Stange, Markus Zygmuntowski It was great fun and always a pleasure to work with you.

I thank Bastian Fessler, Jutta Heinze, Syliva Koch, and Dagmar Rau, who worked tirelessly both offshore and in the laboratories and introduced me to many laboratory and analysis details and practices and provided extensive support with geochemical analyses. My special thanks go to Lulzim Haxhiaj for the great atmosphere and for his professional support in the Kiel ISOLAB.

Sergey Gorbarenko, Sascha Derkachev, Anatoly Obzhirov, Anatoly Salyuk and Valery Sosnin are wholeheartedly thanked for the great collegial help and atmosphere both on board of R/V Akademik Lavrentiev and R/V Sonne, as well as during meetings and visits. It is always great fun and very stimulating to work with you.

I thank Pieter Grootes and Helmut Erlenkeuser for providing their expertise and always being available for many fruitful and stimulating discussion about both stable and radiogenic isotopes, as well as for providing outstanding service in sample analyses.

In addition, I thank the IODP core repository staff at the MARUM in Bremen; especially Walter Hale, Ulla Röhl and Vera Lukies deserve special thanks for introducing me to XRF scanning and providing great technical support during my stays in Bremen.

I am grateful to Silke Steph, who was always open for questions of scientific and other issues. I enjoyed many a fruitful and fun discussion both in Kiel and Bremerhaven, and on conferences, thank you for that.

Of course, sincere thanks go to my colleagues at the Alfred Wegener Institut in Bremerhaven and at GEOMAR Kiel, who over the years directly or indirectly contributed to this work and the good working atmosphere. I especially thank Frank Lamy for his support and motivation during the final days of writing this thesis.

As well, genuine and deep thanks go to my colleagues Lars Max, Jan-Rainer Riethdorf and Hartmut Kühn for a great working atmosphere, many stimulating and fun discussions and ideas.

My thanks also to my AWI colleagues Jørn Thiede, Nicole Biebow, Elena Tschertkow-Paulenz and Veronica Willmott for their support and encouraging interaction with me during the initial stage of writing this thesis.

This thesis was made possible through financial support of the Federal Ministry for Education and Education (BMBF), which is gratefully acknowledged.

A big hug and special thank you to my friend Egon, for never-ending, continuous encouragement, friendship and patience, and great times together.

Finally, a special and truly big(!) thank you to my girlfriend Julia, for unwavering support, patience and perseverance during all the time I was away, and your for understanding and love.

Finally, most grateful I am to my parents, Dorette Lembke-Jene and Walter Jene for their continued interest in my work, encouragement, love and support along the way. Thank you!

Kurzfassung

Der heutige Nordpazifik spielt eine herausragende Rolle in marin-biogeochemischen Kreisläufen. Er beherbergt viele der biologisch produktivsten Meeresregionen auf dem Planeten und stellt hierdurch die größte natürliche Senke für atmosphärisches CO_2 im globalen Ozean dar. Die Remineralisation von Nährstoffen in intermediären Wassertiefen andererseits beeinflusst den Sauerstoffhaushalt des Zwischenwasserstockwerks und begünstigt damit die Entstehung von Sauerstoffminimum-Zonen entlang weiter Teile des pazifischen Kontinentalhangs in mittleren und niederen Breiten. Sauerstoffminimum-Zonen stellen heute eine der größten natürlichen Quellen für CO_2 in die Atmosphäre dar. Diese werden zwar überwiegend durch lokale Prozesse gesteuert, allerdings stellt eine wichtige Modulierungsfunktion zur Erhaltung hinreichender O_2-Konzentrationen innerhalb der Wassersäule die Ventilation durch Bildung neuer Wassermassen in hohen Breiten und deren Belüftung durch Kontakt mit der Atmosphäre dar. Im gesamten Pazifik ist die Bildung neuer Wassermassen eng begrenzt auf zwei Schlüsselregionen: den chilenischen Kontinentalhang (Bildung von Antarktischem Zwischenwasser) und im Nordpazifik das Ochotskische Meer als Bildungsort für Ochotskisches Zwischenwasser, welches durch Vermischungsprozesse das nordpazifische Zwischenwasserstockwerk zwischen ca. 50-20°N mit Sauerstoff, aber auch mit Mikro-Nährstoffen wie Eisen versorgt und so eine entscheidende Rolle in Wassermassen-Austauschprozessen und Stoffkreisläufen einnimmt. Neuere instrumentelle Datensätze legen die Vermutung nahe, dass die Ventilation von Ochotskischem Zwischenwasser nicht nur auf glazialen-interglazialen Zeitskalen schwankt, sondern auch auf kurzen interdekadischen bis Jahrtausender-Zeitskalen hochvariabel ist. Jedoch sind natürliche Hintergrundschwankungen in Sauerstoffgehalten und Primärproduktion sehr ausgeprägt und erschweren die Abgrenzung des natürlichen Signals von möglichen anthropogenen Änderungen.

In dieser Arbeit wird eine Reihe hochauflösender AMS ^{14}C-altersdatierter Sedimentkerne direkt aus der Bildungsregion von Ochotskischem Zwischenwasser zur paläozeanographischen Rekonstruktion der Ventilationsgeschichte benutzt. Der bearbeitete Zeitraum überdeckt den letzten glazial-interglazial Übergangs sowie die gegenwärtige holozäne Warmzeit. Anhand stabiler Kohlenstoff-Isotopen an epibenthischen Foraminiferen und einer Multi-Proxy-Rekonstruktion der Primarproduktion und des terrigenen Sedimenteintrags konnte nachgewiesen werden, dass die letzte Eiszeit-Termination durch rasche und gravierende Schwankungen im Sauerstoff- und Nährstoffgehalt des Zwischenwassers gekennzeichnet ist. Korrelationen zu Referenz-Archiven für den asiatischen Sommer-Monsun legen eine enge Kopplung an ein Progradieren der maximalen Niederschlagszonen im Einzugsgebiet des Amur-Flusses nahe, welches vermutlich verbunden ist mit dem Abschmelzen der Hinterland-

Permafrostboden im Präboreal. Die enge zeitliche Übereinstimmung mit weiteren Proxy-Zeitserien aus dem subarktischen Nordpazifik und der Beringsee während der interstadialen Wärme-Phasen zwischen 18,000-8,000 Jahren impliziert, dass diese deglazialen Perioden schwacher Ventilation und erhöhter Remineralisation großräumig gesteuert werden und gekoppelt sind an Wechsel in der oberflächenahen Stratifizierung der Wassersäule. Ventilationsminima innerhalb der nordpazifischen Zwischenwasser treten zeitgleich mit dem kurzfristigen Expansionen weiträumiger zirkumpazifischer Sauerstoff-Minimum Zonen auf, so dass von einer verstärkenden oder regional gar steuernden Regelung dieser durch Zwischenwassermassen ausgegangen werden kann. Hingegen korrelieren Maxima in der Zwischenwasserventilation während der deglazialen Kälteperioden (Heinrich Stadial 1 und Jüngere Dryas) mit Zusammenbrüchen der nordatlantischen Tiefenwasserzirkulation. Der Gradient zwischen Ochotskischem und Beringsee-Zwischenwasser legt hierbei den Schluss nahe, dass eine hemisphärische Telekonnektion, vermutlich durch Kopplung atmosphärischer Zirkulationsmuster mit Expansionen des Polar Vorte. oder die Intensität der sibirischen Aktionszentren (Aleuten-Tief vs. SibirienßHoch) eine massgebliche Rolle gespielt hat.

Für die jüngste geologische Vergangenheit der letzten 10,000 Jahre kann in dieser Arbeit erstmal nachgewiesen werden, dass drastische Veränderungen im Sauerstoffniveau des Ochotskischen Zwischenwassers keinesfalls auf große Klima-Umschwünge beschränkt waren. Vielmehr ist das frühe bis mittlere Holozän, mit global wie regional ca. 1-2°C höheren Meeresoberflächentemperaturen als heute gekennzeichnet durch eine ca. 50%ige Abnahme in Sauerstoffkonzentrationen. Diese Annahmen basieren auf Abschätzungen durch lokale $\delta^{13}C - O_2$ Regressionen. Vielmehr bestand die heutige Situation mit Ochotskischem Zwischenwasser als Sauerstoff-„Exporteur“ in den Nordpazifik vermutlich nur die vergangenen ca. 2.000 Jahre, während zuvor das Ochotskische Meer überwiegend eine O_2-Senke statt eine Quelle für intermediäre Wassertiefen darstellte. Diesen grundlegenden Schwankungen überlagert sind erstmals nachgewiesene zyklische Schwankungen in der Zwischenwasserventilation auf charakteristischen 1.500 und 2.600 Jahres-Zyklen. Es kann anhand der erarbeiteten Benthos-Kohlenstoff-Isotopenkurven gezeigt werden, dass sich ein dominanter Zyklus von 1.500 Jahren im frühen, ventilationsarmen Holozän verschiebt zu besser ventilierten, von 2.600 Jahr-Zyklen im späten Holozän.

Insgesamt sollen die erbrachten Ergebnisse helfen, das Zusammenwirken von regionalen Klimaschwankungen, wechselnder Flussfracht, biogener Primärproduktivität und Zwischenwasserventilation, sowie deren Kopplung an Stratifizierung und großräumige Klimaschwankungen besser zu verstehen auf Jahrtausender- und kürzeren Zeitskalen. Die mit dieser Arbeit erbrachten Ergebnisse sollen zu einem besseren Grundlagenverständnis der marin-

biogeochemischen Kreisläufe im Bereich des Subarktischen Nordpazifik und seiner Randmeere beitragen.

Abstract

The modern North Pacific plays a critical role in marine biogeochemical cycles, as it is today the largest natural oceanic sink of CO_2 and harbors some of the most biologically productive and least oxygenated regions of the World Ocean. This capacity to sequester CO_2 is limited by variations in the region's biological productivity, and the efficient utilization of preformed nutrients supplied to the upper mixed layer, particularly in the Pacific's subarctic latitudes and marginal seas. Changes in the oxygenation of deeper water masses, on the other hand, are influenced by the remineralization of the settling organic matter through the water column. Today, the entire North Pacific is only weakly ventilated by North Pacific Intermediate Water (NPIW), which receives its relatively higher oxygen concentrations largely from a precursor, the Okhotsk Sea Intermediate Water (OSIW). Past ventilation patterns of OSIW likely have changed profoundly on millennial timescales, making this water mass a prime candidate for shaping variations in deglacial circum-Pacific Oxygen Minimum Zones and reported peaks in biogenic productivity, but their paleoceanographic history over the last glacial termination is not well understood.

In this thesis I present a comprehensive multi-proxy-based reconstruction of Okhotsk Sea Intermediate Water ventilation and productivity variations over the last glacial termination and the Holocene. The results are based on a set of high-resolution AMS ^{14}C-dated sediment cores that were retrieved directly from the source region of modern OSIW formation. Benthic-planktic ^{14}C ages and epibenthic stable carbon isotopes show decreases in OSIW oxygenation during deglacial warm phases from c. 14.7 to 13 ka (Bølling-Allerød) and c. 11.4 to 9 ka (Preboreal), but no concomitant decreases in ventilation ages. I hypothesize that these transient oxygenation decreases are mainly tied to rapid, significantly enhanced organic matter remineralization within OSIW, in line with multi-proxy evidence for maxima in primary productivity and increased supply of organic matter to the mid-depth water column.. Palynological and sedimentological evidence suggests that millennial-scale maxima in fluvial freshwater runoff from the Amur were a primary driver of these significant changes in OSIW oxygen and nutrient concentrations, with runoff changes most likely linked to changes in the East Asian Monsoon and the postglacial melting of permafrost soils in the Siberian hinterland. Correlation of ventilation minima with maxima in nutrient utilization in the open North Pacific implies increased OSIW-sourced mid-depth lateral supply of micronutrients, silicate and organic matter into distant oceanic regions, analog to modern ocean conditions. By invoking such export from marginal seas, the upper ocean open North Pacific was possibly partially relieved from Fe-limiting conditions by

upwelling the mid-depth nutrient-enriched OSIW during wintertime mixing. Such a mechanism would have made the subarctic North Pacific a transient, more efficient CO_2 sink during the B/A and PB and contributed to temporary slowing of the deglacial CO_2 rise. Reconstructed minima in mid-depth oxygen content, on the other hand, provide a reinforcing mechanism for the intermediate-depth circum-Pacific intensification of Oxygen Minimum Zones during the last glacial termination.

Analysis of a suite of Holocene cores provides evidence that such rapid and fundamental changes in mid-depth ocean ventilation and nutrient supply are not limited to deglacial or stadial-interstadial changes. Ventilation reconstructions for the Holocene based on the $\delta^{13}C$ of epibenthic foraminifera prove the modern pattern of Okhotsk Sea Intermediate Water ventilation in the Okhotsk Sea is a relatively recent and non-stable feature that only persisted for the last c. 2,000 years. During the warmer than present early-mid-Holocene, active ventilation was significantly decreased. Estimated dissolved oxygen concentrations of Okhotsk Sea Intermediate Water reached only 50-60 % of modern values, and comparison between in- and outflow sites at the Kamchatka and Sakhalin continental margins suggest that the Okhotsk Sea turned from an early Holocene O_2-sink into the modern O_2-source around 6,000 years ago. Beyond the observed mid-Holocene ventilation shift, millennial-scale cyclic variations were found in the stacked $\delta^{13}C$ ventilation record. Both 1,500 yr and 2,6000 yr cyclic changes in Okhotsk Sea ventilation are evident, with a mid-Holocene shift in dominance from the former to the latter, implying a switch in the dominant forcing between the early and the late Holocene. On a regional scale, the reconstructed interstadial minima correlate with changes in Bering Sea mid-depth ventilation patterns and are in anti-phase to collapses and resumptions of the Atlantic Meridional Overturning Circulation during the Heinrich 1 and Younger Dryas stadial phases. Associated investigations of upper ocean stratification, mixed layer and sea surface temperatures revealed a close interaction and coupling between stratification maxima and ventilation minima during interstadial deglacial phases, whereas stadials were characterized by decreases in sea surface – mixed layer gradients and seasonal contrasts in large swaths of the Northwest Pacific.

Taken together, the results reported here help to further our understanding of complex surface to mid-depth ocean interactions and reorganisations during the last 18,000 years. Initial steps taken towards quantification of the observed changes together with the large regional scope of the investigation will hopefully help to better understand complex biogeochemical cycles in the North Pacific and provide baseline scenarios against which climate model runs can be tested in the future.

Table of Contents

1. Introduction

1.1. Motivation and Aims of the Thesis

The hypothesis that past millennial-scale variations in the oceanic Meridional Overturning Circulation or "Great Ocean Conveyor" cause rapid climate change is in essence less than twenty-five years old (Broecker, 1991). Yet, over these years it has stimulated innumerable paleoceanographic studies on the interaction between the oceans, the atmosphere and such climate shifts. Research was initiated largely in the Atlantic Ocean as the "starting point" of the global Meridional Overturning Circulation (Fig. 1.1, cf. Bond et al., 1997; Duplessy et al., 1988; Sarnthein et al., 2000; Sarnthein et al., 1994). With Greenland and Antarctic ice core records providing both a master chronology and reference climatic time series for temperatures and greenhouse gases (Blunier and Brook, 2001; Dansgaard et al., 1993; Grootes et al., 1993; Kroopnick, 1985a; Petit et al., 1999), oceanic millennial-scale climatic changes could be successfully tied to global climate, and to variations in the global carbon cycle and atmospheric CO_2 concentrations (Sigman and Boyle, 2000; Sigman et al., 2010).

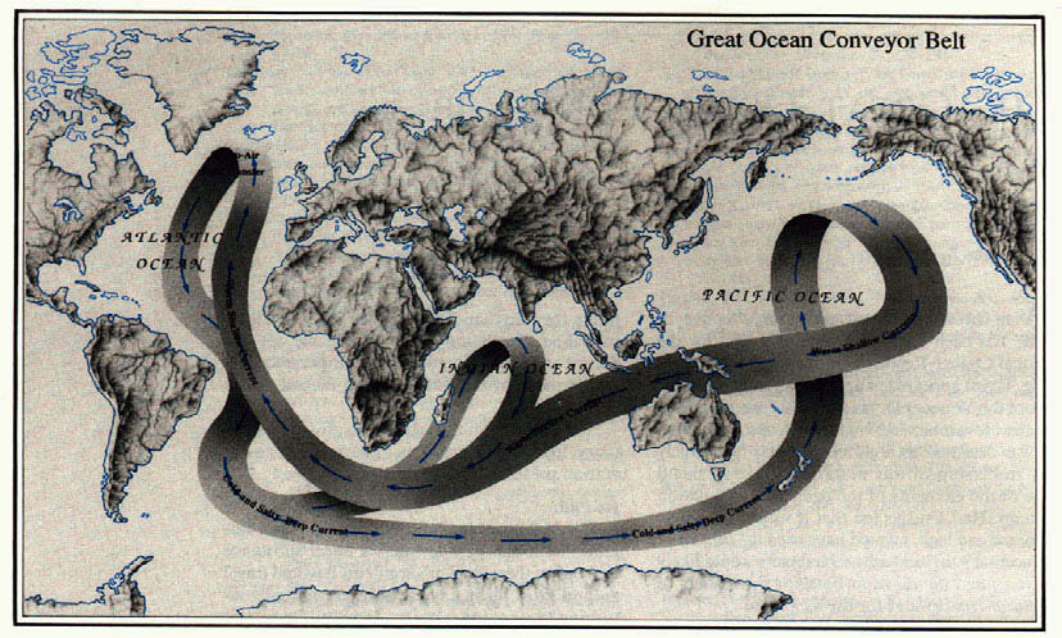

Fig.1.1: The thermohaline circulation or "Great Ocean Conveyor Belt" in simplified illustration. Used conceptually by W. Broecker to propose how rapid paleoceanographic changes were associated with the Younger Dryas climate cold reversal during the last glacial termination (Illustration by John Le Monnier, Natural History Magazine).

Compared to these regions much less is known about the paleoceanographic history of the endpoint of the global Meridional Overturning Circulation in the North Pacific. This lack is especially striking, because the modern North Pacific is thought to play a critical role in the global carbon cycle and ocean-atmosphere CO_2 exchange through changes in its hydrography, biological productivity and use of nutrients both on long glacial-interglacial (Haug et al., 2005; Haug et al., 1999; Jaccard et al., 2005) and short millennial timescales (Galbraith et al., 2007; Lund et al., 2011; Mix et al., 1999).

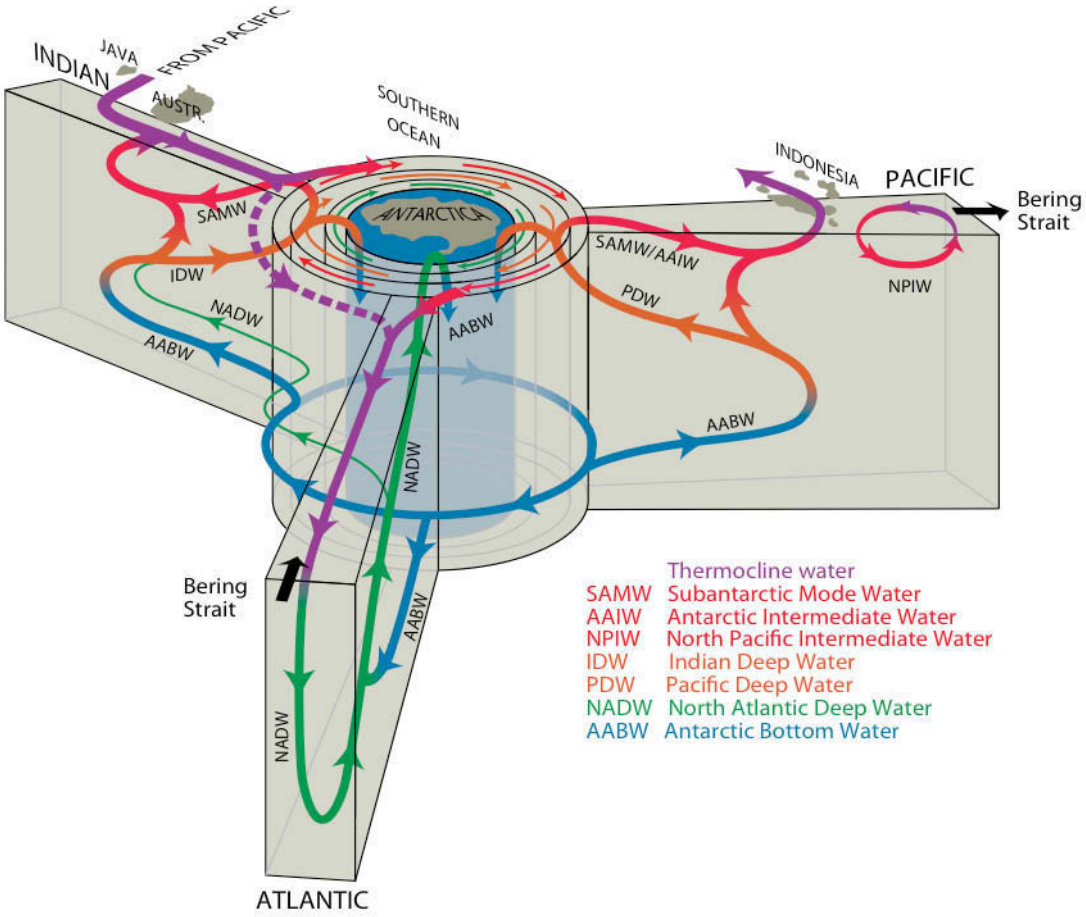

Fig 1.2: Three-dimensional circulation within Atlantic, Indian, and Pacific oceans showing vertical recirculation within and between ocean basins, interchange between oceans via the Antarctic Circumpolar Current and adding cross-basin exchanges via the Indonesian Throughflow and Bering Strait. In this modified version of the original schematic, NPIW and Bering Strait flow are explicitly incorporated for the first time. Observe that NPIW interaction with the Indian Ocean by AAIW/NPIW mixing zones (cf. Zenk et al., 2005) or deeper Pacific water is not shown due to persisting uncertainties of NPIW dynamics, heat and transport capacity. From Talley (2013), modified after (Schmitz, 1996).

In addition, North Pacific mid-depth water masses play a critical role in the ocean nutrient budgets. While their volume contribution to the thermohaline component of the global ocean circulation is only moderate (Lumpkin and Speer, 2007; Talley, 2013), they act as important transport media for nutrients and oxygen to lower latitude regions both on modern (Dugdale et al., 1995; Sarmiento et al., 2004) and longer timescales (Brzezinski, 2002; Galbraith et al., 2004; Matsumoto et al., 2002b). Formation of intermediate waters is focused within only two narrowly defined regions: AAIW is formed in the Southeast Pacific off the Chilean coast (Hartin et al., 2011; Sloyan et al., 2010), The second most important water mass is North Pacific Water (NPIW). It spreads as a salinity minimum between 45°N and 10°N across the subtropical Pacific Ocean, finally feeding into the NEC and contributing to the mid-depth water mixture along the American continental margins (Talley, 1985, 1993). Despite its importance for understanding biogeochemical cycles and the mid-depth Meridional Overturning Circulation, NPIW remains not well understood, both in its formation characteristics, temporal and spatial variations, and sensitivity to changing environmental conditions. However, instrumental datasets that cover the last about five decades show strong evidence for the mid-depth Pacific ocean being a system in transition towards lower oxygen concentrations, warmer temperatures and stronger stratification, with potentially profound consequences for oceanic livestock, primary productivity and repercussions for the global carbon cycle on timescales discernible for humankind. However, within the limited range of instrumental and remote sensing datasets, natural long-term variations are large and may mask true background change.

In this regard, the lack of well-dated paleoceanographic proxy records from the Northwest Pacific leaves our understanding fragmented on how these key regions functioned naturally in the past, and what their contribution to ocean ventilation, biogeochemical budgets or greenhouse gas emissions has been. Underlying processes of atmosphere-ocean-sea ice interactions and continent-ocean coupling mechanisms for climate variability remain largely enigmatic. This holds true for most timescales and temporal resolutions, but especially for rapid and millennial- to centennial-scale changes over the last glacial-interglacial transition and the current Holocene warm period

In the subarctic North Pacific and its marginal seas, a multitude of different atmospheric and oceanic processes exists, which are not well understood, even for the most recent past that is covered, though sparsely, by instrumental datasets and historical records. It is yet not fully known to which extent regional, large-scale, extra-tropical atmospheric patterns such as the East Asian Summer Monsoon (EASM), the Siberian High and Aleutian Low atmospheric action centers patterns influence and condition changes in Okhotsk Sea surface and intermediate water masses.

1.2. Objectives and Structure of the Thesis

The paleo-chemical oceanography, especially the ventilation and productivity characteristics of the upper and intermediate water masses in the Okhotsk Sea are of principal importance for a conceptual understanding of the oceanographic history of the extremely large Pacific region and for constraining the extent of continent-ocean-atmosphere interactions between high and low latitudes. Deciphering the extent, sensitivity and timing of rapid oceanographic variations in key areas like formation regions of new water masses fundamentally helps in establishing knowledge of rapid and profound changes in the global ocean. These data are critically needed by the science community as natural baseline against which to evaluate present and future change in mid-depth oceanic biogeochemistry that are potentially attributable to anthropogenic climate change.

Thus, I aim to reconstruct the paleoceanographic history of Okhotsk Sea and North Pacific intermediate water masses. I will focus on changes in ventilation characteristics and nutrient patterns over the last glacial to interglacial transition and during the Holocene warm period. The implications of changes in these Okhotsk Sea intermediate and surface water characteristics for the extra-tropical North Pacific realm shall be analyzed. Potential forcing factors shall be examined and the potential of Okhotsk Sea water mass variations and changes shall be evaluated with respect to their significance for large-scale regional and global oceanic reorganizations during the studied time intervals.

This thesis is structured into ten chapters:

Chapter 1 gives a short introduction to the rationale for this study and introduces the scientific questions that are covered within the thesis.

In **Chapter 2** a brief introductory overview is given to the regional setting, the modern oceanography and principal climatic forcing mechanisms in the Okhotsk Sea, and neighboring regions. This chapter is restricted to information that is not discussed in the following chapters in detail, but helpful to understand the context of regional settings.

Chapter 3 describes materials and methods that were used for this thesis, and includes a short explanation of the workflow The provided analytical information supplements and references the subsequent use of methods explained within the manuscript sections.

Chapter 4 explains additional aspects and considerations of the age model development of the age models that are used for the high-resolution studies presented in the following manuscripts, in particular with respect to chapters 5 and 6.

Chapter 5–9 present the results of this thesis and are grouped in the form of individual manuscripts that are finalized for submission to international peer-reviewed journals (Chapter 5–7) or have been published (chapter 8–9).

Chapter 5 provides the first detailed study on the OSIW ventilation history during the deglaciation into the early Holocene, covering the time interval from 8,000 to 18,000 years before present. Stable isotope data ($\delta^{13}C$) of epibenthic foraminifera from the OSIW source region are combined with a multi-proxy approach for primary productivity, fluvial freshwater and sediment supply to address the following questions:

- How did the ventilation of Okhotsk Sea Intermediate Water change directly in the source region during the millennial-scale warm and cold phases of last glacial termination?
- How was the OSIW biogeochemical signature influenced by short-term primary productivity peaks during the deglacial Bølling-Allerød and Preboreal warm phases?
- Which potential causes and forcing factors can be identified for deglacial changes in OSIW characteristics?
- How do changes in OSIW biogeochemistry affect mid-depth ventilation, nutrient budgets and their utilisation in the open subarctic North Pacific?

Chapter 6 focuses on the reconstruction of Okhotsk Sea Intermediate Water ventilation during the present Holocene warm period.

- Did Okhotsk Sea Intermediate Water ventilation vary within the relatively, stable current "warmhouse" Holocene?
- How sensitive was the present ventilation process by brine rejection in seasonal sea ice to past higher-than-present surface temperatures and freshwater fluxes?
- What are the influences of ventilation changes in OSIW on oxygen supply to the mid-depth North Pacific?
- What are the potential forcing mechanisms for Holocene variability in OSIW ventilation and circulation? Do we observe cyclic changes analog to North Atlantic records?

Chapter 7 widens the perspective from the Okhotsk Sea into a basin-scale comparative assessment of ventilation changes in the precursor water masses of NPIW, based on analyses of sediment cores form Okhotsk and Bering Sea as the two potential source regions for NPIW ventilation during the last glacial termination. A focus is put on the deglacial cold Heinrich Stadial 1 and Younger Dryas phases, when the collapse of Atlantic Meridional Overturning Circulation (McManus et al., 2004a) and initiation of deep overturning in the subarctic North Pacific were postulated by earlier works (Okazaki

et al., 2010a). This hypothesis is tested by using benthic foraminiferal stable carbon isotopes, radiocarbon-derived paleo-ventilation ages and a basin-wide compilation of radiocarbon ventilation ages are used to address the following questions:

- How important was the contribution of Okhotsk Sea Intermediate Water to deglacial North Pacific ventilation changes in relation to other potential source regions like the Bering Sea?
- Were collapses of the Atlantic Meridional Overturning Circulation during the last deglaciation coupled to enhanced formation and ventilation of the mid-depth and the deep North Pacific?
- Can regional reconstructions of NPIW ventilation in conjunction with information about upper ocean temperature and stratification help to evaluate and constrain existing hypotheses about climate teleconnections and forcings between the North Atlantic and Pacific?

Chapter 8 provides information about deglacial changes in upper ocean temperatures and salinity that were reconstructed based on Mg/Ca and $\delta^{18}O$ measurement of planktic foraminifera, combined with alkenone-derived SST reconstructions. The reported changes in mid-depth ventilation and biogeochemistry of chapter 5–7 are here put into the context of surface and mixed layer stratification variations in the Bering and Okhotsk Sea, thereby addressing the following aspects:

- How do temperature and salinity of the upper mixed layer change in the subarctic North Pacific over the last glacial termination? Do different proxies record the same or different ocean temperature signals?
- Are there regional variations in these upper mixed layer temperature and salinity characteristics between the open subarctic North Pacific and the neighboring marginal seas?
- How does the upper ocean stratification change, based on the combination of SST and (sub)SST reconstruction and what are potential implications for primary productivity changes?

Chapter 9 supplements the results reported in the earlier chapters by addressing the development of sea surface temperature and sea ice characteristics over the deglacial and early Holocene on a basin-wide scale and adds a comparison to previously published records. The findings are integral to understand the role that sea surface temperatures and sea-ice changes exert on ventilation and circulation of deeper water masses and how surface temperature changes are coupled to concurrent changes in the North Atlantic. This chapter addresses the following questions:

- How are millennial-scale changes in Okhotsk Sea Intermediate Water ventilation and primary productivity connected to regional and hemispheric changes in sea surface temperatures?
- Are deglacial changes in sea surface temperatures and mid-depth ventilation characterized by concomitant changes in sea ice distributions?

Chapter 10 presents a brief synthesis of the achieved results. It summarizes the reported findings and highlights the progress achieved in comparison to the previous state of knowledge. The chapter closes out the thesis with an example for future studies.

The **appendix** references selected earlier publications with abstracts for information that were generated within the framework of the KOMEX and KALMAR joint research programs and in collaborations with Russian colleagues, but form no inherent part of the thesis' results.

References of Chapters 5 to 9 are given at the respective end of the chapters. References for the introductory (Chapter 1-4) and closing sections (Chapter 10) are given at the end of the thesis.

2. The Study Area

2.1. Regional Setting and Circulation Patterns

The Okhotsk Sea is the second largest marginal sea of the North Pacific. It is bordered by East Siberia and Sakhalin Island to the west, Northeast Siberia (Magadan Oblast) to the North, the Kamchatka peninsula to the east, the Kuril Island Chain and Hokkaido to the south and southeast. It is covering an approximate area of 1,580,000 km (Tomczak and Godfrey, 2003). Circulation inside the Okhotsk Sea is dominated by the broad Okhotsk Gyre (see fig. 2.1), according to drifter studies (Ohshima et al., 2004; Ohshima et al., 2002). The southward-flowing branch of the Okhotsk Gyre is formed by the East Sakhalin Current, which transports surface and deeper water form the northern shelves into the Kuril Basin.

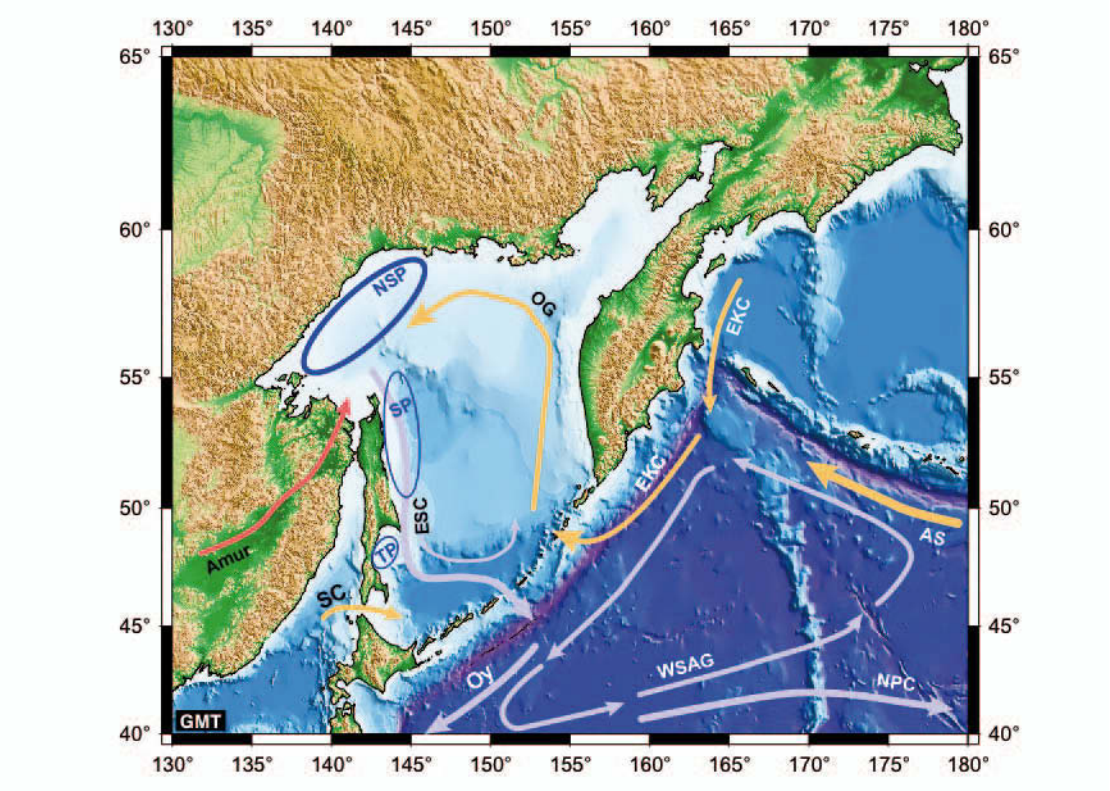

Figure 2.1: Map of study area with major circulation features. EKC = East Kamchatka Current; AS = Alaskan Stream; WSAG = Western Subarctic Gyre; NPC = North Pacific Current; OY = Oyashio; OG = Okhotsk Gyre Current; ESC = East Sakhalin Current; SC = Soya Current; Blue ellipses show average locations of major recurring winter polynias: NSP = Northern Shelf Polynia, SP = Sakhalin and Kashevarov Bank Polynia; TP = Terpeniya Bay Polynia. Red arrow symbolizes freswater influx via the Amur river.

Surface and deeper waters are exchanged between the Okhotsk Sea and the open North Pacific through a series of straits and passages in the Kurile Island with the two most important ones being Busso'l and Kruzensthern Strait (Katsumata et al., 2004; Ohshima et al., 2010). Flow through these straits is highly complex and not well understood, but exhibits a pronounced seasonality (Ohshima et al., 2010) and dependence on tidal forces (Nakamura and Awaji, 2004; Ohshima et al., 2002), leading to strong currents with vertical and horizontal flow reversals on time scales of hours to years, and intense deep, often diapycnal mixing (Katsumata et al., 2004; Nakamura and Awaji, 2004; Rogachev, 2000; Rogachev et al., 2001; Yagi and Yasuda, 2012). Waters mostly enters the Okhotsk Sea from the East Kamchatka Current (EKC, Fig. 2.1), a southward flowing Western Boundary Current that transports Western Subarctic Gyre Water and, to a lesser extent upper Pacific Deep Water to the Kuril Islands. Inside the Okhotsk Sea it enters the gyre and is transported to the northern shelf area, where substantial modification processes occur due to high freshwater flux during spring and autumn, and through the formation of new water masses on the shallow shelf area during winter (Ohshima et al., 2010; Yasuda, 1997; Yasuda et al., 2001).

2.2. Ocean-Atmosphere Forcing on Fluvial Freshwater Flux and Sea Ice

Freshwater flux to the Okhotsk Sea is mainly delivered by precipitation and latent moisture flux to the Amur river drainage basin. The Amur is one of the ten largest rivers worldwide by catchment area and discharges about 333 km^2 freshwater per year (Ogi et al., 2001). As a characteristic feature, the annual runoff is strongly centered in two peak periods, one in early spring and the second in late summer, which are each determined by two different processes (Tachibana et al., 2008). The freshwater in the first peak mainly stems from melting snow and ice in the hinterland and its transport downstream into the Okhotsk Sea. The strength and location of the Siberian High pressure cell over mainland Siberia in wintertime is the dominant factor for the amount of snow cover and the strength of the winter, including the timing of ice breakup and (Honda et al., 1996). A second and much larger peak during September reflects the preceding East Asian Summer Monsoon maximum (July, August) that delivers precipitation to the Amur catchment area (Tachibana et al., 2008). The main discharge of the Amur spreads from the estuary around Cape Elizabeth on northern Sakhalin southward along the continental margin with the East Sakhalin Current (Fig. 2.1 and 2.2). This high supply of freshwater mixed nutrients and terrigenous suspension load contributes to strong stratification of the shallow upper surface waters and causes maxima in productivity on the northeastern Sakhalin margin (Nakatsuka et al., 2004a; Nakatsuka et al., 2004b; Seki et al., 2006). Fluctuations in Amur freshwater discharge play an active role in controlling sea ice formation. Ogi et al. (2001) found evidence for a negative feedback on decadal scales. They suggested that the inflow of warm Amur water tends to increase sea

surface temperatures in the freshwater-influenced part of the Okhotsk Sea, thereby suppressing sea ice formation in winter. This anti-correlation pattern is in turn influenced by the strength and expression of the Arctic Oscillation on instrumental timescales, thus providing a teleconnection pattern between the high Northern latitudes in the North Atlantic and North Pacific realm (Ogi and Tachibana, 2006; Ogi et al., 2004a). It further implies that the hydrological summer cycle of the hinterland, which is largely determined by the strength and northward propagation of the East Asian Summer Monsoon system, is an active player in controlling sea ice. Summer-induced changes in sea ice cover may in turn exert a significant influence on the atmosphere, because the presence of sea ice significantly reduces heat and moisture fluxes from the sea surface and consequently acts to cool the atmosphere above the ice (Honda et al., 1996; Ogi et al., 2004b; Tachibana et al., 2004; Tachibana et al., 2008).

Figure 2.2: Summer Amur river outflow with clearly visible suspension load that is delivered into Okhotsk Sea. Phytoplankton blooms that benefit from delivery of nutrients with river suspension and turbulent mixing on shallow shelf are visible to the mid right of the picture. (Credit: Provided by the SeaWiFS Project, NASA/Goddard Space Flight Center, and ORBIMAGE).

The Okhotsk Sea is covered by sea ice between 6 and 9 months on average per year. It is the southernmost location for such pervasive sea ice formation on the Northern Hemisphere. Formation

processes mainly occur north of Sakhalin Island and along the northern shelf areas (Kimura and Wakatsuchi, 1999; Martin et al., 1998).

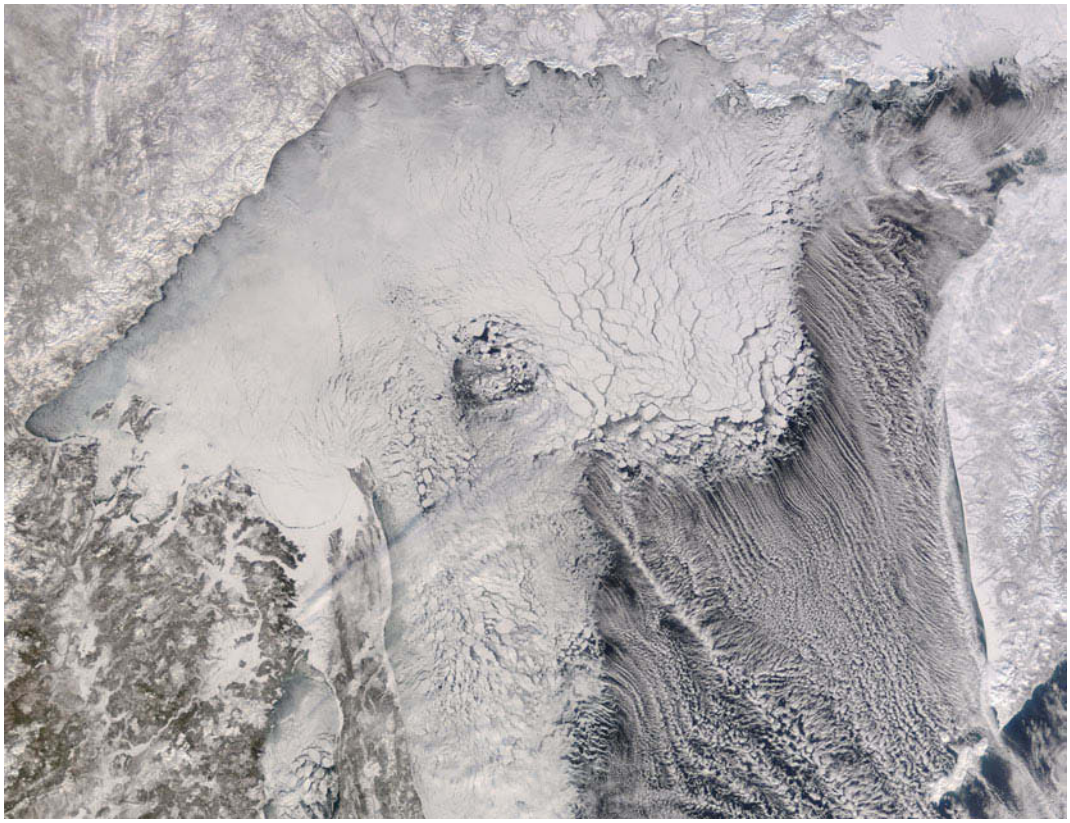

Fig. 2.3: Winter sea ice cover in Okhotsk Sea in true-color Aqua MODIS image from January 26, 2003. Note the accumulation maximum in the northwestern shelf areas (Credit: J. Descloitres, MODIS Rapid Response Team).

While earlier works thought that the large freshwater runoff by the Amur river would foster sea ice formation due to the delivery of low-salinity water before freeze-up starts in autumn, recent studies point to a negative feedback coupling between fluvial runoff and sea-ice concentration on inter-annual and longer timescales due to the amount of latent heat transport into the NE shelf area of the Okhotsk Sea (Ogi et al., 2001; Tachibana et al., 2008). The large amount of latent heat from warmer continental regions under the influence of the South East Asian Summer Monsoon that is transported with the freshwater to the northern shelf suppresses the formation of new ice (Ogi and Tachibana, 2006; Ohshima et al., 2001). Sea ice formation is highly dynamic and variable on inter-annual and longer timescales. It is affecting and in some cases driving force for distinct surface, mixed layer and deeper water characteristics in the Okhotsk Sea (Ohshima et al., 2001; Yamamoto et al., 2002), e.g. by the formation of temperature inversions (the subsurface dichothermal layer) e.g. (Mizuta et al., 2004) and polynias (Fukamachi et al., 2004; Fukamachi et al., 2009). Due to the influence of the relatively warm (compared to the Okhotsk Sea) surface water from the East Kamchatka Current and the distal location

to prevailing cold westerly winds, the western coast of Kamchatka remains mostly ice-free during the entire year. Maximum average concentrations only reach between 0-20% sea ice (Kimura and Wakatsuchi, 1999; Kimura and Wakatsuchi, 2004; Shirasawa et al., 2005), leading to a pronounced difference in vertical water structure between the western and eastern part of the basin.

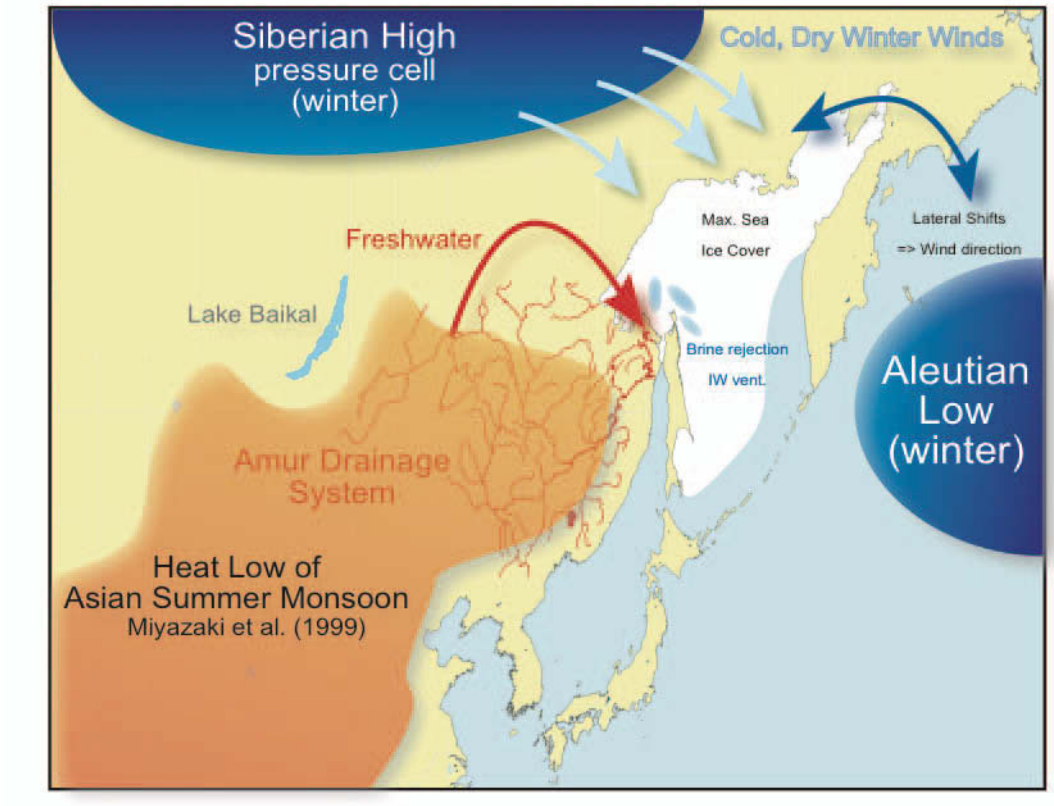

Figure 2.4: Schematic overview of action centers and forcing factors in the study area that influence the formation and ventilation of Okhotsk Sea Intermediate Water and determine sea surface temperatures and salinity (Figure courtesy by R. Tiedemann).

Apart from the connection to the hinterland EASM monsoon system via heat and moisture flux, the study region has been shown to be linked via atmospheric teleconnections to high latitude forcing, usually expressed as changes in the expression of the Arctic Oscillation, or the strength of the Siberian High – Aleutian Low pressure systems (Overland et al., 1999; Pickart et al., 2009; Rodionov et al., 2007). These wintertime patterns exert influence through their modulation of northeasterly winds on the length of the snow season on the duration of sea ice formation, which in turn determine the intensity of polynia formation on the northern shelf areas (Shcherbina et al., 2004a). As a result, the Okhotsk Sea is uniquely located at a junction between strong wintertime high-latitude forcing, and low-latitude monsoon-influenced summertime climate patterns. It features one of the most pronounced interannual and seasonal changes in temperature and precipitation worldwide.

2.3. North Pacific and Okhotsk Sea Intermediate Water

Today, the North Pacific is the endpoint of the global Meridional Overturning Circulation. No new deep water masses are formed (Emile-Geay et al., 2003; Warren, 1983), and the deep North Pacific harbors the oldest and most CO_2-enriched water masses modern in the world ocean (Broecker and Clark, 2010; Broecker et al., 2004). However, the intermediate water layer in the North Pacific is ventilated by newly formed North Pacific Intermediate Water (NPIW), which develops it characteristics in the so-called Mixed Water Region (MWR) between the Kuroshio Extension and the Oyashio Current fronts where waters from subtropical, subpolar and marginal seas origin mix (Talley et al., 1995; Talley, 1985, 1993). NPIW is characterized by a salinity minimum and oxygen maximum along the density surfaces of σ_θ 26.6 to 27.2 (Fig. 2.2., Reid, 1965; Talley, 1993; Van Scoy et al., 1991) and spreads southward into subtropical regions as well as eastward across the North Pacific. It was observed early that these density surfaces do not outcrop on the surface in the modern open North Pacific (Reid, 1965), leading to the hypothesis that the NPIW is mainly ventilated from the Okhotsk Sea and to a lesser extent the Alaskan Gyre (Kitani, 1973) (Talley, 1993; Van Scoy et al., 1991).

While earlier works assumed NPIW formation models of isopycnal mixing-based renewal processes (Reid, 1965; Watanabe and Wakatsuchi, 1998), more recent works have indicated that a substantial amount of ventilation and formation of NPIW precursors occurs by diapycnal mixing induced by tidal variations mainly within the mixed water region off the Kurile Islands and in Bussol' Strait, but also in the Kuril Basin, where DSW and SWW mix into the final OSIW (Nakamura and Awaji, 2004; Nakamura et al., 2004; Ueno and Yasuda, 2003; Yamamoto et al., 2002).

The main water mass responsible for determining the chemical and physical characteristics of NPIW is the Okhotsk Sea Intermediate Water (OSIW), a water mass that is formed by a mixture of:

(1) Western Subarctic Pacific Water (WSAP) that as one principal precursor water mass is transported to the Okhotsk Sea from the North along Kamchatka with the East Kamchatka Current and enters the Okhotsk Sea through the main deep passages, Kruzensthern and Bussol' Strait. It is relatively warmer and more saline than newly formed Okhotsk Sea (Yamamoto et al., 2001; Yamamoto et al., 2002).

(2) Soya Warm Water (SWW), a warm and saline water mass that is transported through the shallow Soya Strait into the southern Okhotsk Sea and mixes with newly formed DSW water in the Kuril Basin before the resulting final OSIW leaves the Okhotsk Sea mainly through to enter the Oyashio. Based calculation using cross-sections and current speed SWW has an annual mean volume transport of about 0.08 Sv (Itoh et al., 2003). The role of SWW in paleoceanographic

reconstructions is not well defined due to the shallow sill depth of Soya Strait (ca. 60 m), which prohibits it entering the Okhotsk Sea during glacial sea-level lowstands.

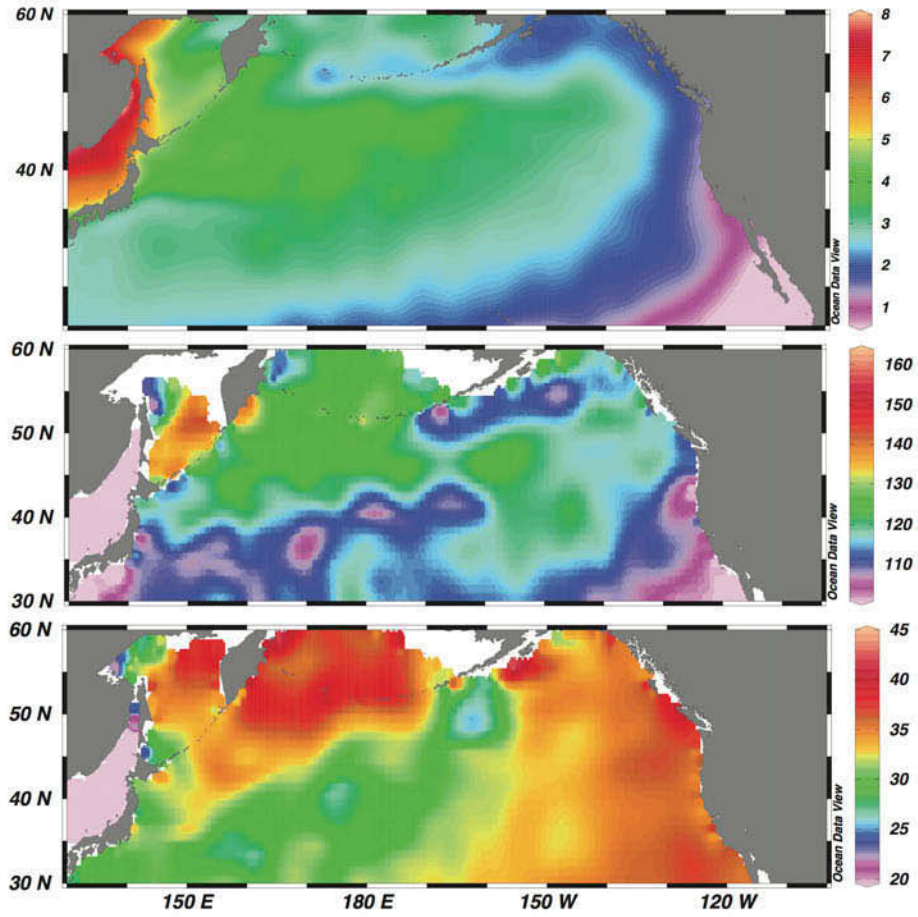

Fig. 2.5: Characteristics of North Pacific mid-depth water masses. Upper panel: Oxygen concentrations in ml/l on density surface σ_θ = 26.8 kg/m^3; middle panel: Silicate concentrations (µmol/l) on density surface σ_θ = 26.8 kg/m^3. Lover panel: Nitrate concentrations (µmol/l) on density surface σ_θ = 26.8 kg/m^3

(3) Dense Shelf Water (DSW) is a newly formed, well ventilated, cold and low salinity water mass . Of these three water masses, DSW commands particular interest as it constitutes the main water mass that imprints a distinct dissolved oxygen and nutrient signature onto the resulting final OSIW. The amount of newly formed DSW varies considerably according to different methodologies and times when studies were carried. Most estimates range between 0.2 and 1 Sv, with early CFC-based calculations gave c. 0.6 Sv (Wong et al., 1998), while hydrographic bottle and CTD data estimations range from 0.2 over 0.6 (Gladyshev et al., 2003) to 0.75 Sv based on mooring and water properties

data (Shcherbina et al., 2004b). Current-based transport calculations reach only the lower end of this range with 0.21 Sv (Fukamachi et al., 2004).

Assuming only isopycnal mixing results in published mixing ratios of 1:1:0.1 among DSW, WSAW, and SWW in order to form OSIW, with formation rate of about 1.4 Sv per year (Itoh et al., 2003). Residence time of finally mixed OSIW in the southern Okhotsk Sea is typically short, based on gridded back-tracking of float trajectories (500-750 m water depth), recent estimates range between mostly 100-400 days before OSIW is exported into the North Pacific (Ohshima et al., 2010). This indicates the potential for a rapid transfer of OSIW-based hydrographic and chemical changes into the open ocean, and was corroborated by recent studies that postulate changes in North Pacific mid-depth water characteristics based on instrumental datasets and were attributed to decreases in the ventilation and formation of Okhotsk Sea Intermediate Water, thereby leading to warming as well as salinity and ventilation decreases in the mid-depth North Pacific (Deutsch et al., 2011; Deutsch et al., 2005; Feely et al., 2004; Nakanowatari et al., 2007).

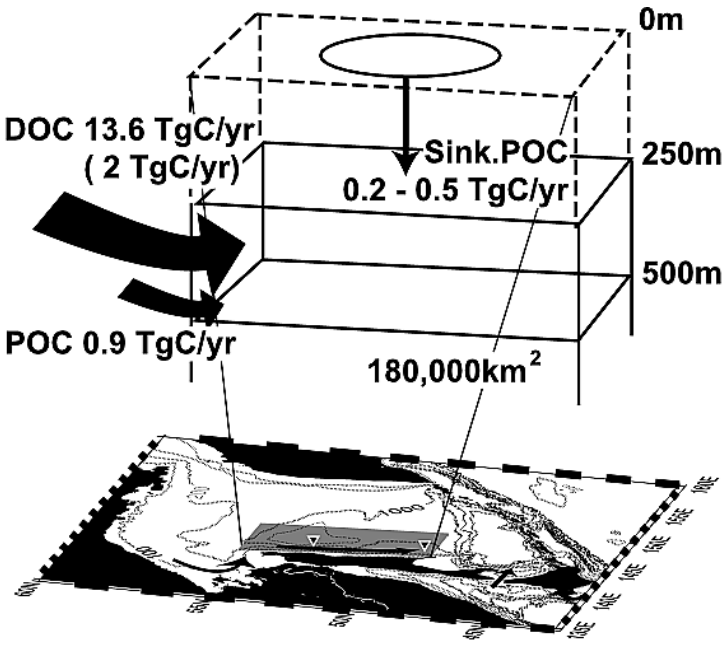

Figure 2.6: Schematic mass balance for Particulate (POC) and Dissolved Organic Carbon (DOC) input to the OSIW along the Sakhalin margin. Calcualtions are based on long-term mooring/sediment trap results(Nakatsuka et al., 2004b). Lithogenic and biogenic fluxes (Fe, detrital terrigenous sedients) co-vary for DSW/OSIW with these transport mechanisms (cf. \(Nakatsuka et al., 2004a; Nishioka et al., 2007). Original figure from (Nakatsuka et al., 2004b).

Today, DSW/OISW is a water mass with a higher O_2 concentration than surrounding water masses along comparable density surfaces (Pacific Deep water and "old" NPIW, Reid, 1965; Talley et al., 1995; Talley, 1985). At the same time, however, it is characterized by a local maximum in nutrients, in particular DOM and POM and also particulate and dissolved iron (Fe). This suspension load is transported with OSIW along the Sakhalin margin and exported to a large extent into the open North Pacific, where it can support high remineralization rates and biological activity in OSIW.(Nakatsuka et al., 1997; Nakatsuka et al., 2004b; Seki et al., 2006). The amounts of POM in the mesopelagic water column, acquired through bottom entrainment on shallow shelves and lateral transport are today slightly higher than the amounts of POM received through vertical settling of particles (the classic "biological pump"), despite the extraordinary high primary productivity in the Okhotsk Sea(Sorokin and Sorokin, 1999). The amount of DOM entrained into OSIW from bottom interaction and fluvial detrital material even surpasses the amount of vertically aquired DOM by an order of magnitude (Fig. 2.6, Nakatsuka et al., 2004b; Nakatsuka et al., 2002).

2.4. Previous Works

Paleoceanographic works in the Okhotsk Sea have intensified over the past decade and increasingly moved to studies both on longer timescales and higher temporal resolution. Most studies focus on the interaction between sea ice, productivity and upper ocean stratification (Gorbarenko et al., 2010b; Harada et al., 2006; Nürnberg et al., 2011; Nürnberg and Tiedemann, 2004; Sakamoto et al., 2006). These works also established understanding of the dominant large-scale oceanic and atmospheric controls on changing parameters in the Okhotsk Sea. For the last million years, Nürnberg and Tiedemann (2004) reconstructed primary productivity, sea ice, sedimentation dynamics coupled to a robust stratigraphic framework and linked changes in terrigenous sediment supply to large orbital-scale climatic changes in the SE Asian hinterland and the East Asian Monsoon system (Nürnberg and Tiedemann, 2004). Other works followed with establishing biostratigraphic control (Matul et al., 2009) and studying changes in productivity patterns as well as organic and lithogenic particle transport on glacial-interglacial timescales (Gorbarenko et al., 2007a; Gorbarenko et al., 2008; Gorbarenko et al., 2010a; Seki, 2005; Seki et al., 2004; Seki et al., 2003; Seki et al., 2009b). These and other works established stratification changes induced by sea ice variations and freshwater transport in combination with glacial-interglacial sea level changes as control mechanisms for primary productivity changes, peaking during glacial terminations. Recent works moved towards the detection and analysis of millennial-scale variations in sea-ice action and productivity, primarily during glacial periods (Sakamoto et al., 2006) (Gorbarenko et al., 2010a; Gorbarenko et al., 2010b; Khim and Sakamoto, 2012; Nürnberg et al., 2011). These studies identified the occurrence of

"Dansgaard/Oeschger"-like millennial variations in the Okhotsk Sea, though sometimes with considerable uncertainties in the used age models. Most works, however, claim an in-phase relationship between North Atlantic and North Pacific warm and cold phases, and postulate that atmospheric teleconnection patterns via Eurasia and/or the Arctic are driving forces for transferring climate oscillations between ocean basins with little time lag as expressed in modern Arctic Oscillation or polar vortex variations (Gorbarenko et al., 2005b; Gorbarenko et al., 2007a; Gorbarenko et al., 2010a; Harada et al., 2006). These teleconnections in turn influence the strength and position of the Aleutian Low – Siberian High pressure system, thus influencing the strength of the East Asian Winter (and to some lesser extent) Summer Monsoon (Gong and Ho, 2002; Overland et al., 1999; Wu and Wang, 2002).

However, most of these studies have been focused on proxy reconstructions that are indicative of upper water mass changes or bear witness to variations in sedimentological parameters, with only indirect relationship to the characteristics of deeper water masses. To date, little to no reliable high-resolution paleoceanographic reconstruction of North Pacific Intermediate Water ventilation changes exist from the Okhotsk Sea as modern source region. This lack of knowledge is even more pressing as a relatively high number of studies in other parts of the North Pacific make inferences about either changing or static NPIW characteristics without having explicit knowledge about the NPIW at its origin (cf. e.g. Cartapanis et al., 2012; Hendy, 2010; Hendy and Kennett, 2003; Zheng et al., 2000).

No studies based on epibenthic $\delta^{13}C$ reconstructions are available for the Okhotsk Sea, with the exception of low-resolution glacial-interglacial time slice reconstructions (Keigwin, 1998a, 2002a). Previous works are mostly based on indirect proxies such as the association of deep-dwelling microfossil assemblages with specific water masses in analogy to modern conditions (Itaki and Ikehara, 2004; Itaki et al., 2008; Katsuki et al., 2010; Okazaki et al., 2004), which remain to be tested over time; or the use of endobenthic foraminiferal isotopes (Gorbarenko et al., 2008; Gorbarenko et al., 2010a) and species assemblages (Bubenshchikova et al., 2010). As a result, knowledge about the role of NPIW and OSIW biogeochemical changes in the larger North Pacific basin over the last 20,000 or so years remain largely enigmatic to date. This thesis thus aims at starting to fill this particular gap in our current understanding of North Pacific and Okhotsk Sea intermediate water mass ventilation patterns, their connection to primary productivity, nutrient utilization dynamics, and relation with near- and far-field forcing factors. Other relevant existing hypotheses and studies will be discussed in more detail in the results chapters 5 to 9.

3. Material and Methods

3.1. Core and Sampling Strategy and Sample Processing

The sample material and the analytical works were embedded in the framework of joint German—Russian collaborative projects „Kurile-Okhotsk Sea Marine Experiment" (KOMEX) I and II and "KOMEX – SONNE SO178". Parts of the results in this work are based on material that originated from the first phase of the KOMEX project and the recently finished joint German—Russian project "KALMAR" to put achieved results into the larger regional context of the subarctic North Pacific.

3.1.1. Site and Sample Selection

Sediment samples from the Okhotsk Sea were selected from gravity and piston cores retrieved during derived from the cruises LV28, LV29 and SO179 to the Okhotsk Sea between 1998 and 2004 in the framework of the joint German—Russian bilateral research projects KOMEX (1998-2001), KOMEX II (2001-2004), KOMEX-SONNE (2004-2006). The used cores were described in the respective cruise reports, which also give an overview about the individual water column and sedimentary regimes at the core locations, and detail the shipboard initial logging, scanning, and sampling procedures for expeditions LV28 (Biebow and Hütten, 1999), LV29 (Biebow et al., 2002b), and SO178 (Dullo and Biebow, 2004). Cores were logged, color-scanned, and sampled jointly by the Shipboard Science Party. Core description and analysis of initial logging and scanning data for the German gravity cores on LV29/2 was carried out by myself, lithostratigraphic inter-core correlations between Russian and German sites and different site locations, as well as selection of cores for further analyses were jointly done by S.A. Gorbarenko, N. Biebow, A. Derkaechev and myself. During SO178 core description, logging and color-scanning was jointly carried out by the Shipboard Paleoceanography Group (Alexander Derkachev, Lester Lembke-Jene, Natalja Nikolaeva), including the lithostratigraphic core-to-core correlation and selection of cores for further paleoceanographic analysis work. A complete overview list with the cores studied in this thesis is given below in Table 3.1 and in Figure 3.1.

Cores LV28-78-3 and LV29-79-3 were chosen for further analysis in order to establish a depth transect of high-resolution Holocene sediment records proximal to the Amur fluvial discharge and the presumed formation site of Okhotsk Sea Intermediate Water (the exact formation process and location of OSIW were hypothesized, but not proven at that time, cf. Shcherbina et al., 2003a). The two sites (LV29-78-3, LV29-79-3) were later amended by core SO178-13-6, as the former cores did not penetrate the last glacial-interglacial transition with sufficiently high temporal resolution or at all.

Table 3.1: Locations and characteristics of all gravity and piston cores used in this thesis

Stat. Nr.	Latitude N	Longitude E	water depth (m)	Recovery (cm)	Location	Remarks
Gravity and Piston Cores Okhotsk Sea (KOMEX, KOMEX II, KOMEX-SONNE)						
LV28-4-4	51°08.475	145°18.582	674	930	E' Sakhalin margin	re-sampled legacy gravity core, KOMEX I, Chapter 5 and 6
LV28-44-3	52°02.514	153°05.949	684	1116	W' Kamchatka margin	re-sampled legacy gravity core, KOMEX I, Chapter 6
LV29-78-3	52°40.388	144°42.203	673	850	NE' Sakhalin margin	KOMEX II gravity core, slightly overpenetrated(20 cm), Chapter 6
LV29-79-3	52°47.272	144°57.318	1082	1072	NE' Sakhalin margin	KOMEX II gravity core, slightly overpenetrated (20 cm), Chapter 5 and 6
LV29-114-3	49°22.540	152°52.676	1762	950	E' slope Kuril Basin	KOMEX II gravity core, Chapter 8 and 9
SO178-13-6	52°43.881	144°42.647	713 (672)	2368	NE' Sakhalin margin	KOMEX-SONNE piston core, Chapter 5 and 7
Piston Cores Bering Sea (KALMAR, investigators: L. Max and J.-R. Riethdorf)						
SO201-2-85KL	57°30.30	170°24.77	967	1813	Shirshov Ridge, W' Bering Sea	Chapter 7, 8 and 9, core sampled and analysed by L. Max and J. Riethdorf
SO201-2-12KL	53°59.47	162°22.51	2170		W' Kamchatka margin, N Pacific	Chapter 8 and 9, core sampled and analysed by L. Max and J. Riethdorf
SO201-2-77KL	56°19.83	170°41.98	2163		Shirshov Ridge, W' Bering Sea	Chapter 8 and 9, core sampled and analysed by L. Max and J. Riethdorf
SO201-2-101KL	58°52.52	170°41.45	630		Shirshov Ridge, W' Bering Sea	Chapter 8 and 9, core sampled and analysed by L. Max and J. Riethdorf
SO201-2-114KL	59°13.87	166°59.32	1394		Shirshov Ridge, W' Bering Sea	Chapter 9, core sampled and analysed by L. Max and J. Riethdorf

These northerly cores are part of a North-South transect along the Sakhalin margin, complementing earlier, more southerly located site LV28-4-4, and a further, southern location off Terpeniya Bay, which comprises a depth transect between 1200 and 2000 m water depth (LV28-2-3, LV29-72-4, LV29-70-3 Biebow et al., 2002b). Unfortunately, on this latter position we unsuccessfully tried to find shallower core sites, i.e. within the 600-1000 m core layer of OSIW. Thus, results from these latter cores are not included in this thesis, but subject to future work. Core LV29-114-3, on the other hand, was chosen as ideal site distal to the immediate influence of fluvial discharge patterns for a more representative reconstruction of regional upper ocean hydrography patterns (cf. chapter 8 and 9). The core was not used in studies of OSIW changes due to its greater water depth, outside the core layer of mid-depth ventilation.

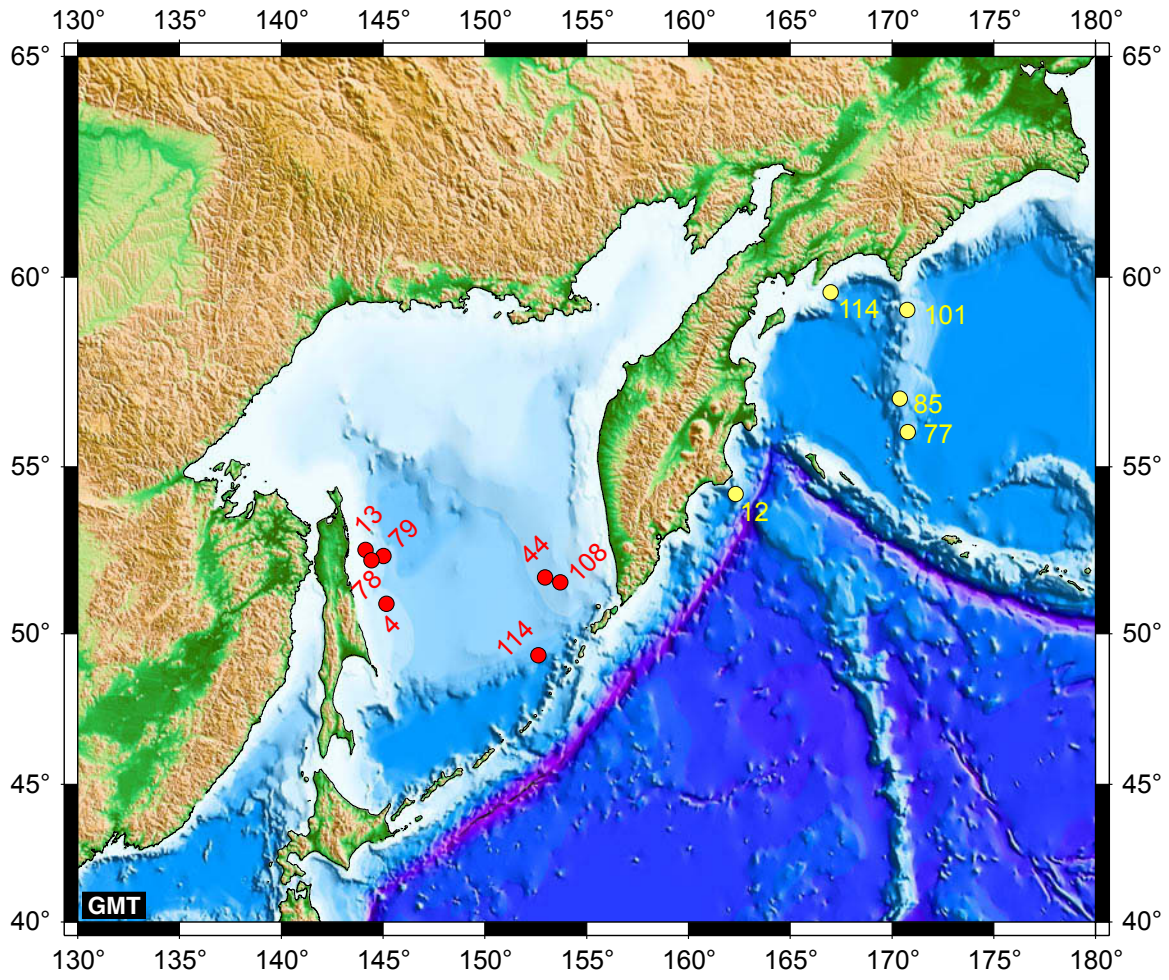

Figure 3.1: map of Study area with core locations. For readability core names are abbreviated to station numbers, with cruise prefix and station suffixes omitted. Red dots mark the primary cores studied in this thesis from the Okhotsk Sea. Yellow dots are core sites that were retrieved during the KALMAR project, primarily analyzed within complementary theses (Max, 2012; Riethdorf, 2012), and used in chapters 7-9 for comparisons between the Okhotsk and Bering Sea. GMT was used for plotting the map.

In addition, in chapters seven, eight and nine, results from Okhotsk Sea cores are compared to data derived from sediment cores of the Bering Sea. Those were retrieved during cruise SO201 with R/V *Sonne* in the framework of the Russian-German project KALMAR. Details for the sampling and coring routines during cruise SO201 are given in the expedition report (Dullo et al., 2009a) and the respective dissertation theses of L. Max and J.-R. Riethdorf, who carried out the sampling and analyses of the Bering Sea cores (Max, 2012; Riethdorf, 2012).

3.1.2. Sample Processing for LV29 and SO178 Cores

Shipboard sampling procedures for all cores have been described in the respective cruise reports (Biebow and Hütten, 1999; Biebow et al., 2002b; Biebow et al., 2000; Dullo and Biebow, 2004). Later onshore sampling of all cores followed for consistency these standard operating procedures. The sampling scheme for older, pre-processed samples from LV28 used to select benthic foraminifera for isotope analyses and radiocarbon dating was described in an earlier thesis (Kaiser, 2001). Core LV28-4-4 (archive) half cores were re-sampled onshore to increase temporal resolution.

The gravity and piston core sampling scheme during the later KOMEX II/KOMEX-SONNE expeditions followed procedures established earlier (Kaiser, 2001) in that the cores were cut into 1 m segments, analyzed for magnetic susceptibility immediately on board and thereafter sliced horizontally into two halves. While the archive half was used for core description and color scanning, the working half was first sampled in 5 or 10 cm intervals for determination of physical properties with syringes. The remaining sediment was thereafter cut into 1 cm-thick slices (outer part of each slice removed to avoid contamination) for subsequent shore-based analyses. LV29-78-3, LV29-79-3, and SO178-13-6 were initially sampled offshore for distribution to the science party, followed by onshore re-sampling in the GEOMAR core laboratory. LV29-114-3 was completely sampled onshore.

All samples taken from sediment cores were placed in polyethylene bags (Whirl-Pak®) or polystyrene hard-shell containers with polyethylene snap lids (Thermo Scientific NUNC®). All samples were stored refrigerated (at temperatures between 2° and 7° C) onboard and in the GEOMAR Lithothek Core Repository thereafter until being further processed or archived. All samples used for subsequent analyses that required dried sediment were freeze-dried, as this method minimizes potential bias and problems during subsequent analyses (e.g. McClymont et al., 2007; Schubert, 2005). Figure 3.1 provides a schematic overview of the sample processing and analysis workflow.

For the retrieval of foraminifera from sediment, slice samples were weighed and washed over a 63µm sieve with tap water, followed by final rinsing with de-ionised water. Samples were dried at 60° C and sieved thereafter into size fractions of 63-150µm, 150-250µm, 250-500 µm, 500-1000 µm and >1000 µm. Subsequent weighed was carried out to calculate coarse fraction content. These samples were used for further studies on foraminifera, including the selection of specimen for isotope analyses and radiocarbon dating.

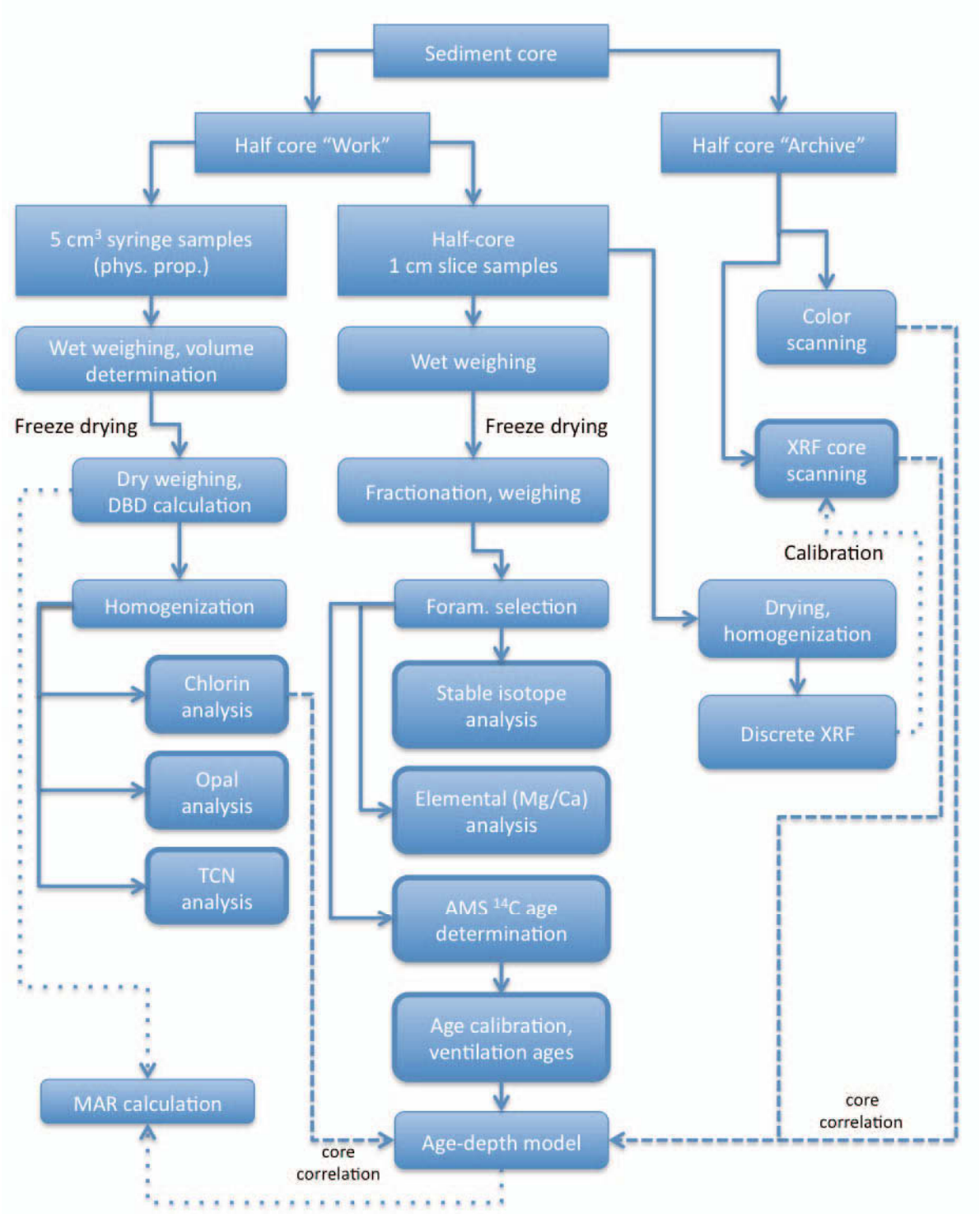

Figure 3.2: Schematic workflow of Okhotsk Sea sample processing and analyses used in this thesis. Blocks with thickened frames indicate processes with final data output mainly used for interpretation.

Samples for analysis of Dry Bulk Density (DBD) were taken directly on board after core opening on cruises *LV29* and *SO178* in 5 cm intervals, in some cases in 10 cm intervals. These Physical Properties

Samples were taken in commercially available, medical plastic syringes in volumetric sizes of five or ten cubic centimeters, with previously cut off heads. Sample syringes were closed with tight-sitting plastic caps, sealed by water- and airtight electrical duct tape and placed in plastic bags that were sealed until processing in shore-based laboratory at IFM-GEOMAR, Kiel. Determination of dry bulk densities (DBD hereafter) followed established protocols (cf. Dadey et al., 1992). All samples were weighed immediately after arrival in the shore-based laboratory, subsequently freeze-dried and again weighed in dry state. After finished DBD determinations and quality control, these samples were used for further anorganic chemistry analysis (*viz.* opal, TCN, chlorin analyses, see methods description below).

3.2. Radiometric Dating — AMS ^{14}C Measurements

Age control was primarily achieved through radiocarbon dating of planktic foraminifera and, in some cases, benthic fauna if the available samples did not yield enough planktic foraminifera. For radiocarbon analysis I picked *all N. pachyderma (s)* and *G. bulloides* of a selected sample from the size fraction 150-250 µm. Specimen with visible overgrowth of diagenetic crystals, with signs of post-depositional alteration, or recrystallisations (e.g. yellowish colour) (Pena, 2005; Pena et al., 2008) were excluded from further use (radiocarbon, stable isotope, elemental analyses). All radiometric dating was carried out in the Leibniz Laboratory for Radiometric Dating and Isotope Research, Kiel. (Grootes et al., 2004; Nadeau et al., 1998; Nadeau et al., 1997)

In the laboratory, samples were routinely cleaned with 15 % H_2O_2 in an ultrasonic bath to remove adhering dust, detrital carbonate and organic surface coatings. The CO_2 was liberated from each sample with 100 % phosphoric acid at 90 °C. This CO_2 was reduced with H_2 over about 2 mg of Fe powder as catalyst, and the resulting carbon/iron mixture was pressed into a pellet in the target holder (P.M. Grootes, pers. communication).

In the Leibniz Laboratory, the ^{14}C concentrations of the samples were measured by comparing the simultaneously collected ^{14}C, ^{13}C, and ^{12}C beams of each sample with those of Oxalic Acid standard CO_2 and pre-Eemian foraminifera as background. Conventional ^{14}C ages were calculated according to Stuiver and Polach (1977a) with a δ^{13}C correction for isotopic fractionation based on the ^{13}C/^{12}C ratio measured by the AMS-system simultaneously with the ^{14}C/^{12}C ratio. For the determination of the laboratory's measuring uncertainty (standard deviation σ) both the counting statistics of the ^{14}C measurement and the variability of the interval results that, together, make up one measurement were measured. The larger of the two was adopted as measuring uncertainty. To this the laboratory adds the uncertainty connected with the subtraction of the "blank". The quoted 1σ uncertainty thus constitutes

the best estimate for the full measurement and is not just based on counting statistics (pers. communication P.M. Grootes and cf. Grootes et al., 2004; Nadeau et al., 1998; Nadeau et al., 1997). While a minimum of about 1,000 specimen is regarded as optimal to deliver enough carbon for dating after sample pre-processing, some samples did not yield sufficient carbonate weight. In these cases sample pre-treatment was modified in the Leibniz Laboratory in order to maintain enough carbon for reliable dating by substituting the H_2O_2 in the cleaning step by repeated rinses with $H_2O_{dem.}$

Dating of two samples carried out at a later stage in addition to the initial set to further constrain the age models was done by the W. M. Keck Carbon Cycle Accelerator Mass Spectrometry Laboratory at University of California, Irvine. Details about the methodology of these age determinations are provided in the online documentation of the facility, including the laboratory's written protocols as Internal Technical Reports in pdf-format (http://www.ess.uci.edu/ams/, last accessed on 01 May 2013).

Radiocarbon data of water samples were courtesy provided by Ralf Tiedemann, samples were measured in the Leibniz laboratory, Kiel as well, methods followed established protocols (cf. http://www.uni-kiel.de/leibniz/ for analytical processes not described in aforementioned references).

The AMS ^{14}C measurements were used for establishing core stratigraphy (chapter 5, 6, 7, 8 and 9) as well as for analysis of paleo-ventilation patterns during the last glacial termination (chapter 5 and 7).

3.3. Stable Isotope Measurements

For each measurement of stable carbon ($\delta^{13}C$) and oxygen ($\delta^{18}O$) isotopes I picked foraminifera from the previously processed coarse fraction samples as follows:

For planktic foraminifera, I selected between 20 and 30 specimen of the non-spinose, non-symbiont-bearing left-coiling variety of *N. pachyderma* (Ehrenberg) 1861 from the 150-250 µm size fraction. I only used clean tests without visible alterations, secondary overgrowths, or discolorations (into yellowish colour) for analysis. Each planktic foraminifera was also checked for contamination by post-depositional sediment fillings and excluded or cleaned before analysis.

For benthic isotope records, I usually analyzed between one and five tests that I chose from the 250-500 µm size fraction. For the identification and selection of all benthic foraminifera data reported in this study, I followed the taxonomic revision and notes of Holbourn and Henderson (2002), with comparisons to Scott et al. (2000b) and van Morkhoven et al. (1986). The used taxonomic assignments were in addition discussed and cross-checked with my Russian collaborator N. Bubenshchikova (cf. \

(Bubenchshikova and Lembke-Jene, 2002; Bubenshchikova et al., 2008). Between three to five tests of the shallow endobenthic foraminifiera *Uvigerina peregrina* were used for analyses. However, I note that in this thesis I use the commonly used designation *U. peregrina*, though N. B. and I largely agree that the taxonomically correcter assignment for the Okhotsk Sea fauna is likely *Uvigerina akitaensis* (in line with reasoning of Scott et al., 2000a).

I use *Cibicides lobatulus* (Walter and Jacob) 1798 (cf. images of specimen in collections of the Natural History Museum, London in Holbourn and Henderson, 2002), which is known to live in an often elevated epibenthic habitat attached to hard substrate or even live macrobenthos (Moore, 1985; Svavarsson and Davidsdottir, 1995). This species is clearly identifiable in the sediment samples of the Okhotsk Sea cores. The second, more abundant cibicid species that is used in this thesis is designated as *C. mundulus* (Brady, Parker, and Jones) 1888, following the arguments of van Morkhoven et al., and, with the often-used name *Cibicides kullenbergi* (Parker) being considered a junior synonym. Holbourn and Henderson (2002) state that *C. mundulus* can be distinguished from *Cibicidoides pachyderma* (Rzehak) 1886 "by looking at the peripheral view: **Cibicidoides pachyderma** has an asymmetrical appearance, reminiscent of the central saucer of the Starship Enterprise, whereas **C. mundulus** exhibits a more symmetrical character reminiscent of a flying saucer from a 1950s sci-fi film (Katz, personal commun., 1998)". While this identification holds true for specimen in the Okhotsk Sea sediment samples, some studied specimen seemingly show intergrading forms between *C. pachyderma* (or respectively C. pseudoungerianus, but cf. discussion in van Morkhoven et al. 1986) and *C. mundulus*, leading to the impression that some, especially *C. mundulus* might be morphologically more closely related to *C. pachyderma* than to "typical" *C. kullenbergi* as known from other regions (Caribbean, Atlantic). Further taxonomic studies might be necessary in the subarctic North Pacific, as the species are widely used for paleoceanographic reconstruction, but are at present such efforts are hampered by the generally low abundance of cibicid species in Okhotsk Sea sediments and sparse coverage of the area with live-sampled fauna.

During picking for isotope analyses, I checked every specimen for preservation state and, if necessary, cleaned the samples. Cleaning was done following established protocols by cracking the foraminiferal tests open, soaking the fragments in ethanol p.a. in an ultrasonic bath, siphoning the supernatant off and drying the samples in a clean oven without ventilation at 50°C over night. This procedure has been shown to not alter the original isotopic composition of the foraminiferal tests before analysis (Ganssen, 1981; Löwemark et al., 2005).

I carried out all analyses of oxygen and carbon isotopes on foraminifera and other carbonate material for this thesis in the Paleoceanography Department's ISOLAB Stable Isotope Laboratory at the IFM-GEOMAR in Kiel, using either a Finnigan Delta-Plus-Advantage Isotope Ratio Mass

Spectrometer (IRMS) coupled to a Finnigan Gas Bench II (with long-term analytical precision better than ± 0.07 ‰ for $\delta^{18}O$ and better than ± 0.05 ‰ for $\delta^{13}C$), or a Finnigan MAT 252 IRMS connected online to an automated Kiel II AUTO CARBO carbonate preparation device (with a long-time reported analytical precision better than ± 0.07 ‰ for $\delta^{18}O$ and ± 0.04 ‰ for $\delta^{13}C$). Both machines are inter-calibrated by using the in-house ST BREMEN ($\delta^{13}C$ = –2.93 ‰, $\delta^{18}O$ = 4.28 ‰) standard that is prepared from Solnhofen Limestone. The ratios of $_{18}O/_{16}O$ and $_{13}C/_{12}C$ are reported as relative deviations (δ-notation) from a laboratory standard, here with reference to the Vienna - Pee Dee Belemnite (V-PDB) notation derived as follows for oxygen isotopes (McKinney et al., 1950):

(3.1)

$$\delta^{18}O(‰) = \left[\frac{(^{18}O/^{16}C)_{sample} - (^{18}O/^{16}O)_{standard}}{(^{18}O/^{16}O)_{standard}} \right] \times 10^3$$

and accordingly for stable carbon isotopes (Craig, 1957):

(3.2)

$$\delta^{13}C(‰) = \left[\frac{(^{13}C/^{12}C)_{sample} - (^{13}C/^{12}C)_{standard}}{(^{13}C/^{12}C)_{standard}} \right] \times 10^3$$

The calibration to the V-PDB standard was obtained the National Bureau of Standards NBS-18 and 19 and the aforementioned internal laboratory standard.

The Thermo Finnigan MAT 252 IRMS was better suited to measure smaller amounts of CO_2 due to the technical layout of the IRMS at the time of measurements and was thus preferentially used for the analyses in this thesis. In the course of the foraminiferal analyses, a high number of single specimen or small carbonate mass measurements were performed due to low abundance of foraminifera in some samples (e.g. chapter 7 and 8). The MAT 252 was accordingly adjusted to small gas volumes by L. Haxhiaj (ISOLAB technician) and myself. These modifications were checked through running repeated in-house standard samples, in addition to regular in-house standard runs. After analysis, I checked each sample measurement result for sample gas volumes, sufficient currents on the IRMS faraday cups, and according maximum standard deviation. Each sample run was validated and corrected by the above-mentioned co-measured in-house standards (of approximately similar sample mass in sample runs).

Results from stable isotope analysis of planktic and benthic foraminifera were used in all reported results (chapters 5-9). Data from cores SO178-13-6, LV28-4-4 and LV29-79-3 were used for the interpretation of paleo-ventilation patterns, changes in hydrography and intermediate water formation

during the last glacial termination (chapter 5, 6 and 7). Stable isotope results from core LV29-114-3 were used for stratigraphy and calculation of $\delta^{18}O$-based salinity approximations (chapter 8). They were also used in additional works about deglacial surface and mixed layer stratification and SST development (see appendix).

3.4. XRF scanning

For major and minor element content analysis of sediment cores I used X-ray fluorescence scanning (Jansen et al., 1998; Richter et al., 2006; Rothwell et al., 2006). I scanned the cores reported in this thesis with one of the two XRF-core scanners available in the IODP Bremen Core Repository (BCR) at the MARUM, University of Bremen during two scanning time slots. I used the newer AVAATECH core scanner model for cores LV29-114-3 and SO178-13-6, while Cores LV29-79-3 and LV28-4-4 were measured on the older CORTEX scanner. The CORTEX Core Scanner is able to measure limited set of elements from potassium (K) through strontium (Sr). The central sensor unit consists of a molybdenum X-ray source (3-50 kV) and a Peltier-cooled PSI detector (KEVEX™) with a 125 µm beryllium window, a multichannel analyzer with a 20 eV spectral resolution and 15 s count time with X-ray current of 0.15 mA (see Röhl and Abrams, 2000). All measurements were performed at 1 cm intervals with 10 kV, except core LV29-79-3, which was measured at 0.5 cm intervals. Gravity core LV28-4-4 was scanned earlier on the same CORTEX scanner by Reinhard Kozdon as part of his Master thesis (Kozdon, 2002), and the data and subsequent processing were taken from that thesis. The AVAATECH XRF scanner can analyze more elements, from Aluminum (Al) through to Uranium (U, atomic number 92) (Richter et al., 2006; Tjallingii, 2006). The AVAATECH scanner had a sensor unit with an Oxford Rhodium (Rh) X-ray source, an Amptek 2-stage Peltier-cooled detector with 25 µm Beryllium window, and multi-channel analyzer with a spectral resolution of 20 eV (Tjallingii, 2006; Weltje and Tjallingii, 2008). The analysis area is Helium-flushed between prism and detector and within the prism to minimize scatter of radiation on both systems.. Prior to XRF-scanning, half cores were covered with Mylar foil for the CORTEX XRF scanner, whereas on the AVAATECH scanner, a 4 µm SPEXCerti Prep Ultralene® foil was applied before scanning in order to achieve a higher transmission of weak fluorescence signals from light elements like Al, Si (compare Tjallingii, 2006; Tjallingii et al., 2007). I took care to bring sediment half core surfaces to room temperature to avoid condensation of water on foils, and to avoid wrinkles and air bubbles along the scanning track.

The inter-comparison of samples measured with both scanners as well as the set-up optimization has been tested and verified by BCR personnel. A number of detailed studies about the two scanners has been published on performance, technical setup and best operating procedures (Croudace et al., 2006;

Richter et al., 2006; Röhl and Abrams, 2000; Tjallingii, 2006; Tjallingii et al., 2007; Weltje and Tjallingii, 2008). These published recommendations were observed for the scanning and analysis works related to this thesis. Values with χ values of more than three on AVAATECH scan runs (Croudace et al., 2006) were discarded from reports. As it has been shown that water content in the sample can affect the accuracy of some lighter elements like SI and Al (Tjallingii et al., 2007), while heavier elements like Ca, Fe, Ti, K remain unaffected. As a result, in this thesis I preferentially use elements proven to be relatively unaffected by the core water content, though no apparent offsets between those and lighter elements e.g. like Al in conjunction with the water content of the cores were observed.

Reported results from XRF scanning in this thesis are largely based on counts or count ratios. However, calibration work was undertaken to (1) ensure that the scanned core results were analyzed with an adequate peak identification and integration quantification model, (2) allow for later quantification of XRF counts into elemental concentrations and (3) assess whether discrete XRF analyses can be used independent of the respective cores they were made on, i.e. whether potential exists for a basin-wide XRF calibration for XRF-scanned cores. Two runs were carried out with 37 and 26 discrete samples that were measured on sequential wavelength dispersive Phillipps PW1400 and X'Unique (RH-tube) X-ray fluorescence spectrometer at the GEOMAR on two different cores (LV28-4-4 and LV29-108-5). Discrete samples were chosen in line with published recommendations (Weltje and Tjallingii, 2008) and show excellent agreement both between XRF scans and discrete samples and between the two different sample datasets from the two cores (Table 3.2), allowing for the use of a combined calibration dataset if needed (cf. Fig. 3.3). Individual plots and regressions of elemental scan counts vs. discrete concentrations are stored in the PANGAEA database.

I ran one gravity core (LV29-108-5) on both scanners with identical set-up for comparison. Core LV29-108-5 is located at c. he same location as LV28-44-3 that is used in this thesis. The environment there is slightly different from the cores off the Sakhalin margin. The former are heavily influenced by fluvial detrital suspension and regularly occurring seasonal sea ice that both deliver high amounts of terrigenous material to the core sites. LV29-108-5, on the other hand is only moderately influenced by terrigenous sediment delivery through rivers, as no river systems comparable to the massive Amur discharge occur on the western Kamchatka margin. In addition, sea ice during the Holocene only intermittently covered the core site, as it lies beneath the inflowing, relatively warm East Kamchatka Current and far from the modern "sea ice formation centers on the shallow northeastern Okhotsk Sea shelf areas. As these two scanning runs were done in 2003 and 2006, well offset from each other, the rationale was to determine whether: (1) The principal elemental concentrations were reproducible on

the two different systems and (2) significant changes in the sediment composition happened due to long-time storage that might have affected the accuracy of the previous scanning results.

Table 3.2: Comparison of linear regressions and correlation coefficients for between discrete and scanned XRF-derived elemental concentrations in two cores from the Okhotsk Sea. "Combined" indicates regressions based on merging datasets of the two different cores to increase the number of data. Bold data indicate elements that were used in thesis (chapters 5, 7, 9).

CORTEX	**Linear Regression: f(x)= m+a*x**			
composite	**const. m**	**a**	**R2**	**Ref. core**
Ti	**1272**	**14.806**	**0.94562**	**combined**
Fe	**9232.7**	**5.2733**	**0.92886**	**combined**
Mn	103.46	3.5037	0.73438	combined
Ca	**2645.7**	**47.686**	**0.70219**	**combined**
K	**6126.9**	**56.175**	**0.91024**	**combined**
Sr	103.45	3.3843	0.36235	combined
Core-specific	**const. m**	**a**	**R2**	**Ref. core**
Ti	**1085.4**	**16.112**	**0.96083**	**LV29-108-5**
	1480.8	**13.309**	**0.94759**	**LV28-4-4**
Fe	**8634**	**5.8259**	**0.95962**	**LV29-108-5**
	10708	**4.662**	**0.96282**	**LV28-4-4**
Mn	177.44	3.1997	0.80695	LV29-108-5
	67.023	3.5703	0.8065	LV28-4-4
Ca	17903	12.235	0.14959	LV29-108-5
	6959.1	12.399	0.29309	LV28-4-4
K	**4496.4**	**57.403**	**0.95613**	**LV29-108-5**
	7783.8	**51.77**	**0.96598**	**LV28-4-4**
Sr	148.5	2.6456	0.35999	LV29-108-5
	105.65	2.6761	0.44462	LV28-4-4
AVAATECH	**Linear Regression: f(x)= m+a*x**			
core-specific	**const. m**	**a**	**R2**	
Ti	**213.11**	**1.3657**	**0.97555**	**LV29-108-5**
Fe	**2377.3**	**1.3572**	**0.97441**	**LV29-108-5**
Mn	-64.994	1.1427	0.68354	LV29-108-5
Mn 3smooth	-118.59	0.45404	0.84691	LV29-108-5
Ca	11431	1.562	0.60858	LV29-108-5
K	**3905.3**	**3.3172**	**0.98729**	**LV29-108-5**
Sr	100.67	0.62235	0.60382	LV29-108-5
Si	382140	-16.328	0.42815	LV29-108-5
Al	-29053	99.054	0.87619	LV29-108-5
Al 3 smooth	-33183	104.63	0.91368	LV29-108-5
Rb	6.77323	0.80368	0.45863	LV29-108-5
Rb 3smooth	-4.5358	1.112	0.76204	LV29-108-5
Ba	121.32	0.46506	0.63092	LV29-108-5
Ba 3smooth	109.32	0.48855	0.76593	LV29-108-5
Zr	33.054	0.53274	0.71254	LV29-108-5
Zr 3smooth	20.648	0.68702	0.899	LV29-108-5

x = XRF scanning counts; f(x)= XRF sequential discrete XRF

Results from the two repeat scanning runs, however, show that the results stay in remarkable similarity. In fact, the counts on all elements that could be analyzed on both scanners showed excellent reproducibility for the elements Fe, K, Ti, Ca. No major offsets due to alteration or other storage-induced artefacts were recognizable in core LV29-108-5 (Fig. 3.3). Interoperability of core scanners and cores as well as core storage induced changes in elemental compositions will be part of a forthcoming intercomparison study that also includes the AWI Bremerhaven XRF-scanner.

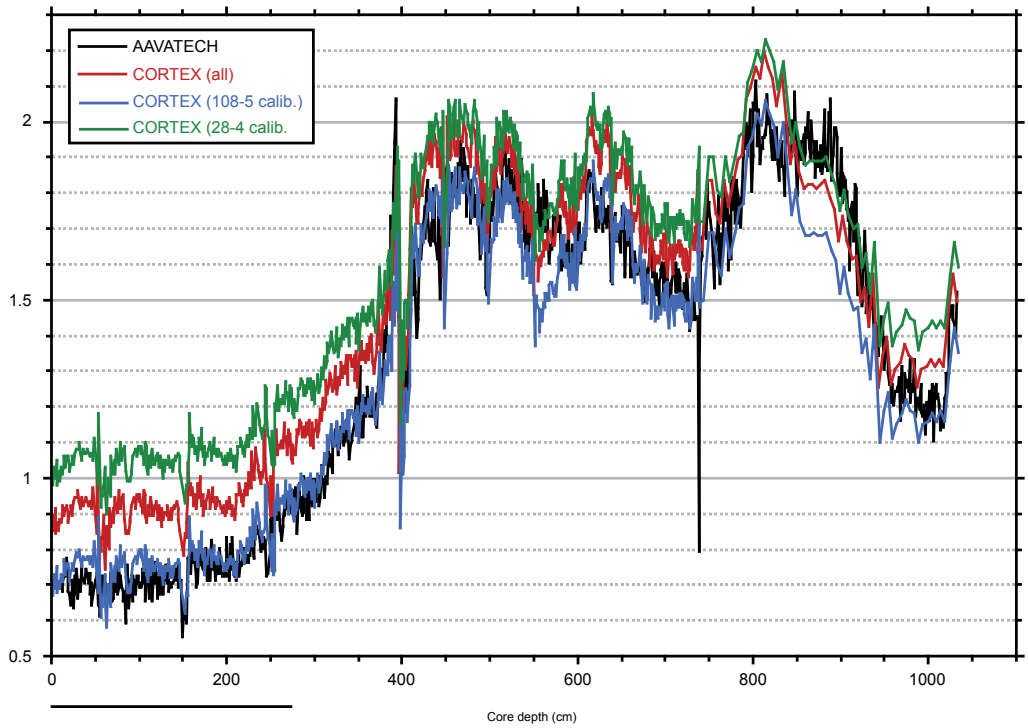

Figure 3.3: Exemplary comparison of different XRF-scanner runs and discrete XRF – based calibrations for potassium (K) on an Okhotsk Sea sediment core (LV29-108-5). Scan runs were carried out in 2003 (CORTEX) and 2006 (AAVATECH). Notice that the overall correspondence between the AAVATECH and CORTEX scan run is small (black and blue lines) when core-specific XRF calibration through discrete is used. Comparison between calibration with core-specific (blue) samples and samples from a core with a different sedimentological setting (fluvial runoff, higher sea ice input) off Sakhalin (LV28-4-4) still results in an overall good match if concentrations are above 1.2-1.5 %. Only for low values below 1.4 % the calibrated concentrations start to diverge significantly. Given that this calibration sensitivity exercise is (1) based on a very limited number of discrete samples (n=25 for LV29-108-5, n=38 for LV28-4-4) and (2) several years passed between both the scanning (>3 yr) and discrete analyses (>5 yr), one can argue that under normal circumstances a basin-wide calibration dataset for all cores can be obtained and that storage, analytical precision and instrument drift play only a negligible role in the XRF-based proxy records presented.

Results from XRF canning were used in the setup of an unified stratigraphic framework between the Bering and Okhotsk Sea (chapter 7) and used to assess the composition of the lithogenic sediment fraction during the last glacial termination (chapter 5) in particular with regard to the iron content.). They were also used in additional works about deglacial surface and mixed layer stratification and SST development (see appendix).

3.5. Chlorin Concentrations

Chlorins are degraded products of phytoplankton that are found in deep-sea sediments and have been shown to represent a good proxy indicator of past primary productivity in a wide range of different oceanographic settings (Harris et al., 1996). They have been used successfully as an indicator of primary productivity within previous multi-proxy studies in the subarctic North pacific and the Okhotsk Sea (e.g. Gebhardt et al., 2008; Gorbarenko et al., 2007a; Nürnberg and Tiedemann, 2004)). For this thesis, the analysis of chlorin concentrations followed standard procedures established in the Geochemistry Laboratory at GEOMAR. Acetone was used to free pigments from previously freeze-dried and homogenized sediment by repeated sonication and centrifugation. Pigments were acidified with Hydrochloric Acid (HCl) to transform chlorophyll-a into phaeopigments. Chlorin concentrations were measured with a Turner Fluorometer (type TD-700) immediately after extraction. The analysis of chlorin concentrations was carried out on about 0.6 g of previously homogenized sediment sample material in duplicate measurements. Prior to analysis, chlorins were extracted with acetone under sonication and subsequent centrifugation in three consecutive steps. The samples were ice-cooled after each extraction. The sediment extracts were thereafter measured with a TD-700 Fluorometer (GAT) immediately after the third extraction, always under low light conditions to hinder decomposition. Chlorophyll-a (sigma), acidified with 2 ml HCl is used as standard. To check extractions and instrument drift an internal standard sample was measured after each dozen measurements. Unless otherwise noted, all chlorin concentrations are reported in ng/g.

Chlorin measurements were used in this thesis to carry out inter-core correlations (chapter 4, 5, 6) and to assess changes in bulk primary productivity during the last glacial termination on the Sakhalin margin (chapter 5).

3.6. TOC, $CaCO_3$, $[C/N]_{atomic}$ ratios

A CARLO ERBA CNS analyzer (Model NA-1500) was used for measuring the carbon and nitrogen content of sediment core samples (Verardo et al., 1990). In most cases, the processed, freeze-dried

sediment samples previously used to determine physical properties were taken for analysis. The total carbon (TC) content was measured from bulk sediment previously homogenised by milling, the Total Organic Carbon (TOC) content was measured on bulk sediment samples previously decalcified with 0.25 M HCl. The $CaCO_3$ content was calculated by subtracting the TOC from the TC value using the formula: $CaCO_3 = 8.333 \cdot (TC - TOC)$. Long-term analytical precision is around 2%. All samples were measured two times and an average value was calculated from these two measurements. In cases of significantly different results, the sample was re-run.

$CaCO_3$ and TOC measurements were used in this thesis to correlate cores and assess changes in primary production and terrigenous matter supply during the last glacial termination (chapter 5). They were also used in the additional works about deglacial surface and mixed layer stratification and SST development (chapter 8 and 9).

3.7. Opal

The measurements of biogenic opal concentrations as well followed well-established procedures in the Sedimentology/Anorganic Geochemistry Laboratory at GEOMAR. The method as been used before on sediments from the Okhotsk Sea and was not modified for this thesis (Nürnberg and Tiedemann, 2004). The methodology follows the automated leaching method (Müller and Schneider, 1993), in which opal is extracted from the previously freeze-dried and homogenized bulk sediment with NaOH at about 85°C over ca. 45 min. time. The leaching solution is continuously analyzed for dissolved silicon by molybdate-blue spectrophotometry (mineral correction applied following DeMaster, 1981; Nürnberg and Tiedemann, 2004). The reported long-term accuracy of the method is ±0.5 weight %, deduced from replicate and standard measurements.

Measurements of biogenic opal were mainly used in this thesis to assess biosiliceous productivity changes during the last glacial termination (chapter 5).

3.8. Archiving and Data Repository

All samples that were used for thesis are permanently stored either in the GEOMAR Lithothek Core and Sample Archive in Kiel or at the AWI Sample Repository in Bremerhaven. All data used and reported in this thesis are permanently stored in the "World Data Center for Marine Environmental Sciences (WDC-MARE) and accessible through the PANGAEA archive and publication system via the online portal (http://www.pangaea.de/).

4. Stratigraphic and Age Model Approach

4.1. Previous Works and Strategies

Establishing a coherent stratigraphic framework for all sediment cores is a mandatory prerequisite for the research targets of this thesis. Early works largely relied on low-resolution bio- and oxygen isotope stratigraphy (Hays and Morley, 2003, 2004; Morley et al., 1991), supplemented by only few radiometric age control points (Keigwin, 1998a, 2002a). A chronostratigraphic approach on a basin scale for the Okhotsk Sea was established by a number of studies in the framework of the first KOMEX phase for longer, orbital timescales (Gorbarenko et al., 2002b; Nürnberg et al., 2011; Nürnberg and Tiedemann, 2004), supplemented by works of other large-scale programs (Sakamoto et al., 2005; Sakamoto et al., 2006; Seki et al., 2004) or works focusing on particular cores (Barash et al., 2008; Bubenshchikova et al., 2010). However, especially for the last glacial termination and the Holocene a comprehensive stratigraphic framework based on independent AMS ^{14}C dating was missing until recently. Progress for the last glacial termination and earliest Holocene that uses an inter-basin correlation approach for the Northwest Pacific led by L. Max is presented in detail in Chapter 9 of this thesis (also: Max et al., 2012a), and thus not repeated here. In that study, core LV29-114-3 from the Kuril Basin is matched to previously published records (Keigwin, 1998a) and cores from the Bering Sea (Dullo et al., 2009a) into one common chronostratigraphy for the region, based on correlation of well-established, AMS ^{14}C-dated $CaCO_3$ peaks (Max, 2012).

This approach works well during the deglaciation, but meets challenges in the cores on the Sakhalin continental margin within the Holocene, the foci of Chapter 5 and 6. Firstly, some of the cores that are used in Chapters 5 and 6 do not completely extend beyond the Holocene into the glacial or the glacial termination, making them less suitable for unambiguously identifying correlating $CaCO_3$ peak patterns during that period. Secondly, these peaks offer little fine structure after the respective the two prominent maxima centered on the Bølling Allerød and early Preboreal interval. This is especially apparent in the cores from the northeastern Sakhalin margin, where due to dilution effects with terrigenous material and high sedimentation rates $CaCO_3$ contents are extremely low and approach zero in some parts (cf. Chapter 5). Thirdly, beyond the prominent peaks during the termination the relatively low $CaCO_3$ content varies locally in different regions of the Okhotsk Sea within the Holocene due to changes in sea ice cover and carbonate vs. siliceous primary producers. As a consequence, I opted to use the chlorin content for inter-core correlations instead. Chlorins are established as a reliable and sensitive proxy for primary production (Harris et al., 1996), have been successfully used as proxies in the Okhotsk Sea before (Gorbarenko et al., 2012; Nürnberg and

Tiedemann, 2004) and display distinct surface productivity patterns within the Holocene. I here assume that neighboring cores on the Sakhalin margin in principle record the same primary productivity patterns and thus can be correlated by matching the chlorin content variations between cores, in analogy to the approach used before by us for deglacial CaCO3 peaks (Max et al., 2012a).

4.2. ^{14}C Age Calibration and Reservoir Age Determinations

Age models for the cores used in this thesis were developed following differing strategies according to the specific nature and needs for temporal resolution and available ^{14}C-dated material. While details about the construction of the age-depth relationships itself are also given in the respective chapters, I here add background information related to the methodological approach for a better understanding of the results reported in Chapters 5, 6 and 7.

Throughout this thesis, unless otherwise noted, I follow the stratigraphic framework and conventions developed by the INTIMATE working group in its most recent version (Blockley et al., 2012; Blockley et al., 2011). All ages, unless specifically given otherwise, are expressed in calibrated calendar years before present according to (Stuiver and Polach, 1977a), the abbreviations “cal. yr BP” or “ka” are used, As these calibrated ages are referenced to A.D. 1950, I applied appropriate corrections to reference curves based on other timescales, e.g. in the case of NGRIP ice core data reported on the GICC05 timescale referenced to yr b2K (A.D. 2000) of –50 yr to adjust all records to one common timescale (Rasmussen et al., 2006a; Svensson et al., 2008).

For all initial age calibrations the software “Calib 6.0” (Stuiver and Reimer, 1993a) was used with the calibration curves MARINE04 and MARINE09 (Hughen et al., 2004; Reimer et al., 2009a). While radiocarbon data once calibrated within the smaller than 12 kyr range remained on the MARINE04 results as the two curves are identical in this time interval, for older dates the MARINE09 curve was used. As part of the age model routine, I cross-checked calibrated ages with MARINE04 because of ongoing discussions in the community whether in fact INTCAL/MARINE04 might be better suited for marine samples than MARINE09 during some deglacial intervals (cf. supplement in: Lund et al., 2011) based on indications in earlier works (Beck et al., 2001; Marchitto et al., 2007a).

Raw radiocarbon ^{14}C ages from marine samples are not in equilibrium with atmospheric ^{14}C, but offset due to adjustment processes at the ocean-atmosphere interface, water mass aging, circulation and mixing, etc. (e.g. Hughen et al., 2006; Reimer et al., 2009a; Shackleton et al., 2004; Skinner, 2008). They thus need to be corrected for either the “total reservoir age” R when calibrated with the terrestrial calibration curve INTCAL09, or for the “local reservoir age” ΔR when the marine calibration curve

MARINE09 is used, which already uses a modeled global marine offset (Hughen et al., 2004; Reimer et al., 2009a).

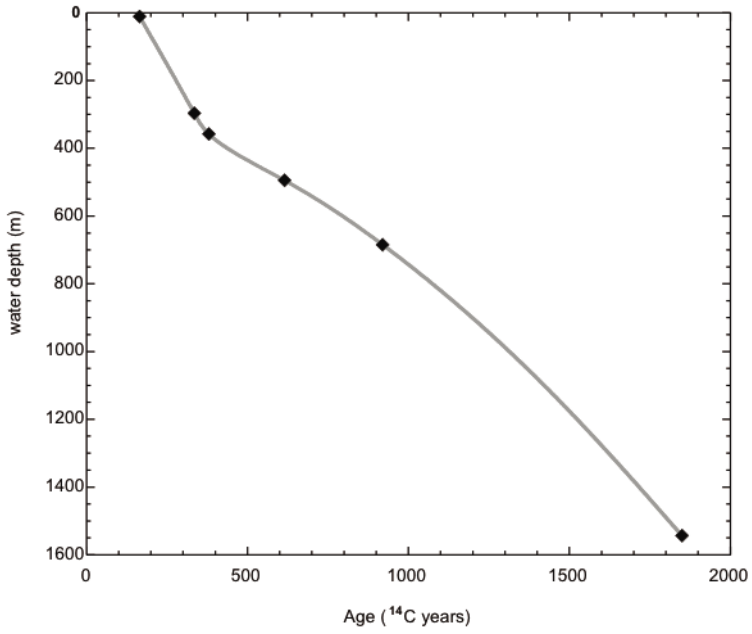

Figure 4.1: Water DIC AMS ^{14}C measurements from legacy samples taken during KOMEX phase I and provided by R. Tiedemann (see table 4.1). Values in raw ^{14}C years were used to constrain ventilation age offsets for benthic ^{14}C measurements that were not used for ventilation age (or b-P age) calculations. However, note that present water DIC measurements can not be transferred directly deduce to reservoir/ventilation ages, due to influence of anthropogenic ("bomb-derived") carbon injected into the atmosphere through nuclear testing in the 1950s (Reimer et al., 2009a).

We used a regional reservoir age correction (ΔR) value of 500 yr ± 50 yr, in line with published correction values for the modern Okhotsk Sea (Kuzmin et al., 2007a). The ΔR values used here potentially changed over the time interval studied (Gebhardt et al., 2008; Sarnthein et al., 2007). However, we are at present unable to constrain such changes for the Okhotsk Sea. The low amount of foraminifera in our samples does, unfortunately, not allow to follow the approach of tuning our sedimentary records to major radiocarbon plateaus as used by other studies (Sarnthein et al., 2007; Sarnthein et al., 2006a). In addition, the application of this technique (and thus also the application of variable reservoir ages derived from its use) meets its own specific set of challenges and limitations that are currently under intense debate (cf. supplementary online discussions in Sarnthein et al., 2013; Skinner, 2008). We thus kept the ΔR values constant over the entire age range used in this thesis. This is in line with reasoning by the original authors of the plateau-tuning technique in that the local reservoir ages in the North Pacific marginal seas have not necessarily been similar to the values in the

open North Pacific (M. Sarnthein, pers. communication and Sarnthein et al., 2007). We set an additional offset for the ventilation age (when we had to use benthic values) of 360 ^{14}C years, based on our own measured benthic-planktic age differences from the same depth interval in shallower cores LV28-4-4 and SO178-13-6 and supported by measurements of ^{14}C of Dissolved Inorganic Carbon (DIC) on water samples from the Sakhalin margin (Fig. 4.1). In deeper core LV29-79-3 the ventilation age value was corrected by an additional 500 ^{14}C years based on published values for the same time interval from corresponding water depths (Gorbarenko et al., 2007a; Gorbarenko et al., 2010b). All AMS ^{14}C dating results that are reported in the results' chapters of this thesis are summarised in table 4.1 at the end of this chapter.

4.3. Age – Depth Model Approach

For developing age–depth relationships between the AMS ^{14}C age control points one can use simple linear interpolation. While this technique robustly avoids artefacts in curve-fitting, the depth-age relationship is in most cases inferior in error regression to higher–order fitting techniques, and results in abrupt sedimentation rates changes at the age control points that are an unlikely, artificial rendering of the actual sedimentation regime (Blaauw, 2012; Blockley et al., 2007; Telford et al., 2004). In addition, a decision has to be made by the researcher through which exact age of the calibrated age distribution this age-depth relationship shall be fit. This decision is often based on arbitrary assumptions, like simply choosing the mean or median value of the 1 sigma error range of the calibrated age distribution for every used age(Blaauw, 2012; Telford et al., 2004). In reality this leads to a statistically (and real) "false" or "too good" precision in constructed age models, which by these methods a priori discard up to one third of the possible curve fitting points fro a given age determination.

To overcome this problem, I used the "CLAMS" routine specifically conceived and programmed for developing age models with a high degree of statistical confidence and highly adaptable various interpolation and smoothing modes (Blaauw, 2010), with linear interpolation being one of them as basic feature for checking the plausibility of derived more complex curve fits. CLAMS is a script run in the "R" language environment that provides standard open source software, and is especially suited for statistical and graphic analyses (available from: http://www.r-project-org, last accessed 25 February 2013). Briefly, CLAMS runs (based on a number of user-defined boundary conditions) a high number of different age models in an iterative mode (Monte Carlo Simulation) with all age datings (AMS ^{14}C, but others can be included, like e.g. tephra layers). The software routine calibrates pre-defined ^{14}C ages of a core with highly flexible user-defined boundary conditions (errors in depth

and time, calibration curve, reservoir ages, hiatuses, etc). Based on these calibrations, it runs a pre-defined number of statistically possible solutions to fitting a regression line through all potential ages, within the respective chosen 1 or 2 σ (68 or 95% confidence intervals) of all AMS ^{14}C ages for a given core. The most plausible age-depth model based on a regression analysis and error minimization is finally provided as result, yielding discrete "best" ages for each cm-sample of a core, together with the 95% confidence interval for each age-depth point and sedimentation rate. The combined output for statistical and quality control data help the user to try out, and decide on final age-depth fits.

While this routine does not reach the sophistication of more precise full bayesian or wiggle-matching analyses, mainly due to lacking a sufficient number of dated samples (Blaauw, 2010; Blaauw and Andres Christen, 2011), I regard it as a good compromise between constraints on analytical efforts (maximum possible number of AMS ^{14}C samples) and a relatively high level of confidence in the resulting age-depth model. As an advantage it provides the user with a number of different fitting algorithms (see. Fig. 4.2 for a comparison of different curve fits on a part of core LV29-79-3)

In the case of primarily ^{14}C-dated cores LV28-4-4, LV29-79-3 and SO178-13-6, a series of test runs was carried out for each core with 1,000 iterations. Each core was initially fit with linear interpolation as baseline against which to perform higher order curve fitting procedures. Linear interpolation is widely used and was also applied to the models presented in Chapter 9. In difference to those age models I also preferred to use 2 σ confidence intervals to better cover (95 %) of statistically plausible age distributions and used the marine calibration curve. The aforementioned use of $\Delta R = 500 \pm 50$ yr with MARINE09 in this thesis and Chapters 5 and 6 does not differ significantly from the R = 900 yr with INTCAL09 approach as used in Chapter 9 (Max et al., 2012a), thus ensuring compatibility between the two approaches. To each core the following regression fits were applied after the linear fits: a set of (1) higher polynomial fits, (2) locally weighted spline, and (2) smooth spline functions, each with various smoothing factors (Blaauw, 2010). Comparisons between results and the resulting confidence intervals led to my decision to use smooth spline functions with a 0.3 smoothing factor for all three cores for consistency, though the manual splicing of higher order polynomial fits in the case of core LV29-79-3 would lead to equally plausible age–depth relationships between control points (not shown here). All cores were then subjected to 10,000x iteration runs to derive final age-depth models with age calculation in 1 cm increments.

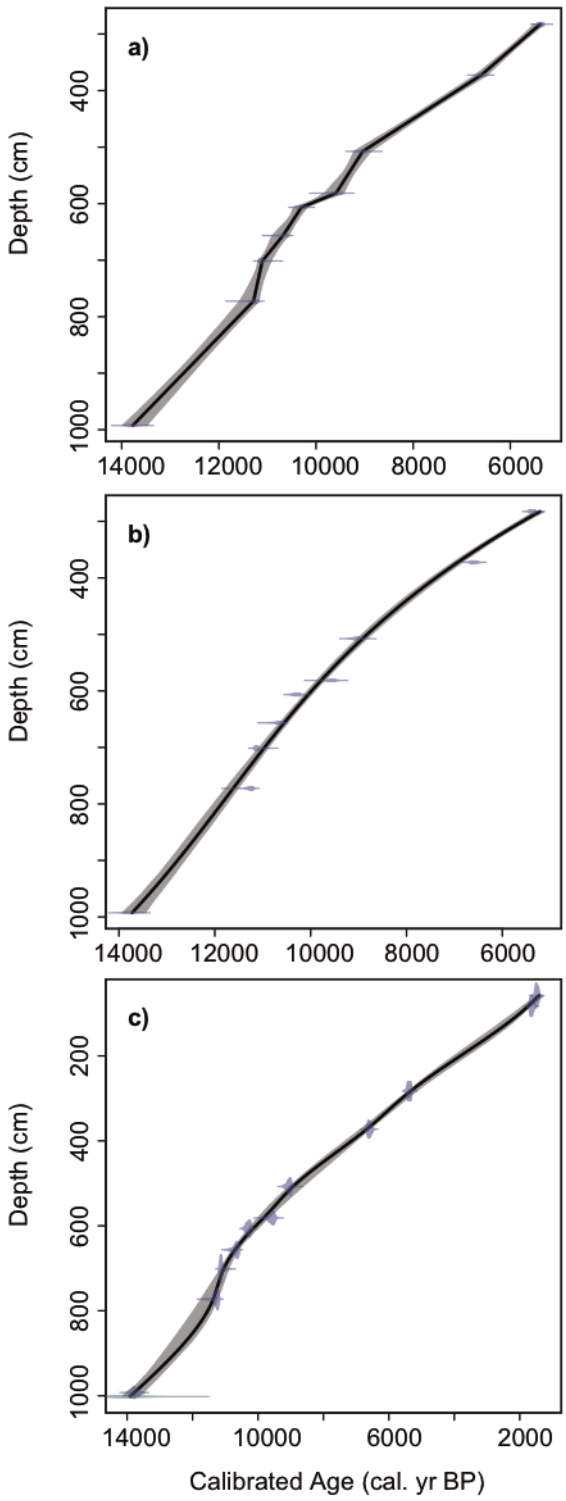

Figure 4.2: Age model examples for core LV29-79-3, graphic output of different age-depth fits through the 2 σ age ranges with different curve fits. Grey areas show the 95 % confidence intervals for each 1 cm-step along the age-depth relationship. a) lower core part (500-1000cm) with linear interpolation. b) same depth interval with 5th order polynomial fit through 2 σ ranges. c) entire core with smooth spline fit, while fit in upper part is sufficient, lower part is better matched by fit shown in b).

These initial, independent age models were then subjected to plausibility tests by inter-core correlations based on measured chlorin concentrations (see following chapter). Correlation patterns were then used to transfer AMS ^{14}C ages from core LV29-79-3 to core SO178-13-6 in the Holocene interval, while for the deglacial part no further dates were added. The resulting compilation of ^{14}C ages for core SO178-13-6 was then subjected to a final series of CLAMS runs, and the final age model based on 10,000 iterations and a smooth spine fit (0.3 smoothing factor) is used for the core (see Fig. 4.4). In the case of LV28-4-4, no transfer of ages and was deemed necessary.

The final age models for the three cores LV28-4-4, LV29-79-3 and SO178-13-6 are shown in the subsequent chapter 5 of this thesis (see Fig. 5.3) and are thus not repeated here.

4.4. Inter-Core Correlation Approach

The AMS ^{14}C dates derived from planktic foraminifera constitute the primary age control points in the age models presented in this thesis. In addition to these AMS ^{14}C dates, I used lithostratigraphic tie points (Biebow et al., 2000; Botsul et al., 2002; Dullo et al., 2004) and cross-correlation of selected proxy records for inter-core correlations between the cores LV29-79-3, LV29-78-3, LV28-4-4 and SO178-13-6. I developed the common stratigraphic framework for the deglaciation and Holocene part of the cores with the following steps involved: After initial calibration of all planktic and benthic AMS ^{14}C ages based on reported reservoir ages and the MARINE09 calibration curve, I used chlorin concentrations to correlate distinct patterns between cores SO178-13-6, LV29-79-3, LV29-78-3 and LV28-4-4 (Fig. 4.3). As a first order approximation, significant changes in surface/export production over time should be recorded in proximal cores with potentially different amplitude but at the same time interval, within the accuracy of the age model. Rather than correlating the cores against each other into a composite age/depth scale, I preferred to identify structural characteristics in the curves and used those to transfer ^{14}C age control points to the respective other cores to consolidate individual cores with additional age control points. Cores LV29-79 and LV28-4-4 had a sufficient numbers of original age control points and thus no ages were transferred to these cores.

In the case of LV28-78-3, which has no independent ^{14}C dates on its own, I correlated the core to LV29-79-3, based on the chlorin content and directly transferred the latter's age scale received from the CLAMS routine to LV29-78-3, resulting in a ^{14}C-based age model for LV29-78-3. As a starting point to this correlation between LV29-78-3 and LV29-79-3, the initial lithostratigraphy derived from shipboard measurements of color scans and changes in lithology and sediment composition was used (Botsul et al., 2002). Thereafter, core LV29-78-3 on the age scale of LV29-79-3 was cross-correlated to southerly core LV28-4-4 with an independent age scale.

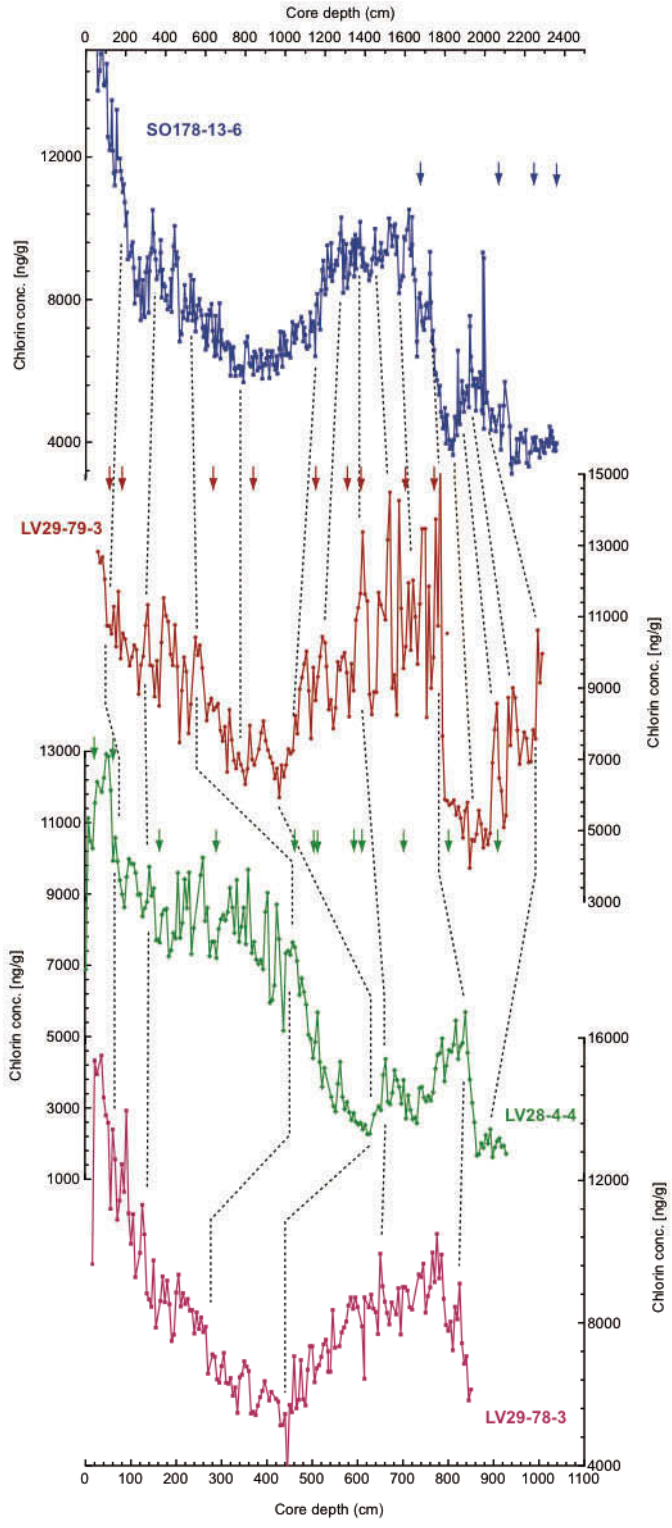

Figure 4.3: Inter-core correlation via chlorin contents between (from top to bottom): SO178-13-6 (blue), LV2979-3 (red), LV28-4-4 (green), and LV29-78-3 (pink) plotted against core depts. Stippled lines indicate correlations between chlorin series and arrows in the core colors the AMS ^{14}C age control points for each core.

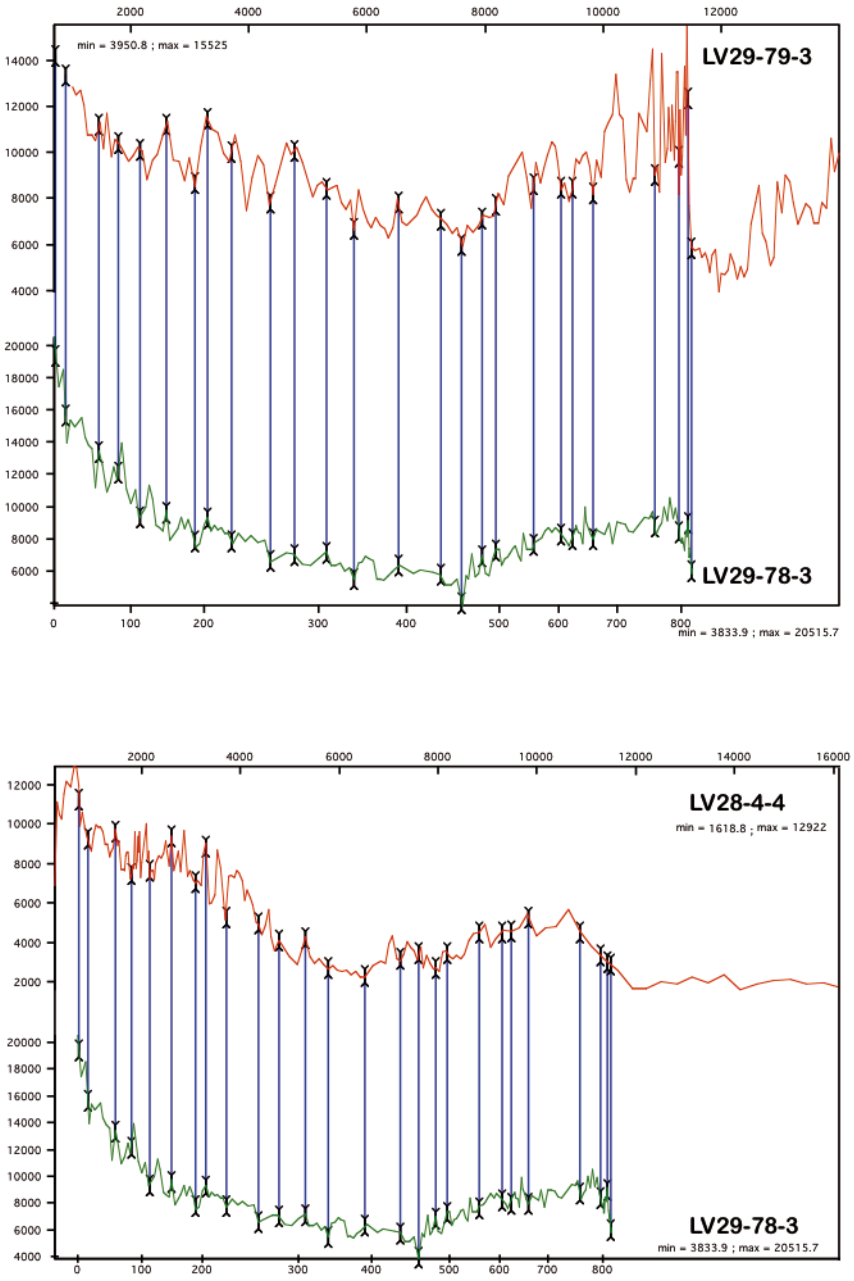

Figure 4.4: Illustration of work steps in age-depth model development for gravity core LV28-78-3 based on chlorin concentrations. Upper panel shows correlation between LV28-78-3 core depth and AMS ^{14}C age scale of core LV29-79-3. Lower graph shows the initial fitting of LV28-78-3 core depth to AMS ^{14}C age scale of core LV28-4-4. Steps were repeated with derived age scales for LV28-78-3 until minimal offsets were achieved between using both reference cores' age scales. Final tie points and correlation maps for LV29-78-3 are available in the online data collection stored in the PANGAEA database.

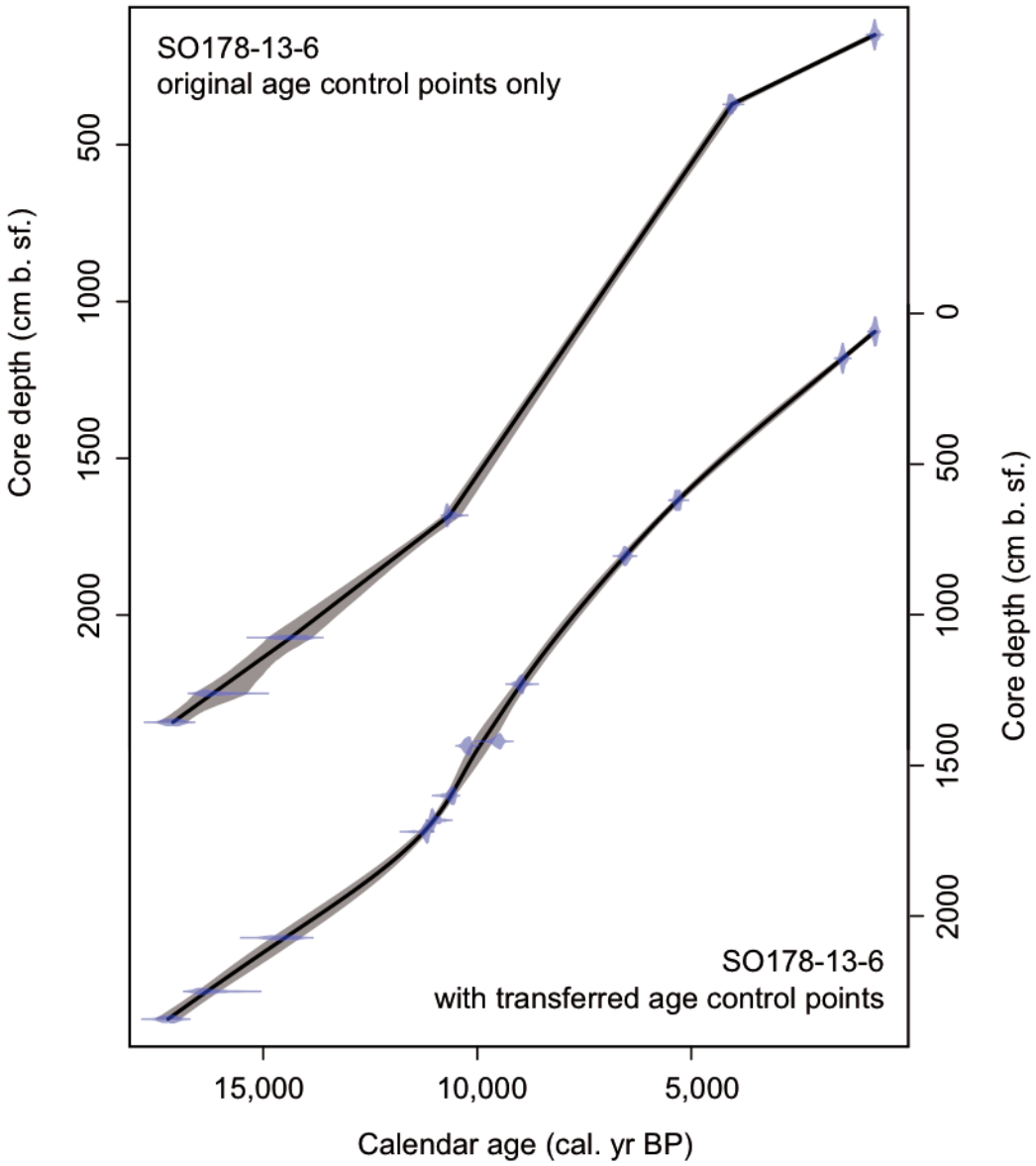

Figure 4.5: Age-depth model development for piston core SO178-13-6. Upper panel shows the linear fit through the age control points based on CLAMS run with AMS ^{14}C ages of SO178-13-6 only. Note that in the upper panel a mollusk-based age at 371 cm is included that was later discarded. Lower graph shows the combined age control points fro SO178-13-6, based on transfer of ^{14}C dates from LV29-79-3 to SO178-13-6 with a smooth spline fit. Black lines denote the "best fit", grey areas are the 95 % confidence intervals, blue probability distributions are the individual age control points with their calibration-based distribution likeliness with 95 % confidence intervals. Tie points and correlation maps for SO178-13-6 are available in the online data collection stored in the PANGAEA database (cf. chapter 3).

This was done especially for the upper part of the core, as LV28-4-4 has a better temporal resolution in the late Holocene and features a modern sediment surface, whereas the upper c. 800 years in core LV29-79-3 are missing (cf. Fig. 4.3). Another aim was to achieve a consistent age framework for all three cores within their respective error envelopes of individual age models' uncertainties. The resulting modified combined "28-4/79-3" age scale was finally cross-checked again with LV29-79-3 as closest neighboring reference core and used as age-depth model for LV29-78-3 (see Fig. 4.4).

Piston core SO178-13-6 was correlated to closely nearby core LV29-79-3 on their respective depth scales (Fig. 4.3). Individual chlorin peak patterns were matched and checked for plausibility with both cores ^{14}C ages in these sections. As a result, eight ^{14}C ages were transferred from LV29-79-3 to the depth scale of SO178-13-6 and incorporated into the age control point set, on which CLAMS was run (Fig. 4.4)

Table 4.1: AMS ^{14}C samples used in this study in Chapters 5 and 6. Additional AMS ^{14}C samples used in Bering Sea stratigraphies are reported in Chapter 8 and 9.

sample ID	depth[1] (cm)	species	weight C (mg)	PMC[2] (corr.)	PMC ±	^{14}C age (^{14}C yr)	dev. +/-	δ^{13}C (‰)	δ^{13}C st. d. (‰)	ΔR (14C yr)[3]	Age 1σ range (cal. yr BP)	Age 2σ range (cal. yr BP)
LV29-79-3												
KIA 21954	57.5	N. p. (s)	0.5	73.87	0.29	2435	30			500	1400-1550	1340-1630
KIA 20964	82.5	N. p. (s)	0.4	72.62	0.31	2570	35	-8.65	0.12	500	1560-1710	1500-1810
KIA 22449	152.5	Mollusk	1.3	55.03	0.25	4800	35	-4.86	0.13	1000 (500)	3600-3880	3470-4030
KIA 21955	282.5	N. p. (s)	0.3	50.25	0.26	5530	40	-4.14	0.33	500	5310-5450	5260-5550
KIA 21956	372.5	N. p. (s)	0.4	43.61	0.28	6665	50	-4.36	0.21	500	6510-6680	6430-6770
KIA 22450	507.5	N. p. (s)	0.3	32.93	0.23	8925	55	-5.05	0.07	500	8940-9150	8790-9260
KIA 21957	581.5	N. p. (s)	0.4	31.02	0.30	9400	80	-5.46	0.15	500	9460-9680	9390-9870
KIA 20965	606.5	N. p. (s)	0.7	29.02	0.20	9940	55	-1.83	0.14	500	10210-10380	10160-10480
KIA 21958	656.5	N. p. (s)	1.1	27.73	0.18	10305	50	-0.20	0.07	500	10560-10770	10520-11000
KIA 21959	701.5	N. p. (s)	1.1	26.74	0.16	10595	50	-0.06	0.09	500	11040-11200	10810-11230
KIA 20966	772.5	N. p. (s)	0.7	26.14	0.21	10780	60	-1.53	0.31	500	11180-11360	11140-11630
KIA 21960	992.5	Mollusk	0.2	19.02	0.21	13330	90	-8.90	0.42	1000 (500)	13470-13970	13270-14520
KIA 22448	48.5	Mollusk	0.9	22.80	0.19	11880	70	-0.59	0.08	not used		
SO178-13-6												
KIA27536	149	Mollusk	1.6	69.15	0.27	2965	30	-5.57	0.38	1000 (500)	1390-1640	1300-1770
KIA27537	371	Mollusk	1.3	50.30	0.22	5520	35	-5.93	0.12	1000 (500)	4570-4830	4420-4970
KIA30870	1542.5	Wood	0.9	30.84	0.24	9450	60	-27.72	0.31	0	10580-10750	10520-11070
KIA30872	1682.5	N. p. & G. bul.	0.4	26.86	0.17	10560	50	-2.67	0.19	500	10940-11170	10780-11200
BETA (LM)	1682.5	benthic foram.				10830						
KIA27538	1973	Mollusk Fragm.	1.5	19.23	0.16	13240	70	1.40	0.12	1000 (500)	13420-13850	13220-14130
KIA30869	2072.5	mix planktics	0.4	18.88	0.24	13390	100	0.89	0.30	500	14230-14900	14090-15090
BETA (LM)	2072.5	benthic foram.				13760						
ICIAMS10967	2250.5	N. p. & G. bul.		17.03	0.00	14220	45			500	16160-16690	15610-16810
BETA (LM)	2250.5	benthic foram.				14580						
ICIAMS10967	2342.5	N. p. & G. bul.		15.29	0.00	15090	60			500	17080-17450	16940-17590
BETA (LM)	2342.5	benthic foram.				15470						
LV29-114-3												
UCIA	197.5	N. p. (s)	1.6	30.15	0.19	9630	50	0.12	0.18	500	10330-10500	10240-10540
KIA30863	232.5	N. p. (s)	0.9	27.18	0.17	10465	50	-0.72	0.13	500	10810-11080	10680-11130
KIA30867	272.5	N. p. (s)	1.0	21.66	0.15	12290	55	-0.47	0.16	500	13160-13310	13110-13380
KIA30865	292.5	N. p. (s)	1.3	19.39	0.15	13180	60	-0.35	0.16	500	13960-14460	13880-14880
KIA30868	317.5	N. p. (s)	0.7	16.66	0.16	14400	80	0.02	1.42	500	16660-16880	16470-16970
KIA30866	352.5	N. p. (s)	0.7	15.20	0.14	15130	80	-3.87	0.17	500	17120-17500	16970-17660
LV28-4-4												
KIA13839	*5.5*	*N. p. & G. bul.*	*0.3*	*87.56*	*0.35*	*1065*	*30*	*-4.16*	*0.05*		*130-270*	*0-300*
KIA13840	*15.5*	*Mollusk*	*1.0*	*78.20*	*0.29*	*1975*	*30*	*-4.62*	*0.05*	*1300 (800)*	*180-460*	*0-520*
KIA13841	*45.5*	*Mollusk*	*1.1*	*74.22*	*0.26*	*2395*	*30*	*4.52*	*0.12*	*1300 (800)*	*520-790*	*420-960*
KIA14648	*62.5*	*N. p. & G. bul.*	*0.3*	*80.60*	*0.30*	*1730*	*30*	*-4.03*	*0.13*	*500*	*700-840*	*670-900*
KIA16838	95.5	Wood	1.0	76.83	0.30	2120	30	-30.07	0.09			
KIA14654	*165.5*	*N. p. & G. bul.*	*0.5*	*71.87*	*0.28*	*2655*	*30*	*-0.43*	*0.07*	*500*	*1680-1830*	*1590-1890*
KIA13844	*285.5*	*N. p. & G. bul.*	*0.1*	*68.14*	*0.42*	*3080*	*50*	*-5.83*	*0.21*	*500*		
KIA13845	*465.5*	*N. p. & G. bul.*	*0.3*	*56.40*	*0.27*	*4600*	*40*	*-5.21*	*0.04*	*500*	*4050-4260*	*3960-4360*
NN[4]	*500.5*	*N. p. & G. bul.*	*0.3*	*N/A*	*N/A*	*4790*	*70*			*500*	*4280-4520*	*4150-4670*
NN[4]	*505.5*	*N. p. & G. bul.*	*0.1*	*N/A*	*N/A*	*4930*	*120*			*500*	*4450-4780*	*4230-4910*
NN[4]	*595.5*	*N. p. & G. bul.*	*0.5*	*N/A*	*N/A*	*6010*	*55*			*500*	*5790-5980*	*5710-6100*
KIA14653	*595.5*	*Mollusk*	*0.1*	*44.31*	*0.35*	*6540*	*60*	*-6.48*	*0.10*	*1000 (500)*	*5740-6120*	*5590-6270*
KIA16837	610.5	Wood	0.5	49.77	0.40	5605	65	-30.29	0.07	terrestrial	7357-7470	7300-7530
KIA16839	*610.5*	*N. p. & G. bul.*	*0.4*	*45.20*	*0.24*	*6380*	*40*	*-6.31*	*0.50*	*500*	*6220-6380*	*6120-6480*
NN[4]	*700.5*	*N. p. & G. bul.*	*0.5*	*N/A*	*N/A*	*7640*	*70*			*500*	*7530-7690*	*7450-7790*
KIA14346	*715.5*	*Mollusk*	*0.1*	*35.02*	*0.42*	*8430*	*100*	*-0.96*	*0.23*	*1000 (500)*	*7700-8050*	*7570-8260*
KIA13846	*800.5*	*N. p. & G. bul.*	*0.6*	*32.00*	*0.21*	*9155*	*55*	*-3.76*	*0.11*	*500*	*9250-9430*	*9120-9480*
KIA13842	*850.5*	*Mollusk*	*1.4*	*25.33*	*0.18*	*11030*	*55*	*-2.77*	*0.06*	*1000 (500)*	*10670-11200*	*10490-11640*
KIA14347	*885.5*	*Mollusk*	*0.2*	*20.11*	*0.21*	*12890*	*80*	*0.33*	*0.22*	*1000 (500)*	*13120-13590*	*12890-13780*
NN[4]	*900.5*	*Mollusk*	*0.6*	*18.45*	*0.18*	*13580*	*80*	*-3.98*	*0.26*	*1000 (500)*	*13750-14500*	*13500-15030*
KIA20305	910.5	N. p. & G. bul.	0.2	17.85	0.20	13840	90	-14.41	0.52	500	15140-15870	15040-16320
KIA14348	*925.5*	*Gastropod*	*0.2*	*16.85*	*0.29*	*14310*	*140*	*-0.94*	*0.08*	*1000 (500)*	*15030-16200*	*14270-16640*
Water Samples (depth is water depth in m)												
KIA10312	*297*	*water DIC*	*1.3*	*95.92*	*0.31*	***335***	*25*	*0.85*	*0.04*		*GE99-16-1*	
KIA10313	*685*	*water DIC*	*0.5*	*89.18*	*0.64*	***920***	*55*	*-43.17*	*0.25*		*GE99-24-1*	
KIA10314	*1544*	*water DIC*	*1.4*	*79.41*	*0.28*	***1850***	*30*				*GE99-31-1*	
KIA10315	*495*	*water DIC*	*1.4*	*92.61*	*0.28*	***615***	*25*	*-0.01*	*0.06*		*GE99-31-1*	
KIA10316	*11*	*water DIC*	*1.2*	*97.96*	*0.28*	***165***	*25*	*3.44*	*0.07*		*CTD41-1*	

Samples in italics were provided by Ralf Tiedemann and measured during KOMEX Phase I, cf. Kaiser (2002)

[1] core or sample depth in sediment

[2] PMC is percent modern carbon according to conventions of Stuiver and Polach (1977)

[3] Local reservoir ages were used in calibration with assigned errors of ±50 14C yr for planktic and ±100/±200 for benthic organisms, respectively.

[4] Samples provided by R. Tiedemann, KIA numbers for these samples in GEOMAR archive

5. Deglacial Variability in Okhotsk Sea Intermediate Water Ventilation and Biogeochemistry: Implications for North Pacific Nutrient Supply and Productivity

Lester Lembke-Jene[1]*, Ralf Tiedemann[1], Dirk Nürnberg[2], Ulla Kokfelt[3], Reinhard Kozdon[4], Lars Max[1], Ursula Röhl[5], Sergey A. Gorbarenko[6]

Manuscript for submission to "Quaternary Science Reviews"

* Corresponding Author: lester.lembke-jene@awi.de

1 Alfred Wegener Institute, Helmholtz Centre for Polar and Marine Research, Am Alten Hafen 26, 27568 Bremerhaven (lester.lembke-jene@awi.de, ralf.tiedemann@awi.de, lars.max@awi.de)

2 GEOMAR Helmholtz Centre for Ocean Research, Am Seefischmarkt 1-3, 24148 Kiel (dnuernberg@geomar.de)

3 University of Copenhagen, Øster Voldgade 10, 1350 København (uk@geo.ku.dk)

4 University of Wisconsin, Madison (rkozdon@geology.wisc.edu)

5 MARUM Center for Marine Environmental Sciences, University of Bremen

6 V.I. Il'ichev Pacific Oceanological Institute FEB-RAS, Baltijskaja Str. 43, RU-690041, Vladivostok, Russia (gorbarenko@poi.dvo.ru)

5.1. Abstract

The modern North Pacific plays a critical role in marine biogeochemical cycles, as it is today the largest natural oceanic sink of CO_2 and harbors some of the most biologically productive and least oxygenated regions of the World Ocean. This capacity to sequester CO_2 is limited by variations in the region's biological productivity, and the efficient utilization of preformed nutrients supplied to the upper mixed layer, particularly in the Pacific's subarctic latitudes and marginal seas. Changes in the oxygenation of deeper water masses, on the other hand, are influenced by the remineralization of the settling organic matter through the water column. Today, the entire North Pacific is only weakly ventilated by North Pacific Intermediate Water (NPIW), which receives its relatively higher oxygen concentrations largely from a precursor, the Okhotsk Sea Intermediate Water (OSIW). Past ventilation patterns of OSIW likely have changed profoundly on millennial timescales, making this water mass a prime candidate for shaping variations in deglacial circum-Pacific Oxygen Minimum Zones and reported peaks in biogenic productivity, but their paleoceanographic history over the last glacial termination is not well understood.

We here present a comprehensive multi-proxy-based reconstruction of Okhotsk Sea Intermediate Water ventilation and productivity variations over the last glacial termination. Our results are based on a set of high-resolution AMS ^{14}C-dated sediment cores that were retrieved directly from the source region of modern OSIW formation. Benthic-planktic ^{14}C ages and epibenthic stable carbon isotopes show decreases in OSIW oxygenation during deglacial warm phases from c. 14.7 to 13 ka (Bølling-Allerød) and c. 11.4 to 9 ka (Preboreal), but no concomitant decreases in ventilation ages. We thus attribute these oxygenation decreases mainly to rapid, significantly enhanced organic matter remineralization within OSIW, in line with multi-proxy evidence for maxima in primary productivity and increased supply of organic matter to the mid-depth water column. Sedimentary C/N ratios and elemental analyses indicate that lateral entrainment of nutrients into OSIW was also higher during these periods and thus increased the overall nutrient load of the OSIW.

Correlation of palynological and sedimentological evidence from our sites with hinterland reference records suggests that millennial-scale changes in fluvial freshwater runoff from the Amur were a primary driver of these significant changes in OSIW oxygen and nutrient concentrations. These runoff changes were most likely linked to a northward propagation of the East Asian Summer Monsoon System that increased precipitation and the postglacial melting of permafrost soils in the Siberian hinterland. During the early, Pre-Bølling deglacial phase provision and entrainment of nutrients into

OSIW was limited, potentially due to the flooding of still frozen permafrost on continental shelves by deglacial sea-level rise.

We hypothesize that correlation of the observed ventilation minima with maxima in nutrient utilization in the open North Pacific implies an increased OSIW-sourced mid-depth lateral supply of micronutrients, silicate and organic matter into distant oceanic regions, analog to modern ocean conditions. By invoking such export from marginal seas, the upper ocean open North Pacific was partially relieved from Fe-limiting conditions by upwelling the mid-depth nutrient-enriched OSIW during wintertime mixing. Such a mechanism would have made the subarctic North Pacific a transient, more efficient CO_2 sink during the B/A and PB and contributed to temporary slowing of the deglacial CO_2 rise. Reconstructed minima in mid-depth oxygen content, on the other hand, provide a reinforcing mechanism for the intermediate-depth circum-Pacific intensification of Oxygen Minimum Zones during the last glacial termination.

5.2. Introduction

Today, the subarctic North Pacific represents the endpoint of the global Meridional Overturning Circulation. No new deepwater is formed there, because the surface water masses are not dense enough to sink to significant water depths and initiate convection due to the presence of low surface salinities and the development of a strong halocline (Emile-Geay et al., 2003; Warren, 1983). Accordingly, the deep North Pacific is weakly ventilated and carries high concentrations of macronutrients, in particular nitrate and phosphate. In contrast, the intermediate-depth level is characterized by a relatively fresh and oxygen-enriched layer of North Pacific Intermediate Water (NPIW, Kitani, 1973; Reid, 1965; Talley, 1993). NPIW is today largely supplied with O_2 through a ventilated precursor water mass, the Okhotsk Sea Intermediate Water (OSIW, Watanabe and Wakatsuchi, 1998). Modern NPIW and OSIW are highly variable in their biogeochemical characteristics even on relatively short instrumental timescales (Emerson et al., 2004; Tadokoro et al., 2009), and keep mid-depth waters in the North Pacific moderately oxygenated.

While the North Pacific is overall the largest modern oceanic regional sink for atmospheric CO_2 (Takahashi et al., 2009), in the Western Subarctic North Pacific (WSNP) the surface utilization of nutrients by primary producers and thus export production of carbon (the “biological pump”) remains incomplete, mainly due to the rapid seasonal depletion of iron (Fe) as micronutrient, (see review by Takeda, 2011) and silicate (Si(OH)4 Harrison et al., 2004). On glacial-interglacial timescales export production and the degree of surface nutrient utilization (as evidenced by studies of $\delta^{15}N$) are anti-correlated, implying more effective use of available nutrients during glacial periods (e.g. Galbraith et

al., 2008; Jaccard et al., 2005). This more effective utilization allowed a lower primary production to export carbon form the surface into the deep ocean more efficiently. Thus, indicators for export production varied in phase with atmospheric CO2 concentrations for at least the last 800 ka (Jaccard et al., 2010).

However, on shorter, millennial timescales this relatively straightforward relationship does not hold. During the last glacial termination the relationship between surface nutrient utilization and export production becomes decoupled in the WSNP (Brunelle et al., 2010b; Kohfeld and Chase, 2011). In the early deglacial phase, or cold Heinrich Stadial 1 (HS-1 hereafter, c. 17.5-15 ka), nutrient utilization decreased without concomitant increases in export production, followed by widespread, extraordinary productivity peaks during the warm Bølling-Allerød interstadial that are characterized by more effective nutrient utilization, contrary to glacial-interglacial patterns (Kohfeld and Chase, 2011). Such millennial-scale patterns call for additional mechanisms that determine the nutrient provision to the upper mixed layer and their biological utilization. Likely candidates are changes in the supply ratio of nitrogen (N, macronutrients) relative to bio-available iron (Fe, micronutrients) to the upper mixed layer (Brunelle et al., 2010b; Kienast et al., 2004; Kohfeld and Chase, 2011). However, the underlying causes and processes for such variations remain unexplained.

In line with these deglacial changes in nutrient supply and utilization, the North Pacific at that time underwent drastic and rapid changes in circulation and ventilation (Ahagon et al., 2003b; Duplessy et al., 1989a; Okazaki et al., 2010a). These variations are closely linked to fundamental and rapid changes in the utilization of nutrients (e.g. Brunelle et al., 2010b; Kienast et al., 2004) and, more generally, in surface and deep biogeochemistry (Crusius et al., 2004; Galbraith et al., 2007; Gebhardt et al., 2008). For cold HS-1, widespread convection and the increased formation of new intermediate–deep water masses (down to 2800 m water depth) has been proposed for the North Pacific (Okazaki et al., 2010a), although newer evidence based both on model results (Chikamoto et al., 2011) and data directly from deepwater sites (Jaccard and Galbraith, 2013) alternatively suggest that a potential Pacific overturning cell did not extend beyond about 1300-1400 m water depth.

This early deglacial episode of better ventilation is sharply contrasted by a subsequent oxygen decreases in intermediate water depths and the deposition of laminated sediments along wide swaths of the open North American Pacific coast (Dean et al., 2006; Van Geen et al., 2003; Zheng et al., 2000), in the Bering Sea (Cook et al., 2005a; Itaki et al., 2012), and on the western Pacific margin off Japan (Ikehara et al., 2006; Sagawa and Ikehara, 2008a) during the Bølling-Allerød (B/A hereafter, 14.7-12.9 kyr BP) and during the earliest Holocene (for recent global summary see Jaccard and Galbraith 2011). In the pelagic abyssal North Pacific, no OMZs develop during this time (Jaccard and

Galbraith, 2011; Jaccard et al., 2009) and no mid-depth open ocean sites to gain knowledge exist, unfortunately, but massive primary productivity peaks do occur during the B/A and early Holocene (Crusius et al., 2004; Galbraith et al., 2007; Gebhardt et al., 2008; Keigwin et al., 1992a). To explain the unusually severe and widespread O_2-depletion of intermediate waters during the Bølling-Allerød and Preboreal increases in export production have been invoked (Davies et al., 2011; McKay et al., 2004; Mix et al., 1999). Alternatively, reduced or ceased ventilation of North Pacific Intermediate Water (NPIW) can constitute another mechanism for decreased O_2 concentrations across the North Pacific. (e.g. Duplessy et al., 1989a; Keigwin et al., 1992a; Zheng et al., 2000). Crusius et al. (2004) proposed that increases in biological productivity in the northwestern Pacific cause a decrease in mid-depth O_2 concentrations of initially well-ventilated NPIW along its pathway across the Pacific before it reaches North American margins by increased respiration of organic matter (OM).

Previous works from the Okhotsk Sea have shown that mixed layer stratification, sea ice action and export production varied on millennial timescales during the deglaciation. This implies that variations were caused by changes in a number of factors, such as surface salinity through freshwater runoff, increases in nutrient supply through flooding of continental shelf areas and river discharge and changes in seasonal availability of light (Gorbarenko et al., 2007a; Gorbarenko et al., 2008; Gorbarenko et al., 2012; Harada et al., 2008; Harada et al., 2012; Riethdorf et al., 2013). However, almost all information used to infer changes in NPIW ventilation stems from locations that are distant to the source regions of modern NPIW formation or are based on indirect, qualitative evidence. Thus, high-resolution records directly from the ventilation source regions of NPIW are needed to discern between principal processes responsible for the widespread occurrence of anoxia along North Pacific continental margins during the deglaciation (Hendy and Kennett, 2003; Jaccard and Galbraith, 2011).

To address this issue, we analyzed a suite of high-resolution sediment cores directly from the main ventilation region of modern OSIW on the continental margin of Sakhalin island in the Okhotsk Sea. We assess changes of ventilation and export production within this most important modern NPIW ventilation source region and compare results with earlier data that showed millennial-scale variations in ventilation and nutrient utilization during the last glacial termination (18,000 to 8,000 cal. yr BP). We constrain likely causes for the observed rapid changes in OSIW/NPIW ventilation and productivity patterns and assess their potential consequences for open-ocean WSNP nutrient supply and biogeochemistry.

5.3. Setting and Modern Hydrography

North Pacific Intermediate Water (NPIW) is defined as a salinity and potential vorticity minimum and spreads between the density lines of c. σ_Θ 26.6 – 27.2 (corresponding to c. 600-800 m water depth) east- and southward across the north Pacific down to a latitude of about 20° N (Fig 2, Talley, 1993; Yasuda et al., 1996). Because water masses with these densities are at present not outcropping on the surface in the open North Pacific, NPIW is thought to be ventilated by one of its main precursor water mass, the Okhotsk Sea Intermediate Water (OSIW) through largely diapycnal mixing processes (Kitani, 1973; Shimizu et al., 2004).

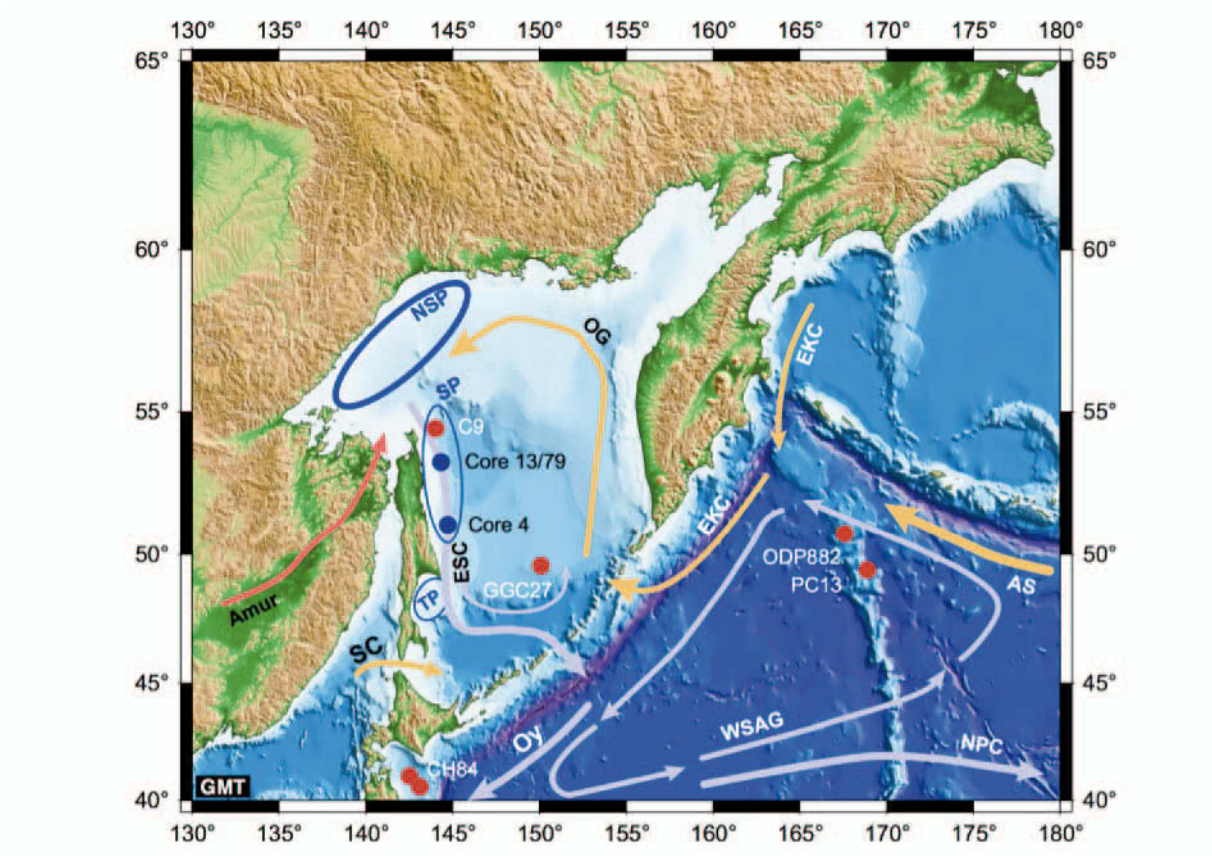

Figure 5.1: Map of the NW Pacific study area. Core locations of this study marked as blue circles see table X for details), core locations of other studies used here as red filled circles. Major regional currents are outlined as arrows (yellow = relatively warmer, light blue = relatively colder) and abbreviated: Alaskan Stream (AS), East Kamchatka Current (EKC), Okhotsk Gyre (OG), Soya Warm Current (SC); East Sakhalin Current (ESC), Oyashio (Oy), Western Subarctic Gyre (WSAG) North Pacific Current (NPC). Red arrow indicates freshwater outflow by Amur into the NE Okhotsk Sea. The blue bold ellipse shows the major modern, recurring Northern Shelf Polynia (NSP) system; the smaller ellipses denote secondary systems: Sakhalin Polynia (SP), Terpeniya Bay Polynia (TBP).

While OSIW itself is a mixture of water masses and formed in the southern part of the Okhotsk Sea, the principal origin for its high O_2 and particle content is Dense Shelf Water (DSW). At present, relatively warm Western Subarctic Pacific Water is transported in the East Kamchatka Current southward as part of the larger Western Subarctic Pacific Gyre and enters the Okhotsk Sea mainly via Kruzensthern Strait and Bussol' Strait. WSAP then flows within the main cyclonic Okhotsk Gyre to the shallow northeastern shelf areas. There, DSW is formed mainly during the sea ice season in autumn and wintertime north of Sakhalin by brine rejection in large persistently recurring polynias (Fukamachi et al., 2009; Shcherbina et al., 2004a) and is characterized by relatively low salinity, very low temperatures and high O_2 content. The newly formed DSW is subsequently entrained into deeper water layers in the highly dynamic region along the N' Sakhalin margin by vertical tidal and diapycnal mixing and transported by the East Sakhalin Current (ESC) (Shcherbina et al., 2004a). It finally enters as OSIW the open North Pacific through deep passages (mainly Bussol' Strait) between the Kuril Islands and is transported with the Oyashio Western Boundary Current into the Mixed Water Region and the Western Pacific Subarctic Gyre circulation (Fig. 1). This well ventilated, cold, low salinity OSIW (relative to NPIW) and the subsequent export of this water mass into the open North pacific is critical for maintaining sufficiently high O_2 levels in the intermediate water layer of the extra-tropical North Pacific. Below the layer of OSIW, the Okhotsk Sea has a weakly developed Oxygen Minimum Zone today along the Sakhalin margin between ca. 1,000 and 1,400 m (Bubenshchikova et al., 2010; Nakatsuka et al., 2004a).

Not only does OSIW ventilate the intermediate-depth North Pacific, it also transports high amounts of both dissolved and particulate terrigenous matter along the Sakhalin margin into the open North Pacific within a turbid layer that has extremely high concentrations of organic carbon, lithogenic particles and suspended material (Hansell, 2002; Nakatsuka et al., 2004b). This material is entrained by vigorous tidal mixing on the northeastern shallow continental shelf into the turbid water layer and transported along the Sakhalin margin along the density surface of OSIW (Nakatsuka et al., 2004b) for long distances. The remnants of this entrainment are visible in the pelagic subarctic North Pacific as intermediate maxima in Dissolved Organic Carbon (DOC) and particulate organic carbon (POC, Goes et al., 2004; Hansell, 2002). In addition, a subsurface to intermediate-depth concentration maximum has been identified in both dissolved and particulate iron in the North Pacific (Nishioka et al., 2007; Nishioka et al., 2003). Its origin was tracked to the Okhotsk Sea, where Fe is entrained both from surface sediments by tidal currents and surface river runoff during intense mixing processes on the shallow northern shelf areas into DSW/OSIW and is transported with OSIW into the open North Pacific (Nishioka et al., 2007; Takeda, 2011).

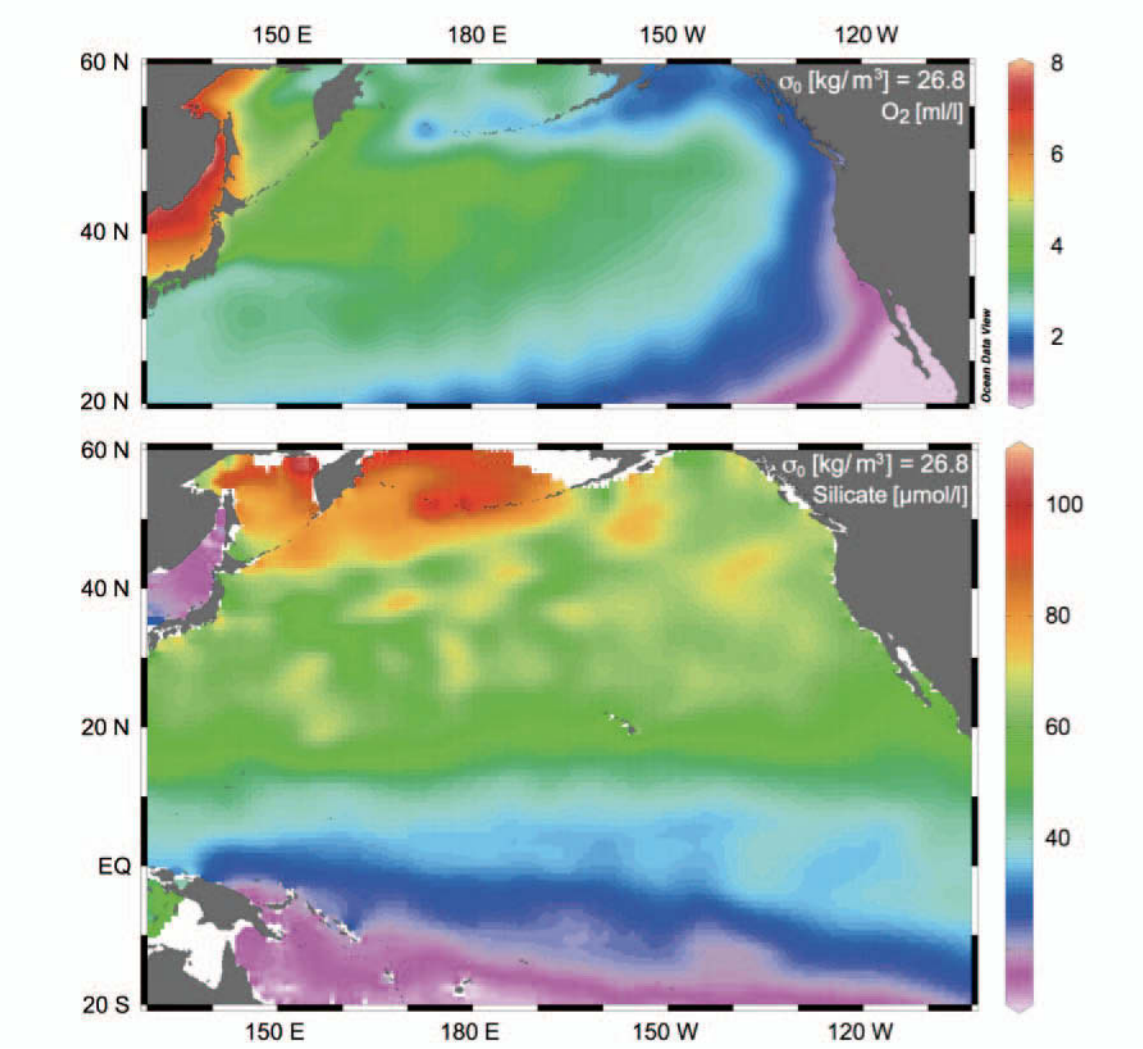

Figure 5.2: Modern lateral distribution of (a) Oxygen in µmol/l and (b) Silicate in µmol/kg according to World Ocean Atlas 2009 data (Garcia et al., 2010a, b) along the main density surface of OSIW and NPIW at σ_Θ = 26.8 kg/m^3. The software ODV (vers. 4.5.1) was used for visualization (Schlitzer, 2002).

The amount of Fe flux to the North Pacific surface water by OSIW and NPIW today is substantial. Results from time-series and modeling studies suggest that it is comparable to the modern Fe flux derived from long-range atmospheric dust transport (Nishioka et al., 2011), which has been conventionally regarded as the major delivery mechanism of Fe to the surface North Pacific to relieve micronutrient limitation (Duce and Tindale, 1991; Mahowald et al., 2005). Thus, the Okhotsk Sea also acts as a modern main source region for both micronutrients, organic matter and macronutrients to distal pelagic regions in the western North Pacific (Misumi et al., 2011; Nishioka et al., 2011; Yamashita et al., 2010). During wintertime wind-induced deep mixing both soluble and particulate Fe are transported into the subsurface and surface water layer, where they become bio-available and induce additional wintertime extensive phytoplankton blooms in this Fe-micronutrient-limited HNLC

region, effectively replenishing depleted stocks of atmospherically-derived Fe (Lam and Bishop, 2008; Misumi et al., 2011; Nishioka et al., 2011).

5.4. Materials and Methods

5.4.1. Core Locations, Sediment Properties

We use three sediment cores in this study: Gravity core LV29-79-3 (core 79 hereafter, 1082 m water depth), gravity core LV28-4-4 (core 4 hereafter, 674 m water depth and piston core SO178-13-6 (core 13 hereafter, 673 m water depth) were recovered from the northeast Sakhalin continental margin from undisturbed, continuous hemipelagic sediment sequences (Biebow and Hütten, 1999; Biebow et al., 2002b). All cores feature similar lithofacies, consisting mainly of silty clays with sand and occasional larger dropstones derived from sea ice-transported terrigenous matter. Sediment content is mostly of terrigenous origin, delivered mainly by two transport mechanisms: (1) river suspension supply via the discharge of the Amur into the NE part of the Okhotsk Sea and (2) transport by sea ice to the core locations. The ice-transported material itself is incorporated into the ice by coastal ad-freezing processes on the large shelf areas in the northern part of the Okhotsk Seas, and by wind-blown aeolian input to the ice surface (Gorbarenko et al., 2002a; Nürnberg et al., 2011; Nürnberg and Tiedemann, 2004). Details of all core locations are given in Table 1. Cores were sampled with varying resolution between 2 and 20 cm, depending on the respective sample protocols for each expedition (cf. Biebow and Hütten, 1999; Biebow et al., 2002b; Dullo and Biebow, 2004). Sediment samples were weighed, freeze-dried and subsequently washed over a 63 µm screen. Dried samples sieved into 63–150, 150-250, 500-1000, and >1000 µm fractions and weighed.

Table 5.1: Sediment cores used in this study

Stat. Nr.	Latitude N	Longitude E	water depth (m)	Recovery (cm)	Location
LV28-4-4	51°08.475	145°18.582	674	930	E Sakhalin margin
LV29-79-3	52°47.272	144°57.318	1082	1072	NE Sakhalin slope
SO178-13-6	52°43.881	144°42.647	713 (672)	2368	NE Sakhalin margin

5.4.2. AMS ^{14}C Measurements

Age control was primarily achieved through radiocarbon dating of planktic foraminifera and, in few cases, benthic fauna if the available samples did not yield enough froaminifera. For radiocarbon analyses all *N. pachyderma* (s) and *G. bulloides* were picked from the size fraction 150-250 µm. Sample size ranged between 1200 and 340 specimen. Foraminifera with diagenetic crystal overgrowth, recrystallisations or other signs of post-depositional alteration (e.g. yellowish colour) were excluded. Most radiometric dating was carried out in the Leibniz Laboratory for Radiometric Dating and Isotope Research, Kiel according to established standard workflow protocols. (Nadeau et al., 1998; Nadeau et al., 1997). Dating of two samples at a later stage was carried out by the W. M. Keck Carbon Cycle Accelerator Mass Spectrometry Laboratory at University of California, Irvine. Details about the methodology of these age determinations are provided in the online documentation of the facility, including the laboratory's written protocols as Internal Technical Reports in pdf format (http://www.ess.uci.edu/ams/, last accessed on 10 May 2013). Conventional ^{14}C ages were calculated and are reported according to Stuiver and Polach (1977a).

To better assess changes in the ventilation of intermediate water masses we supplement our stable carbon isotope results with a set of deepwater ventilation ages derived from published data and measuring planktic foraminifera and benthic organisms from the same core depths. We use raw Benthic-Planktic (or B-P) ages, expressed in ^{14}C years. This technique, while not without errors e.g. due to changing surface reservoir age changes has nonetheless been used in a number of studies in this region before successfully (e.g. Ahagon et al., 2003b; Okazaki et al., 2010a). We do not use the alternative projection age method, because one of the underlying assumptions of this method, the single-source origin of the originating water mass is violated in a region of active water formation such as in this study. The used data and their respective sources are listed in supplementary Tables S1 and S2.

5.4.3. Stable Isotope Measurements

To deduce changes in the ventilation of OSIW we use stable isotopes of benthic foraminifera and paleo-ventilation ages inferred from benthic ^{14}C age determinations. The δ^{13}C of various epibenthic *Cibicides* species is widely used as reliable and well understood proxy for the $\delta^{13}C_{\sum CO2}$ and thus ventilation properties of bottom waters (McCorkle et al., 1997). These species have an epibenthic to slightly elevated epibenthic lifestyle. In addition, this species has relatively low tolerances against longer hypoxic periods in their environment and often are absent in Oxygen Minimum Zones in the Okhotsk Sea (Bubenshchikova et al., 2008). In the Okhotsk Sea, mainly two cibicid species that are

suitable for stable isotope reconstructions have been found, *C. mundulus* and *C. lobatulus*. In this paper, we only use the former due to its more regular abundance in the samples from all three cores and to obtain species-specific timeseries. This species has been shown to reliably record ambient average bottom water $\delta^{13}C$ of the dissolved inorganic carbon (DIC) globally and in the region (McCorkle and Keigwin, 1994), even under high organic matter flux and deposition of phytodetritus layers on the sediment surface (L Lembke-Jene et al., manuscript submitted to Deep-Sea Research I). In the Okhotsk Sea, subsurface and deeper water mass $\delta^{13}C_{DIC}$ is roughly linearly correlated with water column PO_4 (Bauch et al., 2002) and O_2 content (Erlenkeuser, pers. communication), and thus allows using $\delta^{13}C_{Cib}$ as proxy for ventilation of OSIW. In addition, we measured the species *Uvigerina peregrina* as qualitative indicator for sediment oxygenation and changes in pore water O_2 concentrations as a function of organic carbon rain. Specimen for isotope analyses were picked from the 250-500 µm fraction, between one and five specimen were used for each depth interval. All specimens were inspected for preservation; only well-preserved tests with translucent and non-corroded walls were used. All tests were in addition checked for contamination by particles and debris inside the test and cleaned if needed by cracking open the tests and rinsing fragments with de-ionized water in an ultrasonic bath. All stable isotope analyses were carried out in the Paleoceanography Stable Isotope Laboratory at GEOMAR, Kiel with a Thermo Finnigan MAT 252 mass spectrometer, coupled online to an automated Kiel II AUTO CARBO carbonate preparation device. Long-time analytical precision is better than ± 0.07 ‰ for $\delta^{18}O$ and ± 0.04 ‰ for $\delta^{13}C$. Calibration was achieved via an in-house Solnhofen limestone standard and National Institute of Standards (NIST) NBS-19. Results are reported in the δ notation as per mille with reference to Vienna - Pee Dee Belemnite (‰ V-PDB Craig, 1957).

5.4.4. Productivity Proxy Records – Chlorin, TOC, $CaCO_3$, Opal

Productivity proxy analyses followed established procedures in the Sedimentology/Anorganic Geochemistry Laboratory at GEOMAR. All methods have been used before successfully on sediments from the Okhotsk Sea (cf. Nürnberg et al., 2011; Nürnberg and Tiedemann, 2004).

Chlorins were extracted with acetone under sonication and subsequent centrifugation in three consecutive steps; samples were ice-cooled after each extraction. Pigments were acidified with HCl to transform chlorophyll-a into phaeopigments. The sediment extracts were thereafter measured with a Turner TD-700 fluorometer (GAT) immediately after the third extraction, always under low light conditions to hinder decomposition. Chlorophyll-a (sigma), acidified with 2 ml HCl is used as standard. To check extractions and instrument drift an internal standard sample was measured after a

dozen measurements. Precision of the method is about ±2 % and all chlorin concentrations are reported in ng/g.

Measurements of biogenic opal concentrations followed the automated leaching method (Müller and Schneider, 1993), in which opal is extracted from the previously freeze-dried, homogenised bulk sediment with NaOH at about 85°C over c. 45 min. time. The leaching solution is continuously analyzed for dissolved silicon by molybdate-blue spectrophotometry and a mineral correction was applied (DeMaster, 1981; Nürnberg and Tiedemann, 2004). The reported long-term accuracy of the method is ±0.5 weight %, deduced from replicate and standard measurements.

A CARLO ERBA CNS analyzer (Model NA-1500) was used for measuring the carbon and nitrogen content of sediment core samples (Verardo et al., 1990). The total carbon (TC) content was measured from bulk sediment previously homogenised by milling, the Total Organic Carbon (TOC) content was measured on bulk sediment samples previously decalcified with 0.25 M HCl. The $CaCO_3$ content was calculated by subtracting the TOC from the TC value and using the formula: $CaCO_3 = 8.333 \cdot (TC-TOC)$. Long-term analytical precision is around 2%.

5.4.5. Chlorophycean Freshwater Algae

For chlorophycean freshwater algae counts, 32 samples were analysed for *Pediastrum* spp. and *Botryococcus* cf. *braunii*. One to 1.5 g bulk sediment samples were taken in 5-20 cm intervals in core LV28-4-4 (Kokfelt, 2003). Preparation included (1) 10% HCl treatment to dissolve carbonates, sieving with deisonised water through 6µm mesh, (2) 40% cold Hydrofluoric Acid and H_2O washing, (3) hot 10% KOH treatment to remove humic acids, (4) acetolysis treatment with acetic acid - anhydride mix and concentrated sulphuric acid (9:1) to remove cellulosic matter. Sediment was washed in glacial acetic acid and subsequently rinsed with H_2O. Samples were counted under a Zeiss Axiophot light microscope with phase contrast properties under 400x magnification. Total slides were counted to prevent effects of fractionated grain distribution in the slide, and between 229 and 529 (avg. 437) pollen grains were counted in each sample. For algae concentrations the freeze-dried sediments were spiked with *Lycopodium clavatum* tablets and calculation followed:

$$C = (X(spike) / X(sample) * k) / m,$$

where X(spike) was the number of *Lycopodium clavatum* spores added to sediment, X(sample) the number of added *Lycopodium clavatum* spores counted, k is the number of the counted palynomorphs in the sample, and m the weight of freeze-dried sediment in gram.

5.4.6. Bulk Elemental XRF Scanning

We used XRF scanning to determine bulk sedimentary geochemistry with high resolution. Cores were measured on the CORTEX and AVAATECH XRF scanners of the IODP Bremen Core Repository (Jansen et al., 1998; Röhl and Abrams, 2000; Weltje and Tjallingii, 2008) at 1 cm scanning steps. All details of both scanner setups as used during our measurements have been described previously (Richter et al., 2006; Röhl and Abrams, 2000; Tjallingii, 2006; Weltje and Tjallingii, 2008). On the CORTEX system a single run with 10 KV was used for cores LV28-4-4 and LV29-79-3, the AVAATECH scanner was used on core SO178-13-6 with dual runs on 10 KV and 50KV. Here, we use data from XRF-scans as qualitative indicators or relative concentrations in the form of count ratios. However, quantification and inter-calibration of XRF relative scanning intensities was obtained by measuring a set of representative discrete sediment core samples taken at count minima and maxima (cf. Weltje and Tjallingii, 2008) from core LV28-4-4 and LV28-108-5 (Biebow et al., 2002b) on an X'Unique XRF spectrometer with Rh tube housed at GEOMAR (D. Rau, per. communication). All reported elements were inspected if they followed a linear regression between discretely sampled and XRF-scanned samples, all showed excellent correlation with R^2 values between 0.97 and 0.91 (see suppl. for Fe and K regressions).

5.5. Results

5.5.1. Age Models

In this study, we use the term Preboreal (PB) as the period between the start of the Holocene at around 11.6 and 10.1 ka BP, when the NGRIP d18O time series shows an increase into full Holocene conditions. The terms Younger Dryas (YD), Bølling-Allerød (B/A) are used for describing the stadial and interstadial phases during the last glacial termination (19-10 ka), elsewhere identified as GIS-1 and GS-0 (Blockley et al., 2011; Svensson et al., 2008). We use the term Heinrich Stadial 1 (HS-1) to describe entire cold phase encompassing the shorter North Atlantic Heinrich ice-rafting Event 1 itself (cf. Sarnthein et al., 2007). All ages, unless noted otherwise, are given in calibrated years before present with reference to AD 1950 as "cal. yr BP" or "ka". Ice core record timescales referenced to AD 2000 were corrected accordingly.

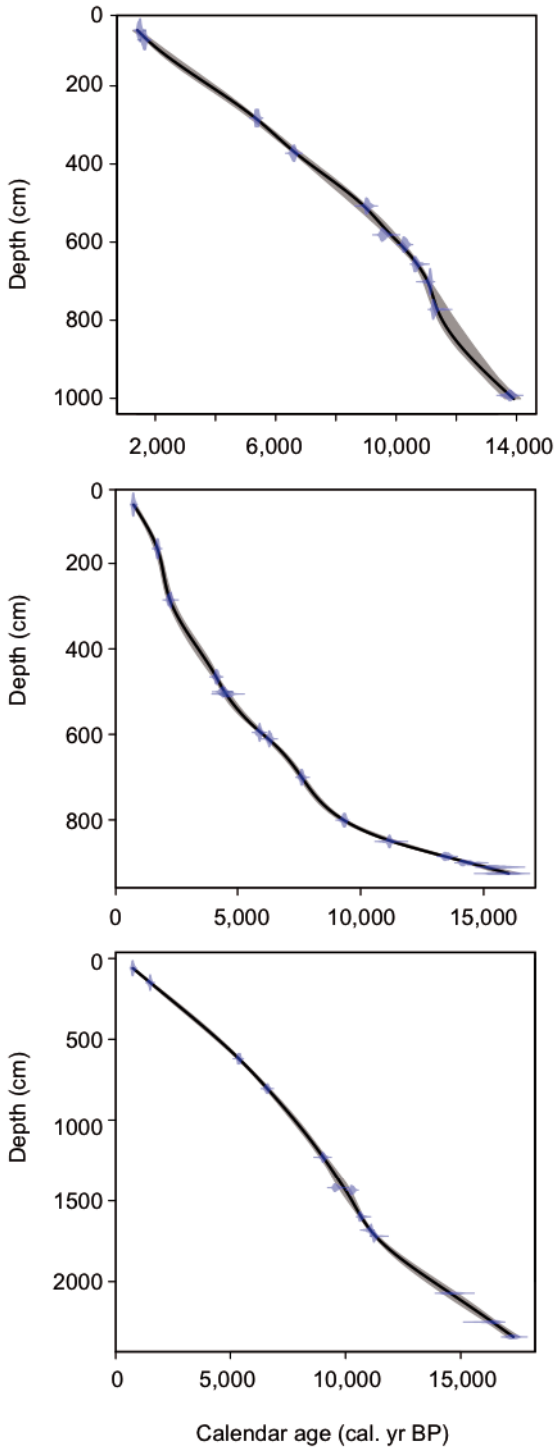

Figure 5.3: Age models for the cores used in this study. Age-depth relationships derived for the individual cores from CLAMS runs. Blue markers show calibrated AMS ^{14}C ages (in cal. yr BP) against core depths (in cm) with respective 2σ error range distributions, Black line represents ideal least squares error fit, grey shaded areas show respective calculated 2σ uncertainty ranges of the smooth spline fit models.

Age models for the three cores are based on AMS ^{14}C dates on planktic foraminifera and in two cases, where abundance of planktic foraminifera was too low to permit dating, on benthic mollusk shells. We used a regional reservoir age correction (ΔR) value of 500 yr ± 50 yr, in line with published correction values for the Okhotsk Sea (Kuzmin et al., 2007a) and earlier works (Max et al., 2012a; Riethdorf et al., 2013). The ΔR values used here potentially changed over the last 18 kyr (Gebhardt et al., 2008; Sarnthein et al., 2007), but as we are at present unable to further constrain such potential changes for the Okhotsk Sea, we kept the values constant over the entire age scale reported here. In the lower part of core 28-4 we used two benthic ages from mollusks. The benthic ^{14}C age value in the lowermost part of the core used to supplement the benthic-planktic ventilation age differences (Fig. 5b) was not used in the construction of the age model. We set an additional offset for the ventilation age correction for benthic values of 360 ^{14}C years, based on our own measured benthic-planktic age differences from the same depth interval in nearby core 13 (Table S2). In the case of core 79 we had to use one additional benthic age control point, this value was corrected by an additional 500 ^{14}C years based on published values for the same time interval from corresponding water depths and nearby cores (Gorbarenko et al., 2007a; Gorbarenko et al., 2010b).

We constrained potential age-depth relationships by comparing the chlorin records on their respective independent age scales against each other (Fig. 3). We assume that major changes in surface productivity patterns at almost identical locations should be broadly similar in timing to each other within the overall error of the individual age models. In the case of core 13, we were thus able to transfer a set of ^{14}C ages measured in core 79 to core 13 (cf. suppl. Table), in a mode similar to earlier stratigraphic correlations from this region (Galbraith et al., 2007; Max et al., submitted; Max et al., 2012a). For core 28-4 no correction of the initial independent age model was deemed necessary. We used the program CALIB 6.1.1 and the MARINE09 calibration curve (Reimer et al., 2009a; Stuiver and Reimer, 1993a) for initial age determinations. All AMS ^{14}C ages, their identification data and calibrated age ranges are given in Table S1.

To establish final age-depth relationships between our age control points we used the routine CLAMS written for the software package R (Blaauw, 2010) as a compromise between manually fitting regressions between age control points and more sophisticated, statistically superior age-depth modeling routines (Blaauw and Andres Christen, 2011; Blaauw et al., 2010; Blockley et al., 2007). The final best-fit runs were performed in CLAMS with 10,000 iterations using a smooth spline function for matching all age control points in their respective 2 σ calibrated age distribution ranges (Fig. 3). Alternative control runs in CLAMS with linear interpolations and higher order polynomial fits displayed only minor offsets within the principal error of the age control points, but the latter yielded higher regression residuals and were thus discarded. Due to the integrative nature of CLAMS

and the chosen fitting procedure, the age-depth relationship is based on the entire core section and thus reported here; however, in this study we investigate only the deglacial and early Holocene time interval between eight and 18 ka. According to the derived age models, average sedimentation rates in the studied time interval (8–18 ka) vary from 15 to 75 cm/ka (southernmost core 28), from 58 to 250 cm/ka (northern deep core 79), and from 88 to 300 cm/ka (northern shallow core 13), thus yielding high, centennial to inter-decadal resolution for most proxy series over the deglacial interval.

5.5.2 Intermediate Water Ventilation Records

All three cores show similar, millennial-scale variations in their epibenthic $\delta^{13}C_{Cib}$ signatures (see Fig. 4b). In the studied time interval of 8 to 18 ka, maxima $\delta^{13}C_{Cib}$ values are reached in core 13 during the early HS-1 with values of up to +0.2 ‰, with other maxima of ca. –0.2 to –0.4‰ during the YD and after the PB. Minima are reached during the warm B/A and PB phases with –0.8 to –1.0‰. Our southernmost core 4 records the lowermost excursions of just –1.5 and –1.2 ‰, respectively (Fig. 4b) during the onsets of the B-A and PB warm phases, whereas its other data fall nearly in line with the records of the northerly cores 13 and 79. The average amplitude of stadial-interstadial $\delta^{13}C_{Cib}$ variations is higher than 0.5 ‰ for both transitions, significantly exceeding the global glacial-interglacial carbon isotope shift of about 0.3 ‰. As modern values for $\delta^{13}C_{DIC}$ in the OS commonly range between –0.3 and –0.5 ‰ (Bauch et al., 2002; Itou et al., 2003), we note that deglacial $\delta^{13}C_{Cib}$ values exceed modern data only during HS-1 and did not recover again during the remainder of the glacial termination. Taken at face value, this indicates that the deglacial OSIW was on average less ventilated. i. e. poorer in O_2 content than today.

The OSIW ventilation (B-P) ages (Fig. 5), though slightly limited in their temporal resolution, help to establish connections between OSIW formation and concurrent deglacial southerly NPIW dynamics as evidenced in sites from the NE Japanese margin. Both the upper and lower OSIW B-P ages show remarkably little variation of less than 200-300 yr over the deglaciation into the Holocene. Absolute B-P ages are comparable to or even slightly lower than modern values in the North Pacific (Broecker, 1991). In fact, if error values are included, the OSIW B-P ages remain nearly unchanged between the cold HS-1, warm B-A and the Holocene. This is contrasted by NE Japan margin B-P ages that show clear variations in B-P ages in the upper NPIW (Fig. 5a). Values similar to the upper OSIW (about 300-500 yr) during the cold HS-1 are followed by drastic and rapid drops to much lower values of 1200-1400 yr during the B/A and a recovery to better ventilated NPIW waters in the subsequent YD and PB. During both he B/A and the PB the B-P ages on the NE Japan margin appear older than in the Okhotsk Sea at comparable water depths (Fig. 5).

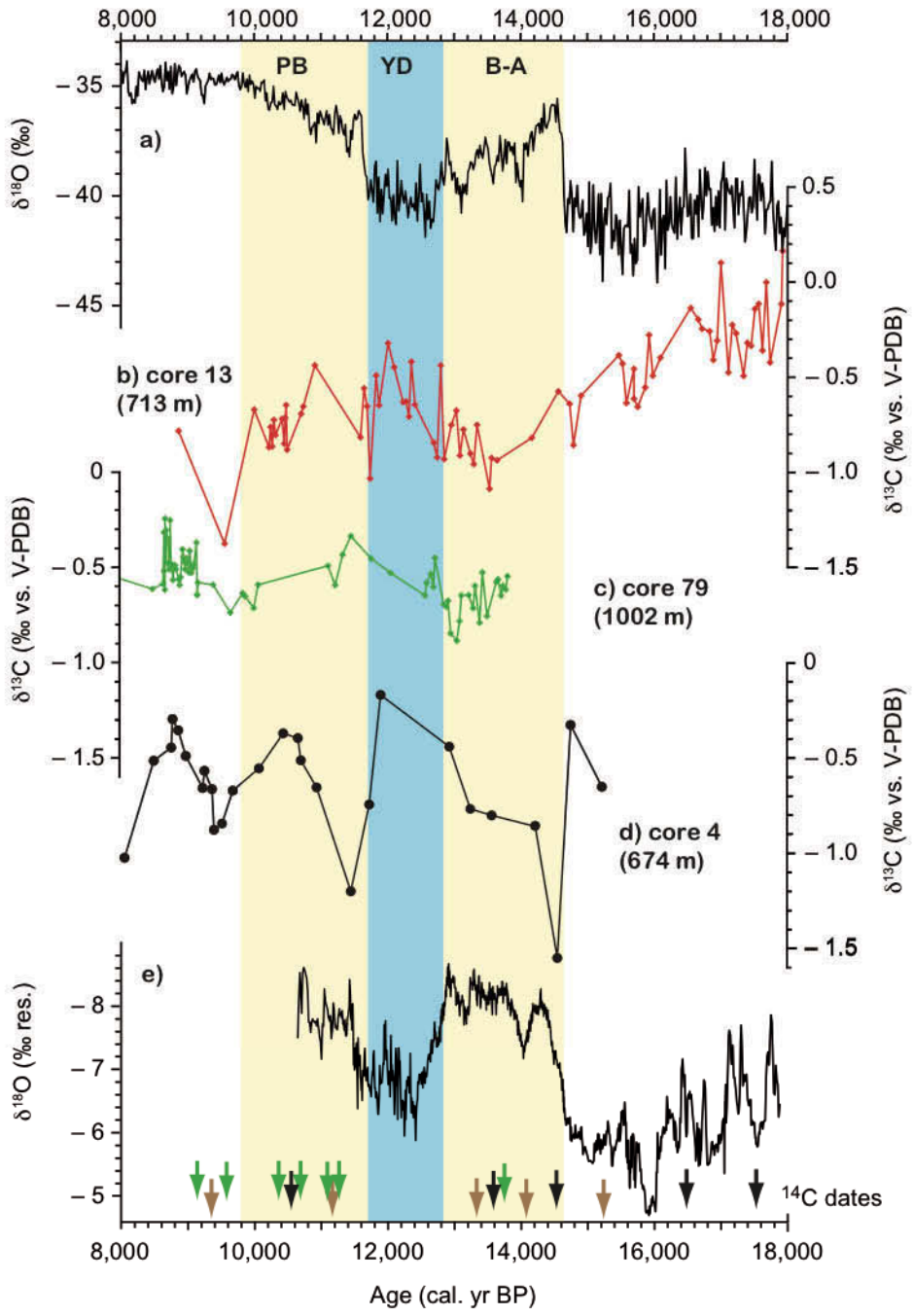

Figure 5.4: Comparison of proxy time series for bottom water ventilation, together with Northern hemispheric reference records from high (Greenland) and low (China) latitudes. (a) Greenland NGRIP $\delta^{18}O$ on the timescale of Rasmussen et al. (2008); (b) stable carbon isotope records of this study's *C. mundulus* ($\delta^{13}C_{cib}$) from northern shallow core 13 (red), (c) northern deep core 79 (green), and (d) southern shallow core 4 (black); (e) $\delta^{18}O$ timeseries of Hulu Cave speleothem record (Wang et al., 2008) on the timescale of Southon et al. (2012). Yellow shadings denote warm interstadial phases B/A and PB, blue shading cold stadial YD phase. Arrows on bottom show AMS ^{14}C dates used of construct age models, colors indicate core 13 (black), core 79 (green) and core 4 (brown).

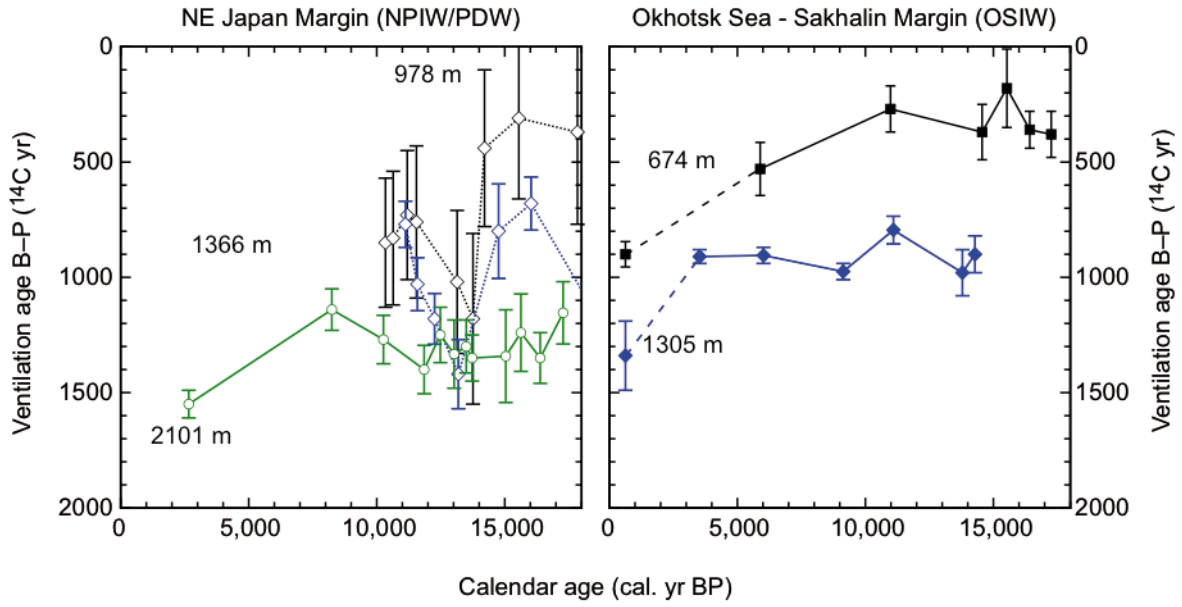

Figure 5.5: Compilation of Benthic – Planktic ventilation ages based on published and this study. (a) Data from the NE Japan Margin off Shimokita. Three cores from intermediate (CH84, black, Duplessy et al., 1989a) , intermediate-deep (Ahagon et al., 2003b; Ahagon and Uchida, 2004; Ohkushi, 2004), and deeper water masses (green, Okazaki et al., 2012).

5.5.3 Productivity Variations

The endobenthic $\delta^{13}C_{Uvi}$ curves of both northerly cores 13 and 79 resemble the epibenthic values in their patterns, though amplitude variations are more pronounced between interstadial low $\delta^{13}C_{Uvi}$ and high $\delta^{13}C_{Uvi}$ stadial data, with average differences of 0.7 ‰ and more (Fig. 6). Absolute minima are reached during the PB and middle to late Allerød, though this assessment might be biased due to the absence of *Uvigerina spp.* in the peak Bølling interval, indicating potentially even lower O_2 pore water concentrations (Bubenshchikova et al., 2008). In line with $\delta^{13}C_{Uvi}$, both TOC and chlorin content follow a similar pattern, evident in all cores with maxima during the mid-late Allerød and peak values during the PB, especially in the more northerly cores 13 and 79 (Fig. 6). Deep Core 79 records maximal chlorin values during the PB and the highest amplitude variations. Notably, southern core 4 does not record a distinct productivity peak in chlorin during the B-A, in contrast to northern cores and other sites further downstream. $CaCO_3$ concentrations in cores 4 and 79 (no data are available for core 13) follow the pattern recorded in the bulk productivity proxies (Fig. 6), while biogenic opal concentrations show a late increase from uniformly low values of about 5 % to steadily increasing early Holocene maxima of about 25 % (Fig. 7). Notably, opal concentrations do not share the rapid millennial-scale variations expressed in all other biological productivity proxies.

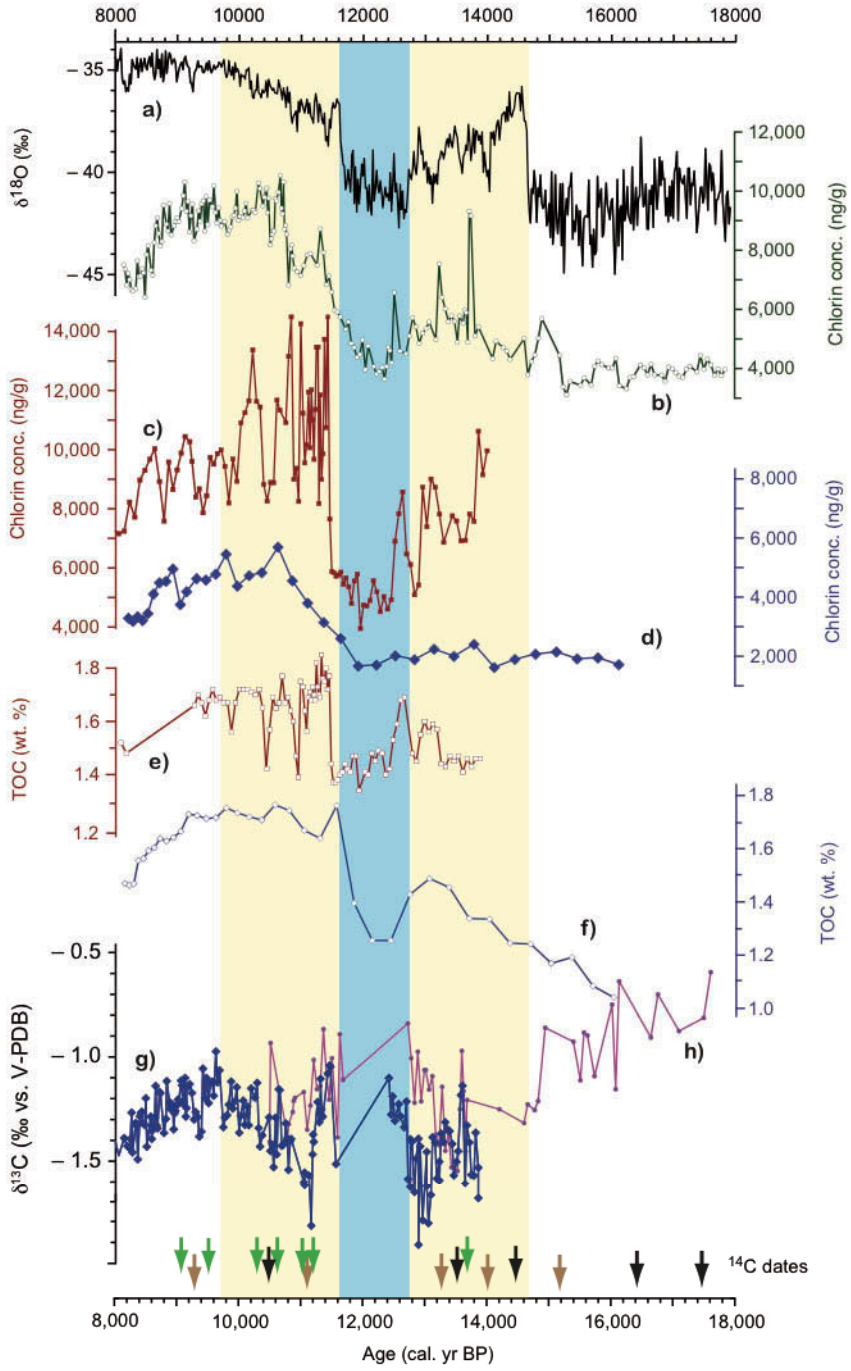

Figure 5.6: Bulk export productivity proxies. (a) Greenland NGRIP $\delta^{18}O$ on the timescale of Rasmussen et al. (2008); chlorin concentration from this study's cores all in (ng/g) from: (b) northern shallow core 13 (dark green, empty circles); (c) northern deep core 79 (dark red, filled circles); and (d) southern shallow core 4 (blue, filled diamonds). Concentrations of total organic carbon (TOC) of this study's cores from (e) northern deep core 79 (dark red as in {c}, but empty squares); (f) southern shallow core 4 (dark blue, empty diamonds). Stable carbon isotope records of this study's *U. peregrina* ($\delta^{13}C_{Uvi}$) from (g) northern deep core 79 (blue) and (h) northern shallow core 13 (violet); Remainder as in figure 4.

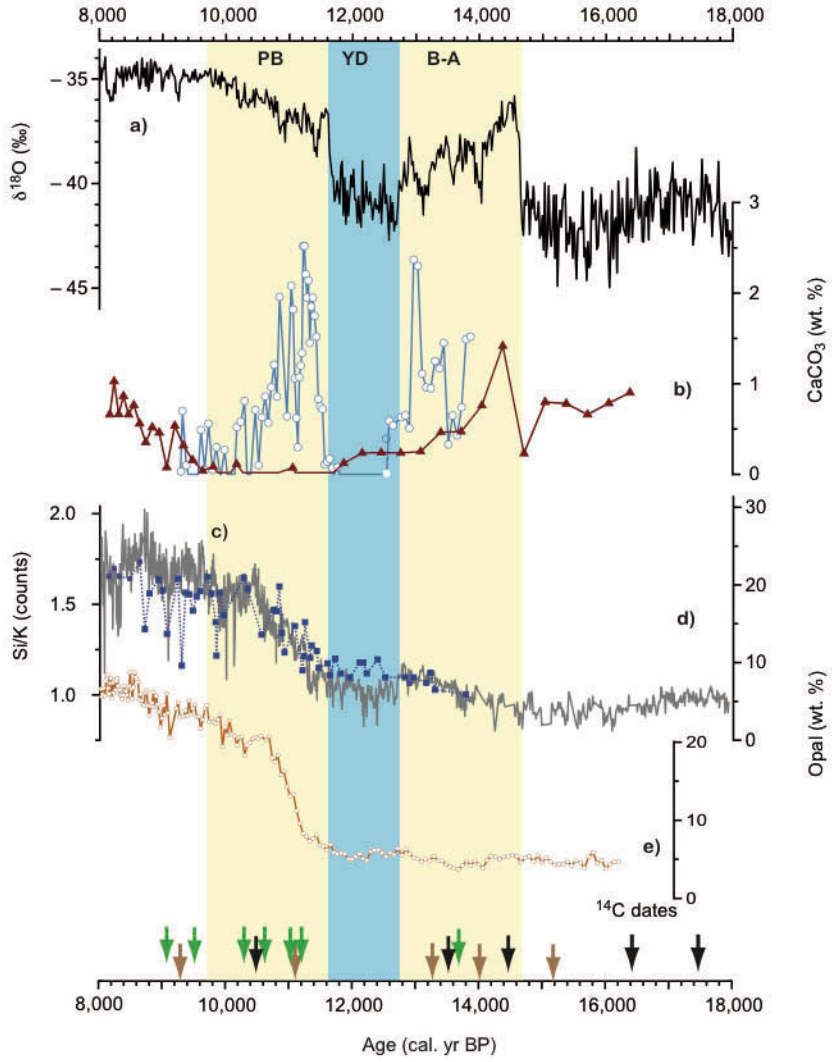

Figure 5.7: Carbonate and siliceous export productivity and terrigenous proxy time series. (a) Greenland NGRIP $\delta^{18}O$ on the timescale of Rasmussen et al. (2008). $CaCO_3$ concentrations from this study's cores (all in weight %) from: (b) northern deep core 79 (light blue, empty circles) and southern shallow core 4 (brown, filled triangles); (c) biogenic opal of northern deep core 79 (blue, filled squares), together with closely matching XRF-derived Si/K ratios as proxy for opal concentrations of nearby shallow northern core 13 (black line). (e) Concentrations of biogenic opal (weight %) of southern shallow core 4.

5.5.4 Lateral Transport and Terrigenous Matter Supply

The studied interval is characterized by large and rapid changes in C/N ratios in cores 4 and 79. High C/N ratios are recorded in both cores during the warm interstadial B/A and PB periods of the termination, with a maximum during the PB phase and early Holocene (Fig. 8). Northern core 79 shows maximum values of 11-14 in the late PB and a second small peak of about 11 in the late

Allerød, indicating a major influence of lateral transport of terrigenous particulate organic carbon (POC) to the core site. Southern core 4 follows the general pattern, however, the overall amplitude of the signal appears more muted with values reaching maxima of only 9-9.5, significantly lower than in core 79 and in line with a more distal location to the northern source areas for terrigenous POC (Fig. 7f).

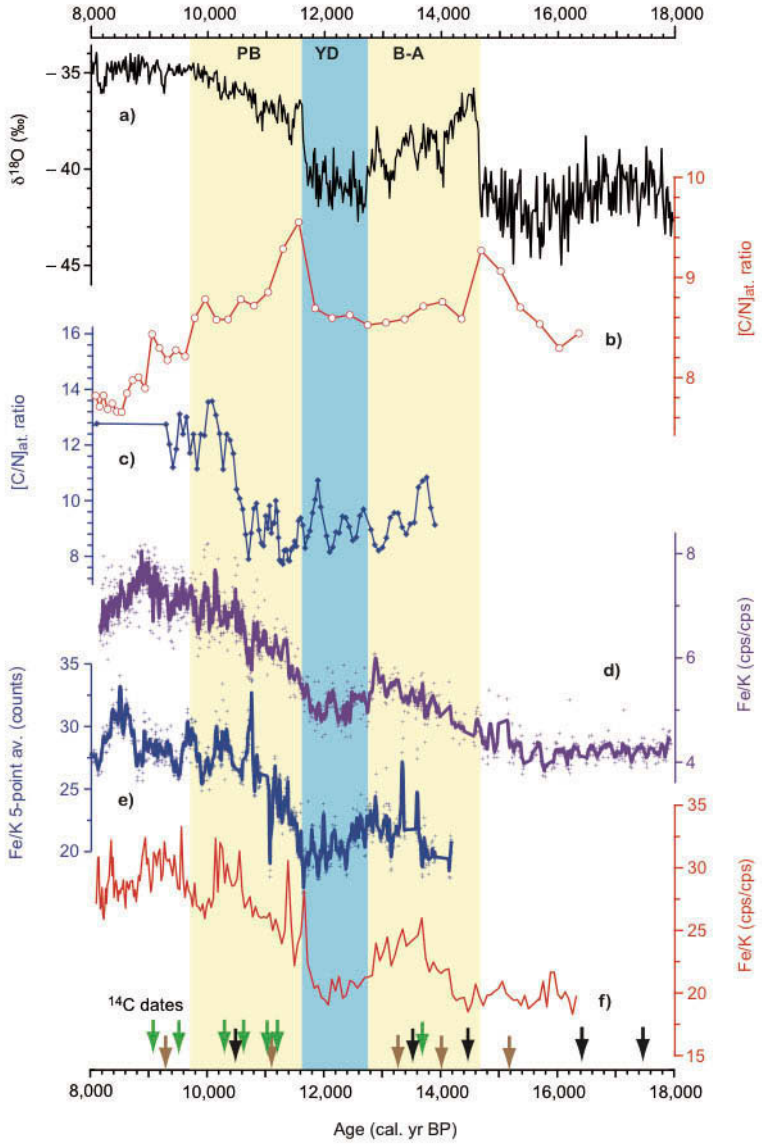

Figure 5.8: Comparison of proxy time-series indicative of terrigenous sediment transport. (a) Greenland NGRIP $\delta^{18}O$ on the timescale of Rasmussen et al. (2008). (b) $[C/N]_{atomic}$ ratios of southern shallow core 4 (dark red, empty circles) and (c) northern deep core 79 (dark blue, filled diamonds). (d-f) XRF-scanning-derived Fe/K ratios for all cores in this study. (d) Fe/K ratio of northern shallow core 13 (violet line 5 point running average, violet crosses individual values). (e) Fe/K ratio of northern deep core 79 (blue line 5 point running average, blue crosses individual values). (f) Fe/K ratio of southern core 4 (red line).

However, we note that the TOC concentration and C/N ratios are not linearly correlated in either of the two cores. This indicates that the TOC peaks primarily reflect biogenic productivity maxima rather than only lateral continental supply of terrigenous carbon. XRF-derived Fe/K ratios, as well as count intensities of Fe indicate an increase in Fe delivery to the core sites during interstadial phases, with an overall increasing trend towards the Holocene (Fig. 8 and 10f). This increase is interrupted by minimal values during the cold HS-1 and YD stadials, whereas local maxima occur during the Allerød and the late PB around 10.2 ka.

5.6. Discussion

5.6.1. Development of OSIW: Collapsed Formation or Decreased Ventilation during Deglacial Warm Phases?

Two principal mechanisms could account for the observed interstadial (B-A and PB, Fig. 4b) ventilation minima of the OSIW layer. Either formation of DSW and thus well-ventilated OSIW ceased due to physical forcing and circulation pattern different from today, leading to no export of OSIW from the Okhotsk Sea into the open North Pacific. Such a collapse of OSIW production would be caused by an absence of seasonal sea ice and thus polynia-induced brine rejection leading to DSW formation. Alternatively, OSIW was still produced, but with less vigorous entrainment of O_2 and exported out of the Okhotsk Sea similarly to modern conditions, but its oxygen content was lower due to shortened atmosphere-ocean exchange and more intense organic matter remineralization after formation because of higher nutrient loads. In the latter case, it must have faced increased POC and DOC respiration already on the Sakhalin margin soon after formation, rapidly decreasing the already lower-oxygenated OSIW even further.

We favor the second explanation for the following reasons: Previous works have shown, based on IRD provenance and abundance studies, that sea ice was present during all phases of the deglaciation in the northeastern part of the Okhotsk Sea and on the Sakhalin margin, even if overall abundances increased and decreased with cold and warm phases (Gorbarenko et al., 2004; Gorbarenko et al., 2010b; Nürnberg et al., 2011; Sakamoto et al., 2005). We thus presume that necessary physical preconditions for sustained formation of DSW masses were fulfilled, i.e. opening of polynias and formation of brine injections during cooling in winter. The maximum duration of the sea-ice season and thus the intensity of atmosphere-ocean exchange and DSW ventilation in winter polynias were likely shortened due to the stronger seasonality and stronger deglacial freshwater flux into the Okhotsk Sea via the Amur. The latter inhibits sea ice growth in winter seasons due to the high amounts of latent heat it carries in its

late summer discharge peaks from lower latitude monsoon-influenced regions (Ogi et al., 2001; Tachibana et al., 2008). Still, some ventilation and O_2 entrainment into OSIW likely persisted even in warm deglacial phases, supported by the notion that despite high productivity the occurrence of prominent laminated intervals in the mid-depth Okhotsk Sea is not observed in the cores 13 or 4, like on most other mid-depth North Pacific indicating transient anoxia during the B/A and PB warm interstadials margins (Jaccard and Galbraith, 2011).

In addition, $\delta^{13}C_{Cib.}$ shows that the vertical extension of OSIW between our shallower and the deeper remained surprisingly homogenous over stadial-interstadial transitions. We speculate that if a substantial weakening of OSIW formation rate or flow volume during warm interstadial phases had happened, an increasing $\delta^{13}C_{Cib.}$gradient between deeper core 79 (1002 m) and shallower core 13 (673 m) should be apparent, becasue core 79 is at the deepest potential extension of intermediate depth water and sensitive to switches between better ventilated OSIW and deeper, oxygen-poorer PDW. However, no such dynamic change can be observed. The observed co-variations of epifaunal $\delta^{13}C_{Cib.}$ and shallow infaunal $\delta^{13}C_{Cib.\ data}$ (Fig. 4 and 6) in addition indicate that the $\delta^{13}C_{DIC}$ and thus O_2 content of OSIW was to a significant extent determined by mesopelagic respiration processes. Analog to modern observations, a minimum of about 30 % of the mesopelagic waters' initial O_2 concentration was likely consumed by organic matter respiration (del Giorgio and Duarte, 2002; Herguera et al., 2009).

The Benthic–Planktic (B-P) ventilation ages derived from our and other cores (Gorbarenko et al., 2008; Gorbarenko et al., 2007b) in the Okhotsk Sea from water depths of 675 m (OSIW core layer) and 1300 m (lower OSIW) support this hypothesis, because they show no major coherent changes towards higher B-P ages during the B/A and PB. We observe that while increases in NPIW ventilation and formation did occur during the cold stadial phases (HS-1 and YD) in the North Pacific (Okazaki et al., 2010a), the warm interstadial phases in contrast did not result in persistent older water masses compared to the modern situation in the OSIW source region, implying a mode similar in strength and volume to modern circulation patterns or even stronger. This reasoning is in line with the notion that the global Meridional Overturning Circulation as one forcing for variations in North Pacific circulation was comparable to modern conditions (McManus et al., 2004a) or stronger as evidenced in records from the Atlantic region during the B/A (Barker et al., 2010).

However, a collapse of NPIW ventilation off Japan between 900-1400 m is indicated by the drop of B-P ages to much older values characteristic of deeper PDW values around 2100 m water depth (Fig. 5a). This pattern implies that either upwelling of old, deeper water masses occurred at the Japan margin into intermediate depths, or that circulation patterns in the intermediate water layer off Japan

significantly changed during the B/A, while leaving deeper PDW around 2000 m relatively unaffected at the same time (Okazaki et al., 2012). Some works indicate that the boundary between Kuroshio and Oyashio currents shifted by several degrees in concert with stadial and interstadial variations during the last glacial and the last termination (Inagaki et al., 2009; Yamamoto et al., 2005), probably affecting the mid-depth waters at the northern Japan margin sites, switching them between a more northern and southern-derived source. As paleo-ventilation ages in the Okhotsk Sea (WSAG). i.e. northward of the Kuroshio-Oyashio extension are unaffected by these changes and show only minor variations over the glacial termination, we presume that during transient warm interstadial phases southern, subtropically influenced intermediate water became more isolated from the northern OSIW-influenced WSAG than today. This would result in the increased injection of more (interstadial low-O_2) OSIW into the northerly subarctic WSAG circulation and effectively decouple subarctic and subtropical-dominated mid-depth water masses in the mid-latitude North Pacific. In contrast, during the remainder of the deglaciation, similar B-P ages on the Okhotsk and Japanese continental margins argue for a southward propagation of OSIW-influenced (stadial high-O_2) intermediate waters into lower latitudes analog to modern conditions.

5.6.2. Timing and Causes for Productivity and OSIW Ventilation Changes During the Deglaciation: Hinterland Environmental Changes and Forcing

The deglacial O_2 decline during the warm B/A indicated in our $\delta^{13}C_{cib}$ data is accompanied by pronounced maxima in surface ocean productivity (Fig 6, 7, 9). However, in contrast to neighboring regions and more southern lower-resolution sites our results place the maxima in primary productivity to the PB (11.6-9 ka) and the Allerød (13.8-13.0 ka), rather than the Bølling or entire B/A phases (Crusius et al., 2004; Gorbarenko et al., 2002a; Khim and Sakamoto, 2012). This timing is not strictly correlated to the rapid warming and MOC changes known from Atlantic (McManus et al., 2004a; Piotrowski et al., 2004). Instead, a first small productivity peak occurs slightly earlier around ca. 15 ka, followed by a second stronger peak centered towards the late Bølling to early Allerød (11.6-11.2 ka, Fig. 6, 7, 9). However, this timing is corroborated by multi-proxy and benthic species assemblage observations from nearby sites (Bubenshchikova et al., 2010; Gorbarenko et al., 2007a; Gorbarenko et al., 2010b; Seki et al., 2004). There, relatively late increases in mainly carbonate-bearing primary producers, occurring only after the Bølling around 13.6-13.1 ka, were tentatively ascribed to a potential lagged transfer of climatic forcing from the North Atlantic region and changes in the AMOC to the North Pacific, but the timing and causation could not be further verified due to potential age model uncertainties in the investigated core (Gorbarenko et al., 2010b). Our new, high-resolution set of cores confirms this particular delayed occurrence (Fig. 6c-f, 9c) in the Okhotsk Sea.

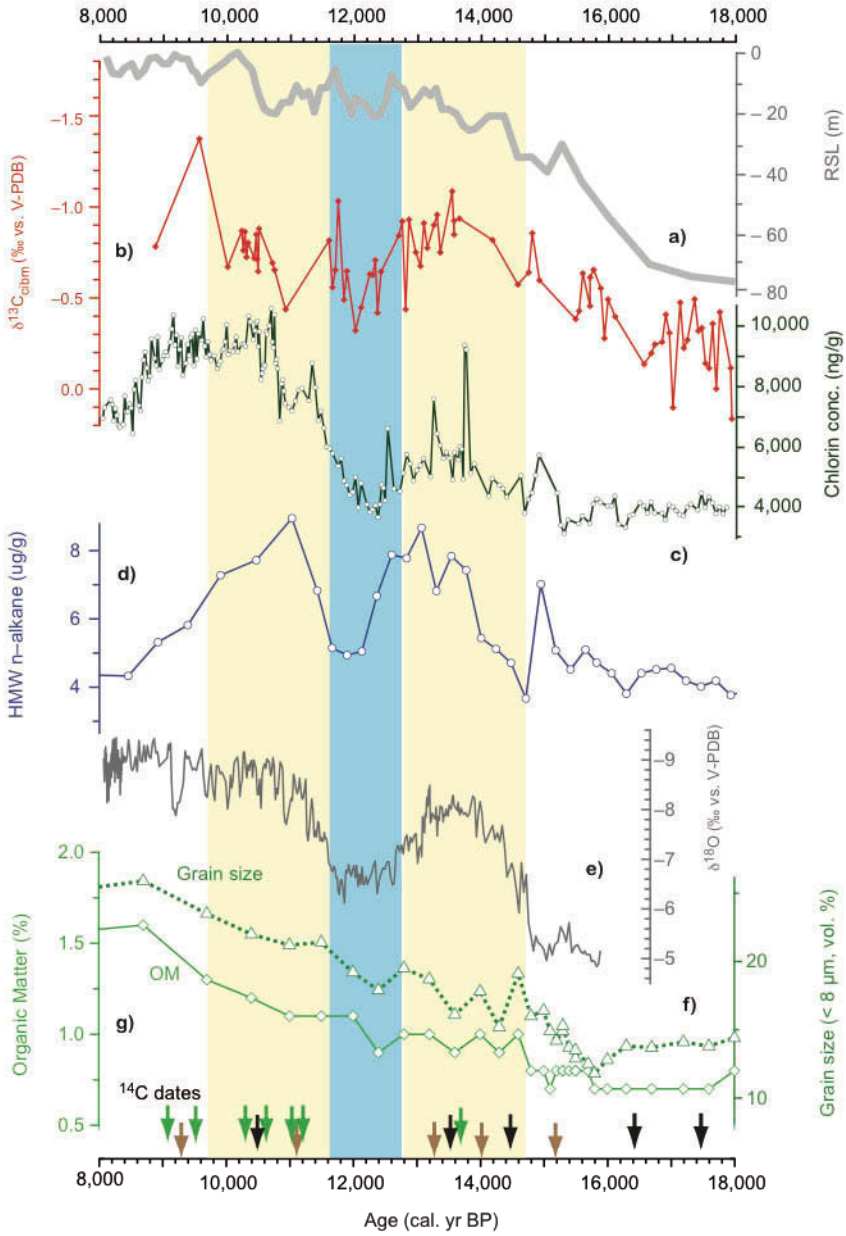

Figure 5.9: Proxy time series related to Sakhalin margin productivity and OSIW changes in comparison to Asian hinterland records to deduce potential causes and forcing mechanisms. (a) eustatic sea level curve (Rohling et al., 2009); (b) this study's OSIW ventilation record based on *C. mundulus* ($\delta^{13}C_{cib}$) from northern shallow core 13 inverted for better comparison (red); (c) chlorin concentration (ng/g) from core 13 (dark green, empty circles). (d) Concentrations of terrestrial plant wax biomarkers C_{25}-C_{35} n-alkanes (µg/g) in nearby core C9 indicating shelf submergence and freshwater runoff (Seki et al., 2012). (e) Proxy record for EASM strength and temperature/precipitation changes: Dongge Cave seleothem $\delta^{18}O$ (in ‰ vs. V-PDB, Dykoski et al., 2005). (f) and (g) Proxy records for precipitation in the SE Asian low latitudes as expressed in Mangshan Loess Plateau sequence MS2008E (Peterse et al., 2011); (f) MS2008E grain size distribution as fraction < 8 µm (in vol. %) and (g) organic matter (OM) content (weight %). Remainder as in figure 4.

In other circum-Pacific regions, sudden deglacial spikes in productivity have been ascribed to various causes, like eustatic sea level rise, mixed layer stratification, lateral material transport or circulation changes (e.g. Addison et al., 2012; Caissie et al., 2010; Cook et al., 2005a; Davies et al., 2011). With regard to effect of these potential causes in the Okhotsk Sea, we assume that flooding of the extensive northern shallow shelf areas during the early deglaciation (18-15 ka) and the pronounced MWP Ia likely caused southward transport of some lithogenic terrestrial material with the East Sakhalin Current. It has been shown that such shelf-derived supply of additional refractory nutrients enhanced primary production further offshore (Davies et al., 2011; Klinkhammer et al., 2009). In the Okhotsk Sea, the first pre-Bølling (15 ka, Fig. 6b and 9b, c-d) and Allerød (13.4-13.0 k) productivity peaks were likely supported by such a mechanism. However, fertilization of marine productivity by se-level alone rise was likely not the main cause for productivity peaks in the Okhotsk Sea due to the following considerations: Absolute deglacial productivity maxima peak later than maximum sea level changes at all sites, namely during the PB with initial spikes around 11.6 to 11.2 ka (Fig. 6b-h, 9). Thus, reported productivity maxima would be offset in timing and lag the sea-level rise maxima by several thousand years. In addition, hypothetically mobilized terrigenous organic matter was highly refractory and, at least during the early phase of the deglaciation, inundated shelf areas were presumably still frozen and thus relatively inert to sediment mobilization, due to their location within the glacial permafrost region (Chlachula, 2003; Vaks et al., 2013).

For an explanation of these discrepancies, we consulted speleothem and loess records from the low-latitude hinterland region, which are indicators for the East Asian Summer Monsoon (EASM) temperature (Fig 9e, Dykoski et al., 2005; Wang et al., 2005) and precipitation history (Fig 9f-g, Peterse et al., 2011). The Donge Cave speleothem record correlates well in overall shape and pattern with our proxy reconstructions of OSIW ventilation and export production (Fig. 9b-c and e), but diverges in the fine structure. Remarkably, the loess-derived precipitation reconstruction shows that the deglacial EASM increases in precipitation were more gradual than the speleothem $\delta^{18}O$ series suggests (Fig. 9e-g) and thus started later than the initial rapid onset of the EASM temperature increases (Peterse et al., 2011). To establish a link between these hinterland reference records indicative of hinterland climatology and the Okhotsk Sea freshwater influx we turned to freshwater algae counts (Fig. 10) from our southernmost core location (core 4). Results show that the first, smaller discharge peak occurred during the B/A, followed by a massive freshwater discharge event between 11.6 and 9 ka. Freshwater algae concentrations during these two peak periods are one to two orders of magnitude higher than Holocene and modern values. Today, neither *Pediastrum* nor *Botryococcus* taxa occur in substantial numbers at site 4 (Fig. 10b), though freshwater flux to the Okhotsk Sea is quite substantial. We thus infer that precipitation increases during the B/A and PB warm phases caused drastic sustained fluvial discharge peaks into the Okhotsk Sea via the Amur.

Land-based records from NE-China peat bogs support this scenario, indicating maxima in effective precipitation in the Amur catchment area (Bazarova et al., 2008; Seki et al., 2009a).

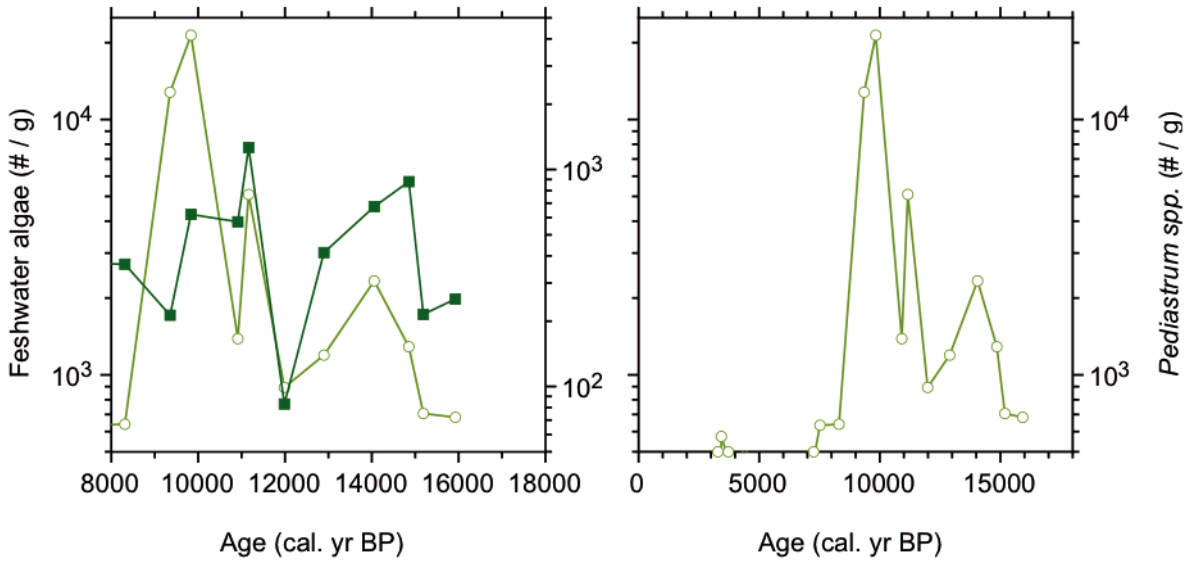

Figure 5.10: Concentrations (in numbers/g sediment) of freshwater-restricted chlorophycean algae *Pediastrum spp.* (light green, open circles) and freshwater-brackish-restricted *Botryococcus spp.* (dark green, filled squares) used as proxies for fluvial freshwater supply to southern site 4 (this study). Note logarithmic scale for concentrations. (a) Interval studied form 8 to 18 ka. (b) entire core section on scale 0 to 18 ka. Note that no freshwater algae are found at this location under modern (still large) fluvial discharge conditions from Amur, implying substantially larger discharge during the deglacial interval.

Concurrent maxima in terrigenous nutrient and detrital iron load derived from the Amur started in the deglacial between 14-12 ka and peaked during the PB as evidenced by maxima in Fe/K ratios (Fig. 8) and matching peaks of terrestrial biomarkers in nearby marine cores (Fig 9d) (Seki et al., 2012; Seki et al., 2003). These higher-than-modern peaks in terrigenous sediment load were in all probability buttressed by the widespread melting of permafrost soils in the Amur hinterland during the late deglaciation. Though temporally poorly constrained, the melting was dated in terrestrial records to the Preboreal (Bazarova et al., 2008; Sakaguchi, 1992). Hinterland records, nearby organic terrestrial biomarker data (Seki et al., 2012), combine with our sedimentological and freshwater algae data (Fig. 9 and 10a) to provide proof that high amounts of fresh organic matter, nutrients and sediment suspension were supplied to the upper water column of the NW Okhotsk Sea during the warm B/A and PB phases (Fig. 9). These elevated nutrient together with indications for maxima in mixed layer

stratification (Riethdorf et al., 2013) and longer sea ice-free summer seasons during the deglacial warm B-A and PB (Gorbarenko et al., 2007a; Gorbarenko et al., 2012) supported primary production increases. This conditioning of the upper mixed layer is also assumed to providing carbonate producers (coccolithophore) with a competitive advantage over diatoms over the deglaciation, thus explaining the lack of an early deglacial biosiliceous productivity peak (Harada et al., 2008; Khim and Sakamoto, 2012; Seki et al., 2009b).

Together, our data (Fig. 9 and 10) indicate that freshwater supply by the Amur was the more important factor in rapidly (i.e. within 10-100s of years) supplying relatively fresh terrigenous matter and nutrients for maximum primary production to the Okhotsk Sea continental margin during the B/A and PB warm phases, while sea level rise was likely a second important contributor of elevated terrigenous refractory organic matter content during the early pre-Bølling and Bølling-Allerød warm phases and productivity peaks. Our results also support a scenario with forcing that is regionalized and differing between particular NW-Pacific areas, being less strictly correlated simply to North Atlantic millennial-scale climatic variability as shown in Greenland ice core records and AMOC changes (Gorbarenko et al., 2008; Harada et al., 2008; Ohkushi et al., 2003). In the Okhotsk Sea, low-latitude forcing by hinterland changes through the migration of the East Asian Summer Monsoon front and deglacial changes in the terrestrial cryosphere played an additional critical role in shaping the deglacial hydrography and biogeochemistry.

5.6.3. Consequences of Variations in OSIW Biogeochemical Signatures for Deglacial North Pacific productivity pulses and OMZ development

Our results provide evidence for significantly higher organic matter and nutrient loads within OSIW during the warm interstadial phases of the last glacial termination (Fig. 8, 9, 11c-d). Based on a number of modern sediment trap and time series results, locations on the Sakhalin margin reliably record the amount of terrigenous and biogenic material entrained in the DSW formation region, which is then transported within a highly turbid water layer southward into the North Pacific (Hansell, 2002; Nakatsuka et al., 2004a; Nakatsuka et al., 2004b; Nakatsuka et al., 2002; Nishioka et al., 2007). Today, the amount of laterally transported POC (0.9 Tg C/yr) and DOC (13.6 Tg C/yr) entrained within DSW is considerably larger than the amount of POC that settles through the water column from surface biogenic productivity (0.2-0.5 Tg C/yr). Thus, lateral entrainment and subsequent transport of suspended material rather than vertical settling of nutrients preconditions the biogeochemistry of OSIW. Our multi-proxy data imply that the flux of the entrained POC and DOC and terrigenous lithogenic material was even higher than today during the B/A and PB warm phases.

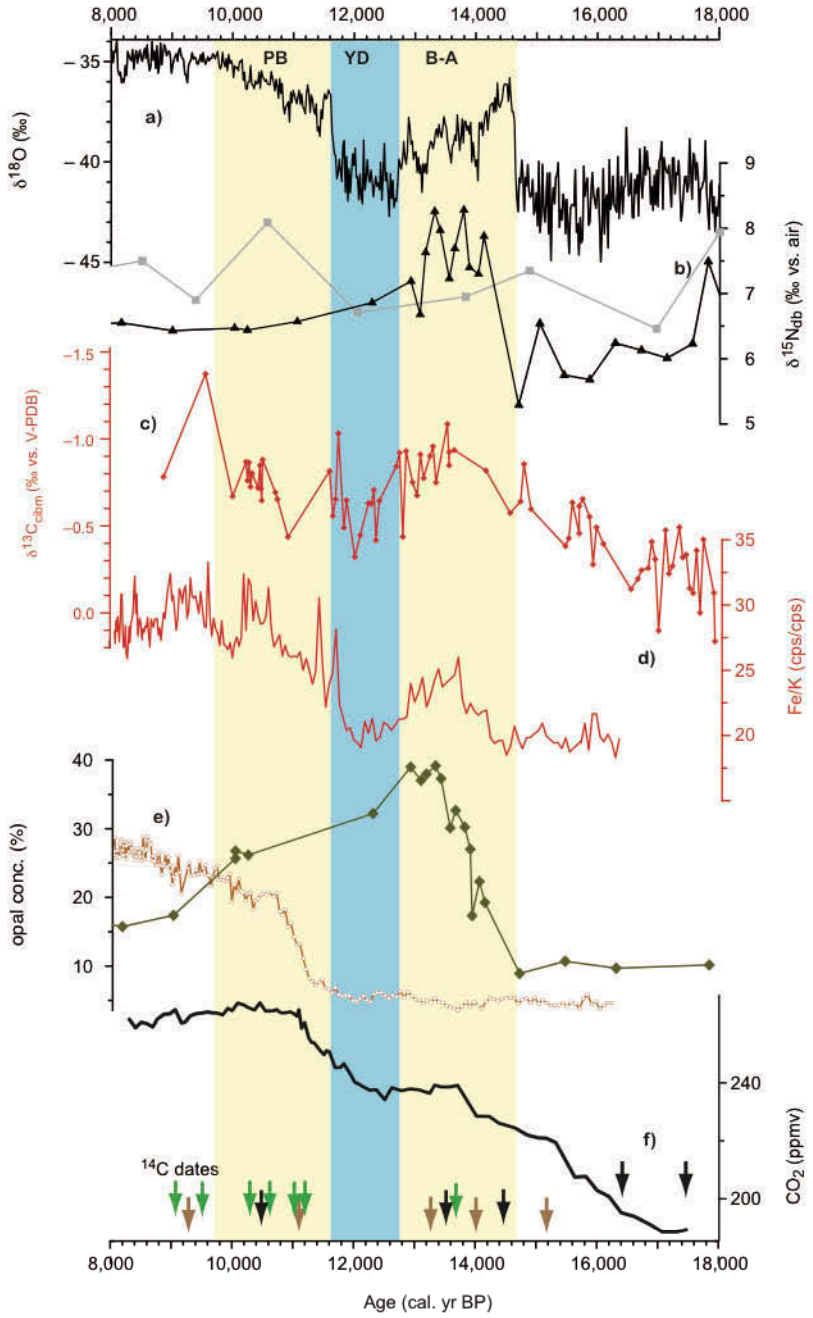

Figure 5.11: Comparison of selected Okhotsk Sea records with subarctic North Pacific (core PC1, Brunelle et al., 2010b) changes in productivity and nutrient utilization to assess consequences of OSIW variability . (a) as in figure 4. (b) nutrient utilization based on $\delta^{15}N$ records for Okhotsk Sea (core GGC27, grey with squares Brunelle et al., 2010b) and the subarctic NW Pacific (core PC13, black with triangles). (c) this study's OSIW ventilation record ($\delta^{13}C_{cib}$) from N' shallow core 13, inverted (red). (d) Fe concentration within the terrigenous fraction based on XRF Fe/K ratio of S' Okhotsk Sea core 4 (red line without markers, cf. Suppl. Fig S2 for Fe/K ratios of N' cores 79 and 13). (e) Biogenic opal concentrations of Okhotsk Sea core 4 (this study, brown, open circles) and Subarctic North Pacific core PC13 (light green line with filled diamonds, Brunelle et al., 2010b). (f)

atmospheric CO_2 concentrations from EPICA Dome C Antarctic ice core (Monnin et al., 2004) on EDC3 timescale.

We thus hypothesize that significant amounts of dissolved and particulate terrigenous carbon, nitrogen and $Si(OH)_4$, were laterally transported within the OSIW during the B/A and PB and exported from the Okhotsk Sea to the open subarctic North Pacific (Fig. 1, 11). Concurrent Fe maxima consistently observed in all sediment records along the pathway of the southward-flowing ESC imply that in addition the amount of lithogenic material increased within the turbid DSW, thus creating a "perfect nutrient mix". The higher (than modern) concentrations of suspended macronutrients together with the essentially needed Fe were likely even reinforced through the observed low primary production of biogenic silica within the Okhotsk Sea, especially during the B-A (Fig. 11e). In combination with maximum fluvial supply such biogenic underutilization probably further conserved $Si(OH)_4$ and bio-available Fe concentrations in the mid-depth highly turbid, weakly ventilated water column.

Independent support for our hypothesis is provided by data from a core located in the southern Okhotsk Sea, far away from the immediate influence of local fluvial transport. There, maxima in terrigenous detrital OM accumulation supply were observed during the deglaciation (Ternois et al., 2001). At that time the authors could not decisively allocate the source mechanism for the material, but concluded that sea ice transport, fluvial supply by the Amur and continental debris from rising sea levels and inundated shallow shelf areas would all be natural candidates. Combined with evidence from our productivity and OSIW ventilation data and the established modern oceanic transport mechanisms of suspended material in the turbid OSIW layer (Hansell, 2002; Nakatsuka et al., 2004a; Nakatsuka et al., 2004b), we suggest that the OSIW acts as an efficient, lateral transport mechanism for nutrient export over wide distances into the open mid-depth North Pacific ocean. There, the low-O_2, and nutrient/Fe-enriched OSIW was upwelled into the upper mixed layer during wintertime turbulent mixing, in analogy to modern conditions (Nakatsuka et al., 2009; Nishioka et al., 2011) and facilitated the transient repletion of nutrients, including Fe, during the B/A and PB . Our hypothesis helps to explain the rather enigmatic pattern of higher than modern nutrient utilization during the deglacial productivity peaks throughout the subarctic NW-Pacific and its marginal seas based on nitrogen isotopes (Fig 11b, Brunelle et al., 2007; Brunelle et al., 2010b; Kohfeld and Chase, 2011). In addition, we suspect that due to the observed ventilation minima in OSIW during the B/A and PB (Fig. 4 and 11c), denitrification was perhaps enhanced, supporting a slightly elevated ^{d15}N OSIW signature (Fig. 11b, Yoshikawa et al., 2006). At the same time, the decreased O_2 content of OSIW and the northward-displaced circulation potentially fostered the establishment of oxygen minimum zones in the North Pacific Ocean, including northward regions like the Bering Sea.

Lastly, the open subarctic North Pacific, though being a sink for atmospheric CO_2 today, constitutes one of the three main modern High Nutrient/Low Chlorophyll regions globally, where Fe-depletion limits the efficiency of the "biological pump" to more effectively sequester atmospheric CO_2 into the deep ocean by better nutrient utilization and higher primary production. The last glacial termination's productivity spikes in the North Pacific (Crusius et al., 2004; Galbraith et al., 2007; Keigwin et al., 1992a) likely contributed to shaping deglacial atmospheric CO_2 changes by an interplay between release of old CO_2-rich deep water masses into the atmosphere and the sequestration of CO_2 into the deep ocean through primary production and changes in the efficiency of carbon export from the upper ocean to the abyss (Galbraith et al., 2007). Notably, our timing of changes in OSIW biogeochemical and ventilation characteristics correlate both with the North Pacific maximum in nutrient utilization/export production, and with transient slowdowns in the deglacial atmospheric CO_2 rise (Fig. 11f, Monnin et al., 2001). Thus, intermediate water masses likely occupy an important role as facilitator for larger regional-scale changes in ocean biogeochemistry and the global carbon cycle, warranting a more detailed understanding on both glacial-interglacial and shorter timescales.

5.7. Conclusions

We carried out a comprehensive multi-proxy-based reconstruction of Okhotsk Sea Intermediate Water ventilation and biogeochemical characteristics over the last glacial termination based on a set of high-resolution AMS ^{14}C-dated sediment cores.

Based on ventilation ages and epibenthic stable carbon isotopes we provided evidence that decreases in OSIW ventilation were largely driven by increases organic matter content and remineralization rates rather than changes in formation rates of Dense Shelf and mid-depth waters in the Okhotsk Sea. From differences in ventilation ages between the northerly Okhotsk Sea and the southerly open Japan margin we deduce that OSIW influence on lower latitude subtropical mid-depth North Pacific waters waned during the during the warm Bølling-Allerød and Preboreal phases. These regional differences might explain large scatter in earlier data compilations (Okazaki et al., 2010a) and indicate more complex intermediate water circulation patterns than previously assumed, in analogy to recently observed regionally differing surface and mixed layer hydrography during the last glacial termination (Max et al., 2012a; Riethdorf et al., 2013). At the same time, OSIW was no source of oxygen for NPIW during the Bølling-Allerød, thus providing a positive feedback for basin-wide intensification of Oxygen Minimum Zones during the last glacial termination, in line with hypotheses that called for elevated respiration rates in the open North Pacific to decrease the O_2 content of NPIW (Crusius et al., 2004).

We observed millennial-scale OSIW ventilation decreases during deglacial warm periods to be in phase with increases in terrigenous suspension load and deposition in the Okhotsk Sea. To a lesser extent terrigenous sediment was supplied by continental shelf flooding through eustatic sea-level rise, mainly during the early-mid deglacial (17-14 ka). However, during Allerød and Preboreal marine productivity maxima on the Sakhalin margin, iron- and nutrient-rich terrestrial material was mainly sourced from the Siberian hinterland and delivered via Amur freshwater discharge peaks. These maxima in river runoff correlate with deglacial increases in precipitation linked to the northward propagation of the East Asian Summer. This closely coupled continent-ocean system provides an example of low-latitude East Asian monsoon forcing exerting direct influence on mid-latitude and subarctic North Pacific oceanography and marine biogeochemistry.

We hypothesize that correlation of the observed ventilation minima with maxima in primary productivity and nutrient utilization in the open North Pacific implies an increase of OSIW-sourced lateral transport of macronutrients and iron into the subarctic North Pacific during the Bølling-Allerød and Preboreal. Variations in this export mechanism could have contributed to pelagic deglacial productivity peaks and simultaneously lead to a higher utilization of nutrients than observed today during deglacial warm phases. In the subarctic North Pacific region, this scenario would have temporarily relieved the upper ocean from micro-nutrient limiting conditions by upwelling the mid-depth nutrient-enriched OSIW during wintertime mixing and switch the region to a transient, more efficient CO_2 sink status during the B/A and PB, two intervals that are marked by a slowdown in atmospheric CO2 rise.

Acknowledgements

We acknowledge the professional support and dedication of masters and crews of R/V Akademik Lavrentiev and R/V Sonne on expeditions LV28, LV29 and SO178. We thank J. Heinze and B. Fessler for help in sample analysis; and N. Stange, M. Zygmuntowski and A. Dix for their support in sediment sampling and processing. This study was carried out within the frameworks of German-Russian multidisciplinary projects KOMEX, KOMEX II and KOMEX-SONNE, and financially supported by the German Ministry for Research and Education (BMBF).

Authors' Contributions

LLJ measured isotope and compiled other data, and wrote paper. LLJ, RT and DN designed study. RK measured opal and XRF on core 4, UK carried out pollen analysis, LM provided B-P data, and UR contributed to XRF measurements, SG provided samples and data. All authors participated in the discussion of results and conclusions and contributed to the final version of the paper.

5.8. References

Addison, J.A., Finney, B.P., Dean, W.E., Davies, M.H., Mix, A.C., Stoner, J.S., Jaeger, J.M., 2012. Productivity and sedimentary $\delta^{15}N$ variability for the last 17,000 years along the northern Gulf of Alaska continental slope. Paleoceanography 27.

Ahagon, N., Ohkushi, K., Uchida, M., Mishima, T., 2003. Mid-depth circulation in the northwest Pacific during the last deglaciation: Evidence from foraminiferal radiocarbon ages. Geophysical Research Letters 30, 2097.

Ahagon, N., Uchida, M., 2004. Transient response of mid-depth circulation in the northwest Pacific around the Younger Dryas event inferred from AMS C-14 ages of foraminifera. Nuclear Instruments & Methods In Physics Research Section B-Beam Interactions With Materials And Atoms 223, 466-470.

Barker, S., Knorr, G., Vautravers, M.J., Diz, P., Skinner, L.C., 2010. Extreme deepening of the Atlantic overturning circulation during deglaciation. Nature Geoscience 3, 567.

Bauch, D., Erlenkeuser, H., Winckler, G., Pavlova, G., Thiede, J., 2002. Carbon isotopes and habitat of polar planktic foraminifera in the Okhotsk Sea: the 'carbonate ion effect' under natural conditions. Marine Micropaleontology 45, 83-99.

Bazarova, V.B., Klimin, M.A., Mokhova, L.M., Orlova, L.A., 2008. New pollen records of Late Pleistocene and Holocene changes of environment and climate in the Lower Amur River Basin, NE Eurasia, Quaternary International, pp. 9-19.

Biebow, N., Hütten, E., 1999. Cruise Reports: KOMEX I and II: RV Professor Gagarinsky Cruise 22, RV Akademik M.A. Lavrentyev Cruise 28, GEOMAR Report. GEOMAR Research Centre for Marine Geosciences, Kiel, p. 188.

Biebow, N., Kulinich, R., Baranov, B., 2002. KOMEX II, Kurile Okhotsk Sea Marine Experiment: Cruise report RV Akademik M.A.Lavrentyev cruise 29, Leg 1 and Leg 2 : Vladivostok - Pusan - Okhotsk Sea - Pusan - Okhotsk Sea - Pusan - Vladivostok ; May 25 - August 05,2002. GEOMAR Forschungszentrum für Marine Geowissenschaften, Kiel.

Blaauw, M., 2010. Methods and code for "classical" age-modelling of radiocarbon sequences. Quaternary Geochronology 5, 512-518.

Blaauw, M., Andres Christen, J., 2011. Flexible Paleoclimate Age-Depth Models Using an Autoregressive Gamma Process. Bayesian Analysis 6, 457-474.

Blaauw, M., Bennett, K.D., Christen, J.A., 2010. Random walk simulations of fossil proxy data. The Holocene 20, 645-649.

Blockley, S.P.E., Blaauw, M., Ramsey, C.B., van der Plicht, J., 2007. Building and testing age models for radiocarbon dates in Lateglacial and Early Holocene sediments. Quaternary Science Reviews 26, 1915-1926.

Blockley, S.P.E., Lane, C.S., Hardiman, M., Rasmussen, S.O., Seierstad, I.K., Steffensen, J.P., Svensson, A., Lotter, A.F., Turney, C.S., Bronk Ramsey, C., 2011. Synchronisation of palaeoenvironmental records over the last 60,000 years, and an extended INTIMATE event stratigraphy to 48,000 b2k. Quaternary Science Reviews 36, 2-10.

Broecker, W.S., 1991. The great ocean conveyor. OCEANOGRAPHY 4, 79-89.

Brunelle, B.G., Sigman, D.M., Cook, M.S., Keigwin, L.D., Haug, G.H., Plessen, B., Schettler, G., Jaccard, S.L., 2007. Evidence from diatom-bound nitrogen isotopes for subarctic Pacific stratification during the last ice age and a link to North Pacific denitrification changes. Paleoceanography 22, PA1215.

Brunelle, B.G., Sigman, D.M., Jaccard, S.L., Keigwin, L.D., Plessen, B., Schettler, G., Cook, M.S., Haug, G.H., 2010. Glacial/interglacial changes in nutrient supply and stratification in the western subarctic North Pacific since the penultimate glacial maximum. Quaternary Science Reviews.

Bubenshchikova, N., Nuernberg, D., Lembke-Jene, L., Pavlova, G., 2008. Living benthic foraminifera of the Okhotsk Sea: Faunal composition, standing stocks and microhabitats. Marine Micropaleontology 69, 314-333.

Bubenshchikova, N.V., Nuernberg, D., Gorbarenko, S.A., Lembke-Jene, L., 2010. Variations of the Oxygen Minimum Zone of the Okhotsk Sea during the Last 50 ka as Indicated by Benthic Foraminiferal and Biogeochemical Data. Okeanologiya 50, 93-106.

Caissie, B.E., Brigham-Grette, J., Lawrence, K.T., Herbert, T.D., Cook, M.S., 2010. Last Glacial Maximum to Holocene sea surface conditions at Umnak Plateau, Bering Sea, as inferred from diatom, alkenone, and stable isotope records. Paleoceanography 25, PA1206-.

Chikamoto, M.O., Menviel, L., Abe-Ouchi, A., Ohgaito, R., Timmermann, A., Okazaki, Y., Harada, N., Oka, A., Mouchet, A., 2011. Variability in North Pacific intermediate and deep water ventilation during Heinrich events in two coupled climate models. Deep Sea Research Part II: Topical Studies in Oceanography.

Chlachula, J., 2003. The Siberian loess record and its significance for reconstruction of Pleistocene climate change in north-central Asia. Quaternary Science Reviews 22, 1879-1906.

Cook, M.S., Keigwin, L.D., Sancetta, C.A., 2005. The deglacial history of surface and intermediate water of the Bering Sea. Deep Sea Research Part II: Topical Studies in Oceanography 52, 2163-2173.

Craig, H., 1957. Isotopic standards for carbon and oxygen and correction factors for mass-spectrometric analysis of carbon dioxide. Geochimica Et Cosmochimica Acta 12, 133-149.

Crusius, J., Pedersen, T., Kienast, S., Keigwin, L., Labeyrie, L., 2004. Influence of northwest Pacific productivity on North Pacific Intermediate Water oxygen concentrations during the Boiling-Allerod interval (14.7-12.9 ka). Geology 32, 633-636.

Davies, M.H., Mix, A.C., Stoner, J.S., Addison, J.A., Jaeger, J., Finney, B., Wiest, J., 2011. The deglacial transition on the southeastern Alaska Margin: Meltwater input, sea level rise, marine productivity, and sedimentary anoxia. Paleoceanography 26, PA2223-.

Dean, W.E., Zheng, Y., Ortiz, J.D., Van Geen, A., 2006. Sediment Cd and Mo accumulation in the oxygen-minimum zone off western Baja California linked to global climate over the past 52 kyr. Paleoceanography 21, PA4209.

del Giorgio, P., Duarte, C., 2002. Respiration in the open ocean. Nature 420, 379-384.

DeMaster, D.J., 1981. Measuring biogenic silica in marine sediments and suspended matter, In: Hurd, D.C., Spenser, D.W. (Eds.), Marine Particles: Analysis and Characterization. American Geophysical Union, Washington, D. C., pp. 363–368.

Duce, R.A., Tindale, N.W., 1991. Atmospheric Transport of Iron and Its Deposition in the Ocean, Limnology and Oceanography, pp. 1715-1726.

Dullo, W., Biebow, N., 2004. SO178-KOMEX Cruise Report: Mass exchange processes and balances in the Okhotsk Sea, IFM-GEOMAR Report. IFM-GEOMAR, Kiel.

Duplessy, J., Arnold, M., Bard, E., JUILLETLECLERC, A., Kallel, N., Labeyrie, L., 1989. Ams C-14 Study of Transient Events and of the Ventilation Rate of the Pacific Intermediate Water During the Last Deglaciation, Radiocarbon, pp. 493-502.

Dykoski, C., Edwards, R., Cheng, H., Yuan, D., Cai, Y., Zhang, M., Lin, Y., Qing, J., An, Z., Revenaugh, J., 2005. A high-resolution, absolute-dated Holocene and deglacial Asian monsoon record from Dongge Cave, China. Earth And Planetary Science Letters 233, 71-86.

Emerson, S., Watanabe, Y.W., Ono, T., Mecking, S., 2004. Temporal trends in apparent oxygen utilization in the upper pycnocline of the North Pacific: 1980–2000. Journal Of Oceanography 60, 139-147.

Emile-Geay, J., Cane, M., Naik, N., Seager, R., Clement, A., Van Geen, A., 2003. Warren revisited: Atmospheric freshwater fluxes and "Why is no deep water formed in the North Pacific''. Journal Of Geophysical Research-Oceans 108, 3178.

Fukamachi, Y., Shirasawa, K., Polomoshnov, A.M., Ohshima, K.I., Kalinin, E., Nihashi, S., Melling, H., Mizuta, G., Wakatsuchi, M., 2009. Direct observations of sea-ice thickness and brine rejection off Sakhalin in the Sea of Okhotsk. Continental Shelf Research 29, 1541-1548.

Galbraith, E.D., Jaccard, S.L., Pedersen, T.F., Sigman, D.M., Haug, G.H., Cook, M., Southon, J.R., Francois, R., 2007. Carbon dioxide release from the North Pacific abyss during the last deglaciation. Nature 449, 890-U899.

Galbraith, E.D., Kienast, M., Jaccard, S.L., Pedersen, T.F., Brunelle, B.G., Sigman, D.M., Kiefer, T., 2008. Consistent relationship between global climate and surface nitrate utilization in the western subarctic Pacific throughout the last 500 ka. Paleoceanography 23, PA2212.

Garcia, H.E., Locarnini, R.A., Boyer, T.P., Antonov, J.I., Baranova, O.K., Zweng, M.M., Johnson, D.R., 2010a. World Ocean Atlas 2009, Volume 3: Dissolved Oxygen, Apparent Oxygen Utilization, and Oxygen Saturation. U.S. Government Printing Office, Washington, D.C.

Garcia, H.E., Locarnini, R.A., Boyer, T.P., Antonov, J.I., Baranova, O.K., Zweng, M.M., Johnson, D.R., 2010b. World Ocean Atlas 2009, Volume 4: Nutrients (phosphate, nitrate, silicate). U.S. Government Printing Office, Washington, D.C.

Gebhardt, H., Sarnthein, M., Grootes, P.M., Kiefer, T., Kuehn, H., Schmieder, F., Röhl, U., 2008. Paleonutrient and productivity records from the subarctic North Pacific for Pleistocene glacial terminations I to V. Paleoceanography 23, PA4212-.

Goes, J.I., Gomes, H.d.R., Limsakul, A., Saino, T., 2004. The influence of large-scale environmental changes on carbon export in the North Pacific Ocean using satellite and shipboard data. Deep Sea Research Part II: Topical Studies in Oceanography 51, 247-279.

Gorbarenko, S., Khusid, T.A., Basov, I., Oba, T., Southon, J., Koizumi, I., 2002. Glacial Holocene environment of the southeastern Okhotsk Sea: evidence from geochemical and palaeontological data. Palaeogeography Palaeoclimatology Palaeoecology 177, 237-263.

Gorbarenko, S., Southon, J., Keigwin, L., Cherepanova, M., Gvozdeva, I., 2004. Late Pleistocene-Holocene oceanographic variability in the Okhotsk Sea: geochemical, lithological and paleontological evidence. Palaeogeography Palaeoclimatology Palaeoecology 209, 281-301.

Gorbarenko, S.A., Goldberg, E.L.a.v., Kashgarian, M., Velivetskaya, T.a.y.A., Zakharkov, S.P., Pechnikov, V.S., Bosin, A.A.a.e., Psheneva, O.Y.a.e., Ivanova, E.D., 2007a. Millennium scale environment changes of the Okhotsk sea during last 80 kyr and their phase relationship with global climate changes. Journal Of Oceanography 63, 609-623.

Gorbarenko, S.A., Harada, N., Malakhov, M.I., Vasilenko, Y.P., Bosin, A.A., Gol'dberg, E.L., 2008. Millennial-scale climatic and environmental oscillations in the Sea of Okhotsk in response to global changes during the last 190 Ka. Doklady Earth Sciences 423, 1410-1413.

Gorbarenko, S.A., Harada, N., Malakhov, M.I., Velivetskaya, T.A., Vasilenko, Y.P., Bosin, A.A., Derkachev, A.N., Goldberg, E.L., d, A.V.I., 2012. Responses of the Okhotsk Sea environment and sedimentology to global climate changes at the orbital and millennial scale during the last 350 kyr. Deep-Sea Research II 61-64, 73-84.

Gorbarenko, S.A., Psheneva, O.Y., Artemova, A.V., Matul, A.G., Tiedemann, R., Nuernberg, D., 2010. Paleoenvironment changes in the NW Okhotsk Sea for the last 18 kyr determined with micropaleontological, geochemical, and lithological data. Deep Sea Research Part I: Oceanographic Research Papers 57, 797-811.

Gorbarenko, S.A., Tsoi, I.B., Astakhov, A.S., Artemova, A.V., Gvozdeva, I.G., Annin, V.K., 2007b. Paleoenvironmental changes in the northern shelf of the Sea of Okhotsk during the Holocene. Stratigraphy and Geological Correlation 15, 656-671.

Hansell, D.A., 2002. Dissolved organic carbon export with North Pacific Intermediate Water formation. Global Biogeochemical Cycles 16, 1007.

Harada, N., Sato, M., Sakamoto, T., 2008. Freshwater impacts recorded in tetraunsaturated alkenones and alkenone sea surface temperatures from the Okhotsk Sea across millennial-scale cycles. Paleoceanography 23, PA3201.

Harada, N., Sato, M., Seki, O., Timmermann, A., 2012. Sea surface temperature changes in the Okhotsk Sea and adjacent North Pacific during the last glacial maximum and deglaciation. … Sea Research Part II: ….

Harrison, P.J., Whitney, F.A., Tsuda, A., Saito, H., Tadokoro, K., 2004. Nutrient and Plankton Dynamics in the NE and NW Gyres of the Subarctic Pacific Ocean. Journal Of Oceanography 60, 93-117.

Hendy, I., Kennett, J., 2003. Tropical forcing of North Pacific intermediate water distribution during Late Quaternary rapid climate change? Quaternary Science Reviews 22, 673-689.

Herguera, J., Peltzer, E., Brewer, P., 2009. Benthic foraminifera habitats and carbon isotopes: new perspective from thermodynamic constrains on intermediate waters respiration. Geophysical Research Abstracts, 2009 EGU General Assembly 2009 11, EGU2009-3831.

Ikehara, K., Ohkushi, K.a.i., Shibahara, A., Hoshiba, M., 2006. Change of bottom water conditions at intermediate depths of the Oyashio region, NW Pacific over the past 20,000 yrs. Global And Planetary Change 53, 78-91.

Inagaki, M., Yamamoto, M., Igarashi, Y., Ikehara, K., 2009. Biomarker records from core GH02-1030 off Tokachi in the northwestern Pacific over the last 23,000 years: Environmental changes during the last deglaciation. Journal Of Oceanography 65, 847-858.

Itaki, T., Kim, S., Rella, S.F., Uchida, M., Tada, R., Khim, B.-K., 2012. Millennial-scale variations of late Pleistocene radiolarian assemblages in the Bering Sea related to environments in shallow and deep waters. Deep Sea Research Part II: Topical Studies in Oceanography 61-64, 127-144.

Itou, M., Ono, T., Noriki, S., 2003. Provenance of intermediate waters in the western North Pacific deduced from thermodynamic imprint on delta C-13 of DIC. Journal Of Geophysical Research-Oceans 108, 3347.

Jaccard, S., Haug, G.H., Sigman, D., Pedersen, T., Thierstein, H., Rohl, U., 2005. Glacial/interglacial changes in subarctic North Pacific stratification. Science (New York, NY) 308, 1003-1006.

Jaccard, S.L., Galbraith, E., 2013. Direct ventilation of the North Pacific did not reach the deep ocean during the last deglaciation. Geophysical Research Letters.

Jaccard, S.L., Galbraith, E.D., 2011. Large climate-driven changes of oceanic oxygen concentrations during the last deglaciation. Nature Geoscience 5, 151-156.

Jaccard, S.L., Galbraith, E.D., Sigman, D.M., Haug, G.H., 2010. A pervasive link between Antarctic ice core and subarctic Pacific sediment records over the past 800 kyrs. Quaternary Science Reviews 29, 206-212.

Jaccard, S.L., Galbraith, E.D., Sigman, D.M., Haug, G.H., Francois, R., Pedersen, T.F., Dulski, P., Thierstein, H.R., 2009. Subarctic Pacific evidence for a glacial deepening of the oceanic respired carbon pool. Earth And Planetary Science Letters 277, 156-165.

Jansen, J.H.F., Van der Gaast, S.J., Koster, B., Vaars, A.J., 1998. CORTEX, a shipboard XRF-scanner for element analyses in split sediment cores. Marine Geology 151, 143-153.

Keigwin, L., Jones, G., FROELICH, P., 1992. A 15,000 Year Paleoenvironmental Record from Meiji Seamount, far Northwestern Pacific. Earth And Planetary Science Letters 111, 425-440.

Khim, B., Sakamoto, T., 2012. Reconstruction of surface water conditions in the central region of the Okhotsk Sea during the last 180 kyrs. Deep Sea Research Part II: ….

Kienast, S., Hendy, I., Crusius, J., Pedersen, T., Calvert, S., 2004. Export production in the subarctic North Pacific over the last 800 kyrs: No evidence for iron fertilization? Journal Of Oceanography 60, 189-203.

Kitani, K., 1973. An oceanographic study of the Okhotsk Sea - particularly in regard to cold waters. Bull. Far Sear Fish. Res. Lab. 9, 45-76.

Klinkhammer, G.P., Mix, A.C., Haley, B.A., 2009. Increased dissolved terrestrial input to the coastal ocean during the last deglaciation. Geochemistry Geophysics Geosystems 10, -.

Kohfeld, K.E., Chase, Z., 2011. Controls on deglacial changes in biogenic fluxes in the North Pacific Ocean. Quaternary Science Reviews.

Kokfelt, U., 2003. An Analysis of Pollen, Spores and Chlorophycean Algae from the Sea of Okhotsk: Implications for Late Glacial and Holocene Climatic Change, Geomar & Geologisk Museum Copenhagen. Copenhagen, Kiel, p. 56.

Kuzmin, Y.V., Burr, G.S., Gorbunov, S.V., Rakov, V.A., Razjigaeva, N.G., 2007. A tale of two seas: Reservoir age correction values (R, Delta R) for the Sakhalin Island (Sea of Japan and Okhotsk Sea). Nuclear Instruments & Methods In Physics Research Section B-Beam Interactions With Materials And Atoms 259, 460-462.

Lam, P.J., Bishop, J.K.B., 2008. The continental margin is a key source of iron to the HNLC North Pacific Ocean. Geophysical Research Letters 35, L07608.

Mahowald, N., Baker, A., Bergametti, G., Brooks, N., Duce, R., Jickells, T., Kubilay, N., Prospero, J., Tegen, I., 2005. Atmospheric global dust cycle and iron inputs to the ocean. Global Biogeochemical Cycles 19, -.

Max, L., Lembke-Jene, L., Riethdorf, J.-R., Tiedemann, R., Nürnberg, D., submitted. Rapid changes in North Pacific Intermediate Water Formation during the Last Glacial Termination. Earth And Planetary Science Letters.

Max, L., Riethdorf, J.-R., Tiedemann, R., Smirnova, M., Lembke-Jene, L., Fahl, K., Nürnberg, D., Matul, A., Mollenhauer, G., 2012. Sea surface temperature variability and sea-ice extent in the subarctic northwest Pacific during the past 15,000 years. Paleoceanography 27, PA3213-.

McCorkle, D., Corliss, B., Farnham, C., 1997. Vertical distributions and stable isotopic compositions of live (stained) benthic foraminifera from the North Carolina and California continental margins. Deep Sea Research Part I: Oceanographic Research Papers 44, 983-1024.

McCorkle, D.C., Keigwin, L.D., 1994. Depth profiles of δ 13C in bottom water and core top C. wuellerstorfi on the Ontong Java Plateau and Emperor Seamounts. Paleoceanography 9, 197.

McKay, J., Pedersen, T., Kienast, S., 2004. Organic carbon accumulation over the last 16 kyr off Vancouver Island, Canada: evidence for increased marine productivity during the deglacial. Quaternary Science Reviews 23, 261-281.

McManus, J.F., Francois, R., Gherardi, J.-M., Keigwin, L.D., Brown-Leger, S., 2004. Collapse and rapid resumption of Atlantic meridional circulation linked to deglacial climate changes. Nature 428, 834-837.

Misumi, K., Tsumune, D., Yoshida, Y., Uchimoto, K., Nakamura, T., Nishioka, J., Mitsudera, H., Bryan, F.O., Lindsay, K., Moore, J.K., Doney, S.C., 2011. Mechanisms controlling dissolved iron distribution in the North Pacific: A model study. Journal of Geophysical Research 116.

Mix, A., Lund, D., Pisias, N., Boden, P., Bornmalm, L., Lyle, M., Pike, J., 1999. Rapid climate oscillations in the northeast Pacific during the last deglaciation reflect Northern and Southern Hemisphere sources. Mechanisms of Global Climate Change at Millennial Time Scales 112, 127–148.

Monnin, E., Indermuhle, A., Dallenbach, A., Flueckiger, J., Stauffer, B., Stocker, T., Raynaud, D., Barnola, J.-M., 2001. Atmospheric CO2 concentrations over the last glacial termination. Science (New York, NY) 291, 112-114.

Monnin, E., Steig, E.J., Siegenthaler, U., Kawamura, K., Schwander, J., Stauffer, B., Stocker, T.F., Morse, D.L., Barnola, J.-M., Bellier, B., 2004. Evidence for substantial accumulation rate variability in Antarctica during the Holocene, through synchronization of CO2 in the Taylor Dome, Dome C and DML ice cores. Earth And Planetary Science Letters 224, 45-54.

Müller, P.J., Schneider, R., 1993. An automated leaching method for the determination of opal in sediments and particulate matter. Deep Sea Research Part I: Oceanographic Research Papers 40, 425-444.

Nadeau, M.-J., Grootes, P.M., Schleicher, M., Hasselberg, P., Rieck, A., Bitterling, M., 1998. Sample throughput and data quality at the Leibniz-Labor AMS facility. Radiocarbon 40 (1), 239-245. 40, 239-245.

Nadeau, M.-J., Schleicher, M., Grootes, P.M., Erlenkeuser, H., Gottdang, A., Mous, D.J.W., Sarnthein, M., Willkomm, H., 1997. The Leibniz-Labor AMS facility at the Christian-Albrechts University, Kiel, Germany. Nuclear Instruments and Methods in Physics Research Section B 123, 22-30.

Nakatsuka, T., Fujimune, T., Yoshikawa, C., Noriki, S., Kawamura, K., Fukamachi, Y., Mizuta, G., Wakatsuchi, M., 2004a. Biogenic and lithogenic particle fluxes in the western region of the Sea of Okhotsk: Implications for lateral material transport and biological productivity. Journal Of Geophysical Research-Oceans 109, C09S13.

Nakatsuka, T., Nishioka, J., Shiraiwa, T., Project, a.m.o.t.A.-O., 2009. Biogeochemical linkage between Amur River basin and western subarctic Pacific by iron transport through Okhotsk Sea Intermediate Water: A new paradigm to explain changes in ocean primary productivity, PICES scientific report, p. 48.

Nakatsuka, T., Toda, M., Kawamura, K., Wakatsuchi, M., 2004b. Dissolved and particulate organic carbon in the Sea of Okhotsk: Transport from continental shelf to ocean interior. Journal Of Geophysical Research-Oceans 109, C09S14.

Nakatsuka, T., Yoshikawa, C., Toda, M., Kawamura, K., Wakatsuchi, M., 2002. An extremely turbid intermediate water in the Sea of Okhotsk: Implication for the transport of particulate organic matter in a seasonally ice-bound sea. Geophysical Research Letters 29, 1757.

Nishioka, J., Ono, T., Saito, H., Nakatsuka, T., Takeda, S., Yoshimura, T., Suzuki, K., Kuma, K., Nakabayashi, S., Tsumune, D., Mitsudera, H., Johnson, W.K., Tsuda, A., 2007. Iron supply to the western subarctic Pacific: Importance of iron export from the Sea of Okhotsk. Journal Of Geophysical Research-Oceans 112, -.

Nishioka, J., Ono, T., Saito, H., Sakaoka, K., Yoshimura, T., 2011. Oceanic iron supply mechanisms which support the spring diatom bloom in the Oyashio region, western subarctic Pacific. Journal Of Geophysical Research-Oceans 116, -.

Nishioka, J., Takeda, S., Kudo, I., Tsumune, D., Yoshimura, T., Kuma, K., Tsuda, A., 2003. Size-fractionated iron distributions and iron-limitation processes in the subarctic NW Pacific. Geophysical Research Letters 30, -.

Nürnberg, D., Dethleff, D., Tiedemann, R., Kaiser, A., Gorbarenko, S.A., 2011. Okhotsk Sea ice coverage and Kamchatka glaciation over the last 350ka — Evidence from ice-rafted debris and planktonic δ 18O. Palaeogeography Palaeoclimatology Palaeoecology 310, 191-205.

Nürnberg, D., Tiedemann, R., 2004. Environmental change in the Sea of Okhotsk during the last 1.1 million years. Paleoceanography 19, PA4011.

Ogi, M., Tachibana, Y., Nishio, F., Danchenkov, M., 2001. Does the fresh water supply from the Amur river flowing into the sea of Okhotsk affect sea ice formation? Journal Of The Meteorological Society Of Japan 79, 123-129.

Ohkushi, K., 2004. Glacial intermediate water ventilation in the northwestern Pacific based on AMS radiocarbon dating. Nuclear Instruments & Methods In Physics Research Section B: Beam Interactions With Materials And Atoms 223-224, 460-465.

Ohkushi, K., Itaki, T., Nemoto, N., 2003. Last Glacial-Holocene change in intermediate-water ventilation in the Northwestern Pacific. Quaternary Science Reviews 22, 1477-1484.

Okazaki, Y., Sagawa, T., Asahi, H., Horikawa, K., Onodera, J., 2012. Ventilation changes in the western North Pacific since the last glacial period. Climate Of The Past 8, 17-24.

Okazaki, Y., Timmermann, A., Menviel, L., Harada, N., Abe-Ouchi, A., Chikamoto, M.O., Mouchet, A., Asahi, H., 2010. Deepwater formation in the North Pacific during the Last Glacial Termination. Science (New York, NY) 329, 200-204.

Peterse, F., Prins, M.A., Beets, C.J., Troelstra, S.R., Zheng, H., Gu, Z., Schouten, S., Damste, J.S.S., 2011. Decoupled warming and monsoon precipitation in East Asia over the last deglaciation. Earth And Planetary Science Letters 301, 256-264.

Piotrowski, A.M., Goldstein, S.L., Hemming, S.R., Fairbanks, R.G., 2004. Intensification and variability of ocean thermohaline circulation through the last deglaciation. Earth And Planetary Science Letters 225, 205-220.

Rasmussen, S.O., Seierstad, I.K., Andersen, K.K., Bigler, M., Dahl-Jensen, D., Johnsen, S.J., 2008. Synchronization of the NGRIP, GRIP, and GISP2 ice cores across MIS 2 and palaeoclimatic implications. Quaternary Science Reviews 27, 18-28.

Reid, J.L., 1965. Intermediate Waters of the Pacific Ocean, The Johns Hopkins Oceanographic Studies. The Johns Hopkins Press, Baltimore, pp. 1-85.

Reimer, P.J., Baillie, M.G.L., Bard, E., Bayliss, A., Beck, J.W., Blackwell, P.G., Ramsey, C.B., Buck, C.E., Burr, G.S., Edwards, R.L., Friedrich, M., Grootes, P.M., Guilderson, T.P., Hajdas, I., Heaton, T.J., Hogg, A.G., Hughen, K.A., Kaiser, K.F., Kromer, B., McCormac, F.G., Manning, S.W., Reimer, R.W., Richards, D.A., Southon, J.R., Talamo, S., Turney, C.S.M., van der Plicht, J., Weyhenmeye, C.E., 2009. INTCAL09 and MARINE09 Radiocarbon Age Calibration Curves , 0-50,000 Years cal. BP. Radiocarbon 51, 1111-1150.

Richter, T.O., van der Gaast, S., Koster, B., Vaars, A., Gieles, R., de Stigter, H.C., De Haas, H., van Weering, T.C.E., 2006. The Avaatech XRF Core Scanner: technical description and applications to NE Atlantic

sediments, In: Rothwell, R.G. (Ed.), New Techniques n Sediment Core Analysis. Geological Society, London, Special Publications. Geological Society, Special Publications, London, pp. 39-50.

Riethdorf, J.-R., Max, L., Nürnberg, D., Lembke-Jene, L., Tiedemann, R., 2013. Deglacial history of (sub) sea surface temperatures and salinity in the subarctic NW Pacific: Implications for upper-ocean stratification. Paleoceanography.

Röhl, U., Abrams, L.J., 2000. High-resolution, downhole, and nondestructive core measurements from Sites 999 and 1001 in the Caribbean Sea: application to the Late Paleocene Thermal Maximum, In: Leckie, R.M., Sigurdsson, H., Acton, G.D., Draper, G. (Eds.), Proceedings of the Ocean Drilling Program, Scientific Results, College Station, TX (Ocean Drilling Program). Ocean Drilling Program, College Station, TX.

Rohling, E.J., Grant, K., Bolshaw, M., Roberts, A.P., Siddall, M., Hemleben, C., Kucera, M., 2009. Antarctic temperature and global sea level closely coupled over the past five glacial cycles. Nature Geoscience 2, 500-504.

Sagawa, T., Ikehara, K., 2008. Intermediate water ventilation change in the subarctic northwest Pacific during the last deglaciation. Geophysical Research Letters 35, L24702.

Sakaguchi, Y., 1992. Cooling Around 9000 BP Caused by Permafrost Melt Water Burst. Bull. Dept. Geogr. Univ. Tokyo 24, 1-6.

Sakamoto, T., Ikehara, M., Aoki, K., Iijima, K., Kimura, N., Nakatsuka, T., Wakatsuchi, M., 2005. Ice-rafted debris (IRD)-based sea-ice expansion events during the past 100kyrs in the Okhotsk Sea. Deep Sea Research Part II: Topical Studies in Oceanography 52, 2275-2301.

Sarnthein, M., Grootes, P.M., Kennett, J.P., Nadeau, M., Schmittner, A., Chiang, J., Hemming, S., 2007. 14C Reservoir Ages Show Deglacial Changes in Ocean Currents and Carbon Cycle, Ocean Circulation: Mechanisms and Impacts, AGU Geophysical Monograph Series. American Geophysical Union, pp. 175-196.

Schlitzer, R., 2002. Interactive analysis and visualization of geoscience data with Ocean Data View. Computers & Geosciences 28, 1211-1218.

Seki, O., Harada, N., Sato, M., Kawamura, K., Ijiri, A., Nakatsuka, T., 2012. Assessment for paleoclimatic utility of terrestrial biomarker records in the Okhotsk Sea sediments. Deep Sea Research Part II: Topical Studies in Oceanography 61-64, 85-92.

Seki, O., Ikehara, M., Kawamura, K., Nakatsuka, T., Ohnishi, K., Wakatsuchi, M., Narita, H., Sakamoto, T., 2004. Reconstruction of paleoproductivity in the Sea of Okhotsk over the last 30 kyr. Paleoceanography 19, PA1016.

Seki, O., Kawamura, K., Nakatsuka, T., Ohnishi, K., Ikehara, M., Wakatsuchi, M., 2003. Sediment core profiles of long-chain n-alkanes in the Sea of Okhotsk: Enhanced transport of terrestrial organic matter from the last deglaciation to the early Holocene. Geophysical Research Letters 30, 1001.

Seki, O., Meyers, P.A., Kawamura, K., Zheng, Y., Zhou, W., 2009a. Hydrogen isotopic ratios of plant wax n-alkanes in a peat bog deposited in northeast China during the last 16 kyr. Organic Geochemistry 40, 671-677.

Seki, O., Sakamoto, T., Sakai, S., Schouten, S., Hopmans, E.C., Damste, J.S.S., Pancost, R.D., 2009b. Large changes in seasonal sea ice distribution and productivity in the Sea of Okhotsk during the deglaciations. Geochemistry Geophysics Geosystems 10, Q10007.

Shcherbina, A., Talley, L., Rudnick, D., 2004. Dense water formation on the northwestern shelf of the Okhotsk Sea: 1. Direct observations of brine rejection. Journal Of Geophysical Research-Oceans 109, C09S08.

Shimizu, Y., IWAO, T., Yasuda, I., Ito, S., Watanabe, T., Uehara, K., Shikama, N., Nakano, T., 2004. Formation process of North Pacific intermediate water revealed by profiling floats set to drift on 26.7 sigma(theta) isopycnal surface. Journal Of Oceanography 60, 453-462.

Southon, J., Noronha, A.L., Cheng, H., Edwards, R.L., Wang, Y., 2012. A high-resolution record of atmospheric 14C based on Hulu Cave speleothem H82, Quaternary Science Reviews, pp. 32-41.

Stuiver, M., Polach, H., 1977. Discussion: Reporting of 14C Data. Radiocarbon 19, 355-363.

Stuiver, M., Reimer, P.J., 1993. Extended 14C database and revised CALIB radiocarbon calibration program. Radiocarbon 35, 215-230.

Svensson, A., Andersen, K.K., Bigler, M., Clausen, H.B., Dahl-Jensen, D., Davies, S.M., Johnsen, S.J., Muscheler, R., Parrenin, F., Rasmussen, S.O., Roethlisberger, R., Seierstad, I., Steffensen, J.P., Vinther, B.M., 2008. A 60 000 year Greenland stratigraphic ice core chronology. Climate Of The Past 4, 47-57.

Tachibana, Y., Oshima, K., Ogi, M., 2008. Seasonal and interannual variations of Amur River discharge and their relationships to large-scale atmospheric patterns and moisture fluxes. Journal of Geophysical Research-Atmospheres 113, D16102.

Tadokoro, K., Ono, T., Yasuda, I., Osafune, S., Shiomoto, A., Sugisaki, H., 2009. Possible mechanisms of decadal‐scale variation in PO 4concentration in the western North Pacific. Geophysical Research Letters 36, L08606-.

Takahashi, T., Sutherland, S.C., Wanninkhof, R., Sweeney, C., Feely, R.A., Chipman, D.W., Hales, B., Friederich, G., Chavez, F., Sabine, C., Watson, A., Bakker, D.C.E., Schuster, U., Metzl, N., Yoshikawa-Inoue, H., Ishii, M., Midorikawa, T., Nojiri, Y., Körtzinger, A., Steinhoff, T., Hoppema, M., Olafsson, J., Arnarson, T.S., Tilbrook, B., Johannessen, T., Olsen, A., Bellerby, R., Wong, C.S., Delille, B., Bates, N.R., De Baar, H.J.W., 2009. Climatological mean and decadal change in surface ocean pCO2, and net sea–air CO2 flux over the global oceans. Deep Sea Research Part II: Topical Studies in Oceanography 56, 554-577.

Takeda, S., 2011. Iron and Phytoplankton Growth in the Subarctic North Pacific. Aqua-BioScience Monographs 4, 41-93.

Talley, L.D., 1993. Distribution and formation of North Pacific intermediate water. Journal Of Physical Oceanography 23, 517-537.

Ternois, Y., Kawamura, K., Keigwin, L., Ohkouchi, N., Nakatsuka, T., 2001. A biomarker approach for assessing marine and terrigenous inputs to the sediments of Sea of Okhotsk for the last 27,000 years. Geochimica Et Cosmochimica Acta 65, 791-802.

Tjallingii, R., 2006. Application and quality of X-ray fluorescence core scanning in reconstructing late Pleistocene NW African continental margin sedimentation patterns and paleoclimate variations, In: Wefer, G., Stein, R. (Eds.), Fachbereich Geowissenschaften. Universität Bremen, Bremen, p. 114.

Vaks, A., Gutareva, O.S., Breitenbach, S.F.M., Avirmed, E., Mason, A.J., Thomas, A.L., Osinzev, A.V., Kononov, A.M., Henderson, G.M., 2013. Speleothems Reveal 500,000-Year History of Siberian Permafrost. Science (New York, NY).

Van Geen, A., Zheng, Y., Bernhard, J., Cannariato, K., Carriquiry, J., Dean, W., Eakins, B., Ortiz, J., Pike, J., 2003. On the preservation of laminated sediments along the western margin of North America. Paleoceanography 18, 1098.

Verardo, D.J., Froelich, P.N., McIntyre, A., 1990. Determination of organic carbon and nitrogen in marine sediments using the Carlo Erba NA-1500 analyzer. Deep Sea Research Part A. Oceanographic Research Papers 37, 157-165.

Wang, Y., Cheng, H., Edwards, R., He, Y., Kong, X., An, Z., Wu, J., Kelly, M., Dykoski, C., Li, X., 2005. The Holocene Asian monsoon: Links to solar changes and North Atlantic climate. Science (New York, NY) 308, 854-857.

Wang, Y., Cheng, H., Edwards, R.L., Kong, X., Shao, X., Chen, S., Wu, J., Jiang, X., Wang, X., An, Z., 2008. Millennial- and orbital-scale changes in the East Asian monsoon over the past 224,000|[thinsp]|years. Nature 451, 1090-1093.

Warren, B., 1983. Why is no deep water formed in the North Pacific? Journal of Marine Research 41, 327-347.

Watanabe, T., Wakatsuchi, M., 1998. Formation of 26.8–26.9 σ θwater in the Kuril Basin of the Sea of Okhotsk as a possible origin of North Pacific Intermediate Water. Journal of Geophysical Research 103, 2849-2865.

Weltje, G.J., Tjallingii, R., 2008. Calibration of XRF core scanners for quantitative geochemical logging of sediment cores: Theory and application. Earth And Planetary Science Letters 274, 423-438.

Yamamoto, M., Suemune, R., Oba, T., 2005. Equatorward shift of the subarctic boundary in the northwestern Pacific during the last deglaciation. Geophysical Research Letters 32, L05609.

Yamashita, Y., Cory, R.M., Nishioka, J., Kuma, K., Tanoue, E., Jaffé, R., 2010. Fluorescence characteristics of dissolved organic matter in the deep waters of the Okhotsk Sea and the northwestern North Pacific Ocean. Deep Sea Research Part II: Topical Studies in Oceanography 57, 1478-1485.

Yasuda, I., OKUDA, K., Shimizu, Y., 1996. Distribution and modification of North Pacific Intermediate Water in the Kuroshio-Oyashio interfrontal zone. Journal Of Physical Oceanography 26, 448-465.

Yoshikawa, C., Nakatsuka, T., Wakatsuchi, M., 2006. Distribution of N* in the Sea of Okhotsk and its use as a biogeochemical tracer of the Okhotsk Sea Intermediate Water formation process. Journal Of Marine Systems 63, 49-62.

Zheng, Y., Van Geen, A., Anderson, R., Gardner, J., Dean, W., 2000. Intensification of the northeast Pacific oxygen minimum zone during the Bolling-Allerod warm period. Paleoceanography 15, 528-536.

Supplementary Material:

Table S1: AMS ^{14}C data of cores used in this study

sample ID	depth[1] (cm)	species	^{14}C age (^{14}C yr)	dev.+ /-	ΔR (14C yr)[3]	Age 2σ range (cal. yr BP)
LV29-79-3						
KIA 21954	57.5	N. pachyderma (s)	2435	30	500	1340-1630
KIA 20964	82.5	N. pachyderma (s)	2570	35	500	1500-1810
KIA 21955	282.5	N. pachyderma (s)	5530	40	500	5260-5550
KIA 21956	372.5	N. pachyderma (s)	6665	50	500	6430-6770
KIA 22450	507.5	N. pachyderma (s)	8925	55	500	8790-9260
KIA 21957	581.5	N. pachyderma (s)	9400	80	500	9390-9870
KIA 20965	606.5	N. pachyderma (s)	9940	55	500	10160-10480
KIA 21958	656.5	N. pachyderma (s)	10305	50	500	10520-11000
KIA 21959	701.5	N. pachyderma (s)	10595	50	500	10810-11230
KIA 20966	772.5	N. pachyderma (s)	10780	60	500	11140-11630
KIA 21960	992.5	Mollusk	13330	90	1000 (500)	13270-14520
SO178-13-6						
KIA27537	371	Mollusk	5520	35	1000 (500)	4,420-4,970
KIA30872	1682.5	N. pachyderma (s)	10560	50	500	10,780-11,200
BETA (LM)	1682.5	benthic foram.	10830			
KIA27538	1973	Mollusk Fragm.	13240	70	1000 (500)	13,220-14,130
KIA30869	2072.5	mix planktics	13390	100	500	14,090-15,090
BETA (LM)	2072.5	benthic foram.	13760			
UCIAMS109675	2250.5	N. pachyderma (s)	14220	45	500	15,610-16,810
BETA (LM)	2250.5	benthic foram.	14580			
UCIAMS109674	2342.5	N. pachyderma (s)	15090	60	500	16,940-17,590
BETA (LM)	2342.5	benthic foram.	15470			
LV28-4-4						
KIA13839	5.5	N. pachyderma (s)	**1065**	30	500	0-300
KIA14648	62.5	N. pachyderma (s)	**1730**	30	500	670-900
KIA14654	165.5	N. pachyderma (s)	**2655**	30	500	1,590-1,890
KIA13844	285.5	N. pachyderma (s)	**3080**	50	500	
KIA13845	465.5	N. pachyderma (s)	**4600**	40	500	3,960-4,360
LJT-1	500.5	N. pachyderma (s)	**4790**	70	500	4,150-4,670
LJT-2	505.5	N. pachyderma (s)	**4930**	120	500	4,230-4,910
LJT-3	595.5	N. pachyderma (s)	**6010**	55	500	5,710-6,100
KIA16839	610.5	N. pachyderma (s)	**6380**	40	500	6,120-6,480
LJT-4	700.5	N. pachyderma (s)	**7640**	70	500	7,450-7,790
KIA14346	715.5	Mollusk	**8430**	100	1000 (500)	7,570-8,260
KIA13846	800.5	N. pachyderma (s)	**9155**	55	500	9,120-9,480
KIA13842	850.5	Mollusk	**11030**	55	1000 (500)	10,490-11,640
KIA14347	885.5	Mollusk	**12890**	80	1000 (500)	12,890-13,780
LJT-5	900.5	Mollusk	**13580**	80		
KIA20305	910.5	N. pachyderma (s)	**13840**	90	500	15,040-16,320
KIA14348	925.5	Gastropod	**14310**	140		
Water Samples (depth is water depth in m)						
KIA10312	297	water DIC	**335**	25		
KIA10315	495	water DIC	**615**	25		
KIA10313	685	water DIC	**920**	55		
KIA10314	1544	water DIC	**1850**	30		

[1] core or sample depth in sediment

[2] PMC is percent modern carbon according to conventions of Stuiver and Polach (1977)

[3] Errors of ±50 ^{14}C yr for planktic and ±100/±200 for benthic organisms, respectively.

Table S2: Compilation of ^{14}C ages from other studies used for Paleoventilation (B-P age) calculations.

Core depth (cm)	Calendar age (cal. yr. BP)	Planktic ^{14}C age (^{14}C yr)	±1 s (yr)	Benthic ^{14}C age (^{14}C yr)	±1s (yr)	BF – PF (yr)	Reference
North Pacific off Shimokita (Japan margin)							
CH84-14 (978 m)							
230	10340	10000	140	10850	140	850	Duplessy et al. (1989)
280	10640	10230	140	11060	150	830	
310	11190	10640	150	11370	130	730	
340	11550	10870	150	11630	180	760	
400	13140	12180	160	13200	150	1020	
480	13760	12750	150	13930	220	1180	
510	14210	13060	140	13500	200	440	
550	15550	13830	150	14140	200	310	
690	17840	15570	210	15940	190	370	
GH02-1030 (1212 m)							
210	10130	9840	40	10700	70	860	Ikehara (2006)
220	10660	10240	60	10800	70	560	Sagawa & Ikehara (2008)
235	10990	10510	60	11190	60	680	
244	11260	10690	60	11370	60	680	(not shown in Fig. 4)
261	11650	10950	60	11610	70	660	but similar features
290	13940	12900	70	13510	80	610	
323.5	14190	13060	70	14500	50	1440	
345.5	14780	13470	40	14160	40	690	
435.5	17250	15010	80	16010	90	1000	
465.5	17370	15140	60	16140	80	1000	
523	18690	16380	60	17230	100	850	
558	20050	17780	70	18730	120	950	
630	21770	19130	180	20590	180	1460	
MR01K03-PC4/5 (water depth 1366 m)							
231	11120	10600	50	11370	50	770	Ahagon et al. (2003)
262	11590	10900	55	11930	60	1030	Hoshiba et al. (2006)
291	12260	11420	60	12600	50	1180	
311	13190	12230	50	13650	100	1420	
363	14760	13450	85	14250	120	800	
405	16030	14150	55	14830	60	680	
540	18760	16450	110	17650	100	1200	
642	20640	18200	65	19650	110	1450	
MD012420 (water depth 2101 m)							
70.1-72.5	2656	3010	25	4560	35	1550	Okazaki et al (2012)
233.4-238.2	8246	7880	40	9020	50	1140	
298.5-302.6	10262	9530	40	10800	65	1270	
339.2-344.1	11852	10700	55	12100	50	1400	
353.8-358.6	12484	11150	55	12400	65	1250	
370.7-375.6	13023	11717	88	13050	60	1333	
382.9-385.3	13497	12150	50	13450	65	1300	
390.1-392.6	13725	12400	45	13750	55	1350	
404.7-407.1	15040	13258	141	14600	60	1342	
419.2-421.6	15632	13510	113	14750	55	1240	
431.3-433.7	16386	13900	50	15250	60	1350	
451.6-454.1	17281	14696	70	15850	65	1154	
489.2-494.2	19132	16457	141	18000	75	1543	
504.1-506.6	19675	17020	50	18350	70	1330	
600.2-602.1	22745	19555	60	21100	100	1545	
Okhotsk Sea (Sakhalin margin)							
LV28-4-4 (674m) / SO178-13-6 (673 m)							
595.5	5890	6010	55	6540	60	530	LV28-4-4
2072.5	14560	13390	100	13760		370	SO178-13-6
910.5	15526	13840	90	14020	200	180	LV28-4-4 (interpolated)
2250.5	16420	14220	45	14580		360	SO178-13-6
2342.5	17260	15090	60	15470		380	SO178-13-6
LV27-2-4 (1306/1312 m)							
170	3523	4205	15	5115	15	910	Gorbarenko (2010)
250	6017	6230	15	7135	20	905	
330	9133	9150	15	10125	20	975	
425	11094	10760	35	11555	25	795	
247	13790	12760	50	13740	50	980	Gorbarenko et al. (2007)
254	14230	13000	60	14230	60	1230	
585	14280	13150	25	14050	40	900	

Figure S1: Downcore records of chlorin contents against respective core depths (in cm b. sf.) used for inter-core correlation. From top to bottom: SO178-13-6 (upper depth scale), LV29-79-3 and LV28-4-4 (lower depth scales). Arrows in the cores' colors denote the AMS ^{14}C measurements for each core (see Table S1 and S2 for details). Correlation lines for transfers of ages to core SO178-13-6 are shown as dashed lines.

This figure is shown in this thesis already in Chapter 4 and thus not repeated here.

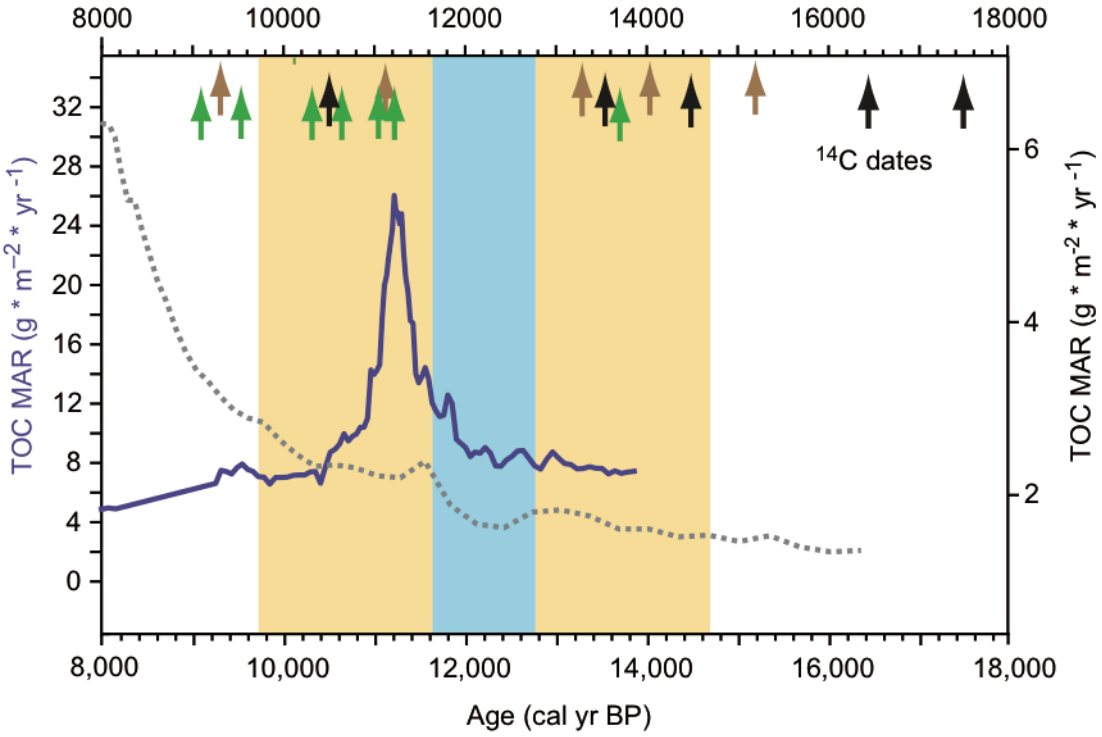

Fig. S2: Comparison of TOC accumulation rates ($g*m^{-2}*yr^{-1}$) for cores 4 and 79.

6. A Mid-Holocene Shift and Millennial-Scale Variations in Mesopelagic North Pacific Ventilation

Lester Lembke-Jene, Ralf Tiedemann, Dirk Nürnberg

(1) Alfred Wegener Institut Helmholtz-Zentrum für Polar- und Meeresforschung, Bremerhaven, Germany

(2) GEOMAR Helmholtz Zentrum für Ozeanforschung, Kiel, Germany

Manuscript for submission to Nature Geoscience (Letter)

The modern North Pacific hosts the largest Oxygen Minimum Zone (OMZ) in the World Ocean(Karstensen et al., 2008). Under future warming, such OMZs are projected to intensify, with severe consequences for ecosystems, marine biogeochemical cycles, and commercial fisheries(Keeling et al., 2010). At present, ventilation of subarctic North Pacific mid-depth water helps to prevent more pronounced OMZ development, but instrumental datasets show decreasing dissolved oxygen concentrations linked to increasing temperatures on decadal timescales(Emerson et al., 2004; Nakanowatari et al., 2007). However, long-term natural variations in O_2 supply to mesopelagic waters are large and prevent precise assessments of ventilation changes by anthropogenic influence against millennial-scale natural background shifts. Here we show that during the Holocene, modern levels of mid-depth North Pacific ventilation are a relatively recent feature of only the last 2,000 years. During the warmer than present early-mid Holocene periods, average O_2 supply was strongly reduced by an estimated 30-50% and featured millennial-scale variations attributed to solar forcing. Our proxy evidence from the Okhotsk Sea, the foremost modern North Pacific ventilation region, implies a close long-term coupling between ventilation and sea surface temperatures, extending this relationship beyond short instrumental timescales. Under past warmer than present conditions, the Okhotsk Sea switched its role from an "O_2 source" to an "O_2 sink" through increased remineralization of organic matter and inhibited ventilation processes with likely consequences for biogeochemical cycles. Our results provide guidance how mesopelagic North Pacific long-term O_2 concentrations might transform under future warming scenarios.

Intermediate waters in the subarctic North Pacific marginal seas play a critical role in supplying oxygen to the North Pacific Oxygen Minimum Zone(Emerson et al., 2004). Recent studies point to decreasing O_2 and increasing temperatures of the mesopelagic North Pacific over the past decades(Nakanowatari et al., 2007). The cause of these changes, however, is hard to unambiguously attribute to either anthropogenic influences or alternatively long-term natural variability, as the latter occur on timescales beyond the reach of instrumental datasets. One decisive factor that today prevents the development of more widespread oxygen limitation is the supply of dissolved oxygen to the mesopelagic water layer via ventilation of subarctic waters. In the North Pacific this ventilation is restricted to marginal seas, where density layers of intermediate waters outcrop in the surface ocean(Reid, 1965)(Fig. 1a, suppl. fig. S1). Today, the Okhotsk Sea constitutes the most important region with active ventilation during the wintertime sea ice season, when polynias open up on the Northeastern shelf areas and dense, O_2-enriched water masses form through brine rejection(Shcherbina et al., 2003b) that are subsequently exported to the open North Pacific as Okhotsk Sea Intermediate Water (OSIW) and ventilate the mid-depth North Pacific(Talley, 1993). This provision of oxygen by OSIW counteracts the occurrence of more widespread hypoxia over vast stretches of the mid-depth North Pacific and is expressed in higher $\delta^{13}C_{DIC}$ values of OSIW compared to precursor Western Subarctic Pacific Gyre Water (Fig 1, Suppl. fig. S1). As the Okhotsk Sea represents a global anomaly in being the world ocean's lowermost latitude where seasonal sea ice occurs, it responds with high sensitivity to changes in climate forcing in short response times(Hill et al., 2003). Previous works are mostly limited to OSIW and connected North Pacific changes during recent glacial periods(Gorbarenko et al., 2012; Keigwin, 1998a). Few studies have addressed paleo-environmental changes in the Okhotsk Sea over warm episodes like the current Holocene(Gorbarenko et al., 2010b; Itaki and Ikehara, 2004).

We here present the first high-resolution proxy records for Holocene changes in OSIW ventilation, using stable carbon isotope ratios of the epibenthic foraminifer *C. mundulus*, which is known to reliably record the $\delta^{13}C$ of $\sum CO_2$ in the bottom water mass it lives in(McCorkle and Keigwin, 1994). Changes in $\delta^{13}C$ of this dissolved inorganic carbon in turn are linearly correlated to water nutrient and oxygen concentrations in the Okhotsk Sea (Bauch et al., 2002) (supplementary text and Fig. S3). We use a suite of four AMS ^{14}C-dated sediment cores to reconstruct OSIW ventilation (supplement, table S1, fig. S1-S2 for age models). Site 44 was retrieved from the Kamchatka continental margin (52°02.514' N, 153°05.959' E, 684 m water depth) along the pathway of inflowing North Pacific water to the formation region of OSIW on the NE continental shelf. This core thus records the precursor water, mainly Western Subarctic Pacific Water (WSAPW), delivered via the East Kamchatka Current to the Okhotsk Sea (Fig. 1). Three sites are used to reconstruct changes in newly

formed OSIW on the eastern Sakhalin continental margin along the export pathway into the North Pacific. Sites 78 (52°40.388' N, 144°42.203' E, 673 m water depth) and 4 (51°08.475' N, 145°18.582' N, 674 m) are within the core layer of OSIW (Biebow and Hütten, 1999; Biebow et al., 2002b). Site 79 (52°47.272' N, 144°57.318' E, 1082 m) complements the records with a deeper location at the lower boundary of OSIW to Pacific Deep Water.

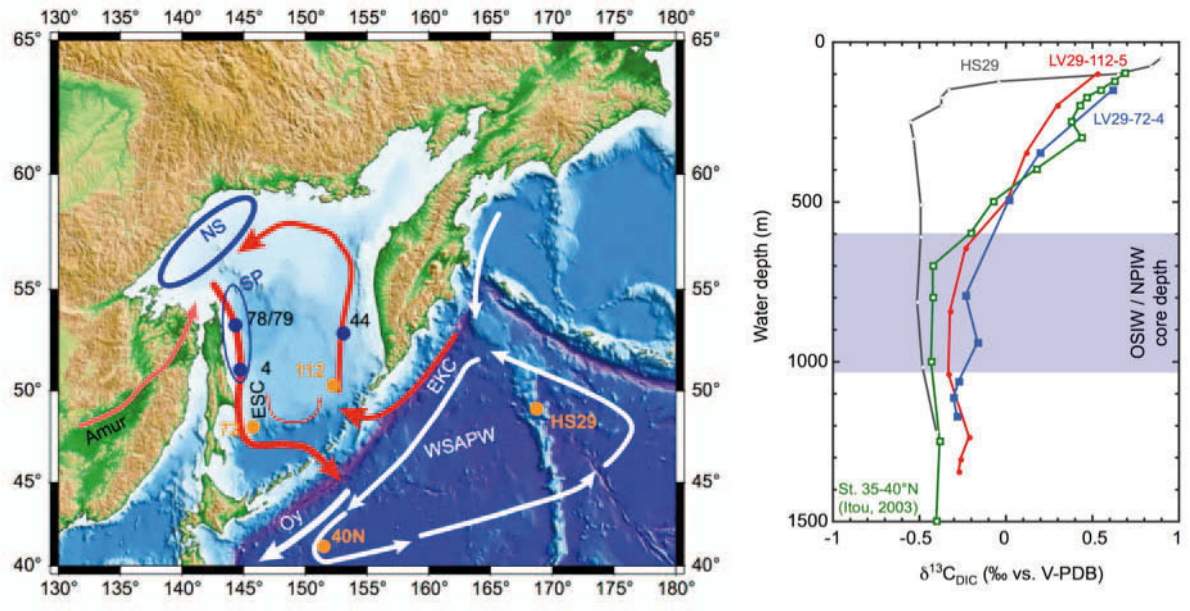

Figure 6.1: Study area, modern circulation patterns and oceanographic characteristics of the study region. a) Bathymetric map with major currents, core locations. Cores are marked in abbreviated number form, for full station information please see text. Abbreviations as follows: NS – Northern Shelf Polynia, SP – Sakhalin Polynia, ESC – East Sakhalin Current, EKC – East Kamchatka Current, WSAPW – Western Subarctic Pacific Gyre Water, Oy – Oyashio. b) Vertical profiles of modern water $\delta^{13}C_{DIC}$ characteristics for the Okhotsk Sea and North Pacific. Station HS29 (black, open circles) records WSAPW before it enters the Okhotsk Sea(Keigwin, 1998a), Station 112 represents Okhotsk Sea Intermediate Water before it is transported to the ventilation areas on the Northern Shelf (red, filled circles, this study), Station 72 monitors the OSIW path "downstream" of the ventilation area before export into the North Pacific (blue, filled squares, this study). Station 40N(Itou et al., 2003) represents final water mix in a southerly position near Kuroshio-Oyashio Extension Region (green, open squares), where new NPIW is formed(Talley, 1993). Note gradient between WSAPW, OSIW before and after ventilation, and resulting change in NPIW (intermediate water core layer: light blue shaded area).

The Sakhalin margin cores that monitor OSIW are characterized by relatively high-amplitude variations on millennial timescales that exceed common glacial-interglacial changes in Pacific deepwater ventilation(Keigwin, 1998a), with values between -0.8‰ and -0.1 ‰ and a close

resemblance between single cores. Sample resolution in deeper core 79 is worse than in shallower cores, but the $\delta^{13}C$ signal matches the former, except for an interval between 3-3.5 ka, probably due to a shoaling of the OSIW and ventilation not extending down to 1000 m. In contrast, the Kamchatka margin core 44, representing WSAPW inflow, shows $\delta^{13}C$ values ranging mostly only between -0.2 and -0,4 ‰, rather similar to modern values (Bauch et al., 2002), with no discernible long-term trend over the Holocene (Fig 2b). Hereafter, we discuss principal characteristics of OSIW based on a stacked record of the two shallow sites 4 and 78 representing the core OSIW layer (Fig. 4a, Fig. S4). In addition, linear correlation in the Okhotsk Sea between dissolved water column O_2 and $\delta^{13}C_{DIC}$ allows us to approximate ranges of past O_2 levels for the major ventilation intervals outlined below (Fig. 3, supplementary information).

Our $\delta^{13}C$ records imply a subdivision of the Holocene into four major periods with differing ventilation patterns, and a principal mid-Holocene baseline shift in average ventilation around 6 ka (Fig. 2c-e, Fig. 4a). The earliest Preboreal (11-8.5 ka) and the subsequent Early Holocene (8.5-6 ka) phases both exhibit significantly lower $\delta^{13}C$ than modern values (Fig. 2). Corresponding O_2 estimates for these two intervals show that during the Preboreal O_2 concentrations barely ever (i.e. in less than 25% of the data) reached the even lower range of modern O_2 concentrations (Fig. 3). During the early Holocene (8.5-6 ka) $\delta^{13}C$ values of all cores suggest abundant ventilation minima in OSIW, comparable to modern regions of old, low-O_2 waters in the open North Pacific (Keigwin, 1998a). Average O_2 estimates for this time interval reach only 90-100 µ mol/l and imply a nearly 50% reduction in mid-depth oxygen This persistent low-O_2 situation is contrasted by increased Middle and Late Holocene ventilation after a sudden shift around 6 ka (Fig. 2c, d and Fig. 3a) towards conditions more akin to modern settings. This later period is separated around 2 ka into a late Holocene (0-2 ka, Fig. 2) and a mid Holocene Phase (6-2 ka), which differ from each other by about 0.2 ‰ in their respective $\delta^{13}C$ ranges. Resulting average O_2 concentrations likewise indicate a ca. 20-30 µ mol/l or 15-20% decrease for the mid Holocene 4-6 ka period compared to modern averages values. A critical result of this $\delta^{13}C$-based ventilation reconstruction is the observation that present-day OSIW and connected mesopelagic North Pacific ventilation has essentially only been prevalent for the last ca. 2 ka.

Superimposed on the long-term step-wise background changes, we detect distinct millennial-scale variations in OSIW ventilation, visible directly in the $\delta^{13}C$ time series and in low-pass filter outputs from the OSIW stacked ventilation record (Fig. 4a). OSIW variations show recurring ca. 2,500 yr cycles over the Holocene, commonly attributed to solar forcing(Debret et al., 2009), and probably connected to 2,500-2,750 yr periodicities assigned to variations in high-latitude polar vortex expansion and wintertime wind circulation(O' Brien et al., 1995).

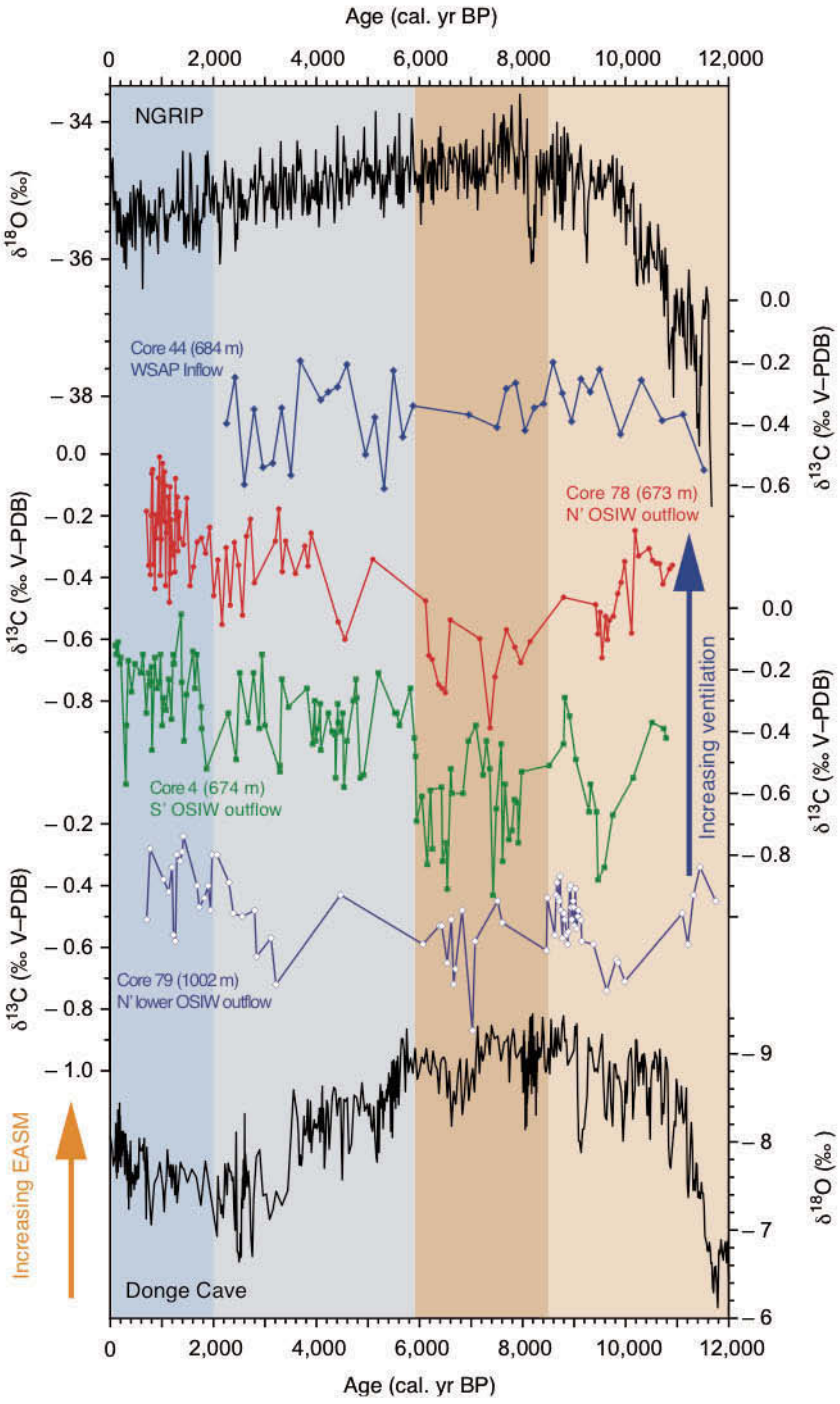

Figure 6.2: Stable isotope records of studied cores indicating changes in OSIW ventilation in relation to global reference records. a) NGRIP ice core $\delta^{18}O$ time series(Blockley et al., 2011). b) Kamchatka margin core 44, indicating WSAP water inflow; c–e) Sakhalin margin cores indicating changes in OSIW ventilation as labeled in figure; f) Dongge Cave speleothem d18O time series, representing changes in South East Asian Summer Monsoon and links to North Atlantic climate(Dykoski et al., 2005). Colored background highlights the four different main ventilation phases from 0-2 ka (late Holocene), 2-6 ka (mid-Holocene), 6-8.5 ka (early-mid Holocene) and 8.5-11 ka (Preboreal).

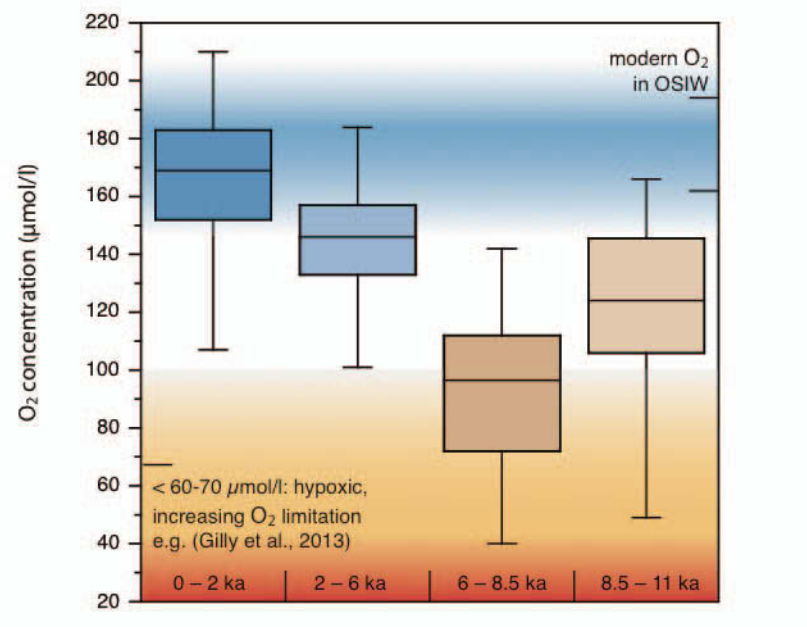

Figure 6.3: Approximation of past levels in dissolved O_2 in OSIW (see supplement S1 and text for calculations) based on $\delta^{13}C_{OSIW}$ stacked record (Fig 4a, blue and grey lines). Box and Whisker plots for four ventilation intervals as described in text and Fig. 2. Boxes represent the inner upper and lower quartiles with median value, whiskers the respective outer quartiles of respective time intervals. Blue background color indicates present O_2 range of OSIW.

These variations support the assumption that OSIW ventilation is partly modulated on millennial timescales by variations in solar activity, probably either through a particular sensitivity of sea ice or wintertime atmospheric patterns to a (yet unspecified) transfer mechanism. Before the 6 ka shift, an additional 1,500 yr periodicity is recognizable (Fig 4b), which has been first reported form North Atlantic drift ice patterns(Bond et al., 1997) and recently re-interpreted as being of internal oceanic origin(Debret et al., 2009).

In the Pacific, evidence for millennial-scale cycles in marine sequences is scarce, however a southerly located Japan margin SST record also shows persistent 1,500 year cycles in SST anomalies(Isono et al., 2009) (i. e. in detrended record, original data in Fig. 4). As such 1,500 yr variations are confined to the early-mid Holocene in our records, we speculate that during periods of overall suppressed OSIW ventilation, the modulation via oceanic internal forcing gains importance. This Early Holocene increased prevalence of 1,500 yr cycles is contrary to North Atlantic time series, where these cycles gain strength after the mid-Holocene 6 ka shift towards a stabilization of the Atlantic MOC into its modern mode; though to date a coherent explanation for their origin and expression remain elusive(Debret et al., 2009).

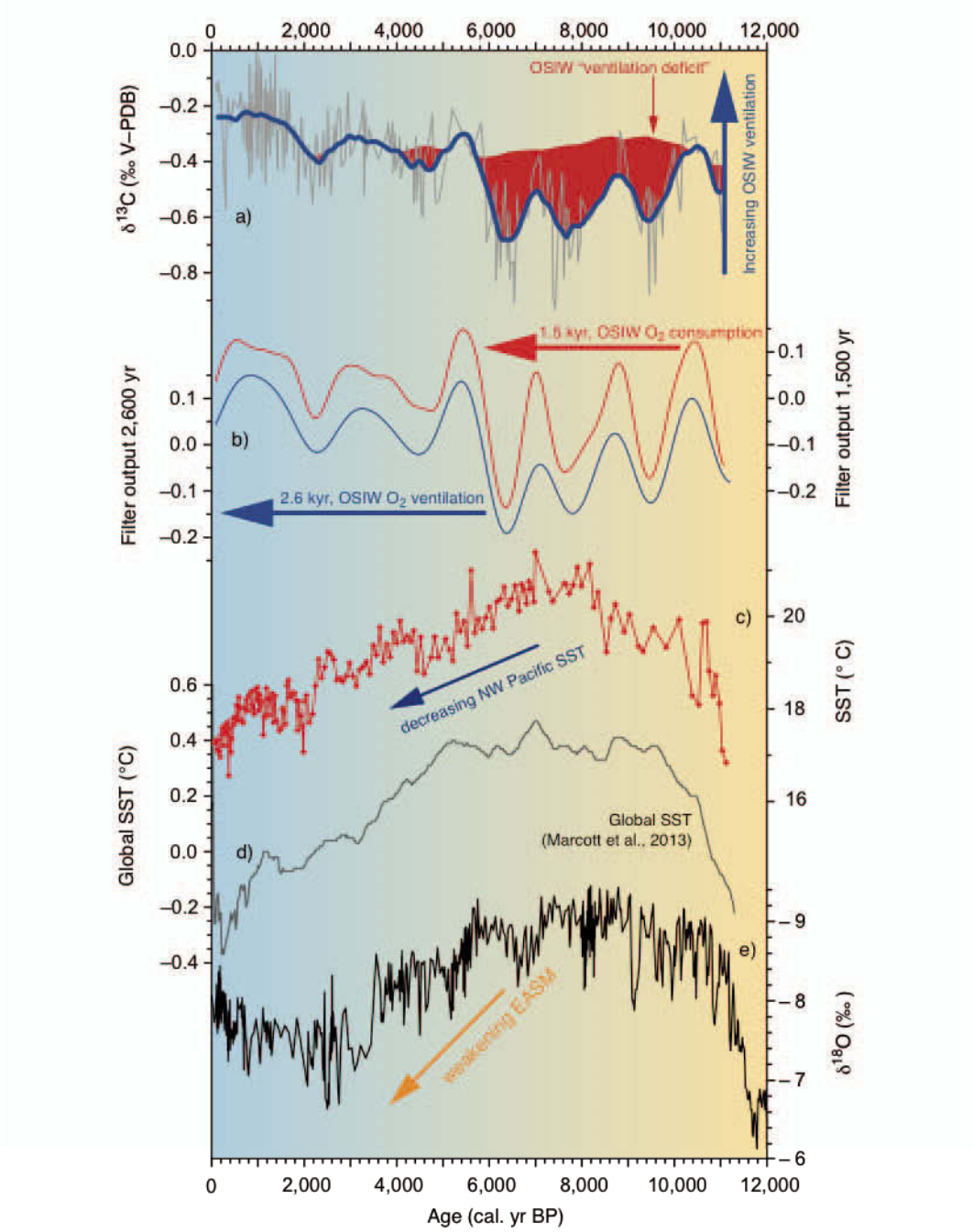

Figure 6.4: Generalized OSIW ventilation dynamics and gradients compared to long-term changes in regional and global climate records. a) $\delta^{13}C_{OSIW}$ stacked record of sites 78 and 4 indicating OSIW ventilation dynamics. Grey line: original data, blue thick line: re-sampled 25-moving average. Red background filling is the 9-moving average of core 44 indicating amount of OSIW ventilation deficiency relative to inflowing WSAP source water. b) Output of $\delta^{13}C_{OSIW}$ ventilation stack, evenly re-sampled in time domain to 100 yr intervals and subjected to 1,500 yr (internal stochastic/oceanic, red curve) and 2,600 yr (high-latitude and solar, blue curve) loss-pass filters. c) composite alkenone-based high-resolution SST record from Japan margin (red curve and diamonds`,

cores MD01-2421`, KR02-06 MC and GC)(Isono et al., 2009). d) $Standard_{5x5}$ SST mean global temperature stack (grey line)(Marcott et al., 2013). e) as in Fig. 2.

The observed variations and in particular the mid-Holocene climatic shift in OSIW ventilation is reflected in records globally(Debret et al., 2009) and in regions influenced by the East Asian Summer Monsoon system (EASM, Fig. 4e). Before 6 ka, a stronger EASM(Dykoski et al., 2005) penetrated further northward than at present, yielding higher precipitation and temperatures in the Okhotsk Sea hinterland, thereby increasing runoff from the Amur river catchment into the Okhotsk Sea(Tachibana et al., 2008). Higher Amur freshwater discharge transports latent heat to the Okhotsk Sea(Ogi et al., 2001; Tachibana et al., 2008), which suppresses sea ice formation and, in concert with stronger thermal stratification of the upper mixed layer(Riethdorf et al., 2013), decreases OSIW ventilation. After 6 ka, a strengthening and expansion of the winter Siberian High atmospheric action center in concert with a southward retreating EASM front is likely responsible for strengthening cold northeasterly winds over the continental shelf region. We infer that this leads to longer sea ice cover, more active polynias and more vigorous mixing of the Upper Mixed Layer, which in concert support formation of new OSIW after 6 ka. In addition, on instrumental timescales the maximum sea ice extent in the Okhotsk Sea is dependent on mean SST conditions in late summer(Nakanowatari et al., 2010). Alkenone-derived SSTs for the Okhotsk Sea and the Japan continental margin (Fig. 3) consistently show maxima in Holocene SSTs between ca. 8 and 6 ka, decreasing SSTs between 4-6 ka and a last shift toward persistent colder SSTs around 2 ka(Isono et al., 2009; Max et al., 2012a). Our decrease in OSIW ventilation during the Early to Middle Holocene is thus in close agreement with increased SSTs (Fig. 4) derived from regional and global reconstructions(Marcott et al., 2013).

Comparison of the WSAPW Kamchatka and the OSIW Sakhalin stacked $\delta^{13}C$ data (Fig. 4a) reveals that OSIW ventilation decreases below values of its precursor WASP water mass before the 6 ka shift. This negative OSIW-WSAPW gradient implies that OSIW export into the North Pacific was either not actively ventilated in the Okhotsk Sea before 6 ka, or that increased remineralization of organic matter through respiration within OSIW relative to today decreased the O_2 content of OSIW below values of WSAPW entering the Okhotsk Sea. Earlier qualitative multi-proxy works on nearby sites in the Okhotsk Sea(Gorbarenko et al., 2010b) also show oceanographic reorganizations at 6 ka. Those studies based on microfossil assemblages suggested higher mesopelagic productivity with increased microbial biomass and higher OM respiration in OSIW before 6 ka together with a reduction in ventilation, while less support for a collapse formation of OSIW was found(Gorbarenko et al., 2010b) (see supplementary information). Either way, ventilation and oxygen supply would have been reduced significantly, turning the Okhotsk Sea from a modern O_2 source into an O_2 sink before 6 ka.

Our study highlights the nonlinear behavior of North Pacific mesopelagic waters on millennial timescales under warmer than present climate. Given the significant importance of mid-depth waters in the global ocean volume and their observed short, almost instant response time within years and decades to changing environmental forcing(Nakanowatari et al., 2007), future studies should aim to elucidate their role for global element cycles that at present remain inadequately understood. As future global SSTs are thought to resemble or surpass early Holocene SST values in the future(Marcott et al., 2013), significant changes to lower oxygen supply from subarctic latitudes coupled with changed ventilation feedback can be expected for the mid-depth Pacific Ocean, a mechanisms that will likely affect oxygen-dependant biogeochemical cycles.

Acknowledgements: We thank masters and crews of R/V Akademik Lavrentiev during cruises LV28 and LV29 for their support. S. Fessler, N. Stange, A. Kaiser and L. Haxhiaj are thanked for their help in sample preparation and laboratory analyses. We sincerely thank H. Erlenkeuser for isotope analyses of seawater samples. This study was funded through BMBF grants KOMEX and KOMEX II.

LLJ, RT and DN designed the study, collected sample material and provided data. LLJ carried out isotope measurements, analyzed data and wrote the paper. All authors discussed results and worked on the final draft of the manuscript.

Material and Methods

To reconstruct changes in mid-depth ventilation patterns of mid-depth water masses, we use the stable carbon isotopic composition ($\delta^{13}C$), of benthic foraminiferal *Cibicides mundulus* tests. This epibenthic species reliably reflects the $\delta^{13}C$ of the $\sum CO_2$ of bottom water masses (see also appendix II for details in this thesis)(Bauch et al., 2002). In the Okhotsk Sea, the $\delta^{13}C$ signature of water Dissolved Inorganic Carbon (DIC) in a first order approximation is linearly correlated to the nutrient and oxygen content of water masses (Fig. S2)(Bauch et al., 2002) and can thus be used to assess changes in past ocean O_2 content (referred simplified to as "ventilation"). Between one and five specimen of *C. mundulus* were picked from the 250-500 µm fraction, cleaned with distilled water from potential dirt, dried at 50°C and measured in the GEOMAR Stable Isotope Laboratory on a Thermo Finnigan MAT252 coupled online to a Kiel CARBO II unit. Calibration was achieved through an in-house carbonate standard (Solnhofen Limestone) and NIST NBS-19, all values are reported in the δ notation with reference to Vienna – Pee Dee Belemnite (‰ V-PDB).

Water samples for isotope analyses were taken during cruise LV29 of R/V Akademik Lavrentiev to the Okhotsk Sea. Directly after retrieval of a CTD water rosette sampler equipped with 12 Niskin bottles, 100ml seawater were filled from Niskin bottles into glass bottles (pre-flushed with ambient seawater). 0.2 ml $HgCl_2$ were immediately added to each sample to stop biological activity. Bottles were closed by airtight crimp seals and stored under refrigerated, dark conditions until further treatment. Measurements of the $\delta^{13}C_{DIC}$ were carried out in the Leibniz Laboratory for Radiometric Dating and Isotope Research, Kiel using an automated Kiel DICI-II device for CO_2 extraction and a Finnigan MAT Delta E mass spectrometer for measurements(Erlenkeuser and Party, 1995; Erlenkeuser et al., 1999). Isotope results are given in the δ-notation and calibration is based on the NBS 20 carbonate isotope standard, the measurement precision of the $\delta^{13}C_{DIC}$ is ± 0.04 ‰.

Two stations in the Okhotsk Sea were used for stable isotope analyses of Dissolved Inorganic Carbon (DIC): LV29-112 at 56° 04' N, 169° 14' E represents the inflow region to the Okhotsk Sea form the North Pacific Western Subarctic Gyre, and LV29-72-4 (52° 42' N, 144° 13' E) is located in the pathway of newly formed OSIW that is exported with the East Sakhalin Current into the North Pacific and enters the Oyashio thereafter. These sites were selected to investigate the modern properties of $\delta^{13}C_{DIC}$ of seawater in the study area (Fig. 1). water samples were collected during the expedition LV29 of R/V Akademik M.A. Lavrentyev in 2002(Biebow et al., 2002b).

Age control for cores LV28-4-4 and LV29-79 in the investigated upper sections relies on ten and twelve, respectively, AMS ^{14}C dates from the planktic foraminiferal species *N. pachyderma* (s) and *G. bulloides*. All AMS ^{14}C measurements were carried out at the Leibniz Laboratory for Radiometric Dating and Isotope Research, Kiel according to established procedures and protocols (see supplementary information). For calibration we used a regional reservoir age correction of $\Delta R = 500$ ^{14}C years with MARINE09(Reimer et al., 2009a). Results, references to methods and the construction of age-depth relationships between age control points are described in detail in the supplementary text and tables.

Supplementary Information:

Site Selection and Age Models:

We use a collection of four sediment cores to track Holocene changes in NPIW/OSIW ventilation. Gravity core LV28-44-3 was retrieved from the western Kamchatka continental margin ("core 44", 52°02.514' N, 153°05.959' E, 684 m water depth) and is located along the pathway of inflowing North Pacific water to the formation region of DSW and OSIW on the northeastern continental shelf

(Biebow and Hütten, 1999). This core thus records the OSIW precursor waters, mainly Western Subarctic Pacific Water (WSAPW hereafter) delivered via the East Kamchatka Current to the Okhotsk Sea. Three gravity cores are used to monitor changes in newly formed DSW/OSIW (simply termed OSIW hereafter) located on the eastern Sakhalin continental margin along the export pathway of newly formed and ventilated OSIW. Northerly cores LV29-78-3 ("core 78", 52°40.388' N, 144°42.203' E, 673 m water depth) and LV29-79-3 ("core 79", 52°47.272' N, 144°57.318' E, 1082 m) are from the core layer of OSIW and it's lower boundary to deeper Pacific Deep Water (PDW), respectively (Biebow et al., 2002b). Core LV28-4-4 ("core 4", 51°08.475' N, 145°18.582' N, 674 m) complements the records with a more southerly location but same intermediate water depth as cores 78 and 44 (Biebow and Hütten, 1999). We are thus confident that observed patterns are not simply caused by highly localized mixing processes, but significant in extent beyond their respective locations.

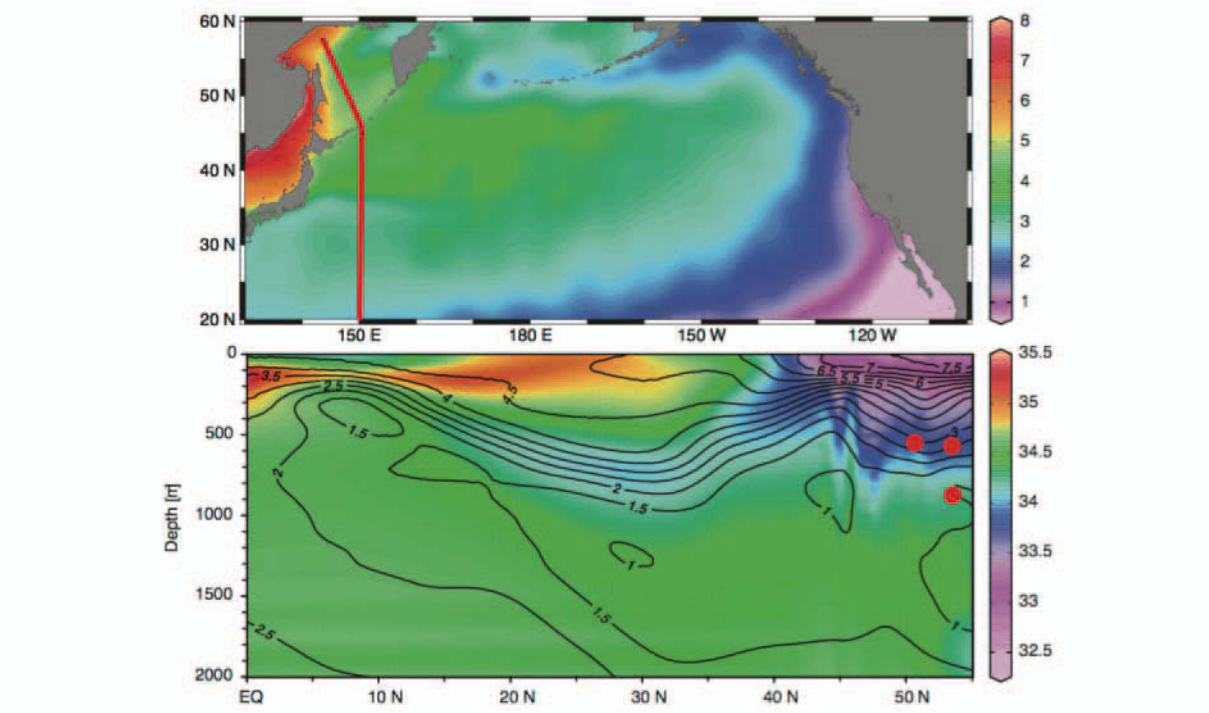

Figure 6.S1: Oceanographic characteristics of the study region. (a) Dissolved O_2 concentrations in the North Pacific (ml/l) on the Okhotsk Sea and North Pacific Intermediate Water density level (σ_Θ=28.8). (b) Cross section through Okhotsk Sea and North Pacific along 150°E. Color shading indicates salinity in practical salinity units and shows salinity minimum between 600 and 1000 m water depth used to define North Pacific Intermediate Water(Talley, 1993). Line contours display O_2 (ml/l) values in 0.5 ml increments. Salinity, density and O_2 data from World Ocean Atlas 2009(Garcia et al., 2010a). ODV and GMT were used for plotting the maps.

We identified representative core sites for OSIW and NPIW according to O_2 maxima and salinity minima along the characteristic density anomalies (Gladyshev et al., 2003; Talley et al., 1995; Talley, 1993). NPIW today spreads across the North Pacific along the Kuroshio-Oyashio Extension and diverges into a smaller northern branch that ultimately enters the Alaskan Gyre and a southern more prominent flow that distributes into the subtropical mid-depth North Pacific (Masujima and Yasuda, 2009; Saito et al., 2011; Shcherbina et al., 2009; Toyama and Suga, 2010). Within the northern, subarctic gyre NPIW looses its defining low-salinity signature due to fresher overlying water masses. In the subtropical circulation arm, NPIW can be detected as local salinity minimum down to c. 20°N (cf. Fig S1).

The derived radiocarbon ages were put into a chronostratigraphic context with published cores and frameworks (Lembke-Jene et al., in this thesis cf. Chapter 4 and 5, Max et al., 2012a; Riethdorf et al., 2013). We calibrated the raw AMS ^{14}C dates with a regional reservoir age correction of $\Delta R = 500$ ^{14}C years (Kuzmin et al., 2007a) and MARINE09 (Reimer et al., 2009a). We used the software Calib 6.01 (Stuiver and Reimer, 1993a) and the program CLAMS written for the software package "R" (Blaauw, 2010) in order to establish an age-depth relationship in cores 4 and 79.

The age model for core 44 is based on a comprehensive, lithostratigraphic and tephrochronological, AMS ^{14}C-supported framework (Derkachev et al., 2012; Gorbarenko et al., 2002b; Nürnberg and Tiedemann, 2004) and has been published previously (Nürnberg et al., 2011). It was used unaltered here. For core 78, age control was achieved by correlating a surface productivity proxy, the sediment chlorin content, to nearby core 79. This strategy of using productivity variations to correlate nearby cores has been successfully employed before on glacial-interglacial and shorter, millennial timescales in the region (Max et al., 2012a; Nürnberg and Tiedemann, 2004). In this way, we were able to transfer chronostratigraphic tie-points to core 78 and establish an age model. While this process might not allow for high-resolution studies with shorter centennial-interdecadal accuracy, it yields sufficient age control in the framework of this study. Tiepoints were supported by lithostratigraphic core correlation based on ship-board core logging and scanning. The program Analyseries 2.0.4 was used for inter-core correlation (Paillard et al., 1996). Within the framework of this thesis the age model for core 78 is explained in more detail in Chapter 4 together with the conceptional approach to age models and core-to-core correlation, it is thus not repeated here.

Use of stable carbon isotopes for assessing OSIW/NPIW ventilation

We use $\delta^{13}C$ of epibenthic foraminifera to address changes in intermediate water ventilation. $\delta^{13}C_{DIC}$ is influenced by more parameters than the nutrient content of the water column (Broecker and Maier-Reimer, 1992; Lynch-Stieglitz and Fairbanks, 1994; Lynch-Stieglitz et al., 1995). Changes in the air-sea exchange by turbulent mixing of the upper mixed layer, the $\delta^{13}C$ of source water masses, and kinetic isotope fractionation all influence the isotope signal and have been addressed in numerous paleoceanographic studies before (Hofmann et al., 1999; Kroopnick, 1985a; Lynch-Stieglitz et al., 1995; McCorkle and Keigwin, 1994). In our case, apart from the apparently significant correlation that is observed in modern water samples between $\delta^{13}C_{DIC}$, O_2 and nutrient content (not shown)(Bauch et al., 2002; Biebow et al., 2011; Pavlova et al., 2008), we feel justified in our approach by the following considerations: The source water masses from which OSIW is formed by brine rejection and subsequent mixing processes in the northern Okhotsk Sea have potentially changed on G-IG timescales. However, during the Holocene, we see no evidence that there was significant variability, supported by the small amplitude variation and unaltered baseline in core 44 (main article, Fig. 2), which should record such source variations. Changes in the air-sea exchange cannot (and are not) excluded in our reasoning. In fact, the late Holocene climatic cooling period after 4-6 ka might have supported stormier winter seasons and an increased entrainment in wintertime and/or more polynias opening, leading to both higher $\delta^{13}C$ and O_2. We cannot quantitatively assess the respective influences of this OSIW "preconditioning" (i.e. O_2 imprint or "ventilation" upon formation) from subsequent drawdown of that preformed $\delta^{13}C$ (and hence O_2) by organic matter degradation and respiration in the mesopelagic water column. Nonetheless, these processes would have changed $\delta^{13}C$, but also O_2, in the same manner and led to export of more or less well ventilated OSIW from the Okhotsk Sea into the North Pacific, under the assumption that the North Pacific Holocene MOC remained comparable in transport rates and volume and water mass exchange to the modern situation. A better understanding of the basin's Holocene physical paleoceanography would be desirable to constrain our assumptions, but adequate quantitative studies are in their infancy.

Correlation between $\delta^{13}C_{DIC}$ and dissolved O_2

For calculating O_2 values from the $\delta^{13}C_{Cib}$ we used published and publicly available data that directly stem from the core locations or nearby sites and were sampled during the same cruises (Bauch et al., 2002; Biebow and Hütten, 1999; Biebow et al., 2011; Biebow et al., 2002a). We excluded the uppermost 50 m of water samples as these are likely directly influenced by ocean-atmosphere exchange processes, thus might be biased by short-term variations in their O_2 and $\delta^{13}C_{DIC}$ signatures. However, adding these few samples to the dataset only slightly modify the overall regression and

relative changes in O_2 concentrations as shown in Fig. 4 still remain. The fact that calculated O_2 values for the 0-2 ka interval as well as for single samples close to the core tops match actual O_2 values measured in these water depths both by CTD sensors and with Winckler titration gives us confidence in providing a reasonable approximation of past O_2 concentrations, which nonetheless should be viewed with an error akin to the featured box plots of perhaps ±30 µmol/l. Compared to modern values for O_2 concentrations in the larger region our regression seems to slightly underestimate O_2 by ca. 20-30 µmol/l, which might be due to large inter-decadal and inter-annual changes in dissolved O2 concentrations(Emerson et al., 2004; Feely et al., 2004).

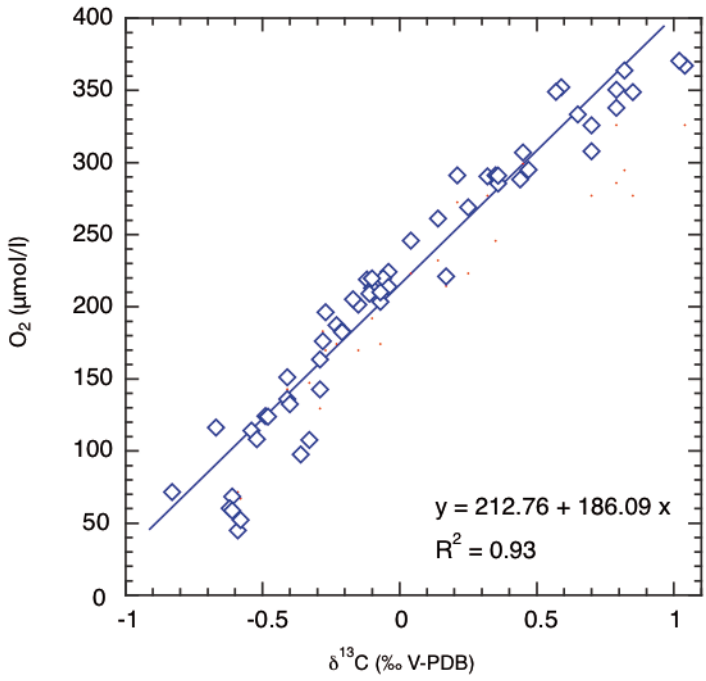

Figure 6.S2: $\delta^{13}C_{DIC}$ vs. O_2 regression based on water (bottle) data from the Okhotsk Sea. Both datasets were taken from Bauch et el. (2002)(2002). Samples influenced by surface exchange processes (i.e. the upper 50 m) were excluded from regression, but would not fundamentally alter the correlation.

We regard our calculated O_2 as a conservative estimate with regard to the lower values reported in the early-mid Holocene interval, because in the Okhotsk Sea below $\delta^{13}C_{DIC}$ values of –0.7 ‰ regression data becomes scarce, but indicates a decoupling of O_2 from the linear relationship to $\delta^{13}C_{DIC}$ whereby lower O_2 concentrations ca. <50 µmol/kg are not accompanied by respective further decreases in DIC and $\delta^{13}C$(Biebow et al., 2002b; Dullo et al., 2005). In any case, the *C. mundulus* species used here is known to become rare from foraminiferal assemblages in the Okhotsk Sea below values of about 65-50 µmol/l and is usually an indicator for well to moderately ventilated water masses (Bubenshchikova et al., 2008). Thus, our calculated O_2 concentrations may well be an underestimation of actual paleo-

O_2 changes. Transient periods during the early-mid Holocene, where *C. mundulus* is absent from the samples, especially in the lower core 79, point to such potential underestimation and factually even lower DO concentrations around 50 µmol/l, but such assumptions cannot be rectified without further evidence.

Comparison to Previous Studies indicating Okhotsk Sea Ventilation Changes

Our results stand in some contrast to previous studies based on the abundance patterns of the radiolarian species *Cycladophora davisiana* in cores form the Okhotsk Sea (Itaki and Ikehara, 2004). This species was used in a number of earlier studies as indicator for the presence of OSIW based on modern abundance patterns (Abelmann and Nimmergut, 2005; Takahashi, 1998) and the indirect inference that such water masses would be well ventilated in analogy to the modern situation(Okazaki et al., 2006; Takahashi, 1998). However, studies that have used the abundance of deep-dwelling radiolarian species *C. davisiana*, which is a good indicator of high amounts of organic detritus in the mesopelagic, show that during times in the early Holocene, when we observe minima in ventilation, maxima in *C. davisiana* are reported (Itaki and Ikehara, 2004). We reconcile these results with our observations by invoking a number of studies both from sediment as well as from water sampling that *C. davisiana* abundance is primarily linked to the provision of bacterial and detrital food in its mesopelagic habitat (Abelmann and Nimmergut, 2005; Nimmergut and Abelmann, 2002; Okazaki et al., 2003). This food source in turn is today delivered via a turbid layer connected to OSIW formation (Nakatsuka et al., 2004b; Nakatsuka et al., 2002). However, our data show that such water mass does not necessarily need to be ventilated. To the contrary, a higher amount of detrital organic material in the mesopelagic water layer would both increase *C. davisiana* abundance and the remineralisation of organic matter, thereby decreasing the O_2 concentrations. In this interpretation, OSIW would bear higher concentrations of nutrients and lower DO in the turbid water layer when *C. davisiana* abundance is high, supported by earlier independent multi-proxy evidence from nearby sites(Gorbarenko et al., 2010b; Gorbarenko et al., 2007b). However, we do not challenge the assumption that the export of mesopelagic waters from the Okhotsk Sea might have been even higher during the early-mid Holocene than today as concluded in some of these works(Itaki and Ikehara, 2004; Itaki et al., 2008). From our stable isotope data alone we do deduce changes in paleo-transport volumes or flow strength of OSIW. Additional studies employing complementary proxies for "paleophysical oceanography" like trace metal or radiogenic isotope studies are needed to separate transport and ventilation signals(cf. Huybers and Wunsch, 2010).

Step detection and software used

The detection of step-like features in the stacked $\delta^{13}C$ series was firstly based on visual inspection of both the stacked time series and the individual records. To corroborate the partitioning into the four reported intervals 0-2, 2-6, 6-8.5 and 8.5-11 ka, we divided the entire time series into single 1,000 yr and 2,000 yr moving windows in 500 yr steps and carried out Wilcoxon-Mann-Whitney tests on the respective series to determine the location of the step changes. For the step intervals selected here, the null hypotheses that the intervals were statistically similar, were rejected with P=<0.001 in normal approximation. Results for the calculated means are given in table S1. Software packages Kaleidagraph, ProFit and R were used to calculate changes and carry out statistical tests. Smoothing, inter-core correlation, and re-sampling of records were done with the software Analyseries 2.0.4 (Paillard et al., 1996). The software Ocean Data View (ODV) was used for visualization of WOA09 data in Fig. 6.S1 (Schlitzer, 2002).

Supplementary table S1: Statistical averages for time intervals in OSIW stacked ventilation record.

	$\delta^{13}C$ 0-2 ka	$\delta^{13}C$ 2-6 ka	$\delta^{13}C$ 6-8.5 ka	$\delta^{13}C$ 8.5-11 ka
Minimum	**-0.57**	**-0.69**	**-0.93**	**-0.88**
Maximum	**-0.01**	**-0.15**	**-0.38**	**-0.25**
Points	92	65	42	36
Mean	**-0.24**	**-0.37**	**-0.65**	**-0.49**
Median	**-0.24**	**-0.36**	**-0.63**	**-0.48**
RMS	0.27	0.39	0.66	0.51
Std Deviation	**0.12**	**0.11**	**0.14**	**0.15**
Variance	0.01	0.01	0.02	0.02
Std Error	0.01	0.01	0.02	0.02
Skewness	-0.33	-0.44	-0.17	-0.76
Kurtosis	-0.21	-0.15	-0.66	0.33

References (main and supplementary text bundled for this thesis)

1 Karstensen, J., Stramma, L. & Visbeck, M. Oxygen minimum zones in the eastern tropical Atlantic and Pacific oceans. *Progress In Oceanography* **77**, 331-350, doi:10.1016/j.pocean.2007.05.009 (2008).

2 Keeling, R. F., Körtzinger, A. & Gruber, N. Ocean Deoxygenation in a Warming World. *Annual Review of Marine Science* **2**, 199-229, doi:10.1146/annurev.marine.010908.163855 (2010).

3 Nakanowatari, T., Ohshima, K. I. & Wakatsuchi, M. Warming and oxygen decrease of intermediate water in the northwestern North Pacific, originating from the Sea of Okhotsk, 1955-2004. *Geophysical Research Letters* **34**, L04602, doi:10.1029/2006GL028243 (2007).

4 Emerson, S., Watanabe, Y. W., Ono, T. & Mecking, S. Temporal trends in apparent oxygen utilization in the upper pycnocline of the North Pacific: 1980–2000. *Journal Of Oceanography* **60**, 139-147 (2004).

5 Reid, J. L. Intermediate Waters of the Pacific Ocean. Report No. 2, 1-85 (The Johns Hopkins Press, Baltimore, 1965).

6 Shcherbina, A. Y., Talley, L. D. & Rudnick, D. L. Direct observations of North Pacific ventilation: Brine rejection in the Okhotsk Sea. *Science* **302**, 1952-1955 (2003).

7 Talley, L. D. Distribution and formation of North Pacific intermediate water. *Journal Of Physical Oceanography* **23**, 517-537 (1993).

8 Hill, K., Weaver, A., Freeland, H. & Bychkov, A. Evidence of change in the Sea of Okhotsk: Implications for the North Pacific. *Atmosphere-Ocean* **41**, 49-63 (2003).

9 Keigwin, L. Glacial-age hydrography of the far northwest Pacific Ocean. *Paleoceanography* **13**, 323-339 (1998).

10 Gorbarenko, S. A. *et al.* Responses of the Okhotsk Sea environment and sedimentology to global climate changes at the orbital and millennial scale during the last 350 kyr. *Deep-Sea Research II* **61-64**, 73-84 (2012).

11 Itaki, T. & Ikehara, K. Middle to late Holocene changes of the Okhotsk Sea Intermediate Water and their relation to atmospheric circulation. *Geophysical Research Letters* **31**, L24309, doi:10.1029/2004GL021384 (2004).

12 Gorbarenko, S. A. *et al.* Paleoenvironment changes in the NW Okhotsk Sea for the last 18 kyr determined with micropaleontological, geochemical, and lithological data. *Deep Sea Research Part I: Oceanographic Research Papers* **57**, 797-811, doi:10.1016/j.dsr.2010.04.004 (2010).

13 McCorkle, D. C. & Keigwin, L. D. Depth profiles of δ 13C in bottom water and core top C. wuellerstorfi on the Ontong Java Plateau and Emperor Seamounts. *Paleoceanography* **9**, 197, doi:10.1029/93PA03271 (1994).

14 Bauch, D., Erlenkeuser, H., Winckler, G., Pavlova, G. & Thiede, J. Carbon isotopes and habitat of polar planktic foraminifera in the Okhotsk Sea: the 'carbonate ion effect' under natural conditions. *Marine Micropaleontology* **45**, 83-99 (2002).

15 Biebow, N., Kulinich, R. & Baranov, B. *KOMEX II, Kurile Okhotsk Sea Marine Experiment: Cruise report RV Akademik M.A.Lavrentyev cruise 29, Leg 1 and Leg 2 : Vladivostok - Pusan - Okhotsk Sea - Pusan - Okhotsk Sea - Pusan - Vladivostok ; May 25 - August 05,2002*. Vol. 110 (GEOMAR Forschungszentrum für Marine Geowissenschaften, 2002).

16 Biebow, N. & Hütten, E. Cruise Reports: KOMEX I and II: RV Professor Gagarinsky Cruise 22, RV Akademik M.A. Lavrentyev Cruise 28. 188 (GEOMAR Research Centre for Marine Geosciences, Kiel, 1999).

17 Itou, M., Ono, T. & Noriki, S. Provenance of intermediate waters in the western North Pacific deduced from thermodynamic imprint on delta C-13 of DIC. *Journal Of Geophysical Research-Oceans* **108**, 3347, doi:10.1029/2002JC001746 (2003).

18 Blockley, S. P. E. *et al.* Synchronisation of palaeoenvironmental records over the last 60,000 years, and an extended INTIMATE event stratigraphy to 48,000 b2k. *Quaternary Science Reviews* **36**, 2-10 (2011).

19 Dykoski, C. *et al.* A high-resolution, absolute-dated Holocene and deglacial Asian monsoon record from Dongge Cave, China. *Earth And Planetary Science Letters* **233**, 71-86, doi:10.1016/j.epsl.2005.01.036 (2005).

20 Debret, M. *et al.* Evidence from wavelet analysis for a mid-Holocene transition in global climate forcing. *Quaternary Science Reviews* **28**, 2675-2688, doi:10.1016/j.quascirev.2009.06.005 (2009).

21 O' Brien, S. R. *et al.* Complexity of Holocene Climate as Reconstructed from a Greenland Ice Core. *Science (New York, NY)* **270**, 1962-1964, doi:10.1126/science.270.5244.1962 (1995).

22 Bond, G. *et al.* A pervasive millennial-scale cycle in North Atlantic Holocene and glacial climates. *Science (New York, NY)* **278**, 1257-1266 (1997).

23 Isono, D. *et al.* The 1500-year climate oscillation in the midlatitude North Pacific during the Holocene. *Geology* **37**, 591-594, doi:10.1130/G25667A.1 (2009).

24 Tachibana, Y., Oshima, K. & Ogi, M. Seasonal and interannual variations of Amur River discharge and their relationships to large-scale atmospheric patterns and moisture fluxes. *Journal of Geophysical Research-Atmospheres* **113**, D16102, doi:10.1029/2007JD009555 (2008).

25 Ogi, M., Tachibana, Y., Nishio, F. & Danchenkov, M. Does the fresh water supply from the Amur river flowing into the sea of Okhotsk affect sea ice formation? *Journal Of The Meteorological Society Of Japan* **79**, 123-129 (2001).

26 Riethdorf, J.-R., Max, L., Nürnberg, D., Lembke-Jene, L. & Tiedemann, R. Deglacial history of (sub) sea surface temperatures and salinity in the subarctic NW Pacific: Implications for upper-ocean stratification. *Paleoceanography* (2013).

27 Nakanowatari, T., Ohshima, K. I. & Nagai, S. What determines the maximum sea ice extent in the Sea of Okhotsk? Importance of ocean thermal condition from the Pacific. *Journal of Geophysical Research* **115**, C12031, doi:10.1029/2009JC006070 (2010).

28 Max, L. *et al.* Sea surface temperature variability and sea-ice extent in the subarctic northwest Pacific during the past 15,000 years. *Paleoceanography* **27**, PA3213-, doi:10.1029/2012PA002292 (2012).

29 Marcott, S. A., Shakun, J. D., Clark, P. U. & Mix, A. C. A Reconstruction of Regional and Global Temperature for the Past 11,300 Years. *Science (New York, NY)* **339**, 1198-1201, doi:10.1126/science.1228026 (2013).

30 Erlenkeuser, H. & Party, T. I. S. S. in *Russian-German Cooperation: Laptev Sea System* Vol. 176 *Berichte zur Polarforschung/Reports on Polar Research* eds H Kassens *et al.*) 170-177 (1995).

31 Erlenkeuser, H., Spielhagen, R. F. & Taldenkova, E. in *The Kara Sea Expedition of RV Akademik Boris Petrov 1997: First Results of a Joint Russian-German Pilot Study* Vol. 300 *Berichte zur Polarforschung/Reports on Polar Research* eds J Matthiessen *et al.*) 80-90 (Alfred Wegener Institute, 1999).

32 Reimer, P. J. *et al.* INTCAL09 and MARINE09 Radiocarbon Age Calibration Curves , 0-50,000 Years cal. BP. *Radiocarbon* **51**, 1111-1150 (2009).

33 Talley, L. *et al.* North Pacific Intermediate Water in the Kuroshio-Oyashio Mixed Water Region. *Journal Of Physical Oceanography* **25**, 475-501 (1995).

34 Gladyshev, S., Talley, L., Kantakov, G., Khen, G. & Wakatsuchi, M. Distribution, formation, and seasonal variability of Okhotsk Sea Mode Water. *Journal of Geophysical Research-Oceans* **108** (2003).

35 Masujima, M. & Yasuda, I. Distribution and Modification of North Pacific Intermediate Water around the Subarctic Frontal Zone East of 150 degrees E. *Journal Of Physical Oceanography* **39**, 1462-1474, doi:10.1175/2008JPO3919.1 (2009).

36 Shcherbina, A. Y., Gregg, M. C., Alford, M. H. & Harcourt, R. R. Characterizing Thermohaline Intrusions in the North Pacific Subtropical Frontal Zone. *Journal Of Physical Oceanography* **39**, 2735-2756, doi:10.1175/2009JPO4190.1 (2009).

37 Toyama, K. & Suga, T. Vertical structure of North Pacific mode waters. *Deep Sea Research Part II: Topical Studies in Oceanography* **57**, 1152-1160, doi:papers2://publication/doi/10.1016/j.dsr2.2009.12.004 (2010).

38 Saito, H., Suga, T., Hanawa, K. & Shikama, N. The Transition Region Mode Water of the North Pacific and Its Rapid Modification. *Journal Of Physical Oceanography* **41**, 1639-1658, doi:10.1175/2011JPO4346.1 (2011).

39 Garcia, H. E. *et al. World Ocean Atlas 2009, Volume 3: Dissolved Oxygen, Apparent Oxygen Utilization, and Oxygen Saturation*. (U.S. Government Printing Office, 2010).

40 Kuzmin, Y. V., Burr, G. S., Gorbunov, S. V., Rakov, V. A. & Razjigaeva, N. G. A tale of two seas: Reservoir age correction values (R, Delta R) for the Sakhalin Island (Sea of Japan and Okhotsk Sea). *Nuclear Instruments & Methods In Physics Research Section B-Beam Interactions With Materials And Atoms* **259**, 460-462, doi:10.1016/j.nimb.2007.01.308 (2007).

41 Stuiver, M. & Reimer, P. J. Extended 14C database and revised CALIB radiocarbon calibration program. *Radiocarbon* **35**, 215-230 (1993).

42 Blaauw, M. Methods and code for "classical" age-modelling of radiocarbon sequences. *Quaternary Geochronology* **5**, 512-518, doi:10.1016/j.quageo.2010.01.002 (2010).

43 Nürnberg, D. & Tiedemann, R. Environmental change in the Sea of Okhotsk during the last 1.1 million years. *Paleoceanography* **19**, PA4011, doi:10.1029/2004PA001023 (2004).

44 Gorbarenko, S. *et al.* Magnetostratigraphy and tephrochronology of the Upper Quaternary sediments in the Okhotsk Sea: implication of terrigenous, volcanogenic and biogenic matter supply. *Marine Geology* **183**, 107-129 (2002).

45 Derkachev, A. N. *et al.* Characteristics and ages of tephra layers in the central Okhotsk Sea over the last 350kyr. *Deep Sea Research Part II: Topical Studies in Oceanography* **61-64**, 179-192, doi:10.1016/j.dsr2.2011.05.015 (2012).

46 Nürnberg, D., Dethleff, D., Tiedemann, R., Kaiser, A. & Gorbarenko, S. A. Okhotsk Sea ice coverage and Kamchatka glaciation over the last 350ka — Evidence from ice-rafted debris and planktonic δ18O. *Palaeogeography Palaeoclimatology Palaeoecology* **310**, 191-205, doi:10.1016/j.palaeo.2011.07.011 (2011).

47 Paillard, D., Labeyrie, L. & Yiou, P. Macintosh program performs time-series analysis. *Eos Transactions AGU* **77**, 379 (1996).

48 Broecker, W. S. & Maier-Reimer, E. The influence of air and sea exchange on the carbon isotope distribution in the sea. *Global Biogeochemical Cycles* **6**, 315, doi:10.1029/92GB01672 (1992).

49 Lynch-Stieglitz, J. & Fairbanks, R. G. A conservative tracer for glacial ocean circulation from carbon isotope and palaeo-nutrient measurements in benthic foraminifera. *Nature News* **369**, 308-310, doi:10.1038/369308a0 (1994).

50 Lynch-Stieglitz, J., Stocker, T. F., Broecker, W. S. & Fairbanks, R. G. The influence of air-sea exchange on the isotopic composition of oceanic carbon: Observations and modeling. *Global Biogeochemical Cycles* **9**, 653, doi:10.1029/95GB02574 (1995).

51 Hofmann, M., Broecker, W. S. & Lynch-Stieglitz, J. Influence of a [CO 2(aq)] dependent biological C-isotope fractionation on glacial 13C/ 12C ratios in the ocean. *Global Biogeochemical Cycles* **13**, 873, doi:10.1029/1999GB900063 (1999).

52 Kroopnick, P. M. The distribution of ^{13}C of $\sum CO2$ in the world oceans. *Deep Sea Research Part I: Oceanographic Research Papers* **32**, 57-84 (1985).

53 Pavlova, G. Y., Tishchenko, P. Y. & Nedashkovskii, A. P. Distribution of alkalinity and dissolved calcium in the Sea of Okhotsk. *Okeanologiya* **48**, 23-32, doi:10.1134/S0001437008010049 (2008).

54 Biebow, N., Hütten, E., Wallmann, K. & Lammers, S. (2011).

55 Biebow, N., Kulinich, R. & Baranov, B. in *GEOMAR Reports* 190 (GEOMAR Research Center for Marine Geosciences, Kiel, 2002).

56 Feely, R. A. *et al.* Oxygen utilization and organic carbon remineralization in the upper water column of the Pacific Ocean. *Journal Of Oceanography* **60**, 45-52 (2004).

57 Dullo, W.-C., Biebow, N. & Georgeleit, K. SO178 KOMEX: Stoffaustauschprozesse und-bilanzen im Ochotskischen Meer: Hintergrund und erste Ergebnisse. 125 (IFM-GEOMAR, Leibniz-Institute for Marine Sciences, Kiel, 2005).

58 Bubenshchikova, N., Nuernberg, D., Lembke-Jene, L. & Pavlova, G. Living benthic foraminifera of the Okhotsk Sea: Faunal composition, standing stocks and microhabitats. *Marine Micropaleontology* **69**, 314-333, doi:10.1016/j.marmicro.2008.09.002 (2008).

59 Takahashi, K. The Bering and Okhotsk Seas: modern and past paleoceanographic changes and gateway impact. *Journal of Asian Earth Sciences* **16**, 49-58 (1998).

60 Abelmann, A. & Nimmergut, A. Radiolarians in the Sea of Okhotsk and their ecological implication for paleoenvironmental reconstructions. *Deep Sea Research Part II: Topical Studies in Oceanography* **52**, 2302-2331, doi:10.1016/j.dsr2.2005.07.009 (2005).

61 Okazaki, Y. *et al.* Cycladophora davisiana (Radiolaria) in the Okhotsk Sea: A key for reconstructing glacial ocean conditions. *Journal Of Oceanography* **62**, 639-648 (2006).

62 Okazaki, Y., Takahashi, K., Nakatsuka, T. & Honda, M. C. The production scheme of Cycladophora davisiana (Radiolaria) in the Okhotsk Sea and the northwestern North Pacific: implication for the paleoceanographic conditions during the glacials in the high latitude oceans. *Geophysical Research Letters* **30**, 1939-, doi:doi:10.1029/2003GL018070 (2003).

63 Nimmergut, A. & Abelmann, A. Spatial and seasonal changes of radiolarian standing stocks in the Sea of Okhotsk. *Deep Sea Research Part I: Oceanographic Research Papers* **49**, 463-493 (2002).

64 Nakatsuka, T., Yoshikawa, C., Toda, M., Kawamura, K. & Wakatsuchi, M. An extremely turbid intermediate water in the Sea of Okhotsk: Implication for the transport of particulate organic matter in a seasonally ice-bound sea. *Geophysical Research Letters* **29**, 1757, doi:10.1029/2001GL014029 (2002).

65 Nakatsuka, T., Toda, M., Kawamura, K. & Wakatsuchi, M. Dissolved and particulate organic carbon in the Sea of Okhotsk: Transport from continental shelf to ocean interior. *Journal Of Geophysical Research-Oceans* **109**, C09S14, doi:10.1029/2003JC001909 (2004).

66 Gorbarenko, S. A. *et al.* Paleoenvironmental changes in the northern shelf of the Sea of Okhotsk during the Holocene. *Stratigraphy and Geological Correlation* **15**, 656-671, doi:10.1134/S0869593807060044 (2007).

67 Itaki, T., Khim, B.-K. & Ikehara, K. Last glacial-Holocene water structure in the southwestern Okhotsk Sea inferred from radiolarian assemblages. *Marine Micropaleontology* **67**, 191-215, doi:10.1016/j.marmicro.2008.01.002 (2008).

68 Huybers, P. & Wunsch, C. Paleophysical Oceanography with an Emphasis on Transport Rates. *Annual Review of Marine Science* **2**, 1-34, doi:papers2://publication/doi/10.1146/annurev-marine-120308-081056 (2010).

69 Schlitzer, R. Interactive analysis and visualization of geoscience data with Ocean Data View. *Computers & Geosciences* **28**, 1211-1218 (2002).

7. Sensitivity of North Pacific Intermediate Water Ventilation to Rapid Climate Oscillations of the Last Deglaciation

Lars Max[a], Lester Lembke-Jene[a], Jan-Rainer Riethdorf[b], Ralf Tiedemann[a], Dirk Nürnberg[c], Hartmut Kühn[a] and Andreas Mackensen[a]

a Alfred Wegener Institut, Helmholtz Centre for Polar and Marine Research, Am Handelshafen 12, D-27570 Bremerhaven, Germany; E-Mail: Lars.Max@awi.de

b Department of Ocean Floor Geoscience, Atmosphere and Ocean Research Institute, University of Tokyo, 5-1-5 Kashiwanoha, Kashiwa, Chiba 277-8564, Japan

c GEOMAR, Helmholtz-Zentrum for Ocean Research, Wischhofstr. 1-3, D-24148 Kiel, Germany

For submission to Earth and Planetary Science Letters

7.1. Abstract

Under modern conditions only the upper portion of the North Pacific Ocean is ventilated by North Pacific Intermediate Water and, in contrast to its Northern Hemisphere counterpart the North Atlantic, lacks any deep water formation. However, some recent studies with General Circulation Models (GCMs) point to a reversed situation and a switch to deep water formation in the subarctic Pacific during the last glacial termination as response to a shutdown or weakening of the Atlantic Meridional Overturning Circulation (AMOC). Here we show first deglacial ventilation proxy records derived from stable carbon isotopes in conjunction with ventilation ages of the Okhotsk Sea and Bering Sea, the potential source regions of past North Pacific ventilation changes. The combination of ventilation proxy data presented here clearly suggest no deep water formation in the North Pacific during the last deglaciation but a strengthened North Pacific intermediate water formation and enhanced shallow overturning during Heinrich 1 and the Younger Dryas. The deglacial source region of strengthened intermediate water ventilation is proposed to be the Okhotsk Sea, where rapid intensifications of intermediate water formation have been observed during times of AMOC reductions. From this, we further infer that the deglacial exchange of nutrient and CO_2-enriched Pacific Deep Water with the atmosphere was probably hampered during times of expanded intermediate water ventilation and strengthened shallow overturning of the subarctic Pacific.

7.2. Introduction

The release of old and deep sequestered carbon from the North Pacific Ocean is widely discussed as mechanism that may have contributed to the rise in atmospheric CO_2 concentrations during the last deglaciation (Boyle, 1988a; Galbraith et al., 2007; Jaccard et al., 2009; Marchitto et al., 2007b; Marchitto et al., 2005). Given that the modern abyssal North Pacific holds the largest quantity of dissolved inorganic carbon, it is of paramount importance to understand its exchange with the atmosphere through changes in ventilation rates in the past. At present, the subarctic North Pacific surface waters are isolated from deeper, nutrient-and CO_2-rich waters by a steep, year-round salinity gradient known as halocline (Haug et al., 1999). The halocline forms a barrier for the heat and gas exchange between the atmosphere and the deep ocean and damps the supply of nutrients into the photic zone. Consequently, the nutrient utilization is nearly complete in the subarctic Pacific (Sarmiento et al., 2004) and lead to one of the highest modern carbon export efficiencies in the world oceans, thus acts as a net sink of atmospheric CO_2 (Honda et al., 2002). Under modern conditions, the formation of new water masses in the North Pacific is restricted to the Okhotsk Sea (Talley, 1993),

where denser waters are produced in coastal polynyas by brine rejection during wintertime sea-ice production (Shcherbina et al., 2003b). These water masses leave the Okhotsk Sea as Okhotsk Sea Intermediate Water, mix with water in the NW-Pacific at intermediate depths and form North Pacific Intermediate Water (NPIW). The NPIW spreads eastward through the North Pacific Ocean between ca. 20° N – 40° N to the proximity of the California Current region, where it can still be recognized as positive oxygen anomaly between 300 – 800 m water depth.

Former reconstructions of changes in deep Pacific hydrography and circulation have been focused mainly on the Last Glacial Maximum (LGM). Available Pacific nutrient proxy records point to an enhancement and deepening of North Pacific ventilation of intermediate water down to 2000 m water depth during the LGM (Keigwin, 1998b; Matsumoto et al., 2002a). Less information exists about millennial-scale deglacial variations in intermediate to deep water circulation due to the limited availability of high-resolution sediment records. However, recent studies with General Circulation Models (GCMs) suggest an onset of deep water formation in the North Pacific during the deglacial cold events Heinrich 1 (H1) and Younger Dryas (YD), which has been linked to strong reductions in AMOC (Okazaki et al., 2010b). Freshwater perturbations in the North Atlantic and associated oceanic-atmospheric interactions have been proposed as a potential mechanism, which induced a redistribution in upper-ocean salinity known as Stommel feedback (Saenko et al., 2004; Stommel, 1961; Timmermann et al., 2005), thereby favoured the establishment of a Pacific Meridional Overturning Circulation (PMOC) and deep water formation to occur in the North Pacific. Main evidence for at least changes in mid-depth ventilation is provided by proxy data, which has been derived from sediment records located east off Japan. In these cores, the difference in radiocarbon ages between planktonic and benthic foraminifers (defined as ventilation age) are reduced during H1 and the YD (Ahagon et al., 2003a; Duplessy et al., 1989b; Sagawa and Ikehara, 2008b) and enhanced NPIW ventilation during these intervals inferred. However, whether the North Pacific itself, the Bering Sea or the Okhotsk Sea formed the source region for “expanded deglacial NPIW” (Jaccard and Galbraith, 2013) is still ambiguous. Available proxy data indicative for changes in intermediate water circulation/ventilation from this key regions are still equivocal, and both the Bering Sea (Rella et al., 2012) (Schlung et al., 2013) as well as the Okhotsk Sea (Tanaka and Takahashi, 2005) are proposed as major contributors of enhanced deglacial NPIW. Another focal point is the timing and rapidity of changes in PMOC. Model simulations propose a rapid switch and a deglacial seesaw mechanism between PMOC and AMOC intensifications, which can not be constrained by available proxy data.

Here, we present new results from stable carbon isotope records in combination with ventilation ages to provide a first comprehensive view on deglacial North Pacific ventilation changes in order to: (1.) infer the timing and extent of intermediate/deep water formation in potential source regions and (2.)

assess its temporal relationship to changes in AMOC, which were associated with large-scale reorganizations in PMOC and upper-ocean heat transport.

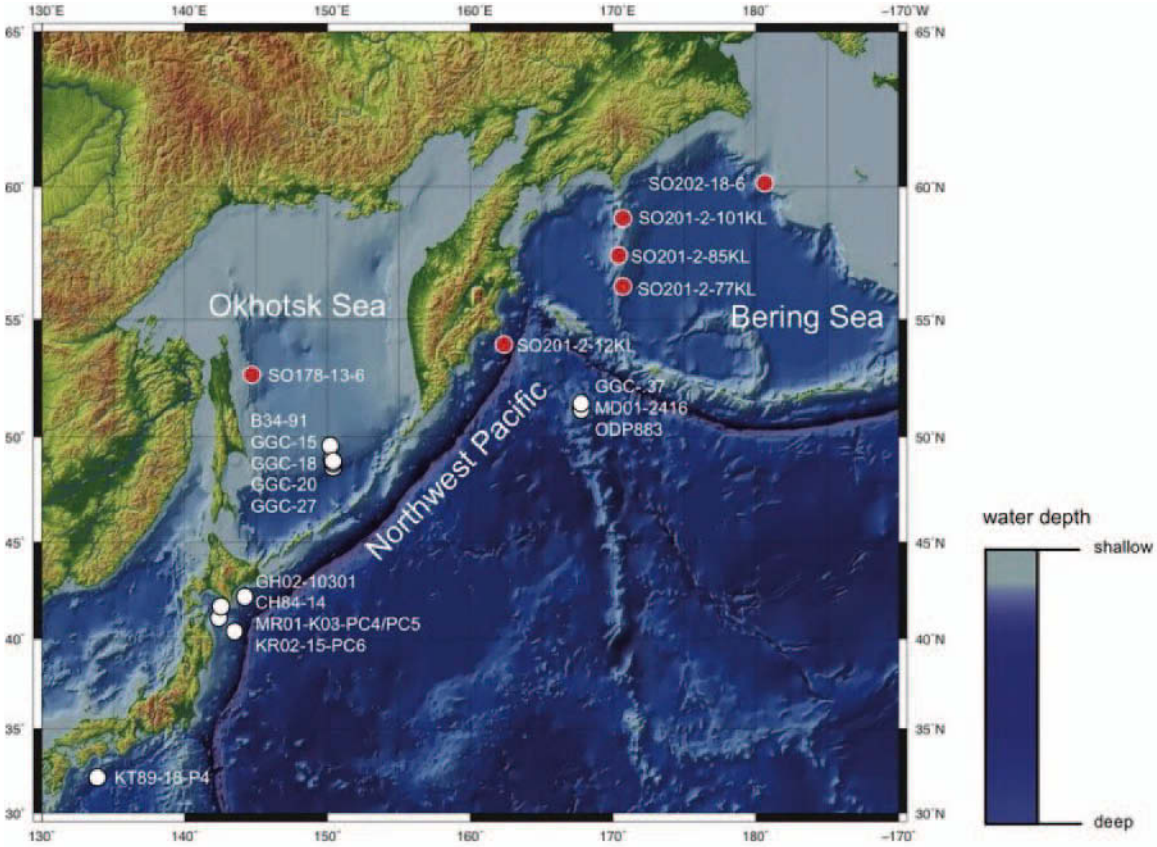

Figure 7.1: Overview of the subarctic northwest Pacific and its marginal seas (Okhotsk Sea and Bering Sea). Red spots give core locations and red boxes mark hydrographic stations obtained in this study. White spots indicate published sediment cores from the northwest Pacific realm considered in this study (please see Table 3 and references therein).

7.3. Chronology

Two sediment cores from intermediate-depth, located in the Okhotsk Sea (SO178-13-6; 52° 43’ N, 144° 42’ E, 713 m water depth) and the western Bering Sea (SO201-2-85KL; 57° 30’ N, 170° 24’ E, 968 m water depth), were selected (Fig.1). For radiocarbon measurements mono-specific samples of planktic foraminifera *Neogloboquadrina pachyderma* sinistral from the 125 – 250 µm size fraction were picked in core SO201-2-85KL, in core SO178-13-6 a mix of planktonic foraminifera species (*G. bulloides* and *Neogloboquadrina pachyderma* sinistral) were picked from 150 – 250 µm size fraction.

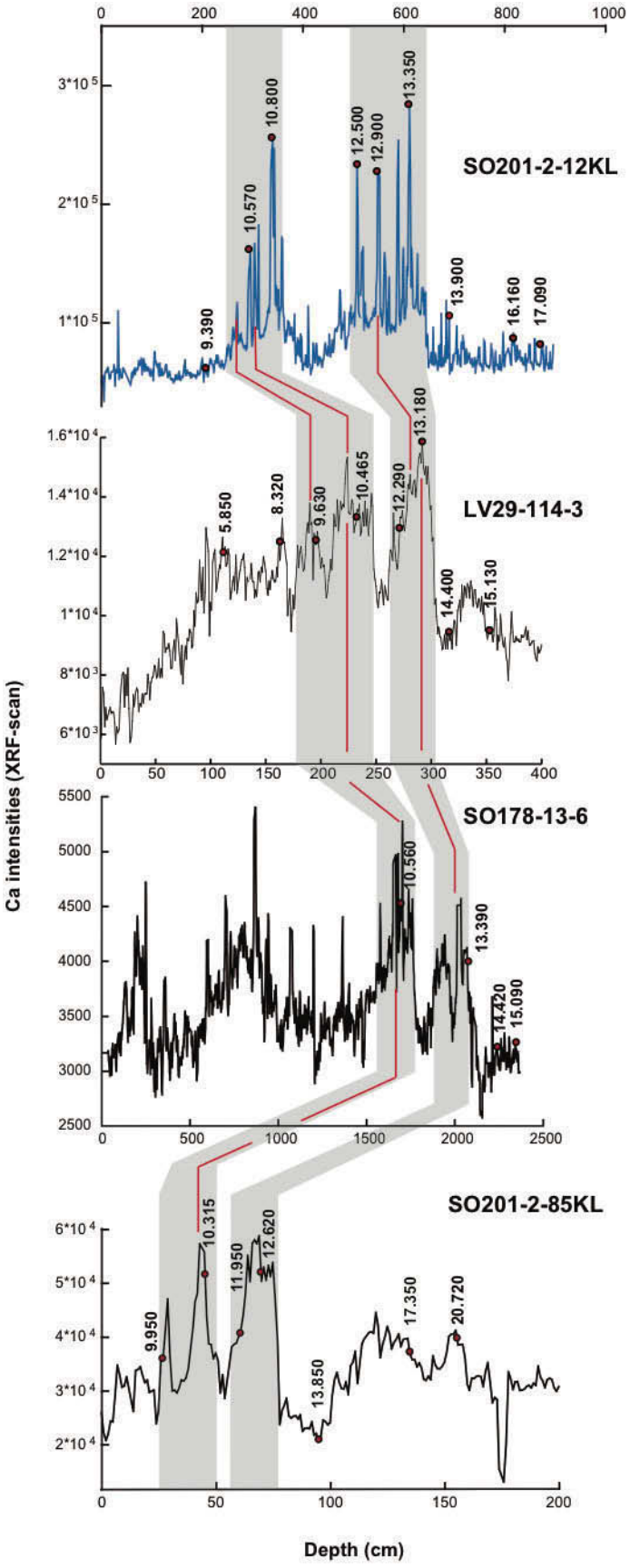
SO201-2-12KL
LV29-114-3
SO178-13-6
SO201-2-85KL
Ca intensities (XRF-scan)
Depth (cm)
9.390
10.570
10.800
12.500
12.900
13.350
13.900
16.160
17.090
5.850
8.320
9.630
10.465
12.290
13.180
14.400
15.130
10.560
13.390
14.420
15.090
9.950
10.315
11.950
12.620
13.850
17.350
20.720

Figure 7.2: Stratigraphic framework of sediment records from the western Bering Sea (SO201-2-85KL) and Okhotsk Sea (SO178-13-6) considered in this study and correlation to the established stratigraphy of Okhotsk Sea record LV29-114-3 and high-resolution sediment core SO201-2-12KL (blue curve) from the subarctic NW-Pacific (Max et al., 2012b). Given are the Ca intensities records achieved from core logging (XRF) together with raw AMS ^{14}C datings (red spots with vertical numbers). Grey shaded areas mark prominent carbonate maxima in the sediment records, red lines indicate correlation points between the sediment cores.

In total sixteen AMS ^{14}C-ages based on planktic foraminifers were determined by BETA Analytics London, the National Ocean Science Accelerator Mass Spectrometry Facility (NOSAMS) at Woods Hole Oceanographic Institute (WHOI) as well as the Leibniz-Laboratory for Radiometric Dating and Isotope Research at Kiel University. Radiocarbon ages are given according to the convention outlined by (Stuiver and Polach, 1977b) and (Stuiver, 1980).

All planktic radiocarbon ages were converted into calibrated 1-sigma calendar age ranges using the calibration tool Calib Rev 6.0 (Stuiver and Reimer, 1993b) with the Intcal09 atmospheric calibration curve (Reimer et al., 2009b) and are summarized in Supplementary Table 1 (see end of article). For reservoir age correction, reservoir ages of 900 years were applied for core SO178-13-6 and 700 years for core SO201-2-85KL, in line with reported correction values for the Bering and Okhotsk Sea, respectively (Kuzmin et al., 2007b; Kuzmin et al., 2001)

Relative sedimentary elemental composition was measured using the Avaatech X-ray Fluorescence (XRF) core scanner at the Alfred Wegener Institute for Polar and Marine Research except Okhotsk Sea core SO178-13-6, where XRF measurements were conducted at the Center for Marine Environmental Science (MARUM), Bremen. Each core segment was triple-scanned for element analysis at 1 mA and tube voltages of 10 kV (Al, Si, S, K, Ca, Ti, Fe) and 50 kV (Ag, Cd, Sn, Te, Ba), using a sampling resolution of 1 cm and 30 s count time.

The deglacial stratigraphy is based on the set of new and already published planktic radiocarbon measurements (AMS ^{14}C ages) and further constrained with X-ray Fluorescence (XRF) core scanner data for inter-core correlation, described in detail by (Max et al., 2012b). In general, the Ca intensity records (XRF) have been used to correlate prominent and similar structures between sediment records from various regions of the subarctic Pacific and its marginal seas. We dated carbonate maxima (maxima in planktic foraminifera abundance), which share common maxima in Ca intensities (XRF) and to avoid age artefacts due to bioturbation effects. Figure 2 gives the Ca intensity records and a detailed core-to-core correlation of the core sites. The Ca intensity pattern shows two intervals with high Ca intensities (carbonate maxima) between 13.390 - 11.950 ^{14}C years and 10.800 – 9.570 ^{14}C years. These pronounced carbonate maxima are well known in the NW-Pacific realm and mark the

B/A and the interval of the early Holocene (Cook et al., 2005b; Gorbarenko et al., 2005a; Gorbarenko et al., 2002c; Keigwin, 1998b; Keigwin et al., 1992b; Seki et al., 2004; Seki et al., 2009c). Hence, core SO178-13-6 was correlated to the established stratigraphy of Okhotsk Sea core LV129-114-3 (Max et al., 2012b) via the Ca intensity records (XRF) and available AMS ^{14}C datings (Fig. 3).

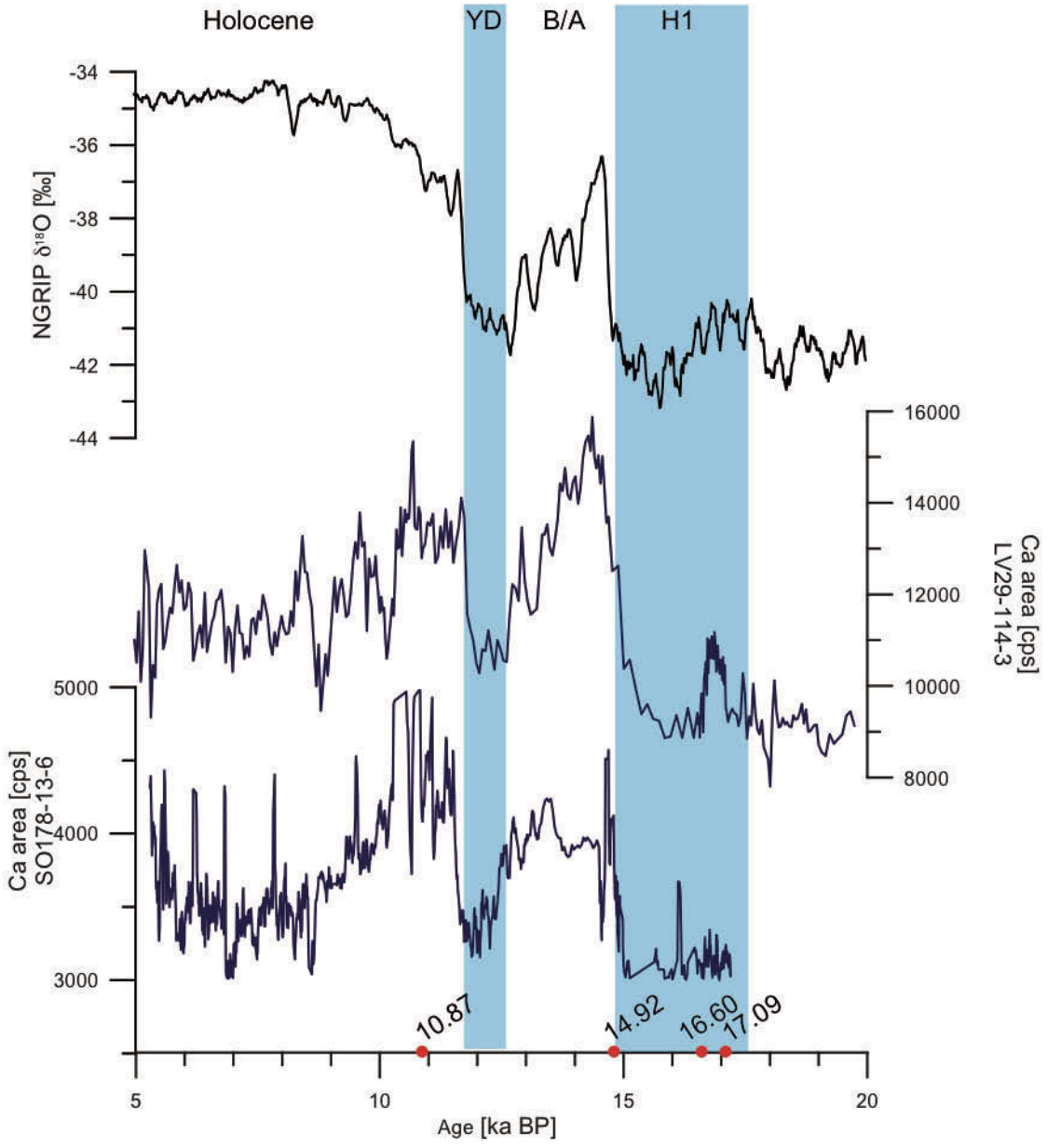

Figure 7.3: Correlation of sediment core SO178-13-6 to the established age model of LV29-114-3 via AMS ^{14}C datings and Ca intensity records (in blue) compared to the NGRIP isotope record (in black) in given above (Rasmussen et al., 2006b). Core SO178-13-6 was correlated to the established stratigraphy of LV29-114-3 (Max et al., 2012b) via Ca intensity studies (XRF) and AMS ^{14}C datings. Red spots with numbers indicate calibrated ^{14}C ages of LV29-114-3 and SO178-13-6, respectively.

7.4. Analytical Methods

7.4.1 Hydrographic measurements of $\delta^{13}C_{DIC}$ of seawater

Two stations proximal to the used core sites SO201-2-85KL (for western Bering Sea station SO201-2-67; 56° 04' N, 169° 14' E) and SO178-13-6 (for Okhotsk Sea station LV29-84-3, 52° 42' N, 144° 13' E) were selected to investigate the modern properties of $\delta^{13}C_{DIC}$ of seawater in the study area (Fig. 1).

For the Bering Sea samples, the water column was sampled during the expedition SO201-2 of R/V Sonne in 2009 in eight depth intervals via a water sampling rosette device (Dullo et al., 2009b). Immediately after sub-sampling of Niskin bottles, water samples were poisoned with a saturated solution of mercury, sealed with wax and stored at 4°C temperature until further treatment. On shore, 1 ml of water was injected through a septum into a vial with ca. 3 ml concentrated phosphoric acid flushed with pure Helium. After storage at room temperature for complete reaction the resultant CO_2 was transferred via a Finnigan Gas Bench II to a Finnigan MAT 252 gas mass spectrometer for determination of stable carbon isotope ratio at the Alfred Wegener Institute for Polar and Marine Research, Bremerhaven. Results are given in δ-notation versus V-PDB. The precision of $\delta^{13}C_{DIC}$ measurements based on an internal laboratory standard has been reported to be better than ±0.1 ‰.

For the Okhotsk Sea, water samples were collected during the expedition LV29 of R/V Akademik M.A. Lavrentyev in 2002 (Biebow et al., 2002). Water samples were slowly filled into 100-ml glass bottles directly after retrieval of a combined CTD water rosette sampler equipped with 12 Niskin bottles. 0.2 ml $HgCl_2$ was immediately added to each sample to stop biological activity. Bottles were closed by airtight crimp seals and stored under refrigerated, dark conditions until further treatment. Measurements of the $\delta^{13}C_{DIC}$ were carried out in the Leibniz Laboratory for Radiometric Dating and Isotope Research, Kiel using an automated Kiel DICI-II device for CO_2 extraction and a Finnigan MAT Delta E mass spectrometer for measurements (see also Erlenkeuser et al., 1995, Erlenkeuser et al., 1999). Isotope results are given in the δ-notation and calibration is based on the NBS 20 carbonate isotope standard, the measurement precision of the $\delta^{13}C_{DIC}$ is ± 0.04 ‰.

7.4.2 Benthic Stable Carbon Isotope Records ($\delta^{13}C$)

Stable carbon isotope records ($\delta^{13}C$) derived from benthic foraminifer tests are believed to be a robust proxy to study past variations in deep water circulation as the $\delta^{13}C$ of dissolved inorganic carbon is closely linked to past ambient seawater nutrient- and oxygen levels (Curry et al., 1988; Curry and Oppo, 2005) whereas high $\delta^{13}C$ values are indicative for lower nutrient concentrations and better

ventilation (Kroopnick, 1985b). In this study, $\delta^{13}C$ measurements were established from sediment samples of core SO178-13-6 (Okhotsk Sea) and SO201-2-85KL (Bering Sea). Discrete sediment samples were taken, freeze-dried, washed over a 63 µm screen, dried and separated in several sub-fractions (63 - 150, 150 - 250, 250 - 500, > 500 µm). For stable isotope analysis, only epibenthic species *Cibicidoides lobatulus* (*C. lobatulus*) were considered and picked from 250 – 500 µm sub-fraction. This species has been observed to preferentially live attached to hard substrate on or slightly above the sediment surface (Lutze and Thiel, 1989; Schweizer et al., 2009) and studies on live specimen indicates that the species faithfully records the $\delta^{13}C_{\sum CO2}$ of overlying bottom waters. Some studies have observed a positive offset in the $\delta^{13}C$ of this species with regard to ambient bottom water for $\delta^{13}C$ at the time of sampling in other high latitude settings. However, this effect was shown to be likely caused by high seasonal variability of the ambient water $\delta^{13}C$ signal as indicated by time-series measurements of water column $\delta^{13}C$ and according calcification of *C. lobatulus* during time intervals of maximum ventilation (Mackensen et al., 2000). We thus regard *C. lobatulus* to reliably reflect the ambient water mass $\delta^{13}C_{\sum CO2}$ signal.

We mostly picked between two and five specimen per sample and restricted our selection to well-preserved specimen with visible pores, clear sutures and unfilled chambers. During some intervals with low foraminifera abundance, we analysed single specimen with sufficient size and preservation. Samples of core SO178-13-6 were cracked open to remove dirt particles from the inside, if necessary cleaned ultrasonically in ethanol p.a. and roasted at 200 °C for 24 h. These samples were measured with a Thermo Finnigan MAT 252 isotope ratio mass spectrometer coupled to an automated KIEL II CARBO preparation device at the Paleoceanography Unit's Stable Isotope Laboratory of the GEOMAR – Helmholtz Centre for Ocean Research, Kiel. Overall analytical reproducibility is ±0.04 ‰ for $\delta^{13}C$ and ±0.06 ‰ for $\delta^{18}O$. Sample measurements of core SO201-2-85KL were done on single specimen due to very low abundance and measured with a Thermo Finnigan MAT 253 isotope ratio mass spectrometer coupled to an automated KIEL CARBO preparation device at the Stable Isotope Laboratory of the Alfred Wegener Institute for Polar and Marine Research, Bremerhaven. Overall analytical reproducibility is ±0.06 ‰ for $\delta^{13}C$ and ±0.08 ‰ for $\delta^{18}O$. Calibration was achieved via National Bureau of Standards NBS19 and NBS 20 material as well as through an internal laboratory standard of Solnhofen limestone. All values are reported as against the Vienna Pee Dee Belemnite Standard (expressed as ‰ vs. V-PDB) and are given in Table 2 (at end of article, supplemenentary information).

7.4.3. Paired Benthic-Planktic Radiocarbon Measurements (Ventilation Ages)

To infer past ventilation ages additional radiocarbon measurements on mono-specific samples of benthic foraminifera *Uvigerina peregrina* or mixed benthos were established. Ventilation ages were calculated from ^{14}C age difference between available planktonic and benthic foraminifers. In total 15 ventilation ages were derived from a set of six sediment cores located in the northwest Pacific realm (Figure 1). Ventilation ages from this study were compiled with published ventilation ages and used to infer ventilation changes in NW-Pacific intermediate and deep water (Figure 1, Table 3).

7.5. Results and Discussion

7.5.1. Modern Properties of Bering Sea and Okhotsk Sea $\delta^{13}C_{DIC}$

The modern distribution of $\delta^{13}C_{DIC}$ show large differences between the Okhotsk Sea and Bering Sea marginal seas as indicated in Figure 4. In the Bering Sea, a large gradient in $\delta^{13}C_{DIC}$ is located around 100 m water depth, which marks today the maximum in mixed layer depth (MLD) of surface water mixing with underlying water masses in winter (Fig. 4a). Beyond the MLD $\delta^{13}C_{DIC}$ values rapidly decline to -0.6 to -0.7 ‰ and indicate the absence of fresh intermediate-water masses in the western Bering Sea today. Modern values of $\delta^{13}C_{DIC}$ are around -0.6 ‰ at the depth of core SO201-2-85KL.

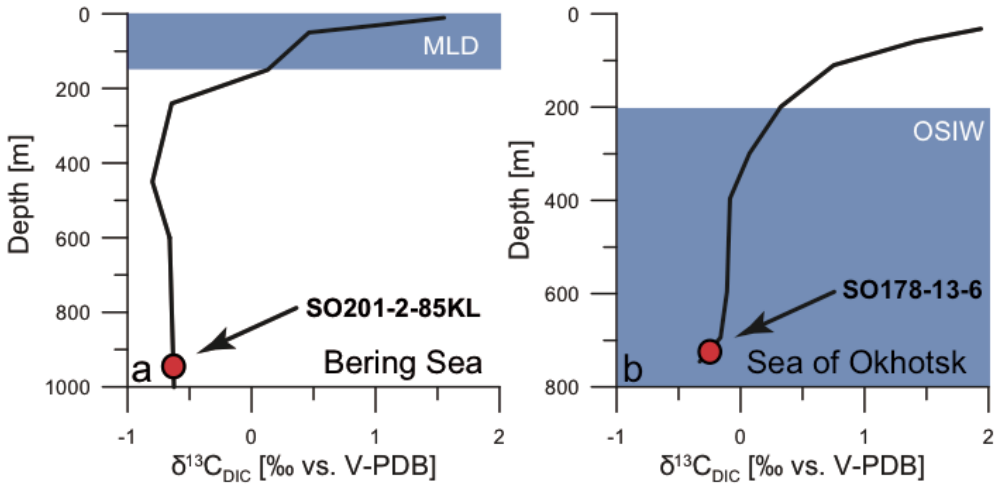

Figure 7.4: Water column profiles of $\delta^{13}C_{DIC}$ in the Bering Sea (station SO201-2-67) and Okhotsk Sea (station LV29-84-3) given as (a) $\delta^{13}C_{DIC}$ profile of the Bering Sea together with the respective depth-interval of SO201-2-85KL (red spot) and (b) $\delta^{13}C_{DIC}$ profile for the Okhotsk Sea together with the corresponding depth-interval of SO178-13-6 (red spot). Blue shaded areas mark the maximum mixed layer depth (MLD) of fresh surface water masses with sub-surface water masses in winter.

The $\delta^{13}C_{DIC}$ profile from the Okhotsk Sea show the presence of enriched $\delta^{13}C_{DIC}$ values within the water column between 200 – 800 m (Fig. 4b). Today, newly formed Okhotsk Sea Intermediate Water (OSIW) spreads across the Okhotsk Sea, expressed as positive $\delta^{13}C_{DIC}$ anomaly in the water column. The modern value of Okhotsk Sea record SO178-13-6 lies at the lower boundary of OSIW with $\delta^{13}C_{DIC}$ values around -0.3 ‰.

7.5.2. Timing and potential source regions for deglacial NPIW changes

In order to assess the timing and nature of past ventilation changes in the subarctic North Pacific and its relationship to major reorganizations in the AMOC we compared our western Bering Sea intermediate-depth benthic δ13C record with published 231Pa/230Th data (proposed to reflect the strength of the AMOC) from the North Atlantic (McManus et al., 2004b) and Greenland ice core record (Rasmussen et al., 2006b) during the last deglaciation (Fig. 5).

The most striking feature is that the western Bering Sea record reveals millennial-scale, rapid oscillations in δ13C that indicate repeated intermediate water ventilation changes, which are strictly opposite in sign (ventilation seesaw) compared to the North Atlantic deep circulation history of the last 20 kyr (Fig. 5). The western Bering Sea δ13C data point to intensified ventilation of intermediate waters during Heinrich 1 (17.5 – 15 ka BP) and the Younger Dryas (12.8 – 11.8 ka BP) as indicated by high δ13C values during times when deep convection in the North Atlantic was strongly reduced. As soon as the North Atlantic deep overturning cell was re-established during the Bølling/Allerød (14.7 – 12.8 ka BP) and the onset of the Holocene, ventilation of western Bering Sea intermediate water rapidly ceased as inferred from low δ13C values.

The deglacial pattern of Okhotsk Sea intermediate water ventilation resembles the mid-depth ventilation history of the Bering Sea (Fig. 6). Although, the timing of changes is similar, the amplitude of changes is much more pronounced in the Okhotsk Sea (differences of up to 1.5 ‰). Lowest δ13C values (-0.4 to -0.7 ‰) are recorded during the Bølling/Allerød interstadial (14.6 – 13.2 ka BP) and the earliest Holocene, similar to the western Bering Sea. However, the δ13C maxima with values of up +0.8 ‰ during H1 (17.5 – 15 ka BP) and of up to +0.7 ‰ during the YD (11.8 – 12.2 ka BP) are significantly higher in the Okhotsk Sea. During H1, Okhotsk Sea Intermediate Water (OSIW) even approached modern NADW δ13C signatures (1 - 1.5 ‰) of the subarctic North Atlantic (Curry and Oppo, 2005). This suggests the presence of well-ventilated, nutrient-depleted and newly formed intermediate water masses in the Okhotsk Sea during deglacial cold stages, which spreads into the NW-Pacific and the Bering Sea. The vertical expansion of this water mass did not reach the deep water level in the NW-Pacific as indicated by a δ13C record recovered from 3300 m water depth

(Keigwin, 1998b). Interestingly the deep water δ13C record shows a temporal variability that is opposite to the intermediate water level with minima during H1 (-0.6 ‰) and the YD (-0.3 to -0.1‰) and thus clearly characterizes a different water mass, which most likely originated from the Southern Ocean (Lund et al., 2011). On the other hand, the deep water δ13C maxima during B/A (-0.1 ‰) and the early Holocene (+0.1 ‰) are significantly higher than at intermediate water depths (-0.4 to -0.7 ‰). This indicates the absence of nutrient-depleted and well-ventilated intermediate water below 700 m water depth most likely in response to reduced intermediate water formation.

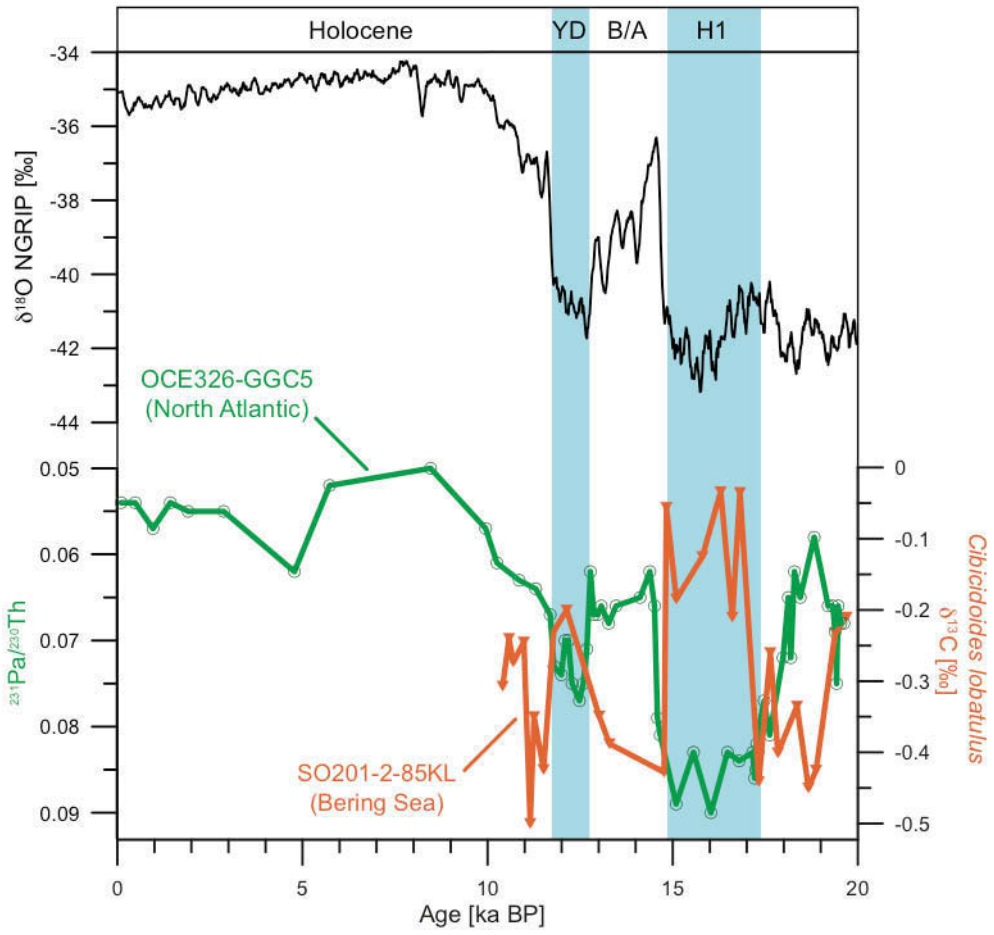

Figure 7.5: Comparison of deglacial circulation changes in the North Atlantic and western Bering Sea during the past 20 kyr. Pa/Th ratio (at the bottom) as proxy for the AMOC strength in the North Atlantic (in green) (McManus et al., 2004b) together with the intermediate-depth δ ^{13}C as proxy for circulation changes in the western Bering Sea (in orange). Blue shaded areas mark stadial Heinrich 1 and the Younger Dryas, respectively. For comparison, the NGRIP ice core record (in black) is given on top (Rasmussen et al., 2006b).

The deglacial variability in δ13C, the timing of ventilation changes as well as the opposing pattern between intermediate- and deep water is also in harmony with changes in ventilation ages, from the

North Pacific and its marginal seas (Fig. 6). At the intermediate water level (980 - 1370 m water depth), northwest Pacific ventilation ages are significantly lower during H1 and the YD than during the B/A (Adkins and Boyle, 1997; Ahagon et al., 2003a; Duplessy et al., 1989b; Sagawa and Ikehara, 2008b). Even younger intermediate water masses (ca. 700 - 980 m water depth) characterize the Bering Sea and the Okhotsk Sea during H1 and YD (Fig. 6). However, our shallow records provide no information about ventilation changes during B/A from the marginal seas. In contrast to the intermediate water level, deep water ventilation ages (Keigwin, 2002b; Minoshima et al., 2007; Murayama et al., 1992; Sarnthein et al., 2006b) deeper than 2170 m water depth interval are highest during H1 and provide the largest age difference between the intermediate and deep water masses within the last deglaciation (Fig. 6). This difference is less pronounced during the YD. The exact opposite is the case during the B/A and the glacial period from ca. 20-19 ka BP as ventilation ages from the intermediate and deep water level are rather similar, indicated by increasing ventilation ages at the intermediate water level and decreasing deep water ages (Fig. 6).

For the periods of H1 and YD, the combination of benthic δ13C and ventilation ages consistently argues for (1.) enhanced NPIW formation/ventilation down to at least 1370 m water depth (but shallower than 2170 m), (2.) a deglacial source of intermediate water formation within or close to the Okhotsk Sea as key region for NPIW changes (3.) a nutrient-rich deep water pool that has been located much deeper, episodically, and thus more isolated from the atmosphere than today. This is consistent with other studies indicating that the abyssal N-Pacific was more isolated and did not contribute to the atmospheric CO2 rise during H1 (Galbraith et al., 2007) but contradicts the model-derived hypothesis of deep water formation in the North Pacific during H1 and the YD (Okazaki et al., 2010b)

7.5.3 What are causes and consequences of rapid switches in North Pacific Intermediate Water ventilation?

During B/A, our results suggest that the formation of intermediate water was significantly weakened or even turned off in the North Pacific while allowing for upward diffusion of nutrient-rich and less-ventilated Pacific Deep Water. This finding is in agreement with the widespread occurrence of laminated sequences at intermediate water depths in the North Pacific realm (Behl and Kennett, 1996; Cook et al., 2005b; Kim et al., 2011) between ca. 600 – 2000 m water depth during B/A and the early Holocene since the formation of laminae has been linked to dysoxic conditions and enhanced biological productivity during this periods. Accordingly, the significantly lower δ 13C values at intermediate water depths can be explained by enhanced re-mineralization of organic matter in response to amplified productivity and carbon export along the continental margins.

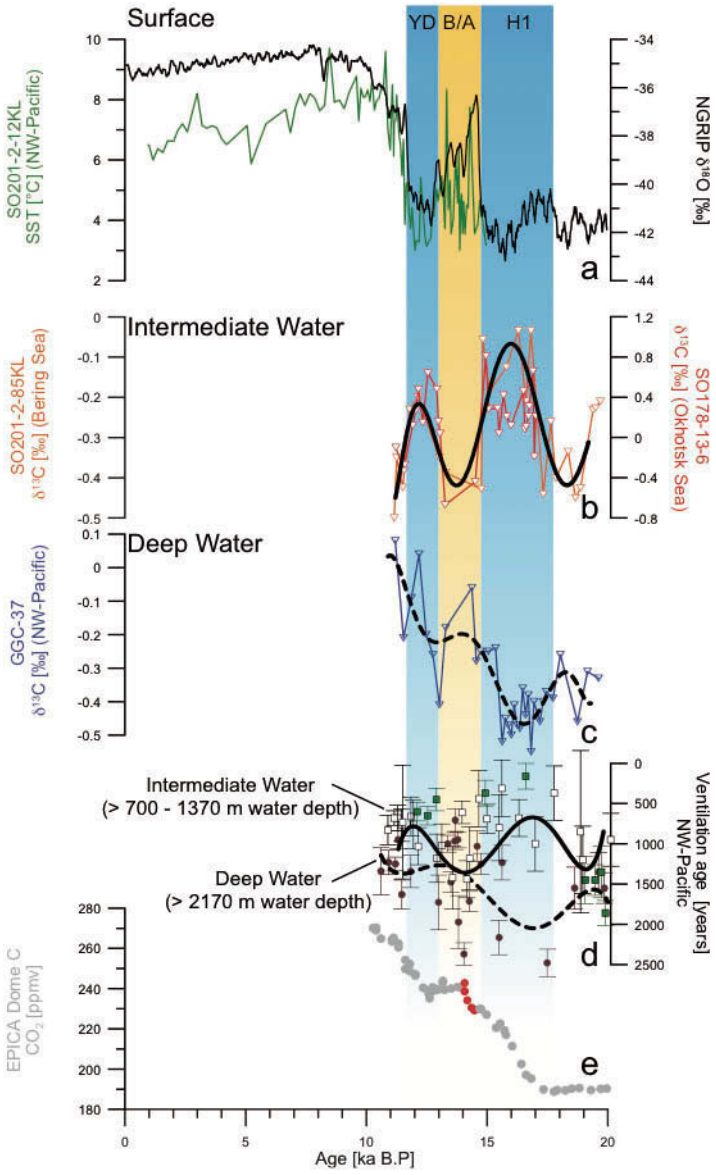

Figure 7.6: Proxy records of surface, intermediate and deep water in NW-Pacific. Blue and yellow shaded bars mark Heinrich-1, Younger Dryas, Bølling/Allerød phases. (a) alkenone-based SST record of SO201-2-12KL (in green) from NW-Pacific (Max et al., 2012b), NGRIP oxygen isotope record in black (Rasmussen et al., 2006b). (b) benthic δ^{13}C-records (*C. lobatulus*) from Okhotsk (red) and Bering Sea (orange) with smoothed spline (thick black line) (c) deep NW-Pacific benthic δ^{13}C-record from core GGC-37 (in blue) from (ca. 3300 m depth, blue curve) and smoothed spline (thick stippled line) (d) published NW-Pacific intermediate (< 1370 m depth; open boxes) and deep water (> 2170 m depth; filled brown circles) B-P ages (Adkins and Boyle, 1997; Ahagon et al., 2003a; Duplessy et al., 1989b; Keigwin, 2002b; Minoshima et al., 2007; Murayama et al., 1992; Sagawa and Ikehara, 2008b; Sarnthein et al., 2006b) and B-P ages from marginal seas (700 – 1000 m depth; filled green boxes) and error bars for each B-P age. Thick black line is smoothed spline interpolation for intermediate and deep water ventilation ages (stippled line), (e) atmospheric CO_2 concentrations from EPICA Dome C ice core (Lourantou et al., 2010). Red spots mark deglacial ~15 ppmv CO_2 rise between ca. 15 – 14.5 ka BP.

Hence, the oceanic conditions during the B/A and the early Holocene may have favoured the opportunity of CO2 release from the North Pacific into the atmosphere as long as upper-ocean stratification and biological nutrient utilization was weak (Sarnthein et al., 2004). If at all, the North Pacific may have contributed to the small-scale (15 ppmv) but rapid atmospheric CO2 rise at ca.14.6 ka BP (Fig. 6), which has been inferred from the EPICA Dome C ice-core record (Lourantou et al., 2010).

The large change in OSIW δ13C values with an amplitude of 1.5 ‰ between H1 and the B/A bears additional information about the boundary conditions of intermediate water formation. The large amplitude requires conditions substantially different from the modern OSIW formation. Under present conditions, intermediate water masses are a blend of surface water and old Pacific Deep Water, which enters the Okhotsk Sea basin through the deepest sills of the Kurile Islands (mainly through Kruzenshtern Strait, ca. 1760 m water depth) (Talley and Roemmich, 1991). Due to the intrusion of old and nutrient-enriched Pacific Deep Water, modern OSIW is marked by relatively high nutrient concentrations and low δ13C values of ca. 0 to -0.3 ‰ (see also Fig.4). Thermodynamic effects due to reduced sea surface temperatures and/or reduced biological productivity cannot solely explain the extremely high δ13C values during H1.

Thus, we speculate that the main source of enhanced OSIW during H1 and the YD was shifted from old Pacific deep water to relatively young and nutrient-depleted surface water masses, which flowed from the North Pacific into the Okhotsk Sea. Once the intensified OSIW formation flushed the deep Okhotsk Sea up to the deep sills, the inflow of old and δ13C-depleted deep-water masses from the North Pacific into the Okhotsk Sea basin was significantly hampered or even blocked during H1 or the YD. The associated deepening of the nutricline within the northwest Pacific region also helps to explain paleo-productivity records that point to reduced biological productivity due to lowered subsurface nutrient supply during H1 and YD (Brunelle et al., 2010a).

7.5.4. Further implications

In general, the finding of a strengthening in meridional overturning in the North Pacific in response to AMOC reductions during H1 and YD is in harmony with results from modelling studies, which simulate enhanced ventilation of NPIW during these intervals (Chikamoto et al., 2012). However, our results do not corroborate model simulations that even argue for a switch to Pacific deep-water formation. The establishment of a deep PMOC is expected to be accompanied by a strengthened northeastward upper-ocean heat transport via the North Pacific Current, thereby warming the N-Pacific during H1 and YD (Krebs and Timmermann, 2007; Okazaki et al., 2010b; Saenko et al., 2004).

SST records in combination with sea-ice reconstructions provide no evidence of surface warming during the H1 and YD in the NW-Pacific (Fig. 6) leaving this scenario unlikely (Max et al., 2012b). From this we infer that the enhancement in NPIW formation was apparently too weak to account for a strengthened poleward heat transport that had the potential of warming the subarctic N-Pacific and promote deep overturning.

On the other hand our results may provide important clues for future changes in marine biogeochemistry that are related to a substantial weakening of Pacific intermediate water formation and its consequences in favouring the expansion of the oxygen minimum zone at the intermediate water level (Jaccard and Galbraith, 2012; Schmittner et al., 2007). During the B/A and early Holocene, hypoxic conditions marked the oceanic continental margins in the NW-Pacific as well as the Bering Sea and culminated in the formation of laminated sediments. Since the intermediate water formation in the Okhotsk Sea is the most important subduction zone of fresh water masses in the subarctic Pacific today, which in turn is closely coupled to sea-ice formation, any significant reduction in sea-ice formation may lead to a rapid switchback to such conditions. This becomes more evident as in the Okhotsk Sea modern seasonal sea ice cover extends south as far as 43°N and marks the southernmost occurrence of sea-ice in the Northern Hemisphere. Environmental changes in the Okhotsk Sea due to a rise in the average temperature of Earth's atmosphere in future may tip the scale for OSIW shutdown and thus could promote the expansion of hypoxic conditions in the N-Pacific as learned from the past.

7.6. Conclusions

The combination of benthic δ13C-records and ventilation ages from the subarctic Pacific consistently argues for rapid switches in intermediate water formation/ventilation during the last deglaciation, ultimately linked to expanded NPIW during times when the Atlantic Meridional Overturning Circulation was substantially weakened. From this we suggest a deglacial seesaw between strengthened (lowered) shallow overtuning of the subarctic Pacific and lowered (strengthened) meridional overturning of the North Atlantic.

The deglacial source of expanded North Pacific Intermediate Water formation was located within the Okhotsk Sea as pacemaker for NPIW changes. To explain the positive excursion δ13C in the Okhotsk Sea we further speculate that the main source of enhanced OSIW during H1 and the YD was shifted from old Pacific deep water to relatively young and nutrient-depleted surface water masses. The expanded OSIW flushed the deep Okhotsk Sea up to the deep sills, thus probably hampered the inflow of old and δ13C-depleted deep-water masses from the North Pacific into the Okhotsk Sea.

The strengthening of NPIW and shallow overturning during H1 and YD would argue for a deepening of the nutricline within the northwest Pacific. This would also have tremendous consequences for the deep Pacific carbon reservoir as the expanded deglacial NPIW hampered the upward diffusion of nutrient- and CO2-rich Pacific Deep Water and its exchange through surface water masses to the atmosphere.

7.7. References

Adkins, J.F., Boyle, E.A., 1997. Changing atmospheric Delta C-14 and the record of deep water paleoventilation ages. Paleoceanography 12, 337-344.

Ahagon, N., Ohkushi, K., Uchida, M., Mishima, T., 2003. Mid-depth circulation in the northwest Pacific during the last deglaciation: Evidence from foraminiferal radiocarbon ages. Geophysical Research Letters 30, -.

Behl, R.J., Kennett, J.P., 1996. Brief interstadial events in the Santa Barbara basin, NE Pacific, during the past 60 kyr. Nature 379, 243-246.

Boyle, E.A., 1988. Vertical Oceanic Nutrient Fractionation and Glacial Interglacial Co2 Cycles. Nature 331, 55-56.

Brunelle, B.G., Sigman, D.M., Jaccard, S.L., Keigwin, L.D., Plessen, B., Schettler, G., Cook, M.S., Haug, G.H., 2010. Glacial/interglacial changes in nutrient supply and stratification in the western subarctic North Pacific since the penultimate glacial maximum. Quaternary Sci Rev 29, 2579-2590.

Chikamoto, M.O., Menviel, L., Abe-Ouchi, A., Ohgaito, R., Timmermann, A., Okazaki, Y., Harada, N., Oka, A., Mouchet, A., 2012. Variability in North Pacific intermediate and deep water ventialtion during Heinrich events in two coupled climate models. Deep-Sea Res. Part II-Top. Stud. Oceanogr. 61-64, 114-126.

Cook, M.S., Keigwin, L.D., Sancetta, C.A., 2005. The deglacial history of surface and intermediate water of the Bering Sea. Deep-Sea Res. Part II-Top. Stud. Oceanogr. 52, 2163-2173.

Curry, W.B., Duplessy, J.C., Labeyrie, L.D., Shackleton, N.J., 1988. Changes in the distribution of delta C-13 of deep water TCO2 between the last glaciation and the Holocene. Paleoceanography 3, 317-341

. Curry, W.B., Oppo, D.W., 2005. Glacial water mass geometry and the distribution of delta C-13 of Sigma CO2 in the western Atlantic Ocean. Paleoceanography 20, -.

Dullo, W.C., Baranov, B., van den Bogaard, C., 2009. FS Sonne Fahrtbericht/ Cruise Report SO201-2 KALMAR, Busan/Korea-Tomakomai/Japan, 30.08-08.10.2009. IFM-GEOMAR Report 35, in: van den Bogaard, C. (Ed.), p. 233.

Duplessy, J.C., Arnold, M., Bard, E., Juilletleclerc, A., Kallel, N., Labeyrie, L., 1989. Ams C-14 Study of Transient Events and of the Ventilation Rate of the Pacific Intermediate Water during the Last Deglaciation. Radiocarbon 31, 493-502.

Galbraith, E.D., Jaccard, S.L., Pedersen, T.F., Sigman, D.M., Haug, G.H., Cook, M., Southon, J.R., Francois, R., 2007. Carbon dioxide release from the North Pacific abyss during the last deglaciation. Nature 449, 890-U899.

Gorbarenko, S.A., Basov, I.A., Chekhovskaya, M.P., Southon, J., Khusid, T.A., Artemova, A., 2005. Orbital and millennium scale environmental changes in the southern Bering Sea during the last glacial-Holocene: Geochemical and paleontological evidence. Deep-Sea Res. Part II-Top. Stud. Oceanogr. 52, 2174-2185.

Gorbarenko, S.A., Khusid, T.A., Basov, I.A., Oba, T., Southon, J.R., Koizumi, I., 2002. Glacial Holocene environment of the southeastern Okhotsk Sea: evidence from geochemical and palaeontological data. Palaeogeogr Palaeocl 177, 237-263.

Haug, G.H., Sigman, D.M., Tiedemann, R., Pedersen, T.F., Sarnthein, M., 1999. Onset of permanent stratification in the subarctic Pacific Ocean. Nature 401, 779-782.

Honda, M.C., Imai, K., Nojiri, Y., Hoshi, F., Sugawara, T., Kusakabe, M., 2002. The biological pump in the northwestern North Pacific based on fluxes and major components of particulate matter obtained by sediment-trap experiments (1997-2000). Deep-Sea Res. Part II-Top. Stud. Oceanogr. 49, 5595-5625.

Jaccard, S.L., Galbraith, E.D., 2012. Large climate-driven changes of oceanic oxygen concentrations during the last deglaciation. Nature Geoscience 5, 151-156.

Jaccard, S.L., Galbraith, E.D., Sigman, D.M., Haug, G.H., Francois, R., Pedersen, T.F., Dulski, P., Thierstein, H.R., 2009. Subarctic Pacific evidence for a glacial deepening of the oceanic respired carbon pool. Earth and Planetary Science Letters 277, 156-165.

Keigwin, L.D., 1998. Glacial-age hydrography of the far northwest Pacific Ocean. Paleoceanography 13, 323-339.

Keigwin, L.D., 2002. Late Pleistocene-Holocene paleoceanography and ventilation of the Gulf of California. Journal of Oceanography 58, 421-432.

Keigwin, L.D., Jones, G.A., Froelich, P.N., 1992. A 15,000 Year Paleoenvironmental Record from Meiji Seamount, Far Northwestern Pacific. Earth and Planetary Science Letters 111, 425-440.

Kim, S., Khim, B.K., Uchida, M., Itaki, T., Tada, R., 2011. Millenial-scale paleoceanographic events and implications for the intermediate-water ventilation in the northrn slope area of the Bering Sea during the last 71kyrs. Global and Planetary Change 79, 89-98.

Krebs, U., Timmermann, A., 2007. Tropical air-sea interactions accelerate the recovery of the Atlantic Meridional Overturning Circulation after a major shutdown. Journal of Climate 20, 4940-4956.

Kroopnick, P.M., 1985. The Distribution of C-13 of Sigma-Co2 in the World Oceans. Deep-Sea Research Part a-Oceanographic Research Papers 32, 57-84.

Kuzmin, Y.V., Burr, G.S., Gorbunov, S.V., Rakov, V.A., Razjigaeva, N.G., 2007. A tale of two seas: Reservoir age correction values (R, Delta R) for the Sakhalin Island (Sea of Japan and Okhotsk Sea). Nuclear Instruments & Methods in Physics Research Section B-Beam Interactions with Materials and Atoms 259, 460-462.

Kuzmin, Y.V., Burr, G.S., Jull, A.J.T., 2001. Radiocarbon reservoir correction ages in the Peter the Great Gulf, Sea of Japan, and eastern coast of the Kunashir, southern Kuriles (northwestern Pacific). Radiocarbon 43, 477-481.

Lourantou, A., Lavric, J.V., Kohler, P., Barnola, J.M., Paillard, D., Michel, E., Raynaud, D., Chappellaz, J., 2010. Constraint of the CO2 rise by new atmospheric carbon isotopic measurements during the last deglaciation. Global Biogeochemical Cycles 24.

Lund, D.C., Mix, A.C., Southon, J., 2011. Increased ventilation age of the deep northeast Pacific Ocean during the last deglaciation. Nature Geoscience 4, 771-774.

Lutze, G.F., Thiel, H., 1989. Epibenthic Foraminifera from Elevated Microhabitats - Cibicidoides-Wuellerstorfi and Planulina-Ariminensis. J Foramin Res 19, 153-158.

Mackensen, A., Schumacher, S., Radke, J., Schmidt, D.N., 2000. Microhabitat preferences and stable carbon isotopes of endobenthic foraminifera: clue to quantitative reconstruction of oceanic new production? Marine Micropaleontology 40, 233-258.

Marchitto, T.M., Lehman, S.J., Ortiz, J.D., Fluckiger, J., van Geen, A., 2007. Marine radiocarbon evidence for the mechanism of deglacial atmospheric CO(2) rise. Science 316, 1456-1459.

Marchitto, T.M., Lynch-Stieglitz, J., Hemming, S.R., 2005. Deep pacific CaCO3 compensation and glacial-interglacial atmosphericCO(2). Earth and Planetary Science Letters 231, 317-336.

Matsumoto, K., Oba, T., Lynch-Stieglitz, J., Yamamoto, H., 2002. Interior hydrography and circulation of the glacial Pacific Ocean. Quaternary Sci Rev 21, 1693-1704.

Max, L., Riethdorf, J.R., Tiedemann, R., Smirnova, M., Lembke-Jene, L., Fahl, K., Nurnberg, D., Matul, A., Mollenhauer, G., 2012. Sea surface temperature variability and sea-ice extent in the subarctic northwest Pacific during the past 15,000 years. Paleoceanography 27.

McManus, J.F., Francois, R., Gherardi, J.M., Keigwin, L.D., Brown-Leger, S., 2004. Collapse and rapid resumption of Atlantic meridional circulation linked to deglacial climate changes. Nature 428, 834-837.

Minoshima, K., Kawahata, H., Irino, T., Ikehara, K., Aoki, K., Uchida, M., Yoneda, M., Shibata, Y., 2007. Deep water ventilation in the northwestern North Pacific during the last deglaciation and the early Holocene (15-5 cal. kyr BP) based on AMS C-14 dating. Nuclear Instruments & Methods in Physics Research Section B-Beam Interactions with Materials and Atoms 259, 448-452.

Murayama, M., Taira, A., Iwakura, H., Matsumoto, E., Nakamura, T., 1992. Northwest Pacific deep water ventilation rate during the past 35,000 years with the AMS 14C foraminifera ages, Summaries of Researchers Using AMS at Nagoya University (Nagoya University Center for Chronological Research), Nagoya, Japan (in Japanese with english abstract). 3, 114-121.

Okazaki, Y., Timmermann, A., Menviel, L., Harada, N., Abe-Ouchi, A., Chikamoto, M.O., Mouchet, A., Asahi, H., 2010. Deepwater Formation in the North Pacific During the Last Glacial Termination. Science 329, 200-204.

Rasmussen, S.O., Andersen, K.K., Svensson, A.M., Steffensen, J.P., Vinther, B.M., Clausen, H.B., Siggaard-Andersen, M.L., Johnsen, S.J., Larsen, L.B., Dahl-Jensen, D., Bigler, M., Rothlisberger, R., Fischer, H., Goto-Azuma, K., Hansson, M.E., Ruth, U., 2006. A new Greenland ice core chronology for the last glacial termination. Journal of Geophysical Research-Atmospheres 111.

Reimer, P.J., Baillie, M.G.L., Bard, E., Bayliss, A., Beck, J.W., Blackwell, P.G., Ramsey, C.B., Buck, C.E., Burr, G.S., Edwards, R.L., Friedrich, M., Grootes, P.M., Guilderson, T.P., Hajdas, I., Heaton, T.J., Hogg, A.G., Hughen, K.A., Kaiser, K.F., Kromer, B., McCormac, F.G., Manning, S.W., Reimer, R.W., Richards, D.A., Southon, J.R., Talamo, S., Turney, C.S.M., van der Plicht, J., Weyhenmeye, C.E., 2009. Intcal09 and Marine09 Radiocarbon Age Calibration Curves, 0-50,000 Years Cal Bp. Radiocarbon 51, 1111-1150.

Rella, S.F., Tada, R., Nagashima, K., Ikehara, M., Itaki, T., Ohkushi, K., Sakamoto, T., Harada, N., Uchida, M., 2012. Abrupt changes of intermediate water properties on the northeastern slope of the Bering Sea during the last glacial and deglacial period. Paleoceanography 27.

Saenko, O.A., Schmittner, A., Weaver, A.J., 2004. The Atlantic-Pacific seesaw. Journal of Climate 17, 2033-2038.

Sagawa, T., Ikehara, K., 2008. Intermediate water ventilation change in the subarctic northwest Pacific during the last deglaciation. Geophysical Research Letters 35, -.

Sarmiento, J.L., Gruber, N., Brzezinski, M.A., Dunne, J.P., 2004. High-latitude controls of thermocline nutrients and low latitude biological productivity. Nature 427, 56-60.

Sarnthein, M., Gebhardt, H., Kiefer, T., Kucera, M., Cook, M., Erlenkeuser, H., 2004. Mid Holocene origin of the sea-surface salinity low in the subarctic North Pacific. Quaternary Sci Rev 23, 2089-2099.

Sarnthein, M., Kiefer, T., Grootes, P.M., Elderfield, H., Erlenkeuser, H., 2006. Warmings in the far northwestern Pacific promoted pre-Clovis immigration to America during Heinrich event 1. Geology 34, 141-144.

Schmittner, A., Galbraith, E.D., Hostetler, S.W., Pedersen, T.F., Zhang, R., 2007. Large fluctuations of dissolved oxygen in the Indian and Pacific oceans during Dansgaard-Oeschger oscillations caused by variations of North Atlantic Deep Water subduction. Paleoceanography 22.

Schweizer, M., Pawlowski, J., Kouwenhoven, T., van der Zwaan, B., 2009. Molecular Phylogeny of Common Cibicidids and Related Rotaliida (Foraminifera) Based on Small Subunit Rdna Sequences. J Foramin Res 39, 300-315.

Seki, O., Ikehara, M., Kawamura, K., Nakatsuka, T., Ohnishi, K., Wakatsuchi, M., Narita, H., Sakamoto, T., 2004. Reconstruction of paleoproductivity in the Sea of Okhotsk over the last 30 kyr. Paleoceanography 19, -.

Seki, O., Sakamoto, T., Sakai, S., Schouten, S., Hopmans, E.C., Sinninghe Damste, J.S., Pancost, R.D., 2009. Large changes in seasonal sea ice distribution and productivity in the Sea of Okhotsk during the deglaciations. Geochemistry, Geophysics, Geosystems 10.

Shcherbina, A.Y., Talley, L.D., Rudnick, D.L., 2003. Direct observations of North Pacific ventilation: Brine rejection in the Okhotsk Sea. Science 302, 1952-1955.

Stommel, H., 1961. Thermohaline Convection with Two Stable Regimes of Flow. Tellus 13, 224-230.

Stuiver, M., 1980. Workshop on C-14 Data Reporting. Radiocarbon 22, 964-966.

Stuiver, M., Polach, H.A., 1977. Reporting of C-14 Data - Discussion. Radiocarbon 19, 355-363.

Stuiver, M., Reimer, P.J., 1993. Extended C-14 Data-Base and Revised Calib 3.0 C-14 Age Calibration Program. Radiocarbon 35, 215-230.

Talley, L.D., 1993. Distribution and Formation of North Pacific Intermediate Water. J Phys Oceanogr 23, 517-537.

Talley, L.D., Roemmich, D., 1991. A TRIBUTE TO REID,JOSEPH,L. IN RECOGNITION OF 40 YEARS OF CONTRIBUTIONS TO OCEANOGRAPHY. Deep-Sea Research Part a-Oceanographic Research Papers 38, R7-R11.

Tanaka, S., Takahashi, K., 2005. Late Quaternary paleoceanographic changes in the Bering Sea and the western subarctic Pacific based on radiolarian assemblages. Deep-Sea Res. Part II-Top. Stud. Oceanogr. 52, 2131-2149.

Timmermann, A., Krebs, U., Justino, F., Goosse, H., Ivanochko, T., 2005. Mechanisms for millennial-scale global synchronization during the last glacial period. Paleoceanography 20.

Author Contributions

L.M. and R.T. designed this study and prepared this manuscript. L.L.-J. and L.M. collected the stable carbon isotope data, A.M. facilitated and oversaw the stable isotope measurements at the Stable Isotope Laboratory of the Alfred Wegener Institute for Polar and Marine Research, Bremerhaven. J.-R.R. and H.K. contributed to the establishment of ventilation ages and discussion. R.T. and D.N. provided important background knowledge on issues regarding this study. All authors contributed to the interpretation and the preparation of the final manuscript.

Supplementary Tables (prepared for electronic supplement)

Table S1: Stable isotope measurement results ($\delta^{18}O$; $\delta^{13}C$) from epibenthic foraminifera *Cibicidoides lobatulus*.

Core:	Core Depth (cm)	Age (ka BP)	$\delta^{18}O$ (‰PDB)	$\delta^{13}C$ (‰PDB)
SO201-2-85KL (western Bering Sea)	43	11.15	3.440	-0.500
	45	11.26	3.288	-0.350
	50	11.51	3.117	-0.424
	53	11.79	3.360	-0.230
	55	12.14	3.387	-0.200
	60	13.01	3.461	-0.349
	63	13.29	3.323	-0.388
	80	14.76	3.307	-0.428
	81	14.83	3.670	-0.056
	85	15.10	3.481	-0.185
	95	15.80	3.988	-0.125
	100	16.30	4.536	-0.034
	103	16.61	3.640	-0.210
	105	16.81	4.231	-0.035
	110	17.33	3.256	-0.441
	113	17.64	3.960	-0.260
	115	17.84	3.817	-0.401
	120	18.36	4.121	-0.335
	123	18.67	3.930	-0.450
	125	18.87	3.965	-0.425
	130	19.39	3.839	-0.232
	131	19.49	3.864	-0.227
	133	19.69	3.900	-0.210
SO178-13-6 (Okhotsk Sea)	1767.5	11.551	3.74	-0.33
	1772.5	11.584	3.45	-0.27
	1822.5	11.915	3.59	0.12
	1842.5	12.048	3.48	0.27
	1857.5	12.154	3.59	0.48
	1870.5	12.334	3.66	0.15
	1885.5	12.542	3.38	0.64
	1912.5	12.915	3.43	0.48
	1917.5	12.984	3.22	0.16
	1922.5	13.053	3.39	0.04
	1937.5	13.261	3.26	-0.67
	1972.5	14.506	4.07	-0.44
	2087.5	14.95	3.1	0.81
	2092.5	15.06	3.05	0.28
	2157.5	15.433	3.81	0.29
	2162.5	15.495	4.04	0.04
	2177.5	15.684	4.05	0.42
	2187.5	15.809	3.82	0.21
	2202.5	15.997	3.88	0.12
	2242.5	16.5	3.9	0.46
	2247.5	16.562	3.81	0.08
	2252.5	16.611	3.86	0.11
	2272.5	16.717	3.78	0.21
	2277.5	16.744	3.88	0.31
	2292.5	16.824	3.64	0.48
	2297.5	16.85	4.12	0.48
	2307.5	16.904	3.75	0.66
	2317.5	16.957	3.11	-0.19
SO178-13-6 (Okhotsk Sea)	2327.5	17.01	3.94	0.21
	2342.5	17.09	3.99	0.27

Table S2: Radiocarbon measurements on paired benthic/planktic foraminiferas (ventilation ages) from NW-Pacific sediment cores. Ventilation ages are given in years and era is indicated by LGM, H1, B/A and Holocene, respectively.

Core	Water Depth (m)	Core Depth (cm)	Planktic ^{14}C-age (yrs)	Benthic ^{14}C-age (yrs)	Calendar Age (ka BP)*	Ventilation Age (years)	Error +/- 1-Sigma (yrs)	Era	Reference
North Pacific (intermediate)									
CH84-14	978	230	10000±140	10850±140	10.33	850	280	Holocene	Duplessy et al., (1989), Adkins and Boyle (1997)
CH84-14	978	280	10230±140	11060±150	10.54	830	290	Holocene	
CH84-14	978	310	10640±150	11370±130	11.03	730	280	Holocene	
CH84-14	978	340	10870±150	11630±180	11.71	760	330	Holocene	
CH84-14	978	400	12180±160	13200±150	13.18	1020	310	B/A	
CH84-14	978	480	12750±150	13930±220	13.66	1180	370	B/A	
CH84-14	978	510	13060±140	13500±200	14.87	440	340	H1	
CH84-14	978	550	13830±150	14140±200	15.52	310	350	H1	
CH84-14	978	690	15570±210	15940±190	17.59	370	400	H1	
GH02-1030	1212	210	9840±40	10700±70	9.52	860	110	Holocene	Sagawa and Ikehara (2008)
GH02-1030	1212	220	10240±60	10800±70	10.07	560	130	Holocene	
GH02-1030	1212	235	10510±60	11190±60	10.39	680	120	Holocene	
GH02-1030	1212	244	10690±60	11370±60	10.64	680	120	Holocene	
GH02-1030	1212	261	10950±60	11610±70	11.02	660	130	Holocene	
GH02-1030	1212	290	12900±70	13510±80	13.37	610	150	B/A	
GH02-1030	1212	323.5	13060±70	14500±50	13.62	1440	120	B/A	
GH02-1030	1212	345.5	13470±40	14160±40	14.03	690	80	B/A	
GH02-1030	1212	435.5	15010±80	16010±90	16.87	1000	170	H1	
GH02-1030	1212	465.5	15140±60	16140±80	16.92	1000	160	H1	
GH02-1030	1212	523	16380±60	17230±100	18.33	850	160		
GH02-1030	1212	558	17780±70	18730±120	19.64	950	190	LGM	
GH02-1030	1212	630	19130±180	20590±180	21.32	1460	360	LGM	
MR01K03-PC4/5	1366	231-232	10600±100	11370±100	11.02	770	200	Holocene	Ahagon et al., (2003)
MR01K03-PC4/5	1366	262-264	10900±110	11930±120	11.46	1030	230	Holocene	
MR01K03-PC4/5	1366	291-293	11420±120	12600±100	12.48	1180	300	YD	
MR01K03-PC4/5	1366	311-313	12230±100	13650±200	13.21	1420	390	B/A	
MR01K03-PC4/5	1366	363-365	13450±170	14250±240	14.77	800	410	H1	

Table S2 (continued):

Core	Water Depth (m)	Core Depth (cm)	Planktic ^{14}C-age (yrs)	Benthic ^{14}C-age (yrs)	Calendar Age (ka BP)*	Ventilation Age (years)	Error +/- 1-Sigma (yrs)	Era	Reference
MR01K03-PC4/5	1366	540-542	16450±220	17650±200	18.74	1200	420		Ahagon et al., (2003)
MR01K03-PC4/5	1366	642-644	18200±130	19650±220	20.62	1450	350	LGM	
Bering Sea (intermediate)									
SO201-2-101KL	630	110	17310±120	18630±200	19.73	1350	320	LGM	this study
SO201-2-85KL	968	45-46	10315±65	10700±40	11.20	385	115	Holocene	this study
SO201-2-85KL	968	135-136	17350±65	19210±90	19.90	1860	155	LGM	
SO202-18	1100	415-417.5	10850±25	11300±50	11.96	450	75	YD	this study
SO202-18	1100	432-434.5	10950±55	11550±40	12.10	600	115	YD	
SO202-18	1100	512-514.5	11150±65	11800±60	12.53	650	115	YD	
SO202-18	1100	592-594.5	11850±60	12300±80	12.90	450	140	YD	
Sea of Okhotsk (intermediate)									
SO178-13-6	713	2072.5	13390±100	13760±60	14.92	370	160	H1	this study
SO178-13-6	713	2250.5	14420±45	14580±60	16.60	160	160	H1	
SO178-13-6	713	2342.5	15090±60	15470±60	17.09	380	160	H1	
Nesmeyanov GGC-27	995	70	16750±200	18200±95	19.06	1450	295	LGM	Keigwin et al., (2002)
B34-91	1227	225	17200±80	18650±110	19.48	1450	190	LGM	Keigwin et al., (2002)
North Pacific (deep)									
SO201-2-12KL	2170	340	10800±65	11750±50	11.31	950	115	Holocene	this study
SO201-2-12KL	2170	508	12500±50	13500±55	13.38	1000	105	B/A	
SO201-2-12KL	2170	550	12900±50	13850±50	13.79	950	100	B/A	
KR02-15 PC6	2215	539.2	10610±90	11840±60	10.91	1230	150	Holocene	Minoshima et al., (2007)
KR02-15 PC6	2215	555.1	10860±70	12490±110	11.46	1630	180	Holocene	
KR02-15 PC6	2215	575.6	13470±70	14500±120	14.59	1030	190	B/A	

Table S2 (continued):

Core	Water Depth (m)	Core Depth (cm)	Planktic ^{14}C-age (yrs)	Benthic ^{14}C-age (yrs)	Calendar Age (ka BP)*	Ventilation Age (years)	Error +/- 1-Sigma (yrs)	Era	Reference
KT89-18-P4	2700	185-190	9800±133	11140±159	10.60	1340	292	Holocene	Murayama et al.,(1992)
KT89-18-P4	2700	200-204	10692±108	12034±94	11.84	1342	202	YD	
KT89-18-P4	2700	236-240	11622±101	13350±238	12.99	1728	339	YD	
KT89-18-P4	2700	268-272	12450±91	14423±237	13.82	1973	328	B/A	
KT89-18-P4	2700	338-342	13447±113	14681±103	15.62	1234	216	H1	
KT89-18-P4	2700	449-453	17275±478	19267±557	20.00	1992	1035	LGM	
KT89-18-P4	2700	534-538	19655±303	21344±205	22.87	1689	508	LGM	
MD01-2416	2317	88	12690±50	13655±55	13.66	965	105	B/A	Sarnthein et al., (2006)
MD01-2416	2317	96	12555±60	14030±70	13.50	1475	130	B/A	
MD01-2416	2317	115	13205±55	14920±70	14.27	1715	125	B/A	
MD01-2416	2317	136	13090±60	15460±80	14.04	2370	140	B/A	
MD01-2416	2317	163	13795±60	15960±100	15.50	2165	215	H1	
MD01-2416	2317	177	15380±70	17850±100	17.49	2480	170	H1	
ODP883	2385	51	12715±50	13420±90	13.68	705	140	B/A	Sarnthein et al., (2006)
Bering Sea (deep)									
SO201-2-77KL	2163	115	10450±40	11650±45	11.20	1250	85	Holocene	this study
SO201-2-77KL	2163	180	13200±45	14450±85	14.75	1250	130	B/A	
Sea of Okhotsk (deep)									
Nesmeyanov GGC-20	1510	230	17350±100	18700±140	19.61	1350	240	LGM	Keigwin et al., (2002)
Nesmeyanov GGC-18	1700	214-216	16250±120	17800±140	18.62	1550	260		Keigwin et al., (2002)
Nesmeyanov GGC-15	1980	170	17650±80	19200±110	19.85	1550	190	LGM	Keigwin et al., (2002)

* recalculated with a constant reservoir age correction of 700 years for the Bering Sea and 900 years for the NW-Pacific and Okhotsk Sea, respectively.

8. Deglacial Development of (sub) sea surface temperature and salinity in the subarctic northwest Pacific: Implications for upper-ocean stratification

Jan-Rainer Riethdorf, Lars Max, Dirk Nürnberg, Lester Lembke-Jene, Ralf Tiedemann

Manuscript published in Paleoceanography, vol. 28, 91-104, 2013.

doi: 10.1002/palo.20014

PALEOCEANOGRAPHY, VOL. 28, 91–104, doi:10.1002/palo.20014, 2013

Deglacial development of (sub) sea surface temperature and salinity in the subarctic northwest Pacific: Implications for upper-ocean stratification

Jan-Rainer Riethdorf,[1,3] Lars Max,[2] Dirk Nürnberg,[1] Lester Lembke-Jene,[2] and Ralf Tiedemann[2]

Received 25 June 2012; revised 13 January 2013; accepted 17 January 2013; published 23 March 2013.

[1] Based on models and proxy data, it has been proposed that salinity-driven stratification weakened in the subarctic North Pacific during the last deglaciation, which potentially contributed to the deglacial rise in atmospheric carbon dioxide. We present high-resolution subsurface temperature ($T_{Mg/Ca}$) and subsurface salinity-approximating ($\delta^{18}O_{ivc\text{-}sw}$) records across the last 20,000 years from the subarctic North Pacific and its marginal seas, derived from combined stable oxygen isotopes and Mg/Ca ratios of the planktonic foraminiferal species *Neogloboquadrina pachyderma* (sin.). Our results indicate regionally differing changes of subsurface conditions. During the Heinrich Stadial 1 and the Younger Dryas cold phases, our sites were subject to reduced thermal stratification, brine rejection due to sea-ice formation, and increased advection of low-salinity water from the Alaskan Stream. In contrast, the Bølling-Allerød warm phase was characterized by strengthened thermal stratification, stronger sea-ice melting, and influence of surface waters that were less diluted by the Alaskan Stream. From direct comparison with alkenone-based sea surface temperature estimates ($SST_{Uk'37}$), we suggest deglacial thermocline changes that were closely related to changes in seasonal contrasts and stratification of the mixed layer. The modern upper-ocean conditions seem to have developed only since the early Holocene.

Citation: Riethdorf, J.-R., L. Max, D. Nürnberg, L. Lembke-Jene, and R. Tiedemann (2013), Deglacial development of (sub) sea surface temperature and salinity in the subarctic northwest Pacific: Implications for upper-ocean stratification, *Paleoceanography*, *28*, 91–104, doi:10.1002/palo.20014.

1. Introduction

[2] No deep water is formed in the modern subarctic North Pacific (N Pacific). There, a relatively steep salinity gradient (permanent halocline) prevents surface water from sinking, isolating it from the underlying nutrient-rich deep water [*Haug et al.*, 1999]. In the N Pacific, upper-ocean stratification most likely developed around 2.7 million years ago [*Haug et al.*, 1999, 2005; *Sigman et al.*, 2004] and is maintained by a restricted meridional exchange between subpolar and subtropical waters, atmospheric low-latitude moisture transport from the Atlantic to the Pacific, and northward moisture flux by the Asian monsoon [*Warren*, 1983; *Emile-Geay et al.*, 2003]. As a consequence of salinity-driven stratification, the exchange of gas, heat, and nutrients between deep and surface water is limited in the N Pacific. In contrast, the modern Southern Ocean releases carbon dioxide (CO_2) to the atmosphere due to upwelling of deep waters. This led to the assumption that high-latitude ocean stratification drives changes in atmospheric CO_2 concentrations during recent glacial-interglacial cycles [*Haug et al.*, 1999; *Sigman and Boyle*, 2000; *Sigman and Haug*, 2003; *Sigman et al.*, 2004, 2010; *Jaccard et al.*, 2005]. However, growing paleoceanographic evidence [e.g., *Okazaki et al.*, 2010] indicates that during the last deglaciation, deep water was formed in the N Pacific and that the regional halocline was not a permanent feature. Hence, the N Pacific might have contributed to the deglacial rise of atmospheric CO_2.

[3] High-resolution records depicting the deglacial paleoceanographic evolution in the subarctic N Pacific are sparse due to a shallow lysocline and corrosive bottom waters limiting $CaCO_3$ preservation. Available reconstructions of sea surface temperature (SST) and salinity indicate strong oceanographic changes and climate oscillations in the subarctic N Pacific realm during the last deglaciation (20–10 ka BP) [e.g., *Ternois et al.*, 2000; *Sarnthein et al.*, 2004, 2006; *Gebhardt et al.*, 2008; *Sagawa and Ikehara*, 2008; *Caissie et al.*, 2010], which are similar to those recorded in Greenland ice [*Grootes et al.*, 1993; *NGRIP members*, 2004]. These are the cold periods of the Heinrich Stadial 1

Additional supporting information may be found in the online version of this article.

[1]Helmholtz Centre for Ocean Research Kiel (GEOMAR), Kiel, Germany.
[2]Alfred Wegener Institute for Polar and Marine Research, Bremerhaven, Germany.
[3]Department of Ocean Floor Geoscience, Atmosphere and Ocean Research Institute, University of Tokyo, Kashiwa, Chiba, Japan.

Corresponding author: Jan-Rainer Riethdorf, Helmholtz Centre for Ocean Research Kiel (GEOMAR), Wischhofstr. 1-3, D-24148 Kiel, Germany. (jriethdorf@geomar.de)

0883-8305/13/10.1002/palo.20014

(H1, 18.0–14.7 ka BP) [*Sarnthein et al.*, 2001] and the Younger Dryas (YD, ~12.9–11.7 ka BP) [*Blockley et al.*, 2012], and the warm phases of the Bølling-Allerød (B/A, ~14.7–12.9 ka BP) [*Blockley et al.*, 2012] and the Preboreal (PB, ~11.7–11.0 ka BP). Recent studies also found evidence for deep water ventilation in the NW Pacific during H1 and the YD [*Ahagon et al.*, 2003; *Ohkushi et al.*, 2004; *Sagawa and Ikehara*, 2008; *Okazaki et al.*, 2010], while at the same time the Atlantic meridional overturning circulation (AMOC) collapsed or declined [*McManus et al.*, 2004]. In contrast, during the B/A, higher ventilation ages have been found in the western N Pacific, which is indicative of reduced deep water ventilation [*Okazaki et al.*, 2010]. In agreement with this observation, general circulation models predict a strengthening of the Pacific meridional overturning circulation (PMOC), which results from a rise in salinity in the N Pacific due to a weakened AMOC [e.g., *Menviel et al.*, 2012]. These studies controversially argue either for an atmosphere-controlled "in-phase" [*Mikolajewicz et al.*, 1997; *Krebs and Timmermann*, 2007; *Okumura et al.*, 2009] or for an ocean-controlled "antiphase" [*Schmittner et al.*, 2003, 2007; *Saenko et al.*, 2004] relationship between the thermal evolution of the North Atlantic (N Atlantic) and the N Pacific. The antiphase relationship is supported by SST and salinity reconstructions from planktonic foraminifera at Site MD01-2416 and ODP Site 883 indicating that during H1, maxima in SST were accompanied by increased salinity [*Kiefer et al.*, 2001; *Sarnthein et al.*, 2006; *Gebhardt et al.*, 2008]. Higher salinity during H1 is supported by Mg/Ca- and $\delta^{18}O$-based results from core GH02-1030 off Japan [*Sagawa and Ikehara*, 2008], which also argues for a potential disappearance of the halocline. The results from core MD01-2416, however, are in conflict with alkenone-based SST reconstructions from the N Pacific realm, which are more supportive of the in-phase models. Results indicate restricted marine productivity during H1 and a SST maximum that occurred during the subsequent B/A in the NE Pacific [*Kienast and McKay*, 2001; *Barron et al.*, 2003], the Bering Sea [*Caissie et al.*, 2010; *Max et al.*, 2012], and the Okhotsk Sea [*Ternois et al.*, 2000; *Harada et al.*, 2006a; *Seki et al.*, 2009]. Mg/Ca-based results from core GH02-1030 also show a rise in SST during the B/A [*Sagawa and Ikehara*, 2008]. In summary, these observations may point to a regionally differing development of the thermocline, because sites MD01-2416 (Detroit Seamount, open subarctic NW Pacific) and GH02-1030 (Kuroshio-influenced NW Pacific) provide quite different oceanographic settings with respect to the N Pacific marginal seas. Consequently, additional reconstructions of SST and salinity, which allow for direct comparisons between alkenone- and Mg/Ca-based results, are essential to understand changes in the structure of the upper water column and the SST development of the subarctic N Pacific.

[4] Here, we report combined stable oxygen isotope and Mg/Ca-based reconstructions of subsurface temperatures ($T_{Mg/Ca}$) and $\delta^{18}O_{ivc\text{-}sw}$ (approximating subsurface salinity) from sediment cores recovered from the southern Okhotsk Sea, the NW Pacific off Kamchatka, and the western Bering Sea covering the last 20 ka BP. Our results, which are compared to alkenone-based SST estimates ($SST_{Uk'37}$) derived from the same samples [*Max et al.*, 2012], indicate deglacial variations in mixed layer stratification (MLS). Moreover, we present supporting evidence that the modern salinity-driven stratification in the N Pacific is a relatively recent feature as suggested by *Sarnthein et al.* [2004].

2. Regional Setting

[5] The subarctic N Pacific is characterized by a large-scale cyclonic surface circulation pattern (Figure 1). At ~40°N, the North Pacific Current, an extension of the subtropical Kuroshio Current, flows eastward and brings relatively warm water (~10°C) into the Alaskan gyre in the NE Pacific. From here, the Alaskan Current, fed by freshwater discharge from the North American continent [*Kowalik et al.*, 1994; *Weingartner et al.*, 2005], transports surface water to the north. Subsequently, the Alaskan Stream flows westward along the Aleutian Island Arc, thereby causing surface water to flow into the Bering Sea through several passes. Within the Bering Sea, a cyclonic surface circulation develops with the East Kamchatka Current (EKC) and the Bering Slope Current acting as boundary currents. Cold and nutrient-rich surface waters leave the Bering Sea through Bering Strait into the Arctic Ocean, but the main outflow occurs back into the NW Pacific via Kamchatka Strait [e.g., *Stabeno et al.*, 1999]. The northern straits of the Kurile Islands provide inflow of Pacific water from the EKC into the Okhotsk Sea [e.g., *Katsumata and Yasuda*, 2010]. In the Okhotsk Sea, the surface circulation pattern is also cyclonic. Notably, brine rejection due to sea-ice formation leads to the production of Okhotsk Sea intermediate water (OSIW), which determines the potential density (σ_0) surface of NPIW in the N Pacific. OSIW flows out of the Okhotsk Sea through the Kurile Straits, thereby mixing with waters from the Western Subarctic Gyre [*Yasuda*, 1997; *You*, 2003]. The Oyashio Current transports this relatively cold (~4°C), low-salinity (~33 psu) water along the Kurile Islands to the east of Japan, where it meets with warmer and saltier water (~34–35 psu) from the Kuroshio. Cabbeling of these water masses then forms NPIW.

[6] Characteristic oceanographic features of the subarctic NW Pacific are the strong seasonal variability of SST and the marked upper-ocean stratification due to the buoyant low-salinity surface layer (Figure 2). Both are linked to the seasonal interplay between the Siberian High and the Aleutian Low, which in the Okhotsk and Bering seas leads to intense winter mixing and to seasonal sea-ice formation [e.g., *Niebauer et al.*, 1999]. Especially during winter, the sea-ice cover is significantly expanded in both marginal seas and in the vicinity of the eastern Kamchatka continental margin. Sea-ice formation releases brines, which sink in the water column resulting in increased subsurface salinity. During summer, MLS arises from increased insolation and melting sea-ice, while a temperature minimum layer (dichothermal layer) remains at ca. 100 m (Figure 2). Waters from this layer are believed to be formed during winter in the Bering and Okhotsk seas and to be subsequently exported to the NW Pacific [*Ohtani et al.*, 1972; *Miura et al.*, 2002]. At our study sites, the modern seasonal thermo- and pycnoclines lie within 0–100 m. The permanent halocline lies deeper (~100–200 m), and it further deepens toward the northern part of the Bering Sea, as do the mixed and the dichothermal layers (Figure 2). Notably, the calcite saturation horizon (CSH) at our sites lies between 150 and

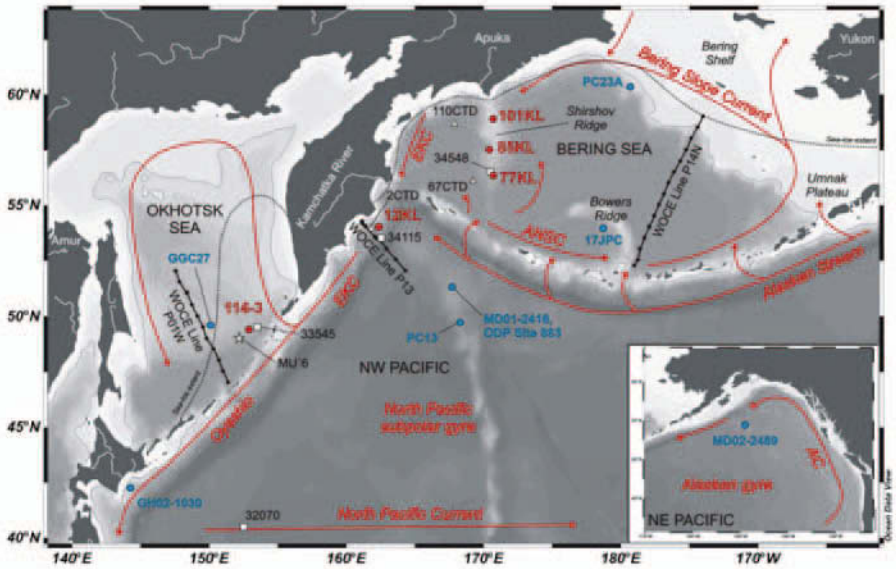

Figure 1. Bathymetric map with 250 m isobathe of the subarctic NW Pacific, Okhotsk Sea, Bering Sea, and NE Pacific (inlet). Red dots indicate sediment cores studied here, blue dots denote published reference records: MD01-2416 and ODP Site 883 [*Sarnthein et al.*, 2004, 2006; *Gebhardt et al.*, 2008], and PC13 [*Brunelle et al.*, 2010] from the NW Pacific, MD02-2489 from the NE Pacific [*Gebhardt et al.*, 2008], GH02-1030 off Japan [*Sagawa and Ikehara*, 2008], GGC27 from the Okhotsk Sea [*Brunelle et al.*, 2010], HLY-02-02-17JPC from Bowers Ridge [*Brunelle et al.*, 2007, 2010], and MR06-04-PC23A from the upper slope of the NE Bering Sea [*Rella et al.*, 2012]. CTD stations from R/V Sonne expedition SO201-2 (white triangles) [*Dullo et al.*, 2009], WOA 2009 stations (white squares) [*Locarnini et al.*, 2010], and stations from the World Ocean Circulation Experiment (WOCE; black dots) referred to in the text are included. The white star marks the position of Okhotsk Sea station MU'6 [*Yamamoto et al.*, 2001]. The general surface circulation pattern [after *Tomczak and Godfrey*, 1994; *Stabeno et al.*, 1999] is indicated by red arrows, and the dotted line marks the modern average winter sea-ice extent (after *Niebauer et al.*, 1999; *IRI/LDEO Climate Data Library*, http://iridl.ldeo.columbia.edu/). AC = Alaskan Current, EKC = East Kamchatka Current, ANSC = Aleutian North Slope Current. This map was generated with "Ocean Data View" [*Schlitzer*, 2011].

300 m, which has implications for our carbonate-based proxy reconstructions (Supplementary Information).

3. Material and Methods

3.1. Sedimentology and Age Models

[7] This study is based on piston cores SO201-2-12KL, -77KL, -85KL, and -101KL recovered during R/V Sonne cruise SO201 KALMAR Leg 2 in the NW Pacific off Kamchatka and in the western Bering Sea [*Dullo et al.*, 2009] (Table 1). Sediments are dominated by siliciclastic material of mainly clay and silt size, which are intercalated by thin layers of diatomaceous ooze/silt. Additional samples stem from core LV29-114-3 retrieved from the southern Okhotsk Sea during cruise LV29 KOMEX Leg 2 with R/V Akademik Lavrentyev [*Biebow et al.*, 2003] (Table 1). In this core, terrigenous sediments are overlain on top by a 175 cm thick layer of diatomaceous sediment. Sites 12KL and 114-3 are influenced by the EKC. All cores contain low contents of $CaCO_3$ (<5 wt %). However, all cores show increased $CaCO_3$ contents of up to 30 wt % during the B/A.

[8] Age models are based on a combined chronostratigraphic approach including high-resolution spectrophotometric (color b*) and X-ray fluorescence (XRF) core logging data for intercore correlations, as well as accelerator mass spectrometry (AMS) radiocarbon dating of planktonic foraminifera. The stratigraphic framework of all cores including the AMS-^{14}C dating results is presented in detail in *Max et al.* [2012] and in the Supplementary Information.

3.2. Stable Isotope and Mg/Ca Analyses

[9] Combined stable oxygen isotope ($\delta^{18}O$) and Mg/Ca analyses were performed on ~500 µg (~100–150 tests) of the polar to subpolar subsurface–dwelling planktonic foraminifer *Neogloboquadrina pachyderma* (sin.) (referred to as *Nps* hereafter), selected from the 125–250 µm size fraction. We focused on the most abundant four-chambered specimen of *Nps*. Abundance of foraminiferal tests was sufficient in all sediment cores, except for core 12KL, which lacked sufficient amounts after 6 ka BP. $\delta^{18}O$ was measured using a MAT 253 mass spectrometer (Thermo Scientific, Germany) coupled with a Kiel IV Carbonate device (Thermo Scientific, Germany). Results were calibrated to the VPDB scale and referenced to the NBS19 standard. Analytical long-term precision ($n > 1000$ samples) of the used in-house carbonate standard (Solnhofen limestone) was

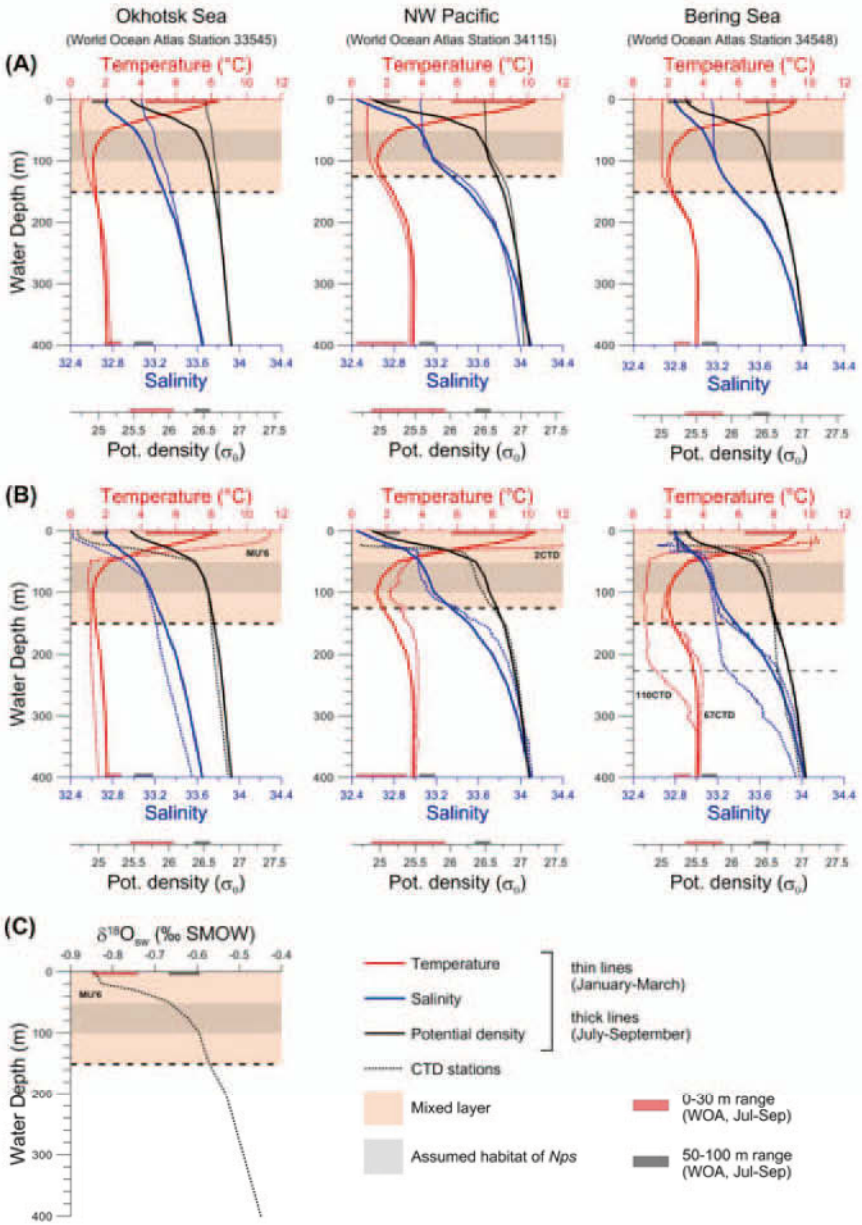

Figure 2. (A, B) Modern seasonal profiles of in situ temperature, salinity, and potential density (σ_0) during boreal winter (January-March, thin lines) and summer (July-September, thick lines), as well as actual seawater $\delta^{18}O_{sw}$ data (C) for the southern Okhotsk Sea, the subarctic NW Pacific, and the western Bering Sea. Stations were chosen from WOA 2009 (stations 33545, 34115, 34548) [*Locarnini et al.*, 2010] (cf. Figure 1). In (B), summer conditions are shown together with CTD data of R/V Sonne expedition SO201-2 from September 2009 (stations SO201-2-2CTD, -67CTD, -110CTD) [*Dullo et al.*, 2009]. $\delta^{18}O_{sw}$ data from Okhotsk Sea station MU'6 are from *Yamamoto et al.* [2001]. The habitat of the planktonic foraminifer *N. pachyderma* (sin.) is assumed to lie in 50–100 m (gray-shaded areas) and to be associated with an isopycnal layer. The modern hydrographic ranges of the photic zone (0–30 m) and of the subsurface in 50–100 m are represented by red and gray bars, respectively, next to the abscissae. Maximum mixed layer depths (dashed line) are inferred from *Miura et al.* [2002] and fit WOA and CTD data. Note the thicker mixed and dichothermal layer at Bering Sea station 110CTD.

Table 1. Site Information

Core	Latitude	Longitude	Depth (mbsl)	Recovery (m)
LV29-114-3	49°22.54'N	152°53.23'E	1765	9.64
SO201-2-12KL	53°59.47'N	162°22.51'E	2145	9.05
SO201-2-77KL	56°19.83'N	170°41.98'E	2135	11.78
SO201-2-85KL	57°30.30'N	170°24.77'E	968	18.13
SO201-2-101KL	58°52.52'N	170°41.45'E	630	18.32

±0.06‰. Cleaning of foraminiferal tests for Mg/Ca analyses followed the protocol of *Barker et al.* [2003] and included an additional reductive cleaning step. Samples were measured on an axial viewing ICP-OES (VARIAN 720-ES) with an analytical long-term precision of ±0.1 mmol mol^{-1} for Mg/Ca of the ECRM752-1 standard. For core 114-3, earlier measurements were included in our data set to improve sampling resolution. These measurements used 30 specimens of *Nps* (150–250 µm size fraction) to determine $\delta^{18}O$ and 50 specimens for Mg/Ca analyses. Cleaning also followed the protocol of *Barker et al.* [2003], but did not include reductive cleaning. A radially viewing ICP-OES (Ciros CCD SOP, Spectro A.I.) was used to determine Mg/Ca. Method details are given in the Supplementary Information.

3.3. Mg/Ca Temperature Signal of *Nps*

[10] As there is no locally established temperature-Mg/Ca calibration for *Nps* in the subarctic N Pacific, we applied the linear equation of *Kozdon et al.* [2009]. It is based on Holocene core-top samples from high-latitude Nordic Seas used in a cross-calibration approach between Mg/Ca and independent $\delta^{44/40}Ca$ measurements.

$$\mathrm{Mg/Ca}\left(\mathrm{mmol\ mol^{-1}}\right) = 0.13\mathrm{Temp.}(^{\circ}\mathrm{C}) + 0.35 \qquad (1)$$

[11] Considering the slope in equation (1), the analytical precision for Mg/Ca translates into an uncertainty of ±0.8°C. Results of *Kozdon et al.* [2009] indicated variable calcification depths of *Nps* that are associated with an isopycnal layer. Most other temperature calibrations for *Nps* are of exponential character and assume constant calcification depths. We consider the habitat of N Pacific *Nps* likely to be related to the seasonal thermo- and pycnoclines, similar to the Nordic Seas and the Arctic Ocean. Other studies conducted there showed that shell calcification of *Nps* mostly occurs at or close to the thermocline in 50–200 m [*Kohfeld et al.*, 1996; *Bauch et al.*, 1997; *Simstich et al.*, 2003]. Based on these studies, *Sarnthein et al.* [2004, 2006] assumed a depth range of 30–100 m in the NW Pacific. For the Okhotsk Sea, *Bauch et al.* [2002] suggested average calcification depths at 50–200 m and concluded that *Nps* lives at the bottom of the thermocline. Tow samples from the NW Pacific showed that the habitat of *Nps* lies below the pycnocline (>20 m) [*Kuroyanagi and Kawahata*, 2004]. Accordingly, we assume that the habitat of *Nps* lies at 50–100 m at our sites. Considering data from the World Ocean Atlas (WOA), this depth range lies below the summer (July-September) pycnocline, extends to the bottom of the summer thermocline, and is associated with an isopycnal layer ($\sigma_0 \approx 26.4\ kg\ m^{-3}$; Figure 2). Additional support for the assumption of calcification at subsurface levels comes from the comparison of the foraminiferal $\delta^{18}O$ signal to what would be predicted for the $\delta^{18}O$ signal of seawater ($\delta^{18}O_{sw}$) when using the hydrographic temperature data (Supplementary Information).

[12] It has been suggested that in the NW Pacific, *Nps* represents late spring and late summer/early fall temperatures [*Sarnthein et al.*, 2006; *Gebhardt et al.*, 2008], which is supported by sediment trap studies [*Takahashi et al.*, 2002; *Kuroyanagi et al.*, 2012]. Results for the southern Bering Sea and the NW Pacific Subarctic Front reveal that the main peak in $CaCO_3$ depositional flux occurs during late summer/early fall [*Takahashi et al.*, 2002; *Mohiuddin et al.*, 2005]. We therefore assume that at our study sites, which are additionally influenced by winter sea-ice, the main Mg/Ca signal of *Nps* likely represents late summer/early fall. This is supported by our reconstructed average Holocene (<8 ka BP) $T_{Mg/Ca}$ estimates of 3–4°C, which is only 1–2°C warmer than during modern summer and fall at 50–100 m. In contrast, modern winter (January-March) and spring temperatures lie below 3°C in 0–100 m (Figure 2).

[13] Our Mg/Ca results might be partly influenced by dissolution of the foraminiferal tests in conjunction with selective removal of Mg^{2+} ions [e.g., *Regenberg et al.*, 2006, and references therein], especially since our sediment cores were recovered below the modern CSH. Variations in Mg/Ca might thus be related to changes in $CaCO_3$ preservation. However, we refrained from correcting the initial Mg/Ca values as clear relationships between $CaCO_3$ contents and foraminiferal Mg/Ca were not found and correction procedures for contamination/dissolution effects were considered unsuitable (Supplementary Information).

3.4. Combined Use of Mg/Ca- and Alkenone-Based Temperatures

[14] We compared our $T_{Mg/Ca}$ records with the $SST_{Uk'37}$ records of *Max et al.* [2012], which were derived from the same samples. *Max et al.* [2012] used the calibration of *Müller et al.* [1998], which is widely used in N Pacific SST reconstructions providing a standard error of ±1.5°C. For the NW Pacific and both marginal seas, it has been shown that alkenones are mainly synthesized by *Emiliania huxleyi* during late summer to early fall within the upper 50 m [*Harada et al.*, 2003, 2006b; *Seki et al.*, 2007]. At our sites, surface sediment $SST_{Uk'37}$ of 5–7°C (not shown) falls within 1–2°C when compared with the modern instrumental range at 0–50 m (Figure 2).

[15] Differences between $SST_{Uk'37}$ and $T_{Mg/Ca}$ can result from seasonal bias [e.g., *Leduc et al.*, 2010]. However, for our sites we assume a restriction of both, coccolithophores and planktonic foraminifera, to the sea-ice-free late summer/early fall season. Nevertheless, we consider that a seasonal bias might have influenced the proxy records under conditions of reduced regional sea-ice influence, e.g., during the B/A. Accordingly, a high temperature gradient (ΔT) between $SST_{Uk'37}$ and $T_{Mg/Ca}$ is thought to reflect enhanced thermal MLS. However, the combined uncertainty for $SST_{Uk'37}$ and $T_{Mg/Ca}$ is substantial (±2.3°C), and significant temporal trends in the records are needed for interpretation of ΔT. In addition, ΔT might be influenced by intensified insolation as well as by variations in the exchange of heat between the upper and the deep ocean [*Kohfeld et al.*, 1996; *Andersson et al.*, 2010].

3.5. Ice Volume–Corrected $\delta^{18}O_{sw}$ and the Influence of Brines

[16] We used ice volume–corrected estimates of the local seawater oxygen isotopic composition ($\delta^{18}O_{ivc\text{-}sw}$; reported in ‰ versus SMOW) to approximate past changes in local salinity. $\delta^{18}O_{sw}$ was calculated by applying the relationship of *Shackleton* [1974]. Finally, we corrected for the global ice-volume signal following *Waelbroeck et al.* [2002]. The conversion of $\delta^{18}O_{sw}$ into salinity relies on regional calibrations. Such calibrations exist for the Okhotsk Sea and the western subarctic Pacific [*Yamamoto et al.*, 2001, 2002]. However, the uncertainty of the $\delta^{18}O_{sw}$ approach (~0.3‰) already translates into a salinity error of ca. ±0.8 when applying the calibration of *Yamamoto et al.* [2001]. Since our study sites show seasonal salinity variations of ~0.4–0.7 at 0–100 m (Figure 2), we did not apply a respective conversion. A shift in $\delta^{18}O_{ivc\text{-}sw}$ toward more positive values, hence, is thought to reflect a rise in local salinity, and vice versa.

[17] In the high latitudes, the salinity-$\delta^{18}O_{sw}$ relationship is not linear due to sea-ice-related brine rejection [e.g., *Bauch et al.*, 1995, 1997; *Yamamoto et al.*, 2002; *Hillaire-Marcel et al.*, 2004]. In general, sea-ice formation in the surface layer produces salty but isotopically light (^{18}O-depleted) brines, which sink in the water column and mix with subsurface waters. Conversely, the surface layer is provided with low-salinity, ^{18}O-enriched water as a result of melting sea-ice [e.g., *Hillaire-Marcel and de Vernal*, 2008]. Isotopic excursions recorded in *Nps* from Arctic Ocean sediments were used to infer variations in sea-ice growth during Heinrich events [*Hillaire-Marcel and de Vernal*, 2008]. For the Okhotsk Sea, a mean $\delta^{18}O_{sw}$ deviation of 0.36 ± 0.02‰ to what would be expected from the salinity-$\delta^{18}O_{sw}$ relationship of *Yamamoto et al.* [2001] was found and ascribed to the influence of brines [*Yamamoto et al.*, 2002]. Hence, our $\delta^{18}O_{ivc\text{-}sw}$ records might not unequivocally reflect past salinity changes. During winter, the northern part of the western Bering Sea is covered with sea-ice [*Niebauer et al.*, 1999; *Zhang et al.*, 2010], which might result in a stronger impact of brine rejection/sea-ice melt on the $\delta^{18}O_{ivc\text{-}sw}$ records toward our northern Bering Sea sites.

3.6. Biogenic Opal and $CaCO_3$

[18] Biogenic opal was measured on freeze-dried bulk sediment samples (20 mg) via molybdate-blue spectrophotometry [*Müller and Schneider*, 1993], and concentrations were calculated after *DeMaster* [1981] with a reproducibility of 1–2 wt %. Total carbon (TC) and total organic carbon (TOC) concentrations were determined using a Carlo Erba CNS Analyzer (model NA-1500), with TOC being measured on previously decalcified samples. Concentrations of $CaCO_3$ were indirectly calculated as the difference between TC and TOC, multiplied by 8.333.

4. Results

4.1. Temperature Reconstructions

[19] Figure 3A shows our $T_{Mg/Ca}$ results for the last 20 kyr together with the $SST_{Uk'37}$ records from *Max et al.* [2012]. Reconstructed $T_{Mg/Ca}$ have a similar range in all cores of about 2° to 6°C. Core 12KL recorded the most pronounced amplitude variations and a $T_{Mg/Ca}$ maximum of ~9°C. Alkenone concentrations before 15 ka BP are below detection limit and afterward the records reflect successively higher $SST_{Uk'37}$ from the north to the south of ~3°C [*Max et al.*, 2012]. No meridional gradients are found for $T_{Mg/Ca}$. Relative temperature changes in $SST_{Uk'37}$ and $T_{Mg/Ca}$ consistently show a warming from H1 into the B/A and a cooling from the B/A into the YD at all sites (Figure 3A). The deglacial $SST_{Uk'37}$ evolution almost parallels the thermal evolution registered in the NGRIP ice core from Greenland, whereas the $T_{Mg/Ca}$ evolution does not. Most notably, $T_{Mg/Ca}$ and $SST_{Uk'37}$ records in part show different trends. All cores show $T_{Mg/Ca}$ values of ~3–4°C during the H1 cold phase, but only at Site 12KL a significant cooling of ~3°C is recorded with respect to the Last Glacial Maximum (LGM) (Figure 3A). At the end of H1 within only 1–2 kyr, $T_{Mg/Ca}$ increase by 2–4°C to maxima of ~5–6°C at all sites, but to ~9°C at Site 12KL. $SST_{Uk'37}$ also increase by 2–6°C to maxima of 6–8°C [*Max et al.*, 2012]. While Bering Sea cores 85KL and 101KL recorded almost similar $T_{Mg/Ca}$ and $SST_{Uk'37}$ until the PB, cores 114-3 and 77KL show ΔT values of ~2–3°C during the B/A (Figure 4). Notably, core 12KL features negative ΔT values that are minimal (-6°C) at the onset of the B/A and subsequently increasing. Following the B/A, cores 114-3, 12KL, and 77KL recorded a $T_{Mg/Ca}$ cooling to minima of ~3–4°C recorded during the YD. Core 85KL still exhibits a strong Mg/Ca variability, but on average decreasing values since the B/A. $SST_{Uk'37}$ also decrease by 2–5°C into the YD [*Max et al.*, 2012]. During the YD, ΔT is reduced to about +2°C at sites 114-3 and 77KL, to 0°C at Site 85KL, and it again becomes negative (-2°C) at Site 12KL (Figure 3A). At Site 12KL, a ~2°C warming from the YD into the PB is recorded with a pronounced $T_{Mg/Ca}$ maximum of ~6°C (~11.5 ka BP), whereas Bering Sea core 77KL shows $T_{Mg/Ca}$ of ~4°C, and Okhotsk Sea core 114-3 does not show significantly increased $T_{Mg/Ca}$. The PB is subject to or followed by a 1–2°C cooling to $T_{Mg/Ca}$ of ~3–4°C at all sites, which remain almost constant afterward. $SST_{Uk'37}$ increase by up to 5°C subsequent to the YD and culminate in maxima of 9–10°C between 11 and 9 ka BP [*Max et al.*, 2012]. The early Holocene $SST_{Uk'37}$ maximum and the summer insolation maximum occur simultaneously (Figure 3A). Consequently, both temperature proxies significantly diverge during or shortly after the PB until ~10 ka BP, with ΔT maxima of up to 6°C. Notably, ΔT at Site 12KL has become positive only since the PB. Holocene $T_{Mg/Ca}$ values are lower than those of the B/A and YD, but are comparable to H1 values. For the last 9 kyr, records from cores 114-3, 12KL, and 77KL point to a gradual ~2°C decrease in $SST_{Uk'37}$, which in core 114-3 is interrupted between 9 and 7 ka BP by a cooling to YD levels [*Max et al.*, 2012]. Hence, the ΔT evolution during the middle to late Holocene overall follows the $SST_{Uk'37}$ signal and records a ΔT minimum between 9 and 7 ka BP in core 114-3 (Figure 3A).

4.2. Reconstruction of $\delta^{18}O_{ivc\text{-}sw}$

[20] Reconstructed $\delta^{18}O_{ivc\text{-}sw}$ values range between -1‰ and +1‰ during the last 20 kyr, with the most prominent variability also being recorded at Site 12KL (Figure 3B). Notably, Bering Sea core 85KL and Okhotsk Sea core

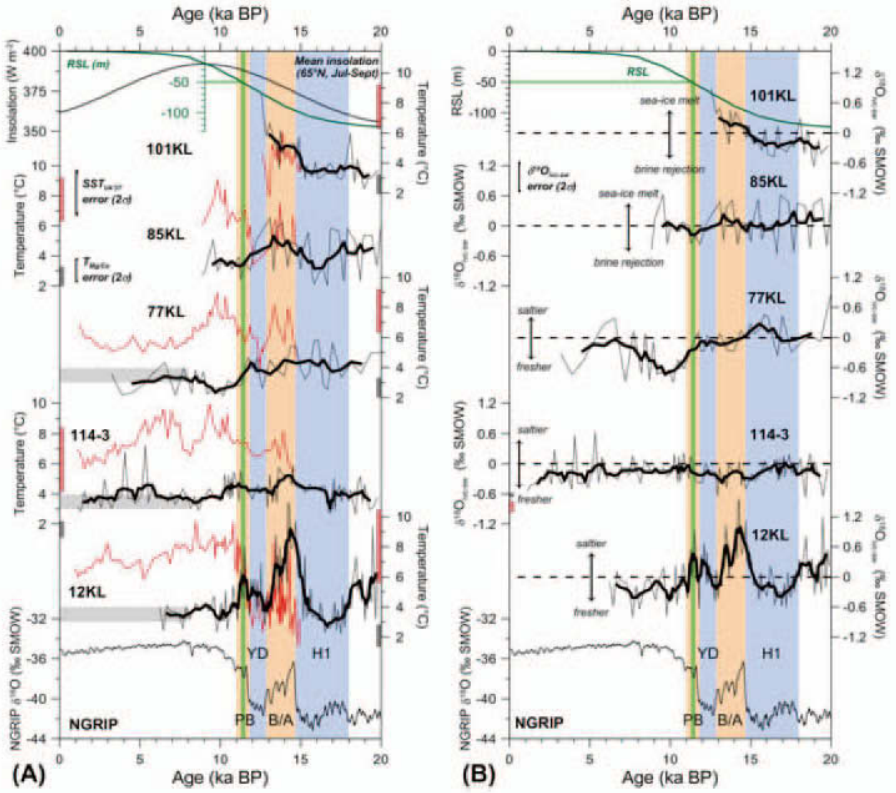

Figure 3. Temperature reconstructions (A) and ice volume–corrected seawater $\delta^{18}O$ estimates ($\delta^{18}O_{ivc\text{-}sw}$; B) over the last 20 kyr from the Bering Sea (SO201-2-101KL, -85KL, -77KL), the subarctic NW Pacific off Kamchatka (SO201-2-12KL), and the southern Okhotsk Sea (LV29-114-3). The NGRIP ice core oxygen isotope record (*NGRIP members*, 2004; GICC05 time scale, *Rasmussen et al*., 2006) is for reference. Running five-point-averages (thick black lines) are given to smooth the records of $T_{Mg/Ca}$ and $\delta^{18}O_{ivc\text{-}sw}$, and the respective uncertainties are indicated. Relative sea level (RSL, green line) is from *Waelbroeck et al*. [2002] and the green vertical bar marks the interval when RSL reached the approximate sill depth of the Bering Strait (~50 m). Pale orange and pale blue shadings represent the B/A and PB, and H1 and YD, respectively. In (A), the $T_{Mg/Ca}$ records (light gray lines) are shown together with the alkenone-based $SST_{Uk'37}$ records (thin red lines) from *Max et al*. [2012], plotted on the same scale. Average middle to late Holocene (<8 ka BP) temperature estimates of 3–4°C are highlighted (gray vertical bars), while the modern photic zone (0–30 m) and subsurface (50–100 m) temperature ranges are represented by red and gray vertical bars, respectively, next to the temperature axes (based on WOA data) [*Locarnini et al*., 2010] (cf. Figure 2). Mean insolation for boreal summer (July-September) at 65°N (thick gray line) was calculated after *Laskar et al*. [2004]. In (B), trends toward heavier (lighter) $\delta^{18}O_{ivc\text{-}sw}$ signatures are equivalent to increasing (decreasing) local subsurface salinity. Toward the northern Bering Sea sites, the $\delta^{18}O_{ivc\text{-}sw}$ signal is assumed to be additionally influenced by ^{18}O-enriched meltwater during sea-ice melt and ^{18}O-depleted brines during sea-ice formation. Dashed lines indicate $\delta^{18}O_{ivc\text{-}sw} = 0‰$ SMOW. Red and gray vertical bars next to the $\delta^{18}O_{ivc\text{-}sw}$ axes mark the modern $\delta^{18}O_{sw}$ ranges for the photic zone (0–30 m) and subsurface (50–100 m), respectively, at Okhotsk Sea station MU'6 [*Yamamoto et al*., 2001]. Notably, all records are characterized by negative average $\delta^{18}O_{ivc\text{-}sw}$ values after the PB.

114-3 show average values of 0‰ and -0.2‰, respectively, with only low and insignificant amplitude variability. Overall, relative changes in $\delta^{18}O_{ivc\text{-}sw}$ are regionally different, and for the Bering Sea sites opposing trends with a maximum gradient of ~0.4‰ are observed. However, at each site, a general covariation between $\delta^{18}O_{ivc\text{-}sw}$ and $T_{Mg/Ca}$ is found. During 20–18 ka BP, cores 12KL and 77KL show on average positive values (0‰ to +0.4‰), whereas $\delta^{18}O_{ivc\text{-}sw}$ is negative at sites 114-3 and 101KL (-0.3‰ to 0‰). During H1, Site 12KL is marked by a $\delta^{18}O_{ivc\text{-}sw}$ minimum of about -0.4‰ (Figure 3B). A similar significant extreme during that time is not observed at any other site. However, on average, core 77KL features positive values of about +0.2‰ during H1, whereas sites 101KL and 114-3 show negative values around -0.2‰. The transition from H1 into the B/A in core 77KL is characterized by decreasing

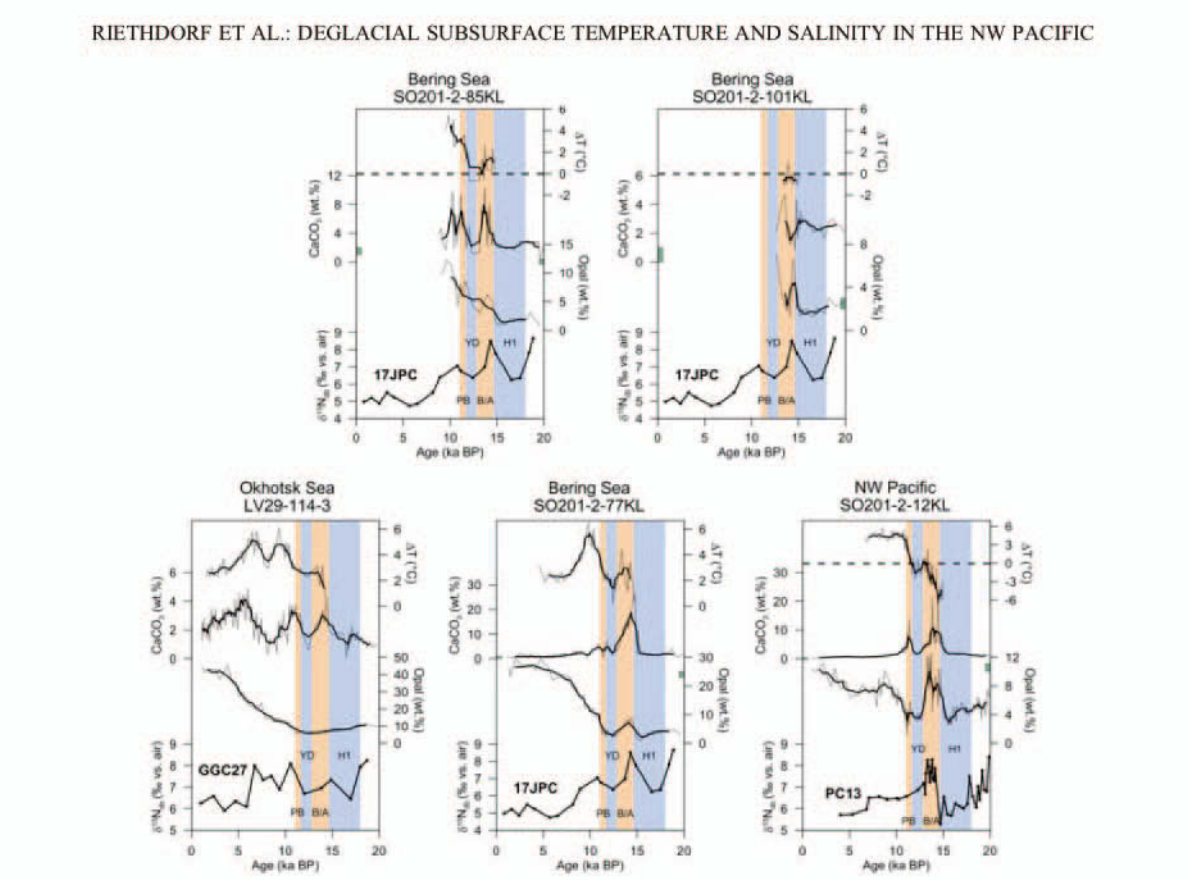

Figure 4. Temperature gradients (ΔT) between $SST_{Uk'37}$ and $T_{Mg/Ca}$, and concentrations of $CaCO_3$ and biogenic opal for cores from the Bering Sea (SO201-2-77KL, -85KL, -101KL), the NW Pacific off Kamchatka (SO201-2-12KL), and the southern Okhotsk Sea (LV29-114-3). Data are smoothed by running five-point-averages (black lines). Dashed lines indicate $\Delta T = 0°C$. Green vertical bars next to the $CaCO_3$ and opal axes mark respective concentrations in surface sediments in the direct vicinity of the sediment core sites (stations SO201-2-11MUC, -76MUC, -83MUC, and -99MUC; Supplementary Information). For comparison, records of $\delta^{15}N_{db}$ from southern Okhotsk Sea core GGC27, southern Bering Sea core HLY02-02-17JPC, and open subarctic Pacific core PC13 are shown (data from *Brunelle et al.*, 2007, 2010; cf. Figure 1). Pale orange and pale blue shadings represent the B/A and PB, and the H1 and YD, respectively.

$\delta^{18}O_{ivc\text{-}sw}$, while cores 12KL and 101KL show increasing values. At Site 12KL, this increase is reflected by a positive shift of about +1.4‰ occurring in less than 2 kyr (Figure 3B). During the B/A, Site 77KL shows negative values of about -0.2‰ prevailing until the onset of the PB. In contrast, positive values are recorded at sites 101KL (+0.3‰) and 12KL (+1‰), where the heaviest deglacial $\delta^{18}O_{ivc\text{-}sw}$ values are found. This core shows a decrease in $\delta^{18}O_{ivc\text{-}sw}$ during the B/A until a minimum of -0.2‰ at the onset of the YD, and a subsequent increase of 0.5‰ at 12.0 ka BP. Furthermore, core 12KL recorded a pronounced maximum of +0.5‰ during the PB (~11.5 ka BP), only found at this site, where it is subsequently followed by a sharp decrease to about -0.5‰ until ~10 ka BP (Figure 3B). Core 77KL also shows decreasing $\delta^{18}O_{ivc\text{-}sw}$ values since the onset of the PB until a minimum of -0.8‰ is reached at 10–9 ka BP. During the Holocene, $\delta^{18}O_{ivc\text{-}sw}$ values are negative at all sites varying between -0.1‰ and -0.8‰. Core 77KL from 9 to 6 ka BP shows a strong variability with on average increasing $\delta^{18}O_{ivc\text{-}sw}$ to about -0.1‰. Even lower values are subsequently preserved in this core until ~4 ka BP but affected by low temporal resolution.

5. Discussion

5.1. Deglacial Variability of Temperature and Salinity

[21] Our reconstructions show synchronous changes in $T_{Mg/Ca}$ and $\delta^{18}O_{ivc\text{-}sw}$ during the last deglaciation. These changes primarily reflect variations between "warm/salty" and "cold/fresh" subsurface waters. Core 114-3, at least during the H1 to B/A transition, appears to show the opposite relationship, but variability of $T_{Mg/Ca}$ and $\delta^{18}O_{ivc\text{-}sw}$ is low for this core and not significantly above measurement uncertainty. Hence, subsurface conditions at Site 114-3 might have remained fairly constant. Regional differences in the deglacial $\delta^{18}O_{ivc\text{-}sw}$ evolution are found, implying saltier subsurface conditions during the B/A and PB in the NW Pacific (Site 12KL), while the Bering Sea cores show opposing trends along the core transect. In contrast to sites 12KL and

101KL, sites 114-3 and 77KL indicate a freshening during the B/A. However, all cores indicate a freshening since the early Holocene. The deglacial $SST_{Uk'37}$ evolution is different from $T_{Mg/Ca}$ and characterized by warmings during the B/A and PB, coolings during the H1 and YD, and a subsequent cooling during the early Holocene. Hence, changes in $SST_{Uk'37}$ and N Atlantic climate occur quasi-synchronous [*Max et al.*, 2012]. The developing gradients between surface and subsurface temperatures indicate changes in thermal MLS, which were different on a regional scale.

[22] Strong amplitude variations in $T_{Mg/Ca}$ and $\delta^{18}O_{ivc\text{-}sw}$ characterize Site 12KL, which might be explained oceanographically in the context of the major Bering Strait reopening. Today, the Alaskan Stream provides the NW Pacific and the Bering Sea with relatively fresh surface waters. Some authors speculated on reduced net inflow of Alaskan Stream waters into the Bering Sea when some of the Aleutian passes were closed due to lower glacial sea level [e.g., *Katsuki and Takahashi*, 2005; *Tanaka and Takahashi*, 2005]. The Bering Strait reopened between 12 and 11 ka BP [*Keigwin et al.*, 2006]. Accordingly, the inflow of waters from the Alaskan Stream into the Bering Sea might have been reduced until the PB allowing for relatively enhanced accumulation of these water masses in the NW Pacific with respect to today. During H1 and the YD, this should consequently have resulted in more invigorated sea-ice formation and brine rejection (providing ^{18}O-depleted water) in the northern Bering Sea, as well as in enhanced accumulation of cold/fresh Alaskan Stream waters in the NW Pacific. In contrast, during the B/A warm phase, sea-ice growth should have been reduced (providing less ^{18}O-depleted brines), and relatively warmer and saltier waters should have accumulated in the NW Pacific. The weaker response at Site 12KL during the PB is then explained by higher sea level and an open Bering Strait, which resulted in stronger inflow of Alaskan Stream waters into the Bering Sea.

5.1.1. Heinrich Stadial 1

[23] The above given considerations explain the presence of cold/fresh subsurface waters at Site 12KL during H1 (Figure 3). *Gebhardt et al.* [2008] also related drops in N Pacific salinity to North American river discharge and its subsequent transport via the Alaskan Current and Alaskan Stream rather than meltwater discharge from glacial ice sheets. This is in agreement with the absence of a Beringian Ice Sheet during the LGM [e.g., *Brigham-Grette et al.*, 2001, 2003; *Karhu et al.*, 2001]. Reduced inflow of Alaskan Stream waters into the Bering Sea can also account for the positive $\delta^{18}O_{ivc\text{-}sw}$ at Site 77KL, implying relatively increased subsurface salinity. At ODP Site 883D and at Site MD01-2416 in the NW Pacific, SSTs were higher than at our sites and characterized by three sharp increases of ~4–6°C [*Sarnthein et al.*, 2006; *Gebhardt et al.*, 2008]. These SST pulses are accompanied by locally increased salinity and were explained by short-term incursions of warm/salty Kuroshio waters. Warm $SST_{Uk'37}$ (20–24°C) of Kuroshio waters are confirmed for the last deglaciation [*Sawada and Handa*, 1998]. At Site GH02-1030, reconstructions from *Globigerina bulloides* show relatively saline conditions prevailing since the LGM, with a maximum at 15.5 ka BP and a subsequent decrease in both salinity and $T_{Mg/Ca}$ [*Sagawa and Ikehara*, 2008]. NE Pacific core MD02-2489 does also not show significantly higher SSTs during H1 [*Gebhardt et al.*, 2008]. Hence, the northern Emperor Seamounts might provide a different oceanographic setting when compared to the far NW Pacific and the N Pacific marginal seas. Prior to ~15 ka BP, nondeterminable alkenone concentrations in our cores indicate restricted alkenone production by coccolithophores, most likely due to temperature limitation. Overall low marine productivity is supported by low biogenic opal concentrations. At the same time, light diatom-bound nitrogen isotope ratios ($\delta^{15}N_{db}$) in the subarctic Pacific realm [*Brunelle et al.*, 2007, 2010] are indicative of a decrease in nitrate utilization in response to the enhanced supply of preformed nutrients from below and limited phytoplankton growth (Figure 4). Qualitative measurements of the sea-ice-related IP_{25} proxy imply sea-ice influence at our sites during H1 and the YD, but absent or at least considerably reduced influence during the B/A and PB [*Max et al.*, 2012]. *Gebhardt et al.* [2008] argued for pronounced phases of sea-ice formation in the subarctic N Pacific that induced vertical mixing during H1. Evidence for increased vertical mixing and/or intensified overturning during H1 and the YD comes from reduced ventilation ages [*Ohkushi et al.*, 2004; *Sarnthein et al.*, 2007; *Sagawa and Ikehara*, 2008; *Okazaki et al.*, 2010], and is supported by climate modeling studies [e.g., *Okazaki et al.*, 2010; *Chikamoto et al.*, 2012; *Menviel et al.*, 2012]. Moreover, benthic $\delta^{18}O$ excursions recorded in the northern Bering Sea imply that the Bering Sea was a proximate source of intermediate water during past stadial episodes [*Rella et al.*, 2012]. Increased ventilation and the potential disappearance of the permanent halocline [*Menviel et al.*, 2012] as a result of higher salinity is consistent with the reconstructions of *Sarnthein et al.* [2006] and *Sagawa and Ikehara* [2008]. It is presumably also supported by our study despite the regional differences in $\delta^{18}O_{ivc\text{-}sw}$, since results for sites 77KL and 114-3 indicate the presence of saltier subsurface waters (Figure 3B). The gradient in $\delta^{18}O_{ivc\text{-}sw}$ along our Bering Sea core transect rather reflects regional differences in sea-ice growth and according brine rejection. We propose that in the north, salty but ^{18}O-depleted brines mixed with subsurface waters explaining the lower $\delta^{18}O_{ivc\text{-}sw}$ values with respect to Site 77KL.

5.1.2. Bølling-Allerød

[24] Our records show maxima in $T_{Mg/Ca}$ at the onset or during the B/A and a subsequent cooling until the YD (Figure 3A). Considering sea–ice influence, more positive $\delta^{18}O_{ivc\text{-}sw}$ values until ~14.0 ka BP imply enhanced sea-ice melt or at least reduced sea-ice growth in the northern Bering Sea, whereas negative and decreasing $\delta^{18}O_{ivc\text{-}sw}$ values were recorded at sites 77KL and 114-3 indicating fresher subsurface conditions (Figure 3B). The recorded evolution of $T_{Mg/Ca}$ and $SST_{Uk'37}$ at our sites is congruent with results from the NW Pacific [*Sagawa and Ikehara*, 2008], the NE Pacific [*Kienast and McKay*, 2001; *Barron et al.*, 2003; *Gebhardt et al.*, 2008], the Bering Sea [*Caissie et al.*, 2010], and the Okhotsk Sea [*Ternois et al.*, 2000; *Harada et al.*, 2006a; *Seki et al.*, 2009]. The high $T_{Mg/Ca}$ of ~9°C at Site 12KL resemble conditions that today prevail in the Kuroshio Extension area (e.g., at WOA station 32070) [*Locarnini et al.*, 2010] (cf. Figure 1), which, thus, argues for the northward expansion of the N Pacific gyre filled with Kuroshio waters as suggested by *Gebhardt et al.* [2008]. At the same time, increased N Pacific ventilation ages [*Adkins*

and Boyle, 1997; *Ahagon et al*., 2003; *Ohkushi et al*., 2004; *Sagawa and Ikehara*, 2008; *Okazaki et al*., 2010] imply reduced formation of deep/intermediate water masses. The presence of alkenones in all cores suggests that temperature limitation of coccolithophores was overcome. ΔT values of 0–1°C indicate weak thermal MLS at sites 85KL and 101KL due to relatively stronger sea-ice influence and still weak seasonal contrasts, which is supported by opal concentrations remaining low (<5 wt %; Figure 4). Sites 77KL and 114-3 also recorded only little higher opal concentrations. However, $T_{Mg/Ca}$ at these sites compare with those of sites 85KL and 101 KL, whereas $SST_{Uk'37}$ estimates are higher by 2–3°C (Figure 3A). This indicates more pronounced thermal MLS as a result of stronger seasonal contrasts. We propose that continuing deglacial sea-level rise resulted in enhanced net inflow of Alaskan Stream waters into the Bering Sea providing Site 77KL with relatively fresher subsurface waters, thereby explaining the decrease in $\delta^{18}O_{ivc\text{-}sw}$ from H1 into the YD (Figure 3B). Relatively fresher subsurface conditions at sites 77KL and 114-3 are consistent with surface freshening off Japan from 14.6 ka BP to 13.6 ka BP [*Sagawa and Ikehara*, 2008]. Previous studies conducted in the southern Bering and Okhotsk seas suggested surface freshening due to invigorated sea-ice melt from the observation of negative shifts in planktonic $\delta^{18}O$ and increasing abundances of the diatom species *Paralia sulcata* [*Gorbarenko et al*., 2004, 2005; *Seki et al*., 2004a]. In contrast, opal concentrations at Site 12KL of up to ~12 wt % are comparable with Holocene values and suggest significantly enhanced marine productivity. At the same time, heavy $\delta^{15}N_{db}$ were recorded in the southern Bering Sea and NW Pacific [*Brunelle et al*., 2010], implying enhanced nitrate utilization or even denitrification of nitrate as a result of stronger upper-ocean stratification (Figure 4). The negative ΔT values in core 12KL during the B/A could be related to a significantly warmer and deepened mixed layer during a prolonged summer season and reduced sea-ice influence. Consequently, for Site 12KL, we consider seasonal bias in $SST_{Uk'37}$ signal formation, and that during the B/A, $SST_{Uk'37}$ more likely represent early spring conditions. Coccolithophorid blooms that in the modern subarctic N Pacific occur already during spring are known [*Takahashi et al*., 2002], and for the Okhotsk Sea seasonal bias has been suggested before to explain similarly high LGM and Holocene $SST_{Uk'37}$ values [*Seki et al*., 2004b].

5.1.3. The Younger Dryas and Preboreal

[25] The $T_{Mg/Ca}$ and $\delta^{18}O_{ivc\text{-}sw}$ evolution observed at sites 114-3, 12KL, and 77KL during the YD and PB (Figure 3) broadly matches that found in the NW Pacific [*Sarnthein et al*., 2004, 2006; *Gebhardt et al*., 2008; *Sagawa and Ikehara*, 2008], although our records show lower $\delta^{18}O_{ivc\text{-}sw}$ values. Lowered $SST_{Uk'37}$ during the YD are in agreement with the suggested southeastward expansion of the W Pacific Subarctic Gyre and the Bering Sea Gyre [*Kienast and McKay*, 2001], as well as with modeling results predicting a strengthened and eastward expanded Aleutian Low, which initiated better ventilation [*Mikolajewicz et al*., 1997]. This is also in agreement with reduced N Pacific ventilation ages [e.g., *Okazaki et al*., 2010]. At the same time, similar $T_{Mg/Ca}$ and $SST_{Uk'37}$ indicate weak but regionally different thermal MLS at our sites as a result of less developed seasonal contrasts. At sites 12KL, 77KL, and 114-3, ΔT values of ~2°C imply relatively stronger thermal MLS than at Site 85KL (ΔT= 0°C), which recorded H1-like conditions (Figures 3 and 4). During the PB, $T_{Mg/Ca}$ and related $\delta^{18}O_{ivc\text{-}sw}$ values imply further subsurface cooling and freshening (77KL) and/or conditions still comparable to the YD (114-3). Concurrent increases in $SST_{Uk'37}$ argue for more pronounced thermal MLS, which is characterized by a deepening of the thermocline, extra cooling of sub-thermocline waters in hand with the formation of the dichothermal layer. We propose that at least our Bering Sea sites were now subject to increased inflow of relatively warmer Pacific surface waters through the Aleutian passes as a result of the reopening of the Bering Strait, and that this process fostered seasonal MLS by reducing the sea-ice growth.

5.1.4. The Holocene

[26] Most notably for all our cores are the differently developing $T_{Mg/Ca}$ and $SST_{Uk'37}$ since the PB (Figure 3A), best explained by insolation changes affecting the surface ocean warming, reduced sea-ice, and increasing seasonal contrasts controlling the shape and position of the thermocline. Holocene $T_{Mg/Ca}$ remain either equal or stay lower than during H1 (Figure 3A). Our $T_{Mg/Ca}$, although being 1–2°C warmer, well reflect modern conditions, which is consistent with the NW Pacific studies [*Sarnthein et al*., 2004, 2006; *Gebhardt et al*., 2008; *Sagawa and Ikehara*, 2008]. Overall, $\delta^{18}O_{ivc\text{-}sw}$ values remain negative at all sites indicating relatively fresh subsurface conditions and almost stable seasonal contrasts. *Sarnthein et al*. [2004] reported on the long-term but stepwise decrease in subsurface salinity at Detroit Seamount during the early to middle Holocene, speculating that the modern salinity-driven stratification developed only since the Holocene. We can not confirm this stepwise salinity decline. However, our results point to a deglacial evolution of subsurface water mass characteristics developing into relatively fresh conditions along with enhanced thermal MLS (strong seasonal contrasts) since the early Holocene. Dominant control on the Holocene subarctic NW Pacific $SST_{Uk'37}$ evolution is attributed to Northern Hemisphere summer insolation [*Okumura et al*., 2009; *Hu et al*., 2010; *Max et al*., 2012]. In consequence, stronger seasonal contrasts developed as the result of a prolonged summer season and reduced sea-ice influence. Stronger winter mixing would have lead to the formation of the dichothermal layer. In this case, our high ΔT values of ~5–6°C would be explained by higher $SST_{Uk'37}$ due to stronger insolation, and by *Nps* recording gradually cooler subsurface temperatures due to the presence of the dichothermal layer. Accordingly, thermal MLS was consolidated and the seasonal halocline developed from sea-ice melt during summer. The largest difference between $T_{Mg/Ca}$ and $SST_{Uk'37}$ at ~10 ka BP coincides with the early Holocene thermal maximum, which in Alaska and northwest Canada occurred between 11 and 9 ka BP [*Kaufman et al*., 2004]. Recent model experiments indicate that besides insolation the reopening of the Bering Strait might have further affected this $SST_{Uk'37}$ maximum [*Okumura et al*., 2009; *Hu et al*., 2010]. Additionally, enhanced precipitation from the Westerlies and strengthened advection of cold/fresh waters from the Alaskan Stream might have contributed to the N Pacific cooling and freshening [*Sarnthein et al*., 2004].

5.2. Cause of Deglacial Stratification Changes and Impact on Atmospheric CO_2

[27] The deglacial $SST_{Uk'37}$ evolution recorded in the subarctic N Pacific realm appears to be related to and in-phase with the thermal evolution recorded in the N Atlantic realm, suggesting an atmospheric coupling [*Ternois et al.*, 2000; *Kienast and McKay*, 2001; *Barron et al.*, 2003; *Harada et al.*, 2006a; *Seki et al.*, 2009; *Caissie et al.*, 2010; *Max et al.*, 2012]. Several modeling studies investigated the sensitivity of the PMOC in response to perturbations of the AMOC on millennial time scales during the last deglaciation. All models predicted an enhanced PMOC at times of a weakened AMOC, whose strength was modulated by freshwater input into the Atlantic or by freshwater extraction from the Pacific [e.g., *Saenko et al.*, 2004]. In the models, the weakened AMOC during H1 and the YD [e.g., *McManus et al.*, 2004] results in the southward shift of the Intertropical Convergence Zone and in weakened Indian and Asian summer monsoons [*Zhang and Delworth*, 2005], which today maintain the salinity gradient between the Atlantic and Pacific [e.g., *Emile-Geay et al.*, 2003]. Consequently, the antiphase models [e.g., *Saenko et al.*, 2004] predicted a warming in the N Pacific due to the weakened AMOC, whereas the in-phase models [e.g., *Mikolajewicz et al.*, 1997] suggested that atmospheric cooling by a strengthened Aleutian Low resulted in a PMOC. Interestingly, modeling results of *Chikamoto et al.* [2012] showed a cooling in the N Atlantic and in the NW Pacific, but ambiguous results for the NE Pacific. This was explained by a salinity increase in the N Pacific due to the weakened east Asian monsoon and changes in the oceanic transport of heat and salt. Both in-phase and antiphase models are supported by low ventilation ages in the N Pacific during H1 and the YD. Overall, our results support the studies of *Chikamoto et al.* [2012] and of *Menviel et al.* [2012], who discussed the effects of the removed halocline in the subarctic N Pacific. However, we cannot confirm strongly enhanced opal production, which was also predicted for H1 as a result of the established PMOC and the removal of the halocline [*Menviel et al.*, 2012]. We rather attribute the low alkenone and opal concentrations observed at our sites to limitation of marine productivity by temperature and sea-ice. The notion of the removed halocline during H1 is supported by the high $\delta^{18}O_{ivc\text{-}sw}$ values recorded in NW Pacific cores MD01-2416 [*Sarnthein et al.*, 2006; *Gebhardt et al.*, 2008] and GH02-1030 [*Sagawa and Ikehara*, 2008]. During H1, our reconstructions indicate cold or decreasing surface and subsurface temperatures (atmospheric cooling), while our results for $\delta^{18}O_{ivc\text{-}sw}$ indicate a subsurface freshening at NW Pacific Site 12KL (strong Alaskan Stream). At the same time, saltier-than-today subsurface conditions are recorded at Bering Sea Site 77KL (weaker halocline), and increasing brine influence toward the north is assumed. The $T_{Mg/Ca}$ and $\delta^{18}O_{ivc\text{-}sw}$ recorded at our sites for the B/A and PB is explained by stronger seasonal MLS, which might be attributed to the reduced PMOC. Subsequent to the PB, the subarctic NW Pacific is subject to enhanced thermal MLS, which for the Bering Sea sites is possibly related to the opening of Bering Strait resulting in stronger inflow of N Pacific surface waters. Moreover, increased surface freshening during the Holocene potentially resulted from enhanced sea-ice melting during summer and enhanced precipitation.

[28] The deep N Pacific is suggested to have stored a greater portion of respired CO_2 during glacials than during interglacials [*Jaccard et al.*, 2009]. During the last deglaciation, when the AMOC was strong, the respired carbon pool was removed from the deep sea, which is considered to have resulted in a deepening of the lysocline and an increase in atmospheric CO_2 [e.g., *Galbraith et al.*, 2007]. Our records confirm increased $CaCO_3$ preservation and higher marine productivity during the B/A. Conversely, *Okazaki et al.* [2010] argued for enhanced N Pacific deep water formation during H1 (i.e., better ventilation when the AMOC was weak), and *Rella et al.* [2012] suggested that the Bering Sea was a proximate source for NPIW during that time. This is in agreement with the notion of a removed halocline, which would result in a rise in atmospheric CO_2 of 5 ppm [*Chikamoto et al.*, 2012; *Menviel et al.*, 2012]. Another aspect involves the efficiency of the biological pump. As recently summarized for the Pliocene, the subarctic N Pacific might have been responsible for higher atmospheric CO_2 in case of deep water formation resulting in a reduced ratio of regenerated-to-preformed nutrients in the ocean, thereby lowering the efficiency of the biological pump [*Studer et al.*, 2012]. The $\delta^{15}N_{db}$ data of *Brunelle et al.* [2007, 2010] indeed argue for reduced nitrate utilization in the NW Pacific and its marginal seas during H1 and the YD (Figure 4). Since we reconstructed changes in thermal MLS, we can neither argue for nor against a change in the position and/or the strength of the permanent halocline. Nevertheless, our $\delta^{18}O_{ivc\text{-}sw}$ data show higher subsurface salinity in the southern Bering Sea (Site 77KL) during H1, but during the B/A in the NW Pacific (Site 12KL). This can at least be taken as supportive evidence for regional changes in subarctic N Pacific permanent halocline stability, which might therefore have contributed to the deglacial rise in atmospheric CO_2.

6. Conclusions

[29] We found regionally different changes in $T_{Mg/Ca}$ and $\delta^{18}O_{ivc\text{-}sw}$ in the subarctic NW Pacific as well as differences in alkenone- and Mg/Ca-based SST reconstructions. Our results indicate deglacial oceanographic changes in the mixed layer, which are most likely related to variations in Northern Hemisphere summer insolation and the strength of atmospheric pressure systems. Both factors control the extent of seasonal contrasts by driving changes in sea-ice formation, thereby altering seasonal MLS. From our results, we propose that seasonal contrasts and, hence, thermal MLS, although being regionally different, were reduced during H1 and the YD, but strong during the B/A. Our sites were characterized by low marine productivity, cold subsurface waters, and weak thermal MLS during the H1 and YD cold phases. This is attributed to an established PMOC and atmospheric cooling resulting in limited phytoplankton growth and enhanced sea-ice formation. Additional influence by increased advection of Alaskan Stream waters accumulating in the NW Pacific due to a closed Bering Strait is proposed. In contrast, warmer subsurface waters and regionally different temperature gradients were recorded during the B/A. At the same time, we found relatively increased $\delta^{18}O_{ivc\text{-}sw}$ in the NW Pacific (Site 12KL) and northern Bering Sea (Site 101KL), but reduced $\delta^{18}O_{ivc\text{-}sw}$ in the southern Okhotsk

and Bering seas (sites 114-3 and 77KL). This is explained by enhanced thermal MLS, accumulation of Alaskan Stream waters in the NW Pacific (at Site 12KL), as well as a stronger impact of brines on the $\delta^{18}O_{ivc\text{-}sw}$ signal in the northern Bering Sea. A decrease in $T_{Mg/Ca}$ and $\delta^{18}O_{ivc\text{-}sw}$ during the early Holocene along with high temperature gradients implies the only recent establishment of modern MLS in the subarctic NW Pacific and argues for subsurface oceanographic changes, which might be related to the reopening of the Bering Strait at 12–11 ka BP.

[30] **Acknowledgements.** This study was funded by the German Federal Ministry of Education and Research (BMBF; grant 03G0672A and B) and resulted from the joint German-Russian research project "KALMAR." Master and crew of R/V Sonne cruise SO201 Leg 2 are gratefully acknowledged for their professional support. E. Maier conducted additional opal measurements for core 77KL. We thank N. Gehre, L. Haxhiaj, B. Domeyer, and D. Poggemann for laboratory assistance and technical support, N. Khelifi for discussions, as well as two anonymous reviewers and the Editor for considerably improving the manuscript. The data are available via the PANGAEA Data Publisher for Earth & Environmental Science (http://doi.pangaea.de/10.1594/PANGAEA.786258).

References

Adkins, J. F., and E. A. Boyle (1997), Changing atmospheric $\Delta^{14}C$ and the record of deep water paleoventilation ages, *Paleoceanography*, *12*(3), 337–344.

Ahagon, N., K. Ohkushi, M. Uchida, and T. Mishima (2003), Mid-depth circulation in the northwest Pacific during the last deglaciation: Evidence from foraminiferal radiocarbon ages, *Geophys. Res. Lett.*, *30*(21), 2097, doi:10.1029/2003GL018287.

Andersson, C., F. S. R. Pausata, E. Jansen, B. Risebrobakken, and R. J. Telford (2010), Holocene trends in the foraminifer record from the Norwegian Sea and the North Atlantic Ocean, *Clim. Past*, *6*(2), 179–193, doi:10.5194/cp-6-179-2010.

Barker, S., M. Greaves, and H. Elderfield (2003), A study of cleaning procedures used for foraminiferal Mg/Ca paleothermometry, *Geochem. Geophys. Geosyst.*, *4*(9), 8407, doi:10.1029/2003GC000559.

Barron, J. A., L. Heusser, T. Herbert, and M. Lyle (2003), High-resolution climatic evolution of coastal northern California during the past 16,000 years, *Paleoceanography*, *18*(1), 1020, doi:10.1029/2002PA000768.

Bauch, D., P. Schlosser, and R. G. Fairbanks (1995), Freshwater balance and the sources of deep and bottom waters in the Arctic Ocean inferred from the distribution of $H_2^{18}O$, *Prog. Oceanogr.*, *35*, 53–80.

Bauch, D., J. Carstens, and G. Wefer (1997), Oxygen isotope composition of living *Neogloboquadrina pachyderma* (sin.) in the Arctic Ocean, *Earth Planet. Sci. Lett.*, *146*, 47–58.

Bauch, D., H. Erlenkeuser, G. Winckler, G. Pavlova, and J. Thiede (2002), Carbon isotopes and habitat of polar planktic foraminifera in the Okhotsk Sea: The 'carbonate ion effect' under natural conditions, *Mar. Micropaleontol.*, *45*, 83–99, doi:10.1016/S0377-8398(02)00038-5.

Biebow, N., R. Kulinich, and B. Baranov (Eds.) (2003), Cruise Report: KOMEX (Kurile Okhotsk Sea Marine Experiment) RV Akademik M.A. Lavrentyev Cruise 29, Leg 1 and Leg 2, Vladivostok–Pusan–Okhostsk Sea–Pusan–Okhotsk Sea–Pusan–Vladivostok, May 25–August 05 2002, *GEOMAR Report*, *110*, 190, 176 pp.

Blockley, S. P. E., et al. (2012), Synchronisation of palaeoenvironmental records over the last 60,000 years, and an extended INTIMATE event stratigraphy to 48,000 b2k, *Quat. Sci. Rev.*, *36*, 2–10, doi:10.1016/j.quascirev.2011.09.017.

Brigham-Grette, J., D. M. Hopkins, V. F. Ivanov, E. B. Basilyan, S. L. Benson, P. A. Heiser, and V. S. Pushkar (2001), Last Interglacial (isotope stage 5) glacial and sea-level history of coastal Chukotka Peninsula and St. Lawrence Island, Western Beringia, *Quat. Sci. Rev.*, *20*, 419–436, doi:10.1029/2003GC000559.

Brigham-Grette, J., L. M. Gualtieri, O. Y. Glushkova, T. D. Hamilton, D. Mostoller, and A. Kotov (2003), Chlorine-36 and ^{14}C chronology support a limited Last Glacial Maximum across central Chukotka, northeastern Siberia, and no Beringian ice sheet, *Quat. Res.*, *59*, 386–398, doi:10.1016/S0033-5894(03)00058-9.

Brunelle, B. G., D. M. Sigman, M. S. Cook, L. D. Keigwin, G. H. Haug, B. Plessen, G. Schettler, and S. L. Jaccard (2007), Evidence from diatom-bound nitrogen isotopes for subarctic Pacific stratification during the last ice age and a link to North Pacific denitrification changes, *Paleoceanography*, *22*, PA1215, doi:10.1029/2005PA001205.

Brunelle, B. G., D. M. Sigman, S. L. Jaccard, L. D. Keigwin, B. Plessen, G. Schettler, M. S. Cook, and G. H. Haug (2010), Glacial/interglacial changes in nutrient supply and stratification in the western subarctic North Pacific since the penultimate glacial maximum, *Quat. Sci. Rev.*, *29*, 2579–2590, doi:10.1016/j.quascirev.2010.03.010.

Caissie, B. E., J. Brigham-Grette, K. T. Lawrence, T. D. Herbert, and M. S. Cook (2010), Last Glacial Maximum to Holocene sea surface conditions at Umnak Plateau, Bering Sea, as inferred from diatom, alkenone, and stable isotope records, *Paleoceanography*, *25*, PA1206, doi:10.1029/2008PA001671.

Chikamoto, M. O., L. Menviel, A. Abe-Ouchi, R. Ohgaito, A. Timmermann, Y. Okazaki, N. Harada, A. Oka, and A. Mouchet (2012), Variability in North Pacific intermediate and deep water ventilation during Heinrich events in two coupled climate models, *Deep-Sea Res. II*, *61-64*, 114–126, doi:10.1016/j.dsr2.2011.12.002.

DeMaster, D. (1981), The supply and accumulation of silica in the marine environment, *Geochim. Cosmochim. Acta*, *45*, 1715–1732.

Dullo, W.-C., B. Baranov, and C. van den Bogaard (Eds.) (2009), FS Sonne Fahrtbericht/Cruise Report SO201-2 KALMAR, Busan/Korea-Tomakomai/Japan, 30.08.-08.10.2009, *IFM-GEOMAR Report*, *35*, 233 pp.

Emile-Geay, J., M. A. Cane, N. Naik, R. Seager, A. C. Clement, and A. van Geen (2003), Warren revisited: Atmospheric freshwater fluxes and "Why is no deep water formed in the North Pacific", *J. Geophys. Res.*, *108*(C6), 3178, doi:10.1029/2001JC001058.

Galbraith, E. D., S. L. Jaccard, T. F. Pedersen, D. M. Sigman, G. H. Haug, M. Cook, J. R. Southon, and R. Francois (2007), Carbon dioxide release from the North Pacific abyss during the last deglaciation, *Nature*, *449*, 890–893, doi:10.1038/nature06227.

Gebhardt, H., M. Sarnthein, P. M. Grootes, T. Kiefer, H. Kuehn, F. Schmieder, and U. Röhl (2008), Paleonutrient and productivity records from the subarctic North Pacific for Pleistocene glacial terminations I to V, *Paleoceanography*, *23*, PA4212, doi:10.1029/2007PA001513.

Gorbarenko, S. A., J. R. Southon, L. D. Keigwin, M. V. Cherepanova, and I. G. Gvozdeva (2004), Late Pleistocene–Holocene oceanographic variability in the Okhotsk Sea: Geochemical, lithological and paleontological evidence, *Palaeogeogr. Palaeoclimatol. Palaeoecol.*, *209*, 281–301, doi:10.1016/j.palaeo.2004.02.013.

Gorbarenko, S. A., I. A. Basov, M. P. Chekhovskaya, J. Southon, T. A. Khusid, and A. V. Artemova (2005), Orbital and millenium scale environmental changes in the southern Bering Sea during the last glacial-Holocene: Geochemical and paleontological evidence, *Deep-Sea Res. II*, *52*, 2174–2185, doi:10.1016/j.dsr2.2005.08.005.

Grootes, P. M., M. Stuiver, J. W. C. White, S. Johnsen, and J. Jouzel (1993), Comparison of oxygen isotope records from the GISP2 and GRIP Greenland ice cores, *Nature*, *366*, 552–554.

Harada, N., K. H. Shin, A. Murata, M. Uchida, and T. Nakatani (2003), Characteristics of alkenones synthesized by a bloom of *Emiliania huxleyi* in the Bering Sea, *Geochim. Cosmochim. Acta*, *67*(8), 1507–1519, doi:10.1016/S0016-7037(02)01318-2.

Harada, N., N. Ahagon, T. Sakamoto, M. Uchida, M. Ikehara, and Y. Shibata (2006a), Rapid fluctuation of alkenone temperature in the southwestern Okhotsk Sea during the past 120 ky, *Global Planet. Change*, *53*, 29–46, doi:10.1016/j.gloplacha.2006.01.010.

Harada, N., M. Sato, A. Shiraishi, and M. C. Honda (2006b), Characteristics of alkenone distributions in suspended and sinking particles in the northwestern North Pacific, *Geochim. Cosmochim. Acta*, *70*, 2045–2062, doi:10.1016/j.gca.2006.01.024.

Haug, G. H., D. M. Sigman, R. Tiedemann, T. F. Pedersen, and M. Sarnthein (1999), Onset of permanent stratification in the subarctic Pacific Ocean, *Nature*, *401*, 779–782.

Haug, G. H., et al. (2005), North Pacific seasonality and the glaciation of North America 2.7 million years ago, *Nature*, *433*, 821–825, doi:10.1038/nature03332.

Hillaire-Marcel, C., A. de Vernal, L. Polyak, and D. Darby (2004), Size-dependent isotopic composition of planktic foraminifers from Chukchi Sea vs. NW Atlantic sediments—Implications for the Holocene paleoceanography of the western Arctic, *Quat. Sci. Rev.*, *23*, 245–260, doi:10.1016/j.quascirev.2003.08.006.

Hillaire-Marcel, C., and A. de Vernal (2008), Stable isotope clue to episodic sea ice formation in the glacial North Atlantic, *Earth Planet. Sci. Lett.*, *268*, 143–150, doi:10.1016/j.epsl.2008.01.012.

Hu, A., G. A. Meehl, B. L. Otto-Bliesner, C. Waelbroeck, W. Han, M.-F. Loutre, K. Lambeck, J. X. Mitrovica, and N. Rosenbloom (2010), Influence of Bering Strait flow and North Atlantic circulation on glacial sea-level changes, *Nat. Geosci.*, *3*, 118–121, doi:10.1038/ngeo729.

Jaccard, S. L., G. H. Haug, D. M. Sigman, T. F. Pedersen, H. R. Thierstein, and U. Röhl (2005), Glacial/interglacial changes in subarctic North Pacific stratification, *Science*, *308*, 1003-1006, doi:10.1126/science.1108696.

Jaccard, S. L., E. D. Galbraith, D. M. Sigman, G. H. Haug, R. Francois, T. F. Pedersen, P. Dulsky, and H. R. Thierstein (2009), Subarctic Pacific

evidence for a glacial deepening of the oceanic respired carbon pool, *Earth Planet. Sci. Lett.*, *277*, 156–165, doi:10.1016/j.epsl.2008.10.017.

Karhu, J. A., S. Tschudi, M. Saarnisto, P. Kubik, and C. Schlüchter (2001), Constraints for the latest glacial advance on Wrangel Island, Arctic Ocean, from rock surface exposure dating, *Global Planet. Change*, *31*, 447–451.

Katsuki, K., and K. Takahashi (2005), Diatoms as paleoenvironmental proxies for seasonal productivity, sea-ice and surface circulation in the Bering Sea during the late Quaternary, *Deep-Sea Res. II*, *52*, 2110–2130, doi:10.1016/j.dsr2.2005.07.001.

Katsumata, K., and I. Yasuda (2010), Estimates of non-tidal exchange transport between the Sea of Okhtosk and the North Pacific, *J. Oceanogr.*, *66*, 489–504, doi:10.1007/s10872-010-0041-9.

Kaufman, D. S., et al. (2004), Holocene thermal maximum in the western Arctic (0–180°W), *Quat. Sci. Rev.*, *23*, 529–560, doi:10.1016/j.quascirev.2003.09.007.

Keigwin, L. D., J. P. Donnelly, M. S. Cook, N. W. Driscoll, and J. Brigham-Grette (2006), Rapid sea-level rise and Holocene climate in the Chukchi Sea, *Geology*, *34*(10), 861–864, doi:10.1130/G22712.1.

Kiefer, T., M. Sarnthein, H. Erlenkeuser, P. M. Grootes, and A. P. Roberts (2001), North Pacific response to millennial-scale changes in ocean circulation over the last 60 kyr, *Paleoceanography*, *16*(2), 179–189, doi:10.1029/2003GC000559.

Kienast, S. S., and J. L. McKay (2001), Sea surface temperatures in the subarctic northeast Pacific reflect millennial-scale climate oscillations during the last 16 kyrs, *Geophys. Res. Lett.*, *28*(8), 1563–1566, doi:10.1029/2003GC000559.

Kohfeld, K. E., R. G. Fairbanks, S. L. Smith, and I. D. Walsh (1996), *Neogloboquadrina pachyderma* (sinistral coiling) as paleoceanographic tracers in polar oceans: Evidence from Northeast Water Polynya plankton tows, sediment traps, and surface sediments, *Paleoceanography*, *11*(6), 679–699, doi:10.1029/2003GC000559.

Kowalik, Z., J. L. Luick, and T. C. Royer (1994), On the dynamics of the Alaska Coastal Current, *Cont. Shelf Res.*, *14*(7/8), 831–845, doi:10.1029/2003GC000559.

Kozdon, R., A. Eisenhauer, M. Weinelt, M. Y. Meland, and D. Nürnberg (2009), Reassessing Mg/Ca temperature calibrations of *Neogloboquadrina pachyderma* (sinistral) using paired $\delta^{44/40}$Ca and Mg/Ca measurements, *Geochem. Geophys. Geosyst.*, *10*(3), Q03005, doi:10.1029/2008GC002169.

Krebs, U., and A. Timmermann (2007), Tropical air-sea interactions accelerate the recovery of the Atlatnic Meridional Overturning Circulation after a major shutdown, *J. Climate*, *20*, 4940–4956, doi:10.1175/jcli4296.1.

Kuroyanagi, A., and H. Kawahata (2004), Vertical distribution of living planktonic foraminifera in the seas around Japan, *Mar. Micropaleontol.*, *53*, 173–196, doi:10.1016/j.marmicro.2004.06.001.

Kuroyanagi, A., H. Kawahata, and H. Nishi (2012), Seasonal variation in the oxygen isotopic composition of different-sized planktonic foraminifer *Neogloboquadrina pachyderma* (sinistral) in the northwestern North Pacific and implications for reconstruction of the paleoenvironment, *Paleoceanography*, *26*, PA4215, doi:10.1029/2011PA002153.

Laskar, J., P. Robutel, F. Joutel, M. Gastineau, A. C. M. Correia, and B. Levrard (2004), A long-term numerical solution for the insolation quantities of the Earth, *Astron. Astrophys.*, *428*, 261–285, doi:10.1051/0004-6361:20041335.

Leduc, G., R. Schneider, J.-H. Kim, and G. Lohmann (2010), Holocene and Eemian sea surface temperature trends as revealed by alkenone and Mg/Ca paleothermometry, *Quat. Sci. Rev.*, *29*, 989–1004, doi:10.1016/j.quascirev.2010.01.004.

Locarnini, R. A., A. V. Mishonov, J. I. Antonov, T. P. Boyer, and H. E. Garcia (2010), World Ocean Atlas 2009, Volume 1: Temperature, in NOAA Atlas NESDIS 68, edited by S. Levitus, 184 pp, U.S. Government Printing Office, Washington, D.C.

Max, L., J.-R. Riethdorf, R. Tiedemann, M. Smirnova, L. Lembke-Jene, K. Fahl, D. Nürnberg, A. Matul, and G. Mollenhauer (2012), Sea surface temperature variability and sea-ice extent in the subarctic northwest Pacific during the past 15,000 years, *Paleoceanography*, *27*, PA3213, doi:10.1029/2012PA002292.

McManus, J. F., R. Francois, J.-M. Gherardi, L. D. Keigwin, and S. Brown-Leger (2004), Collapse and rapid resumption of Atlantic meridional circulation linked to deglacial climate changes, *Nature*, *428*, 834–837, doi:10.1038/nature02494.

Menviel, L., A. Timmermann, O. Elison Timm, A. Mouchet, A. Abe-Ouchi, M. O. Chikamoto, N. Harada, R. Ohgaito, and Y. Okazaki (2012), Removing the North Pacific halocline: Effects on global climate, ocean circulation and the carbon cycle, *Deep-Sea Res. II*, *61-64*, 106–113, doi:10.1016/j.dsr2.2011.03.005.

Mikolajewicz, U., T. J. Crowley, A. Schiller, and R. Voss (1997), Modelling teleconnections between the North Atlantic and North Pacific during the Younger Dryas, *Nature*, *387*, 384–387.

Miura, T., T. Suga, and K. Hanawa (2002), Winter mixed layer and formation of dichothermal water in the Bering Sea, *J. Oceanogr.*, *58*, 815–823, doi:10.1023/A:1022871112946.

Mohiuddin, M. M., A. Nishimura, and Y. Tanaka (2005), Seasonal succession, vertical distribution, and dissolution of planktonic foraminifera along the Subarctic Front: Implications for paleoceanographic reconstruction in the northwestern Pacific, *Mar. Micropaleontol.*, *55*, 129–156, doi:10.1016/j.marmicro.2005.02.007.

Müller, P., and R. Schneider (1993), An automated leaching method for the determination of opal in sediments and particulate matter, *Deep-Sea Res. I*, *40*, 425–444, doi:10.1029/2003GC000559.

Müller, P. J., G. Kirst, G. Ruhland, I. von Storch, and A. Rosell-Melé (1998), Calibration of the alkenone paleotemperature index $U^{K'}_{37}$ based on core-tops from the eastern South Atlantic and the global ocean (60°N–60°S), *Geochim. Cosmochim. Acta*, *62*(10), 1757–1772, doi:10.1029/2003GC000559.

Niebauer, H. J., N. A. Bond, L. P. Yakunin, and V. V. Plotnikov (1999), An update on the climatology and sea ice of the Bering Sea, in Dynamics of the Bering Sea, edited by T. R. Loughlin, and K. Ohtani, pp. 29–59, University of Alaska Sea Grant, doi:10.1029/2003GC000559.

North Greenland Ice Core Project members (2004), High-resolution record of northern hemisphere climate extending into the last interglacial period, *Nature*, *431*, 147–151, doi:10.1038/nature02805.

Ohkushi, K., M. Uchida, N. Ahagon, T. Mishima, and T. Kanematsu (2004), Glacial intermediate water ventilation in the northwestern Pacific based on AMS radiocarbon dating, *Nucl. Instrum. Methods Phys. Res. B*, *223-224*, 460–465, doi:10.1016/j.nimb.2004.04.087.

Ohtani, K., Y. Akiba, and A. Y. Takenouti (1972), Formation of western subarctic water in the Bering Sea, in Biological oceanography of the northern North Pacific Ocean, edited by A. Y. Takenouti, pp. 32–44, Idemitsu Shoten Publ. Co, doi:10.1029/2003GC000559.

Okazaki, Y., A. Timmermann, L. Menviel, N. Harada, A. Abe-Ouchi, M. O. Chikamoto, A. Mouchet, and H. Asahi (2010), Deepwater formation in the North Pacific during the last glacial termination, *Science*, *329*, 200–204, doi:10.1126/science.1190612.

Okumura, Y. M., C. Deser, A. Hu, A. Timmermann, and S.-P. Xie (2009), North Pacific climate response to freshwater forcing in the subarctic North Atlantic: Oceanic and atmospheric pathways, *J. Climate*, *22*, 1424–1445, doi:10.1175/2008jcli2511.1.

Rasmussen, S. O., et al. (2006), A new Greenland ice core chronology for the last glacial termination, *J. Geophys. Res.*, *111*, D06102, doi:10.1029/2005JD006079.

Regenberg, M., D. Nürnberg, S. Steph, J. Groeneveld, D. Garbe-Schönberg, R. Tiedemann, and W.-C. Dullo (2006), Assessing the effect of dissolution on planktonic foraminiferal Mg/Ca ratios: Evidence from Caribbean core tops, *Geochem. Geophys. Geosyst.*, *7*(7), Q07P15, doi:10.1029/2005GC001019.

Rella, S. F., R. Tada, K. Nagashima, M. Ikehara, T. Itaki, K. Ohkushi, T. Sakamoto, N. Harada, and M. Uchida (2012), Abrupt changes of intermediate water properties on the northeastern slope of the Bering Sea during the last glacial and deglacial period, *Paleoceanography*, *27*, PA3203, doi:10.1029/2011PA002205.

Saenko, O. A., A. Schmittner, and A. J. Weaver (2004), The Atlantic—Pacific seasaw, *J. Climate*, *17*(11), 2033–2038, doi:10.1175/1520-0442(2004)017.

Sagawa, T., and K. Ikehara (2008), Intermediate water ventilation change in the subarctic northwest Pacific during the last deglaciation, *Geophys. Res. Lett.*, *35*, L24702, doi:10.1029/2008GL035133.

Sarnthein, M., et al. (2001), Fundamental modes and abrupt changes in North Atlantic circulation and climate over the last 60 ky—Concepts, reconstruction and numerical modeling, in The northern North Atlantic: A changing environment, edited by P. Schäfer, W. Ritzrau, M. Schlüter, and J. Thiede, pp. 365–410, Springer, Berlin.

Sarnthein, M., H. Gebhardt, T. Kiefer, M. Kucera, M. Cook, and H. Erlenkeuser (2004), Mid Holocene origin of the sea-surface salinity low in the subarctic North Pacific, *Quat. Sci. Rev.*, *23*, 2089–2099, doi:10.1016/j.quascirev.2004.08.008.

Sarnthein, M., T. Kiefer, P. M. Grootes, H. Elderfield, and H. Erlenkeuser (2006), Warmings in the far northwestern Pacific promoted pre-Clovis immigration to America during Heinrich event 1, *Geology*, *34*(3), 141–144, doi:10.1130/G22200.1.

Sarnthein, M., P. M. Grootes, J. P. Kennett, and M.-J. Nadeau (2007), ^{14}C reservoir ages show deglacial changes in ocean currents and carbon cycle, in Past and Future Changes of the Oceanic Meridional Overturning Circulation: Mechanisms and Impacts, edited by A. Schmittner, J. C. H. Chiang, and S. R. Hemming, pp. 175–196, AGU Monograph Series, 173, AGU, Washington, D.C.

Sawada, K., and N. Handa (1998), Variability of the path of the Kuroshio ocean current over the past 25,000 years, *Nature*, *392*, 592–595.

Schlitzer, R. (2011), Ocean Data View, http://odv.awi.de.

9. Sea surface temperature variability and sea-ice extent in the subarctic northwest Pacific during the past 15,000 years

Lars Max, Jan-Rainer Riethdorf, Ralf Tiedemann, Maria Smirnova, Lester Lembke-Jene, Kirsten Fahl, Dirk Nürnberg, Alexander Matul, Gesine Mollenhauer

Manuscript published in Paleoceanography, vol. 27, PA3213, 2012.

doi: 10.1002/2012PA002292

PALEOCEANOGRAPHY, VOL. 27, PA3213, doi:10.1029/2012PA002292, 2012

Sea surface temperature variability and sea-ice extent in the subarctic northwest Pacific during the past 15,000 years

Lars Max,[1] Jan-Rainer Riethdorf,[2] Ralf Tiedemann,[1] Maria Smirnova,[3] Lester Lembke-Jene,[1] Kirsten Fahl,[1] Dirk Nürnberg,[2] Alexander Matul,[3] and Gesine Mollenhauer[1]

Received 27 January 2012; revised 2 July 2012; accepted 3 July 2012; published 16 August 2012.

[1] Past changes in North Pacific sea surface temperatures and sea-ice conditions are proposed to play a crucial role in deglacial climate development and ocean circulation but are less well known than from the North Atlantic. Here, we present new alkenone-based sea surface temperature records from the subarctic northwest Pacific and its marginal seas (Bering Sea and Sea of Okhotsk) for the time interval of the last 15 kyr, indicating millennial-scale sea surface temperature fluctuations similar to short-term deglacial climate oscillations known from Greenland ice core records. Past changes in sea-ice distribution are derived from relative percentage of specific diatom groups and qualitative assessment of the IP_{25} biomarker related to sea-ice diatoms. The deglacial variability in sea-ice extent matches the sea surface temperature fluctuations. These fluctuations suggest a linkage to deglacial variations in Atlantic meridional overturning circulation and a close atmospheric coupling between the North Pacific and North Atlantic. During the Holocene the subarctic North Pacific is marked by complex sea surface temperature trends, which do not support the hypothesis of a Holocene seesaw in temperature development between the North Atlantic and the North Pacific.

Citation: Max, L., J.-R. Riethdorf, R. Tiedemann, M. Smirnova, L. Lembke-Jene, K. Fahl, D. Nürnberg, A. Matul, and G. Mollenhauer (2012), Sea surface temperature variability and sea-ice extent in the subarctic northwest Pacific during the past 15,000 years, *Paleoceanography*, *27*, PA3213, doi:10.1029/2012PA002292.

1. Introduction

[2] Knowledge of the deglacial SST development and variability in sea-ice extent in the subarctic Pacific provide important climate boundary conditions to understand oceanic/atmospheric teleconnections between the Atlantic and the Pacific and to evaluate most recent hypotheses related to deep water formation in the North Pacific (N-Pacific). However, the sea surface temperature (SST) variability in the subarctic N-Pacific realm as well as the timing of SST changes during the last glacial termination and the Holocene have remained elusive. In general, the spatial and temporal development of SSTs in the N-Pacific on centennial-millennial timescales is only poorly conceived for several reasons: (1) SST reconstructions from the N-Pacific are sparse (Figure 1); (2) available SST reconstructions are based on a variety of different temperature proxies, which in turn may lead to inconsistent temperature signals since the recording of each proxy can be afflicted with a seasonal bias and/or is related to a different water depth; (3) the availability of carbonate-bearing sediment records with high sedimentation rates is restricted to shallow water depths due to the shallow position of the calcite compensation depth in the N-Pacific (<3000 m); (4) the absence of carbonate for major parts of N-Pacific sediments excludes the application of carbonate-based proxies and ^{14}C-datings on planktonic foraminifers, thus limiting detailed climate reconstructions; and (5) changes in paleo-^{14}C reservoir ages are not well defined and may lead to imprecise age models in the N-Pacific [*Sarnthein et al.*, 2004].

[3] As a consequence, model simulations and proxy-based interpretations have partially led to contradictory results concerning the SST variability in the N-Pacific and its underlying mechanisms during the last deglaciation. Studies with general circulation models (GCMs) suggest both an in-phase behavior of deglacial SST variability between the North Atlantic (N-Atlantic) and the N-Pacific [*Mikolajewicz et al.*, 1997; *Vellinga and Wood*, 2002; *Okumura et al.*, 2009; *Chikamoto et al.*, 2012] as well as an out-of-phase response [*Saenko et al.*, 2004; *Schmittner et al.*, 2007; *Okazaki et al.*, 2010]. The in-phase behavior has been related to rapid atmospheric teleconnections, acting on years to decades. The out-of-phase response has been attributed to oceanic readjustments of the Atlantic meridional overturning circulation (AMOC). More specifically, the simulated

[1]Alfred Wegener Institute for Polar and Marine Research, Bremerhaven, Germany.
[2]GEOMAR, Helmholtz-Zentrum für Ozeanforschung Kiel, Kiel, Germany.
[3]P. P. Shirshov Institute of Oceanology, Moscow, Russia.

Corresponding author: L. Max, Alfred Wegener Institute for Polar and Marine Research, Am Handelshafen 12, DE-27570 Bremerhaven, Germany. (lars.max@awi.de)

0883-8305/12/2012PA002292

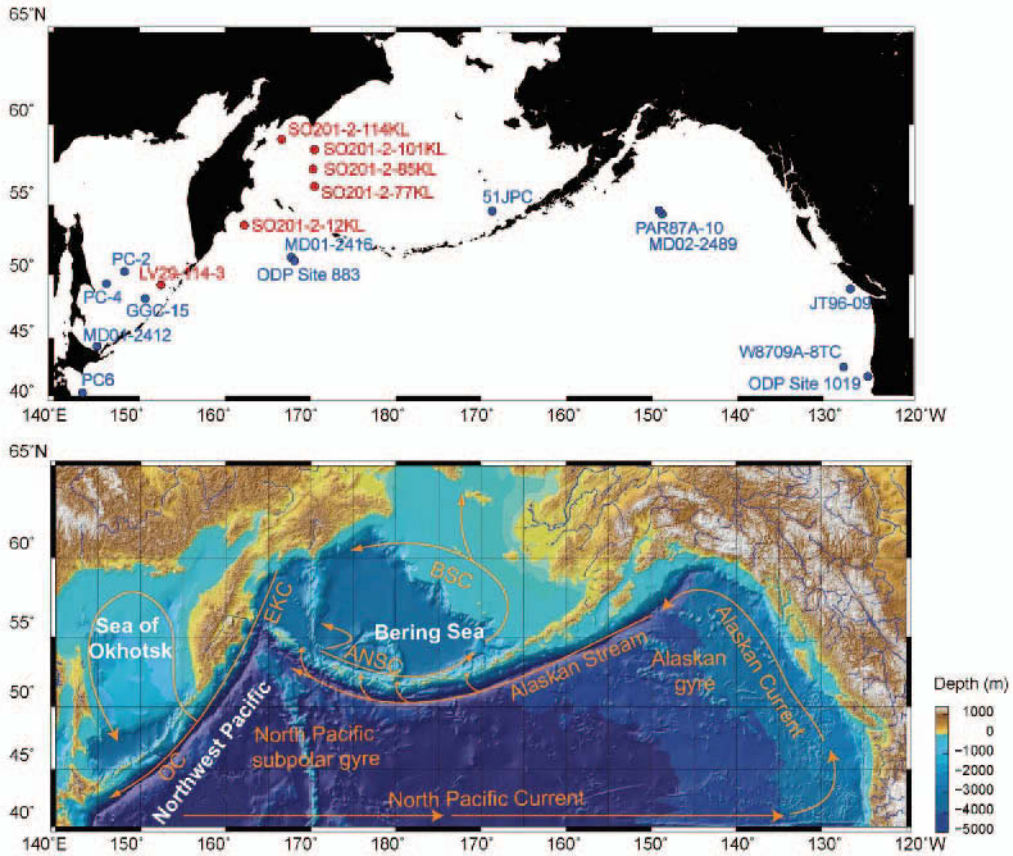

Figure 1. (top) Core sites in the subarctic Pacific from this study (in red), together with published sediment records (in blue) in the Sea of Okhotsk (PC-2 and PC-4 [*Seki et al.*, 2004a], GGC-15 [*Ternois et al.*, 2000], MD01–2412 [*Harada et al.*, 2006b]) the Bering Sea (51JPC [*Caissie et al.*, 2010]) and the N-Pacific (PC6 [*Minoshima et al.*, 2007], ODP Site 883 [*Kiefer et al.*, 2001], MD01–2416 [*Sarnthein et al.*, 2004], PAR87A-10 [*Pisias et al.*, 2001], MD02–2489 [*Gebhardt et al.*, 2008], JT96–09 [*Kienast and McKay*, 2001], W8709A-8TC [*Pisias et al.*, 2001], ODP Site 1019 [*Barron et al.*, 2003]). (bottom) Bathymetric chart of the subarctic N-Pacific with the general surface circulation pattern indicated by orange arrows (modified after *Stabeno et al.* [1999]). OC = Oyashio Current; EKC = East Kamchatka Current; ANSC = Aleutian North Slope Current; BSC = Bering Slope Current.

reduction of the AMOC as a consequence of enhanced sea surface freshening in the N-Atlantic (as during Heinrich 1 and the Younger Dryas) resulted in a strengthening of the Pacific meridional overturning circulation (PMOC) and an associated warming in the N-Pacific. The warming resulted from an enhanced poleward heat transport from the subtropics to the N-Pacific. Accordingly, the proposed seesaw between AMOC reduction and PMOC intensification suggests a N-Pacific warming during Heinrich 1 (H1) and the Younger Dryas (YD). In turn, the reestablishment of the AMOC (shutdown of PMOC) led to a surface cooling in the N-Pacific during the Bølling/Allerød (B/A) and the early Holocene. Consequently, the interplay between the two meridional overturning cells is expected to provide millennial-scale out-of-phase fluctuations in SST between the N-Atlantic and the N-Pacific [e.g., *Saenko et al.*, 2004].

[4] The few available deglacial SST proxy records from the N-Pacific and its adjacent seas also provide a quite inconsistent picture. The records support both an in-phase and out-of-phase relationship with regard to the N-Atlantic SST development or show continuously cold SSTs from the last glacial to the onset of the Holocene (no warming event during the B/A). For example, a remarkable similarity between the Greenland/N-Atlantic temperature evolution and SST records, based on alkenone paleothermometry, radiolarian assemblages and dinocyst studies, was derived from sediment records of the subarctic northeast Pacific (NE-Pacific) [*Kienast and McKay*, 2001; *Pisias et al.*, 2001; *Seki et al.*, 2002; *Barron et al.*, 2003], the Bering Sea [*Caissie et al.*, 2010] and the Sea of Okhotsk [*Ternois et al.*, 2000]. These records rather argue for an in-phase relationship of temperature fluctuations between the N-Pacific and N-Atlantic. On the other hand, N-Pacific SST records from pelagic core MD01–2416 and MD02–2489, derived from planktonic Mg/Ca ratios and from census counts of planktonic foraminifera using the SIMMAX transfer function,

indicate a different SST development. These records suggest temperature maxima during H1 and the YD and thus millennial-scale fluctuations out-of-phase with the Greenland/N-Atlantic temperature evolution [*Sarnthein et al.*, 2004; *Kiefer and Kienast*, 2005; *Sarnthein et al.*, 2006; *Gebhardt et al.*, 2008]. The timing of these temperature changes is possibly best constrained in sediment record MD01–2416 from the pelagic NW-Pacific. Unfortunately, this record does not allow a direct comparison between Mg/Ca- and alkenone-derived SSTs. Other records provide inconsistent trends of deglacial SST variability. For example, some records derived from the Sea of Okhotsk and the Pacific continental margin of Japan show no SST maximum during the B/A, and the deglacial temperature rise does not appear before the end of the YD [*Seki et al.*, 2004a; *Minoshima et al.*, 2007].

[5] For the Holocene, *Kim et al.* [2004] summarized alkenone-based SST reconstructions from the N-Pacific and the N-Atlantic using a coupled atmosphere-ocean general circulation model to assess the inter-oceanic teleconnected climate variability. Their investigations led to the hypothesis of a long-term temperature seesaw between the N-Atlantic and the N-Pacific. The model-supported proxy-study suggests a warming trend in the N-Pacific and a cooling trend in the N-Atlantic for the time period of the last 7 kyr. The inverse SST trends between the N-Atlantic and the N-Pacific have been attributed to an atmospheric interaction of the positive Pacific North American (PNA) pattern and the negative North Atlantic Oscillation (NAO) phase. However, the derived warming trend in the N-Pacific relies on a single proxy record from the NW-Pacific only [*Ternois et al.*, 2000], which is marked by low alkenone concentrations (close to the detection limit) within the time interval spanning the last 8 kyr BP.

[6] Irrespective of the differences in Holocene and deglacial Pacific SST variability, an exact chronostratigraphic correlation between Greenland ice core records and ^{14}C-dated deglacial marine climate records is limited by assumptions about the ^{14}C reservoir age of the surface water, the habitat in which planktonic foraminifera incorporate the ^{14}C signal into their carbonate shells. Knowledge of the ^{14}C reservoir age is a necessary precondition for converting radiocarbon ages into calendar years in order to balance for the ^{14}C disequilibrium between the upper ocean and the atmosphere. Since the variability of past reservoir ages is largely unknown, most studies assume a constant reservoir effect over time, thereby taking an uncertainty of several hundred years into account. Such uncertainties may increase to more than thousand years within time intervals associated with prominent atmospheric ^{14}C-plateaus (i.e., intervals of very low ^{14}C change with calendar age). Such plateaus especially mark the period of the last deglaciation. Accordingly, the lead and lag of different proxies, indicative of rapid climate change in the subarctic Pacific, are difficult to constrain in comparison to the Greenland climate signal.

[7] Here, we present the first alkenone-derived high-resolution SST estimates from the subarctic NW-Pacific continental margin and the western Bering Sea as well as a new record from the southeastern Sea of Okhotsk. Our study provides a stratigraphic framework for the NW-Pacific realm, which is based on detailed core-to-core correlations and 37 AMS ^{14}C datings. This framework is well constrained between 20 to ~6 ka BP and can be used via X-ray Fluorescence (XRF) core scanner data (e.g., Ca intensities) to transfer ages to other available and future sediment records. The relatively high sedimentation rates enable us to investigate past SST changes on multicentennial to millennial timescales in comparison to rapid climate oscillations known from other parts of the N-Pacific and the N-Atlantic for the last 15 kyr. Additionally, relative percentages of specific diatom groups in combination with qualitative measurements of the C_{25} monounsaturated hydrocarbon (IP_{25}) are used to assess past changes in the sea-ice extent [*Belt et al.*, 2007; *Müller et al.*, 2009] with regard to short-term warm/cold fluctuations. Our data suggest that the subarctic NW-Pacific region is characterized by deglacial SST fluctuations, which show strong similarities to the Greenland/N-Atlantic SST evolution. The sea-ice distribution is closely coupled to the SST variability. The SST records from the NW-Pacific realm presented here provide new insights into the spatio-temporal pattern of millennial-scale SST variability during the deglacial period and the Holocene, which in turn will aid to further constrain the impact of past rapid climate oscillations on N-Pacific oceanography. Our results shed new light onto the discussion of whether the deglacial temperature development in the NW-Pacific supports an in-phase or an out-of-phase behavior with respect to the N-Atlantic SST development and the related seesaw between AMOC and PMOC. With respect to the Holocene, the SST reconstructions are also used to reconsider the hypothesis of a seesaw mechanism that has been proposed to have led to contrasting long-term temperature trends between the N-Atlantic and the N-Pacific (temperature seesaw) during the past 7 kyr.

2. Regional Setting

[8] The subarctic Pacific regions are characterized by a large, seasonal variability in SST and sea-ice distribution, tightly coupled to atmospheric pressure cells which in turn are influenced by large-scale interannual-decadal variability associated with the Pacific–North American (PNA) pattern and the Pacific Decadal Oscillation (PDO) [*Niebauer*, 1988; *Mantua et al.*, 1997; *Niebauer*, 1998; *Overland et al.*, 2002]. During winter, the contrast between the Siberian High and Aleutian Low-Pressure System (ALPS) brings cold air masses from the Arctic to the subarctic Pacific, which results in strong sea surface cooling and mixing of nutrient-rich subsurface waters and favors the expansion of sea-ice in the Bering Sea and Sea of Okhotsk. During summer, both increased insolation and weakening of the ALPS lead to warm SSTs, ice-free conditions and strong upper-ocean stratification [*Ohtani et al.*, 1972]. This leads to strong, seasonal temperature differences between winter (0–2°C) and summer (8–10°C) SSTs in the subarctic NW-Pacific and its marginal seas. Maxima in biogenic productivity occur during spring (dominated by diatoms) and late summer (dominated by coccolithophorids).

[9] The structure of the upper water column is characterized by the presence of a strong halocline, which is a permanent feature of the subarctic Pacific. It forms a barrier for the heat and gas exchange between the deep ocean and the atmosphere as well as for the supply of nutrients into the photic zone. It leads to the highest carbon export efficiency

Table 1. Core Locations in the Subarctic NW-Pacific, Sea of Okhotsk and Western Bering Sea as Well as the Performed Proxy Studies

Sediment Core	Latitude (°N)	Longitude (°E)	Depth (mbsl)	Study Area	Performed Proxy Studies[a]
LV29-114-3	49°22.54′	152°53.23′	1765	Sea of Okhotsk	$U^{K'}_{37}$, IP_{25}, $CaCO_3$, CL, ^{14}C
SO201-2-12KL	53°59.47′	162°22.51′	2145	NW-Pacific	$U^{K'}_{37}$, IP_{25}, Opal, DS, CL, ^{14}C
SO201-2-77KL	56°19.83′	170°41.98′	2135	western Bering Sea	$U^{K'}_{37}$, IP_{25}, CL, ^{14}C
SO201-2-85KL	57°30.30′	170°24.77′	968	western Bering Sea	$U^{K'}_{37}$, IP_{25}, CL, ^{14}C
SO201-2-101KL	58°52.52′	170°41.45′	630	western Bering Sea	$U^{K'}_{37}$, IP_{25}, CL, ^{14}C
SO201-2-114KL	59°13.87′	166°59.32′	1376	western Bering Sea	$U^{K'}_{37}$, IP_{25}, CL, ^{14}C

[a] $U^{K'}_{37}$: alkenone paleothermometry; IP_{25}: sea-ice diatoms biomarker; Opal: wt.% biogenic opal; $CaCO_3$: wt.% $CaCO_3$; CL: Core logging; ^{14}C: AMS ^{14}C datings; DS: Diatom studies.

in the world oceans and acts as a net sink of atmospheric CO_2 today [*Honda et al.*, 2002].

[10] The surface circulation of the subarctic NW-Pacific follows a large-scale cyclonic pattern of surface currents, which regulate the exchange of heat and nutrients between different ocean regions. The dominant large-scale circulation pattern in the subpolar N–Pacific consists of the Kuroshio–North Pacific Current system in the South and two counterclockwise circulating systems: the Alaskan gyre in the East and the western North Pacific subpolar gyre (Figure 1). The North Pacific Current (the Kuroshio extension) transports relatively warm water masses eastward into the Alaskan gyre. The Alaskan Stream forms the northern boundary current and transports water masses from the Alaskan gyre along the Aleutian Islands into the western subpolar gyre, thereby entering the Bering Sea through several passages between the Aleutian Islands. This inflow drives a large-scale counterclockwise surface circulation in the Bering Sea. The surface waters leave the Bering Sea via the Bering Strait into the Arctic Ocean but mainly through the Kamchatka Strait back into the N–Pacific via the East Kamchatka Current (EKC). The EKC delivers nutrient-rich waters from the Bering Sea into the NW-Pacific [*Stabeno et al.*, 1999] and represents the western branch of the North Pacific subpolar gyre. On its path to the South, a part of the EKC enters the Sea of Okhotsk through the Kurile Island Arc, thereby influencing the water mass signature of the Okhotsk gyre. During winter, the intrusion of the relatively warm EKC promotes ice-free conditions around the southern tip of Kamchatka [*Seki et al.*, 2004b] (Figure 1).

3. Material and Methods

[11] We investigated six piston cores from the western Bering Sea, the continental slope of east Kamchatka and the southeastern Sea of Okhotsk (Figure 1). Sediment records were obtained during cruises LV29 KOMEX Leg 2 with R/V *Akademik Lavrentyev* in 2002 and R/V *Sonne* during SO201 KALMAR Leg 2 in 2009. Core site selection was done by intensive sediment echo-sounding studies onboard to detect high-resolution sediment deposits, which are located well above the shallow calcite compensation depth (CCD). Our sediment records provide sufficient amounts of carbonate-bearing material for detailed paleoceanographic reconstructions (Table 1) except the younger part of the Holocene. During the last 6 kyr, the productivity of calcareous plankton was generally low in the NW-Pacific and the productivity dominated by siliceous diatoms. The high amounts of silicious diatom tests further diluted the quantity of planktonic carbonate shells within the sediments [*Gorbarenko et al.*, 2002].

3.1. Stratigraphic Approach

3.1.1. AMS-^{14}C-Dating

[12] AMS ^{14}C-ages were measured on monospecific samples of the planktonic foraminifera *Neogloboquadrina pachyderma* sinistral (*N. pachyderma* sin.) from 125–250 μm fraction. The radiocarbon dating has been performed by the National Ocean Science Accelerator Mass Spectrometry Facility (NOSAMS) at Woods Hole Oceanographic Institute (WHOI) and Leibniz-Laboratory for Radiometric Dating and Isotope Research at Kiel University. Radiocarbon ages have been reported according to the convention outlined by *Stuiver and Polach* [1977] and *Stuiver* [1980]. All radiocarbon ages were converted into calibrated 1-sigma calendar age ranges using the calibration tool Calib Rev 6.0 [*Stuiver and Reimer*, 1993] with the Intcal09 atmospheric calibration curve [*Reimer et al.*, 2009] and considering a constant reservoir age throughout the time period covered by the sediment records (Table 2).

3.1.2. Biogenic Opal and $CaCO_3$

[13] Biogenic opal and $CaCO_3$ were measured at GEOMAR, Kiel. Biogenic opal concentrations were determined from bulk sediment, using the automated leaching method according to *Müller and Schneider* [1993] by molybdate-blue spectrophotometry. Results are given with respect to the mineral correction of *DeMaster* [1981].

[14] Total carbon contents (TC) were determined with a CARLO ERBA Model NA 1500 CNS analyzer. TC was measured on bulk sediments and total organic carbon was derived from decalcified samples. The inorganic carbon ($CaCO_3$) content was calculated by the difference between TC and TOC as follows:

$$CaCO_3 = (TC - TOC) \times 8.333. \quad (1)$$

3.1.3. Core Logging Data

[15] Relative sedimentary elemental composition was measured using the Avaatech X-ray Fluorescence (XRF) core scanner at the Alfred Wegener Institute for Polar and Marine Research, Bremerhaven. Each core segment was triple-scanned for element analysis at 1 mA and tube voltages of 10 kV (Al, Si, S, K, Ca, Ti, Fe), 30 kV (Cu, Zn, Br, Rb, Zr, Sr, Mo) and 50 kV (Ag, Cd, Sn, Te, Ba), using a sampling resolution of 1 cm and 30 s count time.

[16] Color and light reflectance properties of the sediment cores have been measured with a Minolta CM 508d handheld spectrophotometer directly after core splitting onboard [*Dullo et al.*, 2009]. Measurements were conducted at 1 cm interval. Reflectance data was converted into L*, a* and b* color space with the software Spectramagic.

Table 2. AMS ^{14}C Ages of the Sediment Records With Calibrated Calendar Age $\pm 1\sigma$ (Years) and Applied Reservoir Age Correction Used in This Study

Laboratory Number	Sediment Core	Core Depth (cm)	Radiocarbon Age (years)	Calendar Age $\pm 1\sigma$ (years)	Reservoir Age (years)
Transferred age	LV29-114-3	108	5850 ± 60[a]	5607–5730	900
OS-88042		162	8320 ± 40	8236–8310	900
KIA30864		197	9630 ± 50	9764–10067	900
KIA30863		232	10465 ± 50	10808–11080	900
KIA30867		272	12290 ± 55	13164–13308	900
KIA30865		292	13180 ± 60	13960–14457	900
KIA30868		317	14400 ± 80	16538–16827	900
KIA30866		352	15130 ± 80	17117–17497	900
OS-85655	SO201-2-12KL	210	9390 ± 40	9484–9527	900
KIA44680		295	10570 ± 50	11080–11191	900
OS-87895		340	10800 ± 65	11231–11368	900
OS-92047		508	12500 ± 50	13340–13498	900
OS-87891		550	12900 ± 50	13782–13918	900
OS-87902		610	13350 ± 65	14219–14752	900
OS-92150		695	13900 ± 55	15227–15872	900
KIA44682		820	16160 ± 80	18491–18666	900
KIA44683		875	17090 ± 90	19254–19457	900
OS-85671	SO201-2-77KL	105	9570 ± 45[b]	10051–10152	700
OS-85658		115	10450 ± 40[c]	11174–11222	700
OS-90700		155	11500 ± 50	12608–12727	700
OS-85657		167–170	12750 ± 50	13823–13967	700
OS-85664		180	13200 ± 45	14501–14945	700
OS-85665	SO201-2-85KL	26	9950 ± 40[b]	10378–10507	700
KIA42231		45	10315 ± 65[c]	10791–10966	700
OS-85669		60	11950 ± 45	13104–13217	700
KIA42232		70	12620 ± 90	13665–13887	700
OS-87896		95	13850 ± 55	15803–15822	700
OS-87890		135	17350 ± 65	19575–19895	700
KIA42233		155	20720 ± 160	23706–24194	700
OS-87887	SO201-2-101KL	10	12600 ± 55	13686–13838	700
OS-88041		90	14950 ± 60	17165–17506	700
KIA42229		110	17310 ± 120	19541–19919	700
Transferred age		140	20720 ± 160[d]	23706–24194	700
KIA42230		190	22510 ± 190	25876–26351	700
KIA42506		260	29270 ± 440	32121–33539	700
KIA42235	SO201-2-114KL	39	10200 ± 70	10600–10805	700
KIA42236		76–78	10645 ± 50	11249–11404	700
KIA42237		114	12160 ± 80	13249–13403	700
KIA42238		153	13410 ± 100	14727–15237	700

[a]The ^{14}C age transferred from sediment core V34–98 [*Gorbarenko et al.*, 2002].
[b]The ^{14}C ages used to define the carbonate spike 1.
[c]The ^{14}C ages used to define the carbonate spike 2.
[d]The ^{14}C age transferred from sediment core SO201-2-85KL.

3.2. Alkenone Analysis and Sea Surface Temperatures ($U^{K'}_{37}$)

[17] Discrete samples (5–10 g) were taken from bulk sediment, freeze-dried and stored frozen until further analysis. Samples were extracted with an accelerated solvent extractor (ASE-200, Dionex) at 100°C and 1000 psi for 15 min by using dichlormethane (DCM) as a solvent. Remaining extracts were separated by silica gel column chromatography into three sub-fractions with the following mixture of solvents: fraction 1, 5 ml hexane; fraction 2, a mixture of 5 ml DCM\hexane (1:1); fraction 3, 5 ml DCM. Alkenones were eluted in the third fraction and prepared in 100 μl hexane. The third fraction was measured at the Alfred Wegener Institute for Polar and Marine Research (AWI) by using a HP 6890 gas chromatograph, equipped with a cold injection system, a DB-1MS fused silica capillary column (60 × 0.32 mm inner diameter, film thickness of 0.25 μm) and a flame ionization detector. Individual alkenone (C37:3, C37:2) identification was based on the retention time and the comparison with an external standard, which were also used for controlling the instrument stability. The detection threshold for the alkenones is almost 10 ng/g. The alkenone unsaturation index ($U^{K'}_{37}$) as proxy for SST [*Brassell et al.*, 1986; *Prahl and Wakeham*, 1987] was calculated following the relationship between $U^{K'}_{37}$ and temperature as proposed by *Müller et al.* [1998], which is based on a global core top calibration (60°N–60°S):

$$U^{K'}_{37} = 0.033T(°C) + 0.044. \quad (2)$$

[18] The standard error of this calibration is reported as +/−0.050 $U^{K'}_{37}$-units or +/−1.5°C. However, it has to be mentioned that for the lower end of the used temperature calibration a larger error is reported but still keeps its significance in conjunction to other results from this study. It is also known that in the subpolar N-Pacific, alkenone producers are limited to specific seasons and represent more likely the late summer/early fall SST [*Harada et al.*, 2003, 2006a; *Seki et al.*, 2007]. Nevertheless, for a direct comparison to other studies, we decided to use the calibration

after *Müller et al.* [1998] mentioned above, which is widely used in the N-Pacific and other regions rather than the polar temperature function of the Southern Ocean as proposed by *Sikes et al.* [1997].

3.3. Qualitative Assessment of Sea-Ice Distribution (IP_{25}) and Microfossil Studies (Diatoms)

[19] Recently it has been recognized that when detected in marine sediments, the C_{25} isoprenoid lipid (IP_{25}) biosynthesized by Arctic sea-ice diatoms acts as a proxy for previous spring sea-ice occurrence and subsequent melt [*Belt et al.*, 2007]. We performed qualitative IP_{25} analysis on selected samples, based on significant changes in our proxy records and reflecting different climate intervals according to our age model. For this purpose the hydrocarbon fraction (fraction 1, see above) of selected samples were measured with an Agilent 6850 GC (30 m HP-5MS column, 0.25 mm i.d., 0.25 μm film thickness) coupled to an Agilent 5975 C VL mass selective detector. The GC oven was heated from 60°C to 150°C at 15°C min^{-1}, and then at 10°C min^{-1} to 320°C (held 15 min.). Operating conditions for the mass spectrometer were 70 eV and 230°C (ion source). Helium was used as carrier gas. Identification of IP_{25} is based on comparison of its retention time and mass spectra with published data [*Belt et al.*, 2007]. The measurements were carried out using SIM (selected ion monitoring) mode (for further details see *Müller et al.* [2011] and *Fahl and Stein* [2012]). The Kovats index is 2085.

[20] Diatom analysis was carried out on discrete samples (approximately every 10 cm) for NW-Pacific core SO201-2-12KL. Observations by using a compound light-microscope were made at 1000× magnification. At least 300–500 valves were counted per sample. The number of diatom valves per gram of sediments was estimated. Results are given as relative percentage of diatom species *Fragilariopsis oceanica* (Cleve) Hasle (*F. oceanica*) as sea-ice indicator, and *Neodenticula seminae* (Simonsen and Kanaya) Akiba and Yanagisawa (*N. seminae*) related to open-water conditions.

4. Results

4.1. Age Model

[21] The color and XRF records have been used to correlate prominent and similar structures between sediment records. This approach also enabled a transfer of conventional ^{14}C ages from one core to another (Figure 2 and Table 2). We preferentially dated carbonate maxima (maxima in planktonic foraminifer abundance), which are indicated by maxima in Ca intensities (XRF), to avoid age artifacts due to bioturbation effects. Figure 2 shows the Ca intensity records and a detailed core-to-core correlation of our studied core sites. The pattern is marked by two intervals with high Ca intensities. These pronounced carbonate maxima are well known in the NW-Pacific realm and mark the B/A and the interval of the early Holocene [*Keigwin et al.*, 1992; *Keigwin*, 1998; *Gorbarenko et al.*, 2002, 2005; *Caissie et al.*, 2010]. The prominent carbonate maxima range from ca. 13,410 (SO201-2-114KL) to 11,950 ^{14}C years (SO201-2-85KL) and from ca. 10,800 (SO201-2-12KL) to 9,570 ^{14}C years (SO201-2-77KL). The structure of these carbonate maxima is best resolved in NW-Pacific sediment record SO201-2-12KL, which provides sedimentation rates of up to 80 cm/kyr for these intervals. However, this record suggests that the maxima consist of a sequence of carbonate spikes that are not fully resolved in the other cores. At Shirshov Ridge, the interplay of lower sedimentation rates and bioturbation effects may have led to stratigraphic uncertainties in the early Holocene. In Shirshov cores SO201-2-77KL and SO201-2-85KL, the match between carbonate spikes 1 and 2 (Figure 2) and their corresponding ^{14}C ages provide an uncertainty of up to a few hundred years. In this case, we calculated and used an average ^{14}C age for each carbonate spike (spike 1 = 9,760 ^{14}C years; spike 2 = 10,383 ^{14}C years). At high-resolution core SO201-2-114KL from the northwestern continental margin of the Bering Sea, laminated sediment deposits characterize the intervals of both carbonate maxima (Figure 2).

[22] The mid to late Holocene time interval is marked by low carbonate contents in the NW-Pacific realm. Accordingly, the low abundance or complete absence of foraminifers prevented any planktonic ^{14}C-dating of our records. However, for core LV29-114-3 from the Sea of Okhotsk, we improved the age control via correlation to the well-dated neighbor core V34–98 [*Gorbarenko et al.*, 2002] and assigned one additional ^{14}C age to core LV29-114-3 (5,850 years) as shown in Figure 3.

[23] In addition, we also correlated the Ca intensity pattern of NW-Pacific core SO201-2-12KL and Sea of Okhotsk core LV29-114-3 to the pattern of NW-Pacific cores RAMA 44PC [*Keigwin et al.*, 1992] and MD01–2416 [*Sarnthein et al.*, 2004; *Gebhardt et al.*, 2008]. This correlation provides a good match with the RAMA 44PC carbonate record. Sediment record MD01–2416 provides an excellent age model, including 15 planktonic ^{14}C-datings, which covers the interval of the first pronounced carbonate maximum between H1 and the B/A. However, the carbonate maximum is less clearly developed in comparison to all other records presented here (Figure 2). A clear correlation is only possible by considering the ^{14}C ages. Furthermore, the Ca and $CaCO_3$ structure at 9,985 ^{14}C years in core MD01–2416, which possibly marks the first Ca-spike of the second carbonate maximum in the early Holocene, appears to be several hundred years too young in comparison to the age assignments of our Ca-records from the NW-Pacific, the Bering Sea and the Sea of Okhotsk (Figure 2). Consequently, we did not transfer any ^{14}C ages from core MD01–2416 to our records.

[24] In general, the sequence of ^{14}C data and their assignment to prominent carbonate structures is consistent between the investigated cores (within a range of a few hundred years) and can be traced from the Bering Sea to the NW-Pacific (except for core MD01–2416) and even into the Sea of Okhotsk. Hence, the registered temporal pattern of the carbonate maxima seems not to be significantly biased by water depth-dependent differences in carbonate dissolution at our investigated records, which range from 630 to 2200 m water depth. However, the ^{14}C ages of the carbonate maxima at our sediment records from the western Bering Sea (630 to 2200 m water depth) are about 200 years younger than in the NW-Pacific (2170 m water depth) and the Sea of Okhotsk (1765 m water depth). Since the Shirshov Ridge records cover the full range of water depth (630 to 2200 m), we ascribe the temporal offset to regionally different ^{14}C surface ocean reservoir effects rather than to changes in carbonate dissolution.

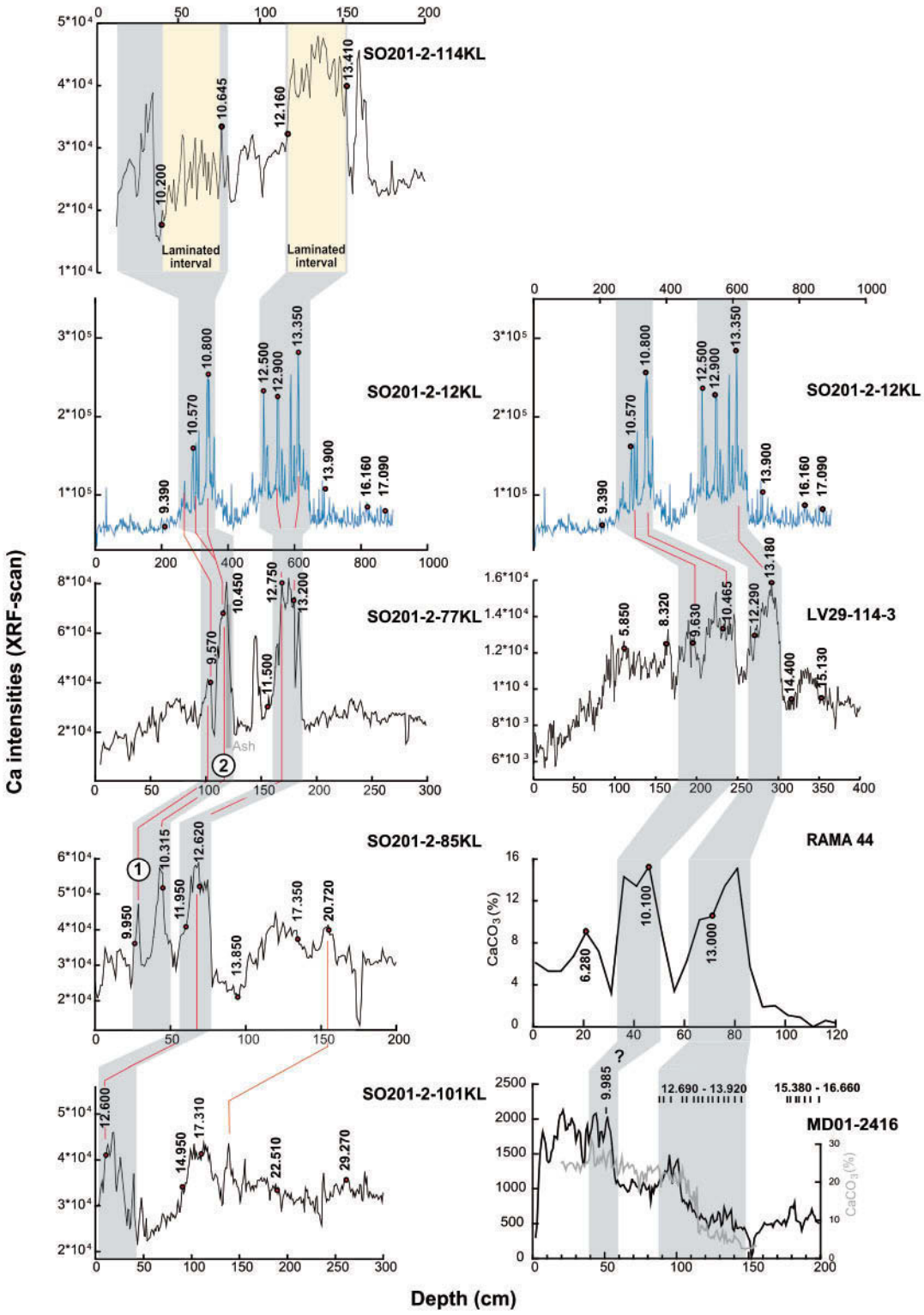
SO201-2-114KL
Laminated interval
Laminated interval
SO201-2-12KL
SO201-2-77KL
Ash
SO201-2-85KL
SO201-2-101KL
LV29-114-3
RAMA 44
MD01-2416
12.690 - 13.920
15.380 - 16.660
Ca intensities (XRF-scan)
CaCO3 (%)
Depth (cm)

Figure 2

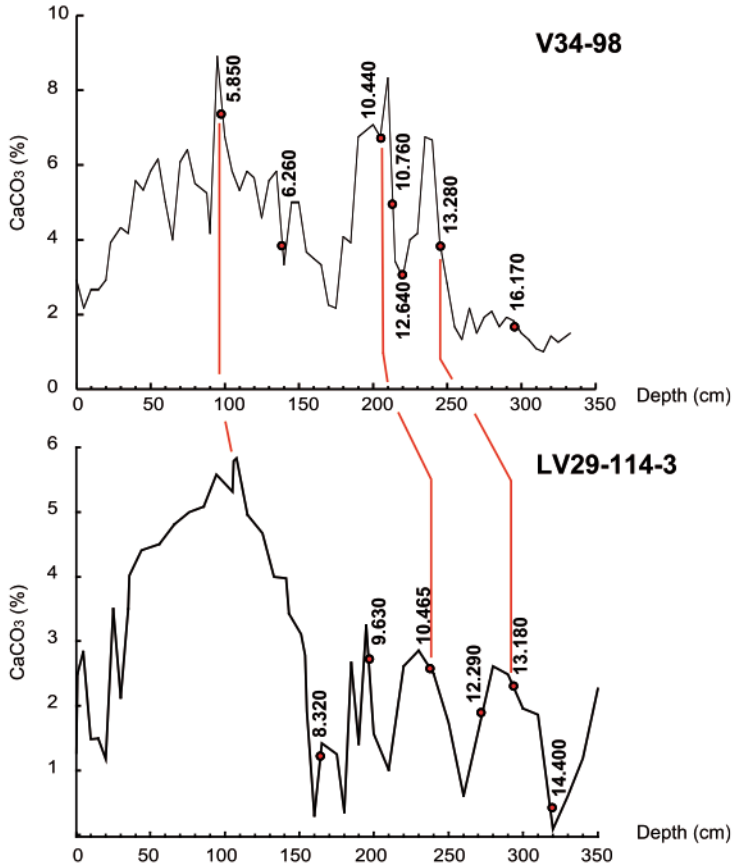

Figure 3. Correlation of sediment record LV29-114-3 with core V34–98 [*Gorbarenko et al.*, 2002] based on $CaCO_3$ (%) data. Numbers with red spots indicate raw ^{14}C ages and red lines give correlation points. However, only the raw ^{14}C age of 5,850 years was transferred to sediment record LV29-114-3 to improve stratigraphic control in the upper part of this sediment core.

[25] The conversion of radiocarbon ages in calendar years requires a correction for the surface ocean reservoir age to balance out the ^{14}C effect of disequilibrium between the atmosphere and the upper ocean as well as the input of deep waters into the mixed layer. In the N-Pacific, the surface ocean reservoir age has been reported to range from 600 to 1,000 years [*Southon et al.*, 1990; *Kuzmin et al.*, 2001; *McNeely et al.*, 2006; *Yoneda et al.*, 2007]. There is increasing evidence that the reservoir age has also varied over the course of the last 20 kyr, which has been attributed to global thermohaline reorganizations as well as to changes in the upper-ocean stratification. For the N-Pacific, *Sarnthein et al.* [2006] and *Gebhardt et al.* [2008] suggest variable ^{14}C reservoir ages for the last 20 kyr, which have been derived by ^{14}C-plateau tuning. For the ^{14}C-plateaus at 12.3 kyr, 12.8–13.4 kyr and 14.9–15.3 kyr (raw ^{14}C ages), reservoir ages of 450, 300 and 1150 years have been suggested [*Sarnthein et al.*, 2007], respectively. In contrast, a more recent study claims that the surface ocean reservoir age was close to 730 years and varied by less than ±200 years during the last deglaciation in the NE-Pacific [*Lund et al.*, 2011]. Since our ^{14}C datings are not dense enough to

Figure 2. (left) Stratigraphic framework of sediment records from the western Bering Sea and correlation with high-resolution record SO201-2-12KL record (blue curve) from the subarctic NW-Pacific. The stratigraphy is based on Ca intensity studies, derived from core logging data (XRF), together with raw AMS ^{14}C datings (red spots with vertical numbers). Grey shaded areas mark prominent carbonate maxima. Defined carbonate spikes (spike 1 = 9,760 ^{14}C years; spike 2 = 10,383 ^{14}C years) are numbered, and red lines indicate correlation points between the sediment records. (right) Comparison of Ca intensity data from high-resolution record SO201-2-12KL from the NW-Pacific (in blue) and LV29-114-3 from the Sea of Okhotsk to already published records from the open NW-Pacific (RAMA 44 [*Keigwin*, 1998] and MD01–2416 [*Gebhardt et al.*, 2008]) Ca intensity and $CaCO_3$ (%) data. Red spots (vertical numbers) mark raw AMS ^{14}C datings, and grey shaded areas indicate carbonate maxima in the sediment records. Sediment record MD01–2416 provides best age control based on ^{14}C-plateau tuning. However, no correlation was done to the records of this study due to discrepancies between the carbonate records of MD01–2416 and our sediment records.

identify the age-calibrated ^{14}C- plateaus, we were not able to assess the variability of paleo-reservoir ages. Instead, we used constant reservoir ages over time with 700 years for the western Bering Sea cores and 900 years for the NW-Pacific and the Sea of Okhotsk records, which are within the range of NW-Pacific modern surface ocean reservoir ages. After converting the ^{14}C ages into calendar years, the difference in regional reservoir ages provides the best chronostratigraphic match between our high-resolution core-logging records (color b* and XRF-Ca/Ti ratios). This assumes that the pattern of XRF-Ca/Ti ratios and color b* occurred synchronously in the NW-Pacific realm. Trends in color b* generally correlate with those of biogenic opal (Figure 4). Color b* is reported to provide a good proxy for variations in biogenic opal and total organic matter content of anoxic sediments [*Debret et al.*, 2006]. The Sea of Okhotsk is marked by an increase in $CaCO_3$ content rather than an increase of diatom production during the deglaciation [*Seki et al.*, 2009]. Thus, we used the pattern of Ca/Ti ratios in the Sea of Okhotsk record, which reflects changes in carbonate contents versus terrigenous siliciclastic input. Our age-depth control points within each record have been moved within the 1-sigma calendar age ranges to improve the fit between records. This also results in a good correlation to the Greenland temperature record (NGRIP) [*Rasmussen et al.*, 2006] shown in Figure 4.

4.2. SST Reconstructions

[26] Calculated alkenone SSTs spanning the time period of the last 15 kyr BP are shown in Figure 5. As expected, the SST records reflect successively increasing temperatures from north to south. At the southernmost site (core LV29-114-3), the SSTs are about 3°C warmer than at the northernmost site (core SO201-2-114KL). A general feature of all records is the consistent temperature variability during the last glacial termination from 15 ka BP to 10 ka BP. This temperature evolution is very similar to that reconstructed from Greenland ice core records, which mark the temperature rise from the end of H1 into the B/A, the subsequent cold spell of the YD and the following warming into the early Holocene (Figure 5). The early warming into the B/A does not capture the full amplitude of the SST increase, since all of our records are characterized by alkenone contents below the detection limit prior to 15 ka BP. Hence, the amplitudes of the early temperature increase represent minimum ranges between 3 and 5°C at our studied sites, with lowest SSTs of 2–5.5°C at 15 ka BP and highest values ranging between 6 and 8°C during the B/A. The temperature decrease that followed into the YD is marked by amplitudes of 1.5–5°C with lowest amplitudes observed in Sea of Okhotsk core LV29-114-3. At each site, the subsequent temperature increase of up to 5°C consistently culminates in an early Holocene SST maximum between 11 and 9 ka BP. All records display a maximum in SSTs of 9–10°C except for the northernmost core SO201-2-114KL from the Bering Sea, where the SST maximum remains approx. 3°C colder. The temperature development during the Holocene is only preserved in Bering Sea core SO201-2-77KL, northwest Pacific core SO201-2-12KL and Sea of Okhotsk core LV29-114-3. These records point to a smooth and gradual SST decrease over the past 9 kyr. However, in Sea of Okhotsk core LV29-114-3, the temperature trend is interrupted by a cold spell between 9–7 ka BP. This pronounced SST minimum displays temperatures as cold as those found during the YD. Nevertheless, the SST trend in this record also suggests a gradual cooling in SST (3°C), which is best developed since 6 ka BP. Another subtle difference can be observed for the time interval of the last 3.5 kyr. While the Bering Sea record suggests a slight warming, records from the NW Pacific and the Sea of Okhotsk indicate a further decline in SST.

4.3. Sea-Ice Distribution

[27] To assess past variations in sea-ice extent, we compared relative percentages of diatom species *F. oceanica* (indicative of sea-ice presence) and *N. seminae* (indicative of open water conditions) from sediment record SO201-2-12KL with qualitative measurements of the IP_{25} proxy (indicative of sea-ice presence), derived from specific time slices in all sediment records. The percentages of the diatom species (*F. oceanica* and *N. seminae*) point to millennial-scale variability in sea-ice presence, which is consistent with the SST development during the last 15 kyr (Figure 6). Moderate amounts of *F. oceanica* mark the last glacial. Extremely low contents are typical for the B/A. Highest percentages characterize the YD and the subsequent warming phase at the end of termination 1. The SST maximum between approx. 10.5–9 ka BP is marked by the absence of *F. oceanica.* The last 9 kyr are marked by a slight increase in *F. oceanica. N. seminae* provides an opposite trend between 15–10.5 ka BP, suggesting open water conditions with reduced sea-ice presence during the B/A and the Holocene SST maximum between 10.5–9 ka BP. Moderate contents of both *F. oceanica* and *N. seminae* are observed during the past 9 kyr and may indicate temporal variations in sea-ice cover, allowing for both open water conditions as well as sea-ice presence.

[28] As mentioned above, we further applied the IP_{25} proxy, which is indicative of past variations in sea-ice extent. In all records (LV29-114-3, SO201-2-12KL, SO201-2-77KL, SO201-2-85KL, SO201-2-101KL, SO201-2-114KL) we measured IP_{25} at selected time slices (15.1 ka BP, 14.3 ka BP, 12.2 ka BP and 10.5 ka BP), which are representative for distinct climate extremes (H1, B/A, YD, early Holocene SST maximum) recognized in our SST records (Figure 5). As shown for NW-Pacific core SO201-2-12KL, by direct comparison between *F. oceanica* content and the occurrence of the IP_{25} biomarker, a consistent variability in sea-ice extend is documented and supports the applicability of the IP_{25} biomarker as sea-ice proxy in the subarctic NW-Pacific (Figure 6). The IP_{25} time slice reconstructions suggest that sea-ice was present during phases of H1 and the YD at each core location in the study area. Conversely, IP_{25} was not found in any sediment sample from samples covering the B/A and the early Holocene SST maximum. Accordingly, ice-free conditions mark the positions of all cores during these intervals.

5. Discussion

5.1. Deglacial SST Development in the Subarctic NW-Pacific

[29] The deglacial SST development in the subarctic NW-Pacific realm is reminiscent of the temporal evolution associated with millennial-scale climate variations revealed

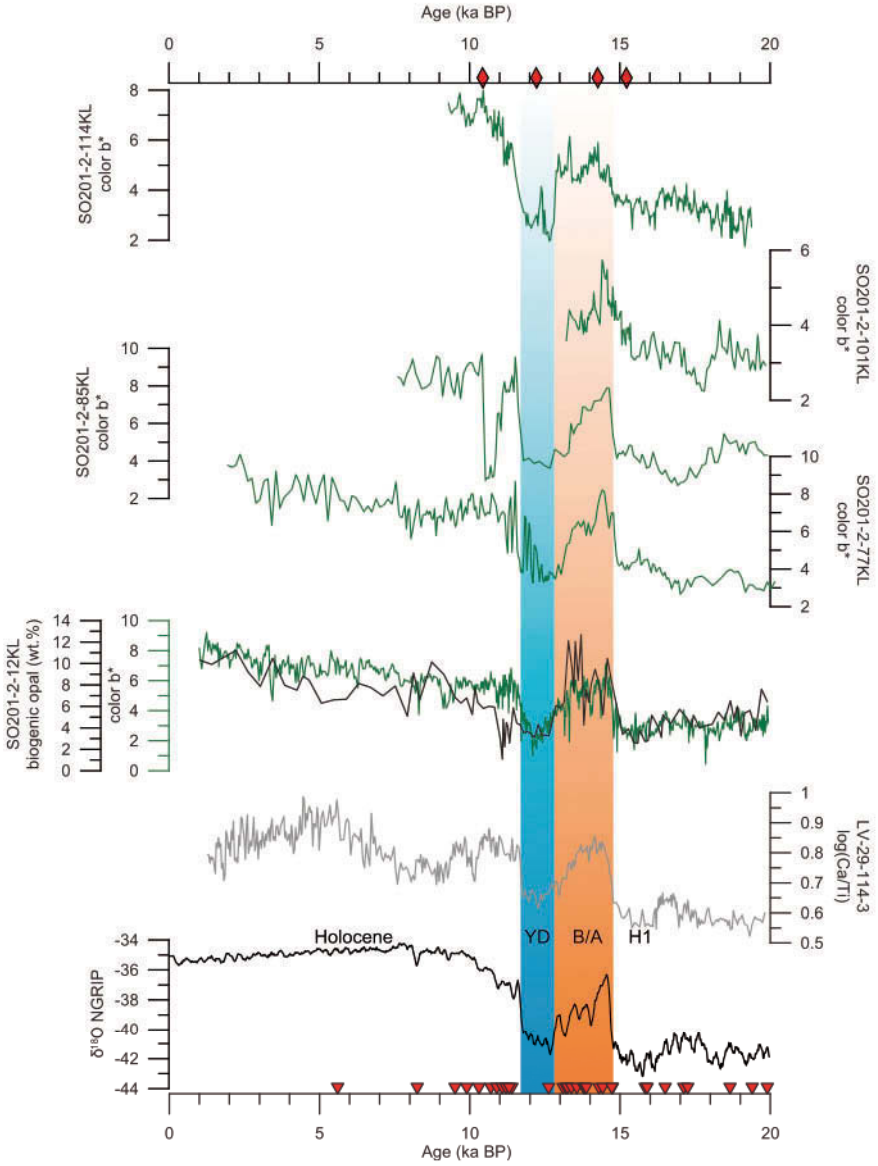

Figure 4. Spectrophotometric measurements (color b*, green curves) from sediment records of the western Bering Sea, together with SO201-2-12KL from the NW-Pacific and log Ca/Ti ratio (XRF element intensities) of LV29-114-3 from the Sea of Okhotsk (in grey) against the NGRIP isotope record (in black) for the last 20 kyr BP. Additionally, biogenic opal (%) (thin black line) is given for SO201-2-12KL. Red triangles at the bottom mark ^{14}C age control points used in this study. Note the excellent correlation of all studied sediment records with the Greenland isotope record during the last 15 kyr BP. Prominent climate stages as the B/A (shaded in red), the YD (shaded in blue) as well as the onset of the early Holocene are mimicked in the color b* and logCa/Ti proxy records. Red diamonds on top (representative of all sediment records) mark time slices used for the qualitative assessment of the IP_{25} sea-ice proxy. IP_{25} measurements were conducted on individual sediment records from samples according to the selected time slice.

by temperature records from Greenland and the N-Atlantic [e.g., *Bard et al.*, 2000]. The alkenone temperature records obtained from the subarctic NW-Pacific, the Sea of Okhotsk and the Bering Sea suggest a deglacial warming, with a first warming at the onset of the B/A (14.7–12.9 ka BP), which was subsequently interrupted by a cooling phase associated with the YD cold phase (12.8–11.8 ka BP) and continued by a second and more pronounced warming into the early Holocene. Hence, this SST development matches the millennial-scale temperature fluctuations recognized in Greenland ice core records and N-Atlantic SST records and has also been reported in previous studies, which established

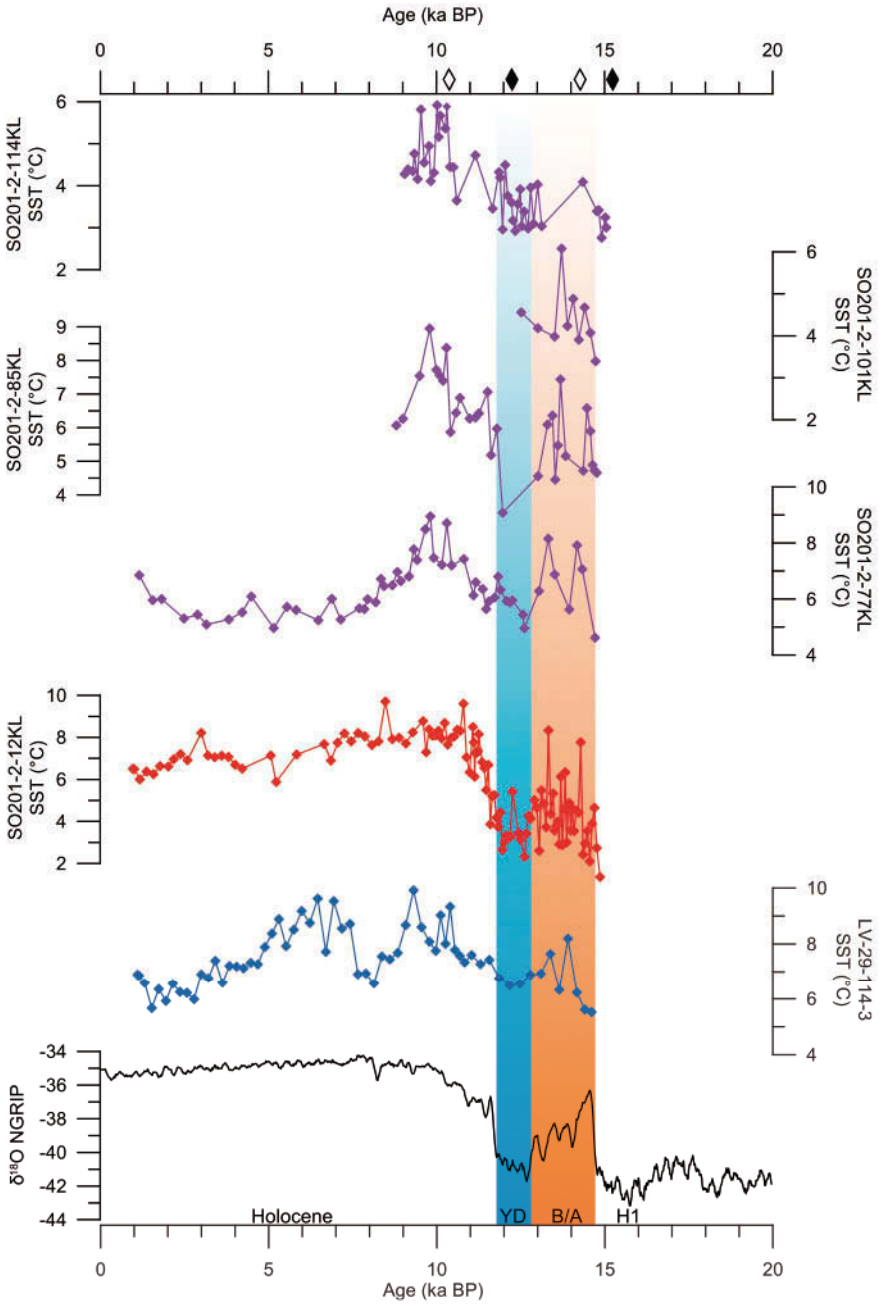

Figure 5. Results of the SST reconstructions from the western Bering Sea (in purple), the NW-Pacific (in red) and Sea of Okhotsk (blue curve) compared with the Greenland ice core record for the last 15 kyr BP. Red shaded area marks the B/A and blue shaded bar indicate the YD cold spell in the records. Diamonds on top mark time slices used for the qualitative assessment of the IP_{25} sea-ice proxy (representative of all sediment records). Black diamonds on top mark time slices (H1 and YD), where the IP_{25} biomarker was found at all core sites and thus the presence of sea-ice inferred. In turn, white diamonds indicate time slices (B/A and early Holocene) where IP_{25} biomarker was absent at all core sites and no sea-ice cover inferred.

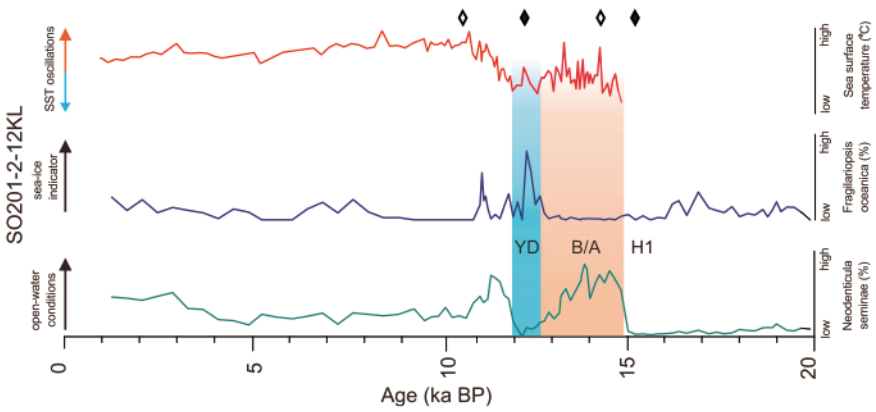

Figure 6. Results of the SST reconstructions from sediment record SO201-2-12KL (NW-Pacific) in red together with relative percentage of diatom *Fragilariopsis oceanica* (in blue) and *Neodenticula seminae* (in green). Red shaded area marks the B/A and blue shaded bar indicate the YD cold spell in the sediment records. Diamonds on top mark time slices used for the qualitative assessment of the IP_{25} sea-ice proxy (representative of all sediment records). Black diamonds on top mark time slices (H1 and YD), where the IP_{25} biomarker was found at all core sites and therefore the presence of sea-ice inferred. In turn, white diamonds indicate time slices (B/A and early Holocene) where no IP_{25} biomarker was found at all core sites and thus no sea-ice cover inferred.

alkenone-derived SST records from other parts of the N-Pacific realm as the NE-Pacific [*Kienast and McKay*, 2001; *Barron et al.*, 2003], the eastern Bering Sea [*Caissie et al.*, 2010], the Sea of Okhotsk [*Ternois et al.*, 2000; *Harada et al.*, 2006b; *Seki et al.*, 2009; *Harada et al.*, 2012] and off Japan [*Harada et al.*, 2012]. On the basis of our age models, the deglacial SST variability in the NW-Pacific realm seems to be rather in-phase than out-of-phase with Greenland/N-Atlantic temperature changes (Figure 7). This would suggest a quasi-synchronicity between the N-Atlantic and N-Pacific SST development during the last glacial termination and argues for a strong atmospheric coupling between the N-Pacific and the N-Atlantic.

[30] The majority of model results also favors this interpretation and provides insights into the underlying mechanisms linking the development of SST between the N-Atlantic and the N-Pacific. Numerous studies with coupled General Circulation Models (GCMs) have examined whether and how the millennial-scale climate oscillations in the N-Atlantic would impact the N-Pacific SST development via atmospheric and oceanic teleconnections during the last glacial termination. All models propose a close linkage to deglacial variations in AMOC. The temperature changes in the N-Atlantic region are closely coupled to a change in the strength of the AMOC, which is strongly modulated by freshwater forcing due to the instability of the Northern Hemisphere ice sheets and melting icebergs [*Rahmstorf*, 1995; *McManus et al.*, 2004; *Yin and Stouffer*, 2007]. The freshwater input into the N-Atlantic led to a reduced thermohaline overturning, which also resulted in a reduced northward advection of saline and warm subtropical surface waters into the N-Atlantic [*Manabe and Stouffer*, 1988]. *Manabe and Stouffer* [1988] were among the first who demonstrated that the climatic impact of an AMOC shutdown is of global significance. Subsequent freshwater perturbation experiments also suggest, beyond the Atlantic basin, a robust response over the N-Pacific [e.g., *Mikolajewicz et al.*, 1997; *Vellinga and Wood*, 2002; *Okumura et al.*, 2009; *Timmermann et al.*, 2010]. When the AMOC is substantially weakened (e.g., during H1 and the YD), N-Pacific summer and winter SSTs are suggested to have cooled by up to 3–6°C. Most studies attribute the cooling to enhanced thermal advection of cold air masses from the N-Atlantic via westerly winds [*Manabe and Stouffer*, 1988]. As a result, the deepening of the Aleutian Low, the intensification in ocean-to-atmosphere heat flux and southward Ekman transport in combination with the southward shift of the oceanic frontal system would have further cooled the N-Pacific. More recently, model experiments also provide hints for another atmospheric bridge between the N-Pacific and the subtropical Pacific/Atlantic that may have the potential to influence the strength of the Aleutian Low. Tropical SST anomalies in both the Atlantic and Pacific are found to be important for the barotropic response of the Aleutian Low [*Okumura et al.*, 2009]. These mechanisms represent AMOC-induced fast-acting atmospheric teleconnections on decadal timescales and suggest a similar temperature development between the N-Atlantic and the N-Pacific.

[31] In contrast, *Kiefer and Kienast* [2005] and *Gebhardt et al.* [2008] found inversed millennial-scale SST oscillations with SST maxima at H1 and the YD in the NW-Pacific (core MD01–2416 and ODP883), as indicated by Mg/Ca-derived and planktonic foraminiferal SIMMAX-based SSTs. This temporal NW-Pacific SST development is in harmony with model results from *Huang et al.* [2000] and *Okazaki et al.* [2010]. According to *Huang et al.* [2000], a slowdown of the Meridional Overturning Circulation in the N-Atlantic (like during H1 and YD) may result in N-Pacific warming due to a reduction in upwelling of cold and nutrient-rich Pacific Deep Water in the N-Pacific subpolar gyre. However, the model experiments of *Huang et al.* [2000] do not consider the environmental background

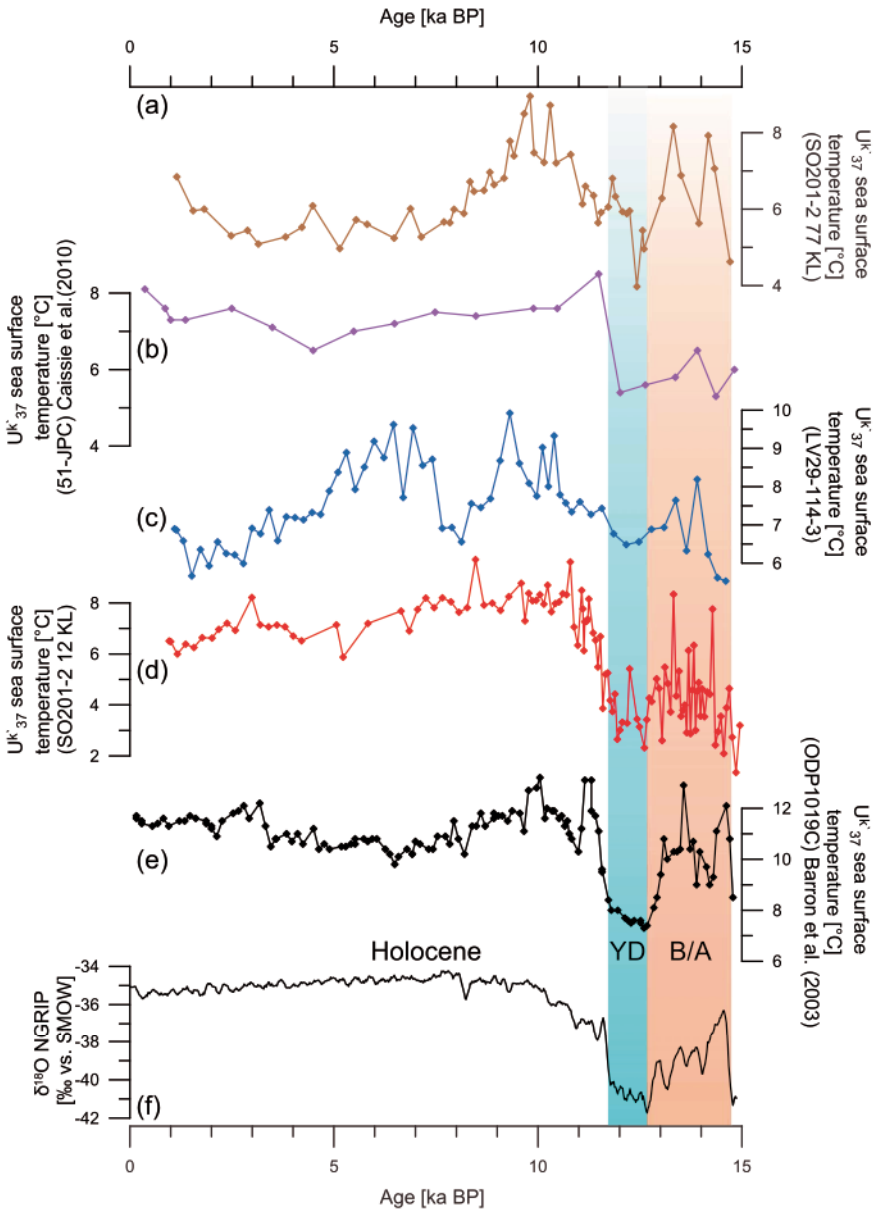

Figure 7. Alkenone-based SST reconstructions for the subarctic N-Pacific, including detailed comparison of (a) western Bering Sea, (b) eastern Bering Sea, (c) Sea of Okhotsk, (d) NW-Pacific, and (e) NE-Pacific compared with (f) NGRIP isotope record for the past 15 kyr. Red shaded area marks the B/A and blue shaded bar indicates the YD cold spell in the records.

conditions associated with expanded Northern Hemisphere ice sheets during H1 and YD. The study of *Okazaki et al.* [2010] also suggests a warming in the N-Pacific during times of AMOC slowdown but due to the establishment of the PMOC. Thus, enhanced meridional overturning would result in strengthened northeastward upper-ocean heat transport via the North Pacific Current, thereby warming the N-Pacific, in particular in the Pacific Northeast. Recently, *Chikamoto et al.* [2012] simulated an AMOC shutdown using glacial boundary conditions (hereby considering a closed Bering Strait) and examined the impact on N-Pacific climate history by using two different models. Their results indicate that the spatial temperature pattern in the N-Pacific is strongly coupled to the strength of the PMOC. These model experiments suggest cooler SSTs in the subarctic NW-Pacific for both cases, a strong and a weak PMOC. However, in case of a strong PMOC, the NE-Pacific would experience surface warming due to an enhanced poleward transport of heat and salt from the subtropics to the extratropics via the Kuroshio–North Pacific

Current system. Hence, the PMOC associated impact on SSTs seems to be too weak to compensate for the SST cooling in the NW-Pacific during times of expanded Northern Hemisphere ice sheets. These results favor AMOC-induced atmospheric teleconnections as the main driver for the SST development in the subarctic N-Pacific and are in accordance with our SST reconstructions from the NW-Pacific.

[32] However, the inconsistent deglacial trends between alkenone-derived SSTs (this study) and Mg/Ca-derived and planktonic foraminiferal SIMMAX-based SSTs [*Kiefer and Kienast*, 2005; *Gebhardt et al.*, 2008] in the subarctic N-Pacific raise the question of whether the differences can be explained by stratigraphic uncertainties, in particular through the use of different SST proxies and/or are related to regional oceanographic deviations. The stratigraphic differences are mainly based on the application of different paleo-reservoir ^{14}C ages (chapter 4). Compared to our age model, their radiocarbon-based age constraints rely on variable reservoir ages [*Sarnthein et al.*, 2006, 2007]. If we apply this variable reservoir correction to our age model (not shown), it would slightly and comparably affect the stratigraphic position of the B/A temperature maximum in all our records. The temperature increase at the transition from the glacial into the B/A would lead, relative to our age model, by 100–200 years. The end of this temperature maximum would lead that of our age model by up to 350 years. As a result, the temperature maximum would remain within the interval of the B/A and will not result in an anti-phased SST evolution between the N-Pacific and the N-Atlantic in our records. Thus, the different appearance of the temperature maxima between our and other records (core MD01–2416, ODP-Site 883) cannot easily be ascribed to age model discrepancies. Assuming that the original planktonic ^{14}C ages (uncorrected) within the NW-Pacific region are marked by similar reservoir ages over time, the SST maxima and minima would occur at different time intervals in any case. For example, the most pronounced temperature maximum at core MD01–2416 occurs between 14,430–13,820 ^{14}C years (original) and has been assigned to the beginning of a ^{14}C-plateau that ranges between 16,700–15,300 calendar years BP. The most pronounced temperature maximum in our SST records occurs between 13,350–12,500 ^{14}C years (original). These ages would correspond to another ^{14}C-plateau, which marks the beginning of the B/A from 14,900–14,200 calendar years BP [*Gebhardt et al.*, 2008]. However, core MD01–2416 provides no SST maximum at this stratigraphic position.

[33] Hence, we speculate that the different SST proxies are afflicted with diverse temperature signals due to seasonal bias and formation of the proxy signal at different water depths. The modern alkenone signal has been shown to reflect the late summer/autumn SST (0–30 m) in the NW-Pacific [*Harada et al.*, 2003, 2006a; *Seki et al.*, 2007]. The Mg/Ca-based temperatures are derived from the planktonic foraminifer *N. pachyderma* sin. and may reflect the winter signal due to its preferred habitat depth below or close to the thermocline [e.g., *Bauch et al.*, 2002]. In particular, the modern water masses below the summer thermocline originate from intense and deep mixing during winter. Hence, a stronger temperature gradient between the depth habitat of the coccolithophorides and *N. pachyderma* sin. may result from enhanced stratification, intensified insolation and/or extra cooling of sub-thermocline waters in response to enhanced heat exchange with deeper and colder water masses [*Kohfeld et al.*, 1996; *Andersson et al.*, 2010]. Accordingly, such differences do not simply reflect changes in seasonality.

5.2. Holocene SST Variability of the N-Pacific and its Marginal Seas

[34] Alkenone-derived SST reconstructions from the NW-Pacific region are characterized by a pronounced temperature maximum during the early Holocene between 11 and 9 ka BP (Figures 5 and 8). This temperature maximum coincides with the maximum in Northern Hemisphere summer insolation (June–August) [*Laskar et al.*, 2004]. In addition, recent model experiments suggest a reopening of the Bering Strait as another forcing mechanism [*Okumura et al.*, 2009; *Hu et al.*, 2010]. The reopening, which has been dated to approx. 11 ka BP [e.g., *Elias et al.*, 1997] may have led to increased meridional heat transport from the tropics to the extratropics and also warmed N-Pacific surface waters. The gateway-induced forcing may have been active for a restricted time interval, which may represent the phase of progressive marine inundation of the Bering Strait during rapid early Holocene sea level rise (11–8 ka BP) [*Fleming et al.*, 1998]. Whether the N-Pacific SST maximum (11–9 ka BP) is affected by the opening of the Bering Strait remains elusive since the maximum also coincides with the maximum in Northern Hemisphere summer insolation.

[35] Our SST records in combination with existing SST records from the N-Pacific are further used to reassess the hypothesis of the long-term inverse temperature development between the N-Atlantic and N-Pacific from the middle to late Holocene [*Kim et al.*, 2004]. According to *Kim et al.* [2004], SST trends have resembled a basin-scale, long-term N-Pacific warming while the N-Atlantic has cooled during the last 7 kyr. However, the interpretation of *Kim et al.* [2004] is based on a single record from the subarctic NW-Pacific (GGC-15 [*Ternois et al.*, 2000]), located in the Sea of Okhotsk. Our more comprehensive compilation of alkenone-based SST records from the N-Pacific and its marginal seas reveal no basin-scale, long-term warming trend over the past 7 kyr. The compilation of SST records from the N-Pacific realm hints to complex regional differences in the temperature development during the middle to late Holocene (Figure 8).

[36] In the Sea of Okhotsk, the middle to late Holocene SST development is characterized by different trends with relatively large temperature fluctuations (Figure 8). Core LV29-114-3 from the southeastern Sea of Okhotsk shows a clear cooling trend (−3°C) during the last 7 kyr. In contrast, the neighbor core GGC-15, considered in the study of *Kim et al.* [2004], shows increased temperatures during this interval [*Ternois et al.*, 2000]. However, this SST record is possibly biased by low alkenone contents in the middle to late Holocene interval [*Ternois et al.*, 2000]. Three SST records from the central Sea of Okhotsk (XP98-PC 2 and -PC4, *Seki et al.*, 2004a) and the southwestern Sea of Okhotsk (MD01–2412 [*Harada et al.*, 2006b]) are marked by a pronounced temperature minimum between 6–3 ka BP. Only core MD01–2412 shows a clear SST trend, which points to a warming during the late Holocene (Figure 8).

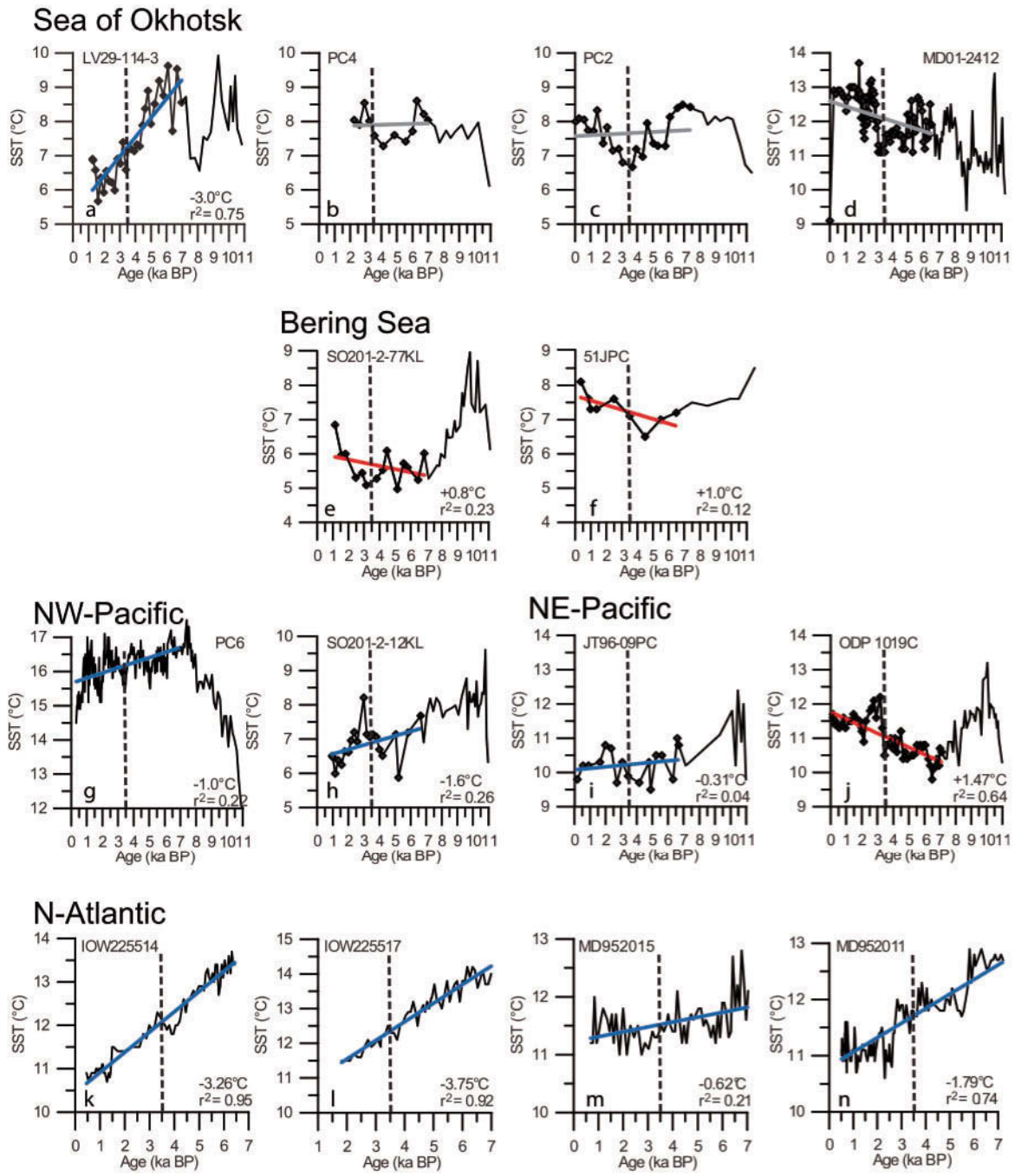

Figure 8. Holocene compilation of alkenone-based SST reconstructions for the (a–d) Sea of Okhotsk, (e and f) Bering Sea, (g and h) subarctic NW-Pacific, and (i and j) subarctic NE-Pacific compared with subarctic N-Atlantic alkenone-derived SSTs (k and l) *Emeis and Dawson* [2003]; (m and n) *Marchal et al.* [2002]) from the middle to late Holocene. The stippled vertical lines indicate the middle to late Holocene boundary in every record. Linear regression trends are given for all records (blue, red and grey thick lines) for the last 7 kyr BP. Correlation coefficients r^2 are shown in the lower right corners, respectively.

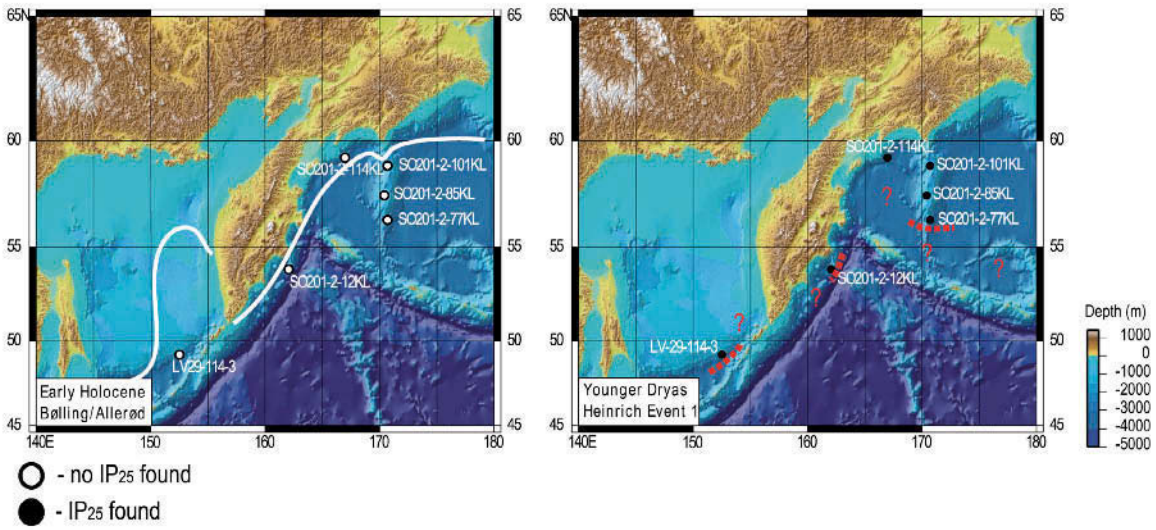

Figure 9. Sea-ice extent derived from occurrence/absence of IP_{25} sea-ice diatoms biomarker measured on a set of six sediment records during time slices of (left) the Bølling/Allerød and Early Holocene together with the modern sea-ice distribution (solid white line [*Zhang et al.*, 2010]) and (right) the Younger Dryas and Heinrich Event 1 (dashed red lines) of the subarctic NW-Pacific. Question marks indicate regions where no information of the past sea-ice coverage is available. White circles indicate that no IP_{25} was found in the samples and black circles mark samples where IP_{25} was detected at the core site according to the time slice, respectively. Note the strong expansion of sea-ice in the subarctic NW-Pacific during times of H1 and YD, where IP_{25} was detected at every core site and thus the sea-ice boundary was shifted several hundred miles to the South (especially in the western Bering Sea) compared to today. During phases of the B/A and early Holocene, IP_{25} was absent in all sediment records and thus no sea-ice presence inferred at the core sites.

Altogether, we partly ascribe the differences in SST development to a variable inflow of surface water masses from the N-Pacific and the Japan Sea. Core LV29-114-3 is located at the main entrance of Pacific water masses delivered by the EKC (via Krusenstern Strait), which transports relatively cold water masses to the Sea of Okhotsk. Thus, the Holocene cooling trend at core LV29-114-3 might be related to temperature changes in the source region of the EKC. On the other hand, core MD01–2412 is influenced by the inflow of warm water masses from the Japan Sea via the Soya Strait. The warming trend may indicate a strengthened influence of the Japan Sea.

[37] In the Bering Sea, the middle to late Holocene SST development is derived from two sediment records (HLY0202–51JPC [*Caissie et al.*, 2010]; SO201-2-77KL, this study). Both temperature records reveal a consistent SST development with a net warming indicated by the linear regression trend (Figure 8). This trend seems to be related to a SST rise around the mid- to late Holocene transition (ca. 3.5 ka BP).

[38] The subarctic NW-Pacific SST records reveal a cooling trend from the middle to late Holocene (PC6 [*Minoshima et al.*, 2007]; SO201-2-12KL (this study); Figure 8). Available temperature records from the subarctic NE-Pacific margin show no consistent picture of SST development during the last 7 kyr (JT96–09PC [*Kienast and McKay*, 2001]; ODP 1019C [*Barron et al.*, 2003]; Figure 8). As the SST record from core JT96–09PC indicates weak cooling over the last 7 kyr, SSTs at ODP site 1019 are marked by a clear warming trend.

[39] In summary, the compilation of alkenone-derived SST records from the N-Pacific and its marginal seas show no consistent SST trends and thus do not corroborate the basin-scale, long-term warming from the middle to late Holocene in the N-Pacific [*Kim et al.*, 2004]. Regionally consistent trends in SST development are observed for the Bering Sea and the subarctic NW-Pacific, however, with opposing trends during the last 7 kyr. The Bering Sea is marked by a warming trend and the subarctic NW-Pacific is characterized by a cooling trend from the middle to late Holocene. The SST development within the Sea of Okhotsk is rather diverse. The cooling trend in the NW-Pacific could be partly attributed to the decrease in summer insolation. On the other hand, the opposing SST development in the Bering Sea as well as the diverse SST trends in the Sea of Okhotsk also call for a strong imprint of other processes (internal forcing), involving atmosphere–ocean interactions. AMOC-induced changes, which apparently played a key role for the deglacial SST development in the subarctic N-Pacific, seem to be of minor importance since the thermohaline circulation has been reported to be relatively stable during the middle to late Holocene [e.g., *McManus et al.*, 2004].

5.3. Changes in Sea-Ice Extent

[40] The variability in sea-ice distribution during the last glacial termination is closely coupled to the general SST

development in the subarctic Pacific realm, although the alkenone-derived SSTs most likely reflect summer-autumn temperature variations and are not associated with the seasonal maximum in sea-ice extent. The qualitative assessment of sea-ice extent (IP_{25}) in the subarctic NW-Pacific suggests a highly dynamic sea-ice cover (Figure 9), which oscillated at least over several hundred miles during the last deglaciation. In the study area, the advancement of sea-ice reached all core sites during cold phases of H1 and the YD and was accompanied by coldest temperatures as derived from our SST records (Figure 5). The common occurrence of IP_{25} in the sediments clearly points to vast expansion of sea-ice in a generally colder climate during H1 and YD in the subarctic NW-Pacific. However, due to the limited spatial coverage of sediment cores, the maximum expansion in seasonal sea-ice cover may have been much larger during these intervals. Conversely, the absence of IP_{25} suggests ice-free conditions at all our core locations during phases of the B/A and the early Holocene warm intervals, which also matches warmest intervals derived from our SST records (Figure 5). During the early Holocene, the maximum in sea-ice extent was even more limited compared to today [*Zhang et al.*, 2010] (Figure 9). This is suggested by the absence of IP_{25} at the northernmost core site SO201-2-114KL, which today is influenced by sea-ice advances during winter. These findings are underpinned by pronounced millennial-scale shifts in diatom assemblages at core SO201-2-12KL, indicative for changes in seasonal sea-ice cover during the past 15 kyr (Figure 6). High percentages of *F. oceanica* suggest the presence of sea-ice during the YD. High percentages of *N. seminae* reflect open water conditions during the B/A and the early Holocene. Combining the information of both proxies (IP_{25} and diatom assemblages) also enables us to identify different stages of sea-ice conditions, e.g., permanent sea-ice coverage versus seasonal or no sea-ice presence. With respect to the position of core SO201-2-12KL, high amounts of *F. oceanica* during the YD and relatively low amounts during the last glacial do not necessarily represent a discrepancy. Since *N. seminae* is marked by extremely low values during both intervals, we infer that the glacial position of the sea-ice margin was further offshore of core SO201-2-12KL, compared to the YD. At the core site, perennial sea-ice cover prevailed during the glacial, and the retreat of the summer sea-ice boundary may have reached the core location only occasionally. This interpretation is also supported by low total diatom abundance during the last glacial. The low diatom abundance is probably a result of enhanced sea-ice coverage, which further limits phytoplankton growth. After ~15 ka BP (beginning of the B/A), total diatom abundance is higher by an order of magnitude (not shown). In general, our results are in harmony with previous sea-ice reconstructions based on diatom assemblages and paleo-productivity studies in the subarctic Pacific realm [*Sancetta*, 1983; *Sancetta and Robinson*, 1983; *Sancetta*, 1992; *Cook et al.*, 2005; *Katsuki and Takahashi*, 2005; *Okazaki et al.*, 2005; *Sakamoto et al.*, 2006; *Katsuki et al.*, 2009; *Caissie et al.*, 2010]. The conclusive variability between SST and the IP_{25}-proxy highlights the potential of this relatively new sea-ice proxy as tool for more detailed spatial time slice reconstructions in the N-Pacific realm in order to further assess the climate dynamics and feedback mechanisms during millennial-scale climate fluctuations of the last deglaciation.

6. Conclusions

[41] Our conclusions can be summarized into four main points.

[42] 1. Alkenone-temperatures derived from high-resolution sediment records in the subarctic NW-Pacific, the Sea of Okhotsk and the western Bering Sea show a deglacial temperature evolution similar to the NE-Pacific and even to the N-Atlantic and Greenland temperature variability. From this we suggest a close linkage to deglacial variations in AMOC associated with rapid atmospheric teleconnections, which resulted in a quasi-synchronous SST development between the N-Atlantic and the N-Pacific during the last glacial termination. Although the SST variability between the N-Atlantic and N-Pacific show striking temporal similarities, uncertainties in age control related to a lack of knowledge in ^{14}C reservoir ages may bias the timing of SST changes by up to several hundred years.

[43] 2. During the middle to late Holocene, the subarctic N-Pacific reveals complex SST trends, suggesting strong regional overprints. The compilation of alkenone-derived SST records from the NW-Pacific, the Bering Sea and the Sea of Okhotsk does not support the hypothesis of a long-term Holocene temperature seesaw between the N-Atlantic and N-Pacific associated with a basin-scale warming trend in the N-Pacific during the last 7 kyr. Only the Bering Sea records reveal a tendency toward warmer temperatures compared to a slight cooling in the NW-Pacific. The records from the Sea of Okhotsk exhibit both cooling and warming trends as well as large fluctuations during the middle to late Holocene.

[44] 3. Past sea-ice expansion were reconstructed from a set of six sediment records by qualitative assessment of the IP_{25} biomarker for cold (H1 and YD) and warm (B/A and early Holocene) stages and compared to diatom studies during the last glacial termination in the NW-Pacific. Our results suggest a strong variability of sea-ice extent and a close coupling to SST fluctuations in the N-Pacific. The sea-ice advanced at least by several hundred miles during phases of H1 and YD. During the phases of B/A and the early Holocene the maximum in sea-ice cover seems to have been even more reduced compared to today.

[45] 4. Our SST records in combination with the sea-ice reconstructions provide no evidence of surface warming during the YD and H1, which has been suggested by several climate models to occur in response of enhanced deep water formation in the N-Pacific.

[46] **Acknowledgments.** This study resulted from the German-Russian multidisciplinary research project "KALMAR–Kurile-Kamchatka and Aleutean Marginal Sea-Island Arc Systems: Geodynamic and Climate Interaction in Space and Time." We gratefully acknowledge the Master and crew of R/V *Sonne* cruise SO201-2 and thank them for their professional support onboard. Lukas Belz and Adelina Manurung are thanked for technical assistance in the geochemical laboratory. We also would like to thank the three anonymous reviewers, who helped to improve the quality of this manuscript. This study was funded by the German Federal Ministry of Education and Research (BMBF) grant 03G0672B and 03G0672A.

References

Andersson, C., F. S. R. Pausata, E. Jansen, B. Risebrobakken, and R. J. Telford (2010), Holocene trends in the foraminifer record from the Norwegian Sea and the North Atlantic Ocean, *Clim. Past*, *6*(2), 179–193, doi:10.5194/cp-6-179-2010.

Bard, E., F. Rostek, J. L. Turon, and S. Gendreau (2000), Hydrological impact of Heinrich events in the subtropical northeast Atlantic, *Science*, *289*(5483), 1321–1324, doi:10.1126/science.289.5483.1321.

Barron, J. A., L. Heusser, T. Herbert, and M. Lyle (2003), High-resolution climatic evolution of coastal northern California during the past 16,000 years, *Paleoceanography*, *18*(1), 1020, doi:10.1029/2002PA000768.

Bauch, D., H. Erlenkeuser, G. Winckler, G. Pavlova, and J. Thiede (2002), Carbon isotopes and habitat of polar planktic foraminifera in the Okhotsk Sea: The 'carbonate ion effect' under natural conditions, *Mar. Micropaleontol.*, *45*(2), 83–99, doi:10.1016/S0377-8398(02)00038-5.

Belt, S. T., G. Masse, S. J. Rowland, M. Poulin, C. Michel, and B. LeBlanc (2007), A novel chemical fossil of palaeo sea ice: IP25, *Org. Geochem.*, *38*(1), 16–27, doi:10.1016/j.orggeochem.2006.09.013.

Brassell, S. C., G. Eglinton, I. T. Marlowe, U. Pflaumann, and M. Sarnthein (1986), Molecular stratigraphy: A new tool for climatic assessment, *Nature*, *320*(6058), 129–133, doi:10.1038/320129a0.

Caissie, B. E., J. Brigham-Grette, K. T. Lawrence, T. D. Herbert, and M. S. Cook (2010), Last Glacial Maximum to Holocene sea surface conditions at Umnak Plateau, Bering Sea, as inferred from diatom, alkenone, and stable isotope records, *Paleoceanography*, *25*, PA1206, doi:10.1029/2008PA001671.

Chikamoto, M. O., L. Menviel, A. Abe-Ouchi, R. Ohgaito, A. Timmermann, Y. Okazaki, N. Harada, A. Oka, and A. Mouchet (2012), Variability in North Pacific intermediate and deep water ventialtion during Heinrich events in two coupled climate models, *Deep Sea Res., Part II*, *61–64*, 114–126, doi:10.1016/j.dsr2.2011.12.002.

Cook, M. S., L. D. Keigwin, and C. A. Sancetta (2005), The deglacial history of surface and intermediate water of the Bering Sea, *Deep Sea Res., Part II*, *52*(16–18), 2163–2173, doi:10.1016/j.dsr2.2005.07.004.

Debret, M., M. Desmet, W. Balsam, Y. Copard, P. Francus, and C. Laj (2006), Spectrophotometer analysis of Holocene sediments from an anoxic fjord: Saanich Inlet, British Columbia, Canada, *Mar. Geol.*, *229*(1–2), 15–28, doi:10.1016/j.margeo.2006.01.005.

DeMaster, D. J. (1981), The supply and accumulation of silica in the marine environment, *Geochim. Cosmochim. Acta*, *45*(10), 1715–1732, doi:10.1016/0016-7037(81)90006-5.

Dullo, W.-C., B. Baranov, and C. van den Bogaard (Eds.) (2009), FS Sonne Fahrtbericht/Cruise Report SO201–2, *IFM-GEOMAR Rep. 35*, 233 pp., IFM-GEOMAR, Kiel, Germany.

Elias, S. A., S. K. Short, and H. H. Birks (1997), Late Wisconsin environments of the Bering Land Bridge, *Palaeogeogr. Palaeoclimatol. Palaeoecol.*, *136*(1–4), 293–308, doi:10.1016/S0031-0182(97)00038-2.

Emeis, K. C., and A. G. Dawson (2003), Holocene palaeoclimate records over Europe and the North Atlantic, *Holocene*, *13*(3), 305–309, doi:10.1191/0959683603hl622ed.

Fahl, K., and R. Stein (2012), Modern seasonal variability and deglacial/Holocene change of central Arctic Ocean sea-ice cover: New insights from biomarker proxy records, *Earth Planet. Sci. Lett.*, in press.

Fleming, K., P. Johnston, D. Zwartz, Y. Yokoyama, K. Lambeck, and J. Chappell (1998), Refining the eustatic sea-level curve since the Last Glacial Maximum using far- and intermediate-field sites, *Earth Planet. Sci. Lett.*, *163*(1–4), 327–342, doi:10.1016/S0012-821X(98)00198-8.

Gebhardt, H., M. Sarnthein, P. M. Grootes, T. Kiefer, H. Kuehn, F. Schmieder, and U. Rohl (2008), Paleonutrient and productivity records from the subarctic North Pacific for Pleistocene glacial terminations I to V, *Paleoceanography*, *23*, PA4212, doi:10.1029/2007PA001513.

Gorbarenko, S. A., T. A. Khusid, I. A. Basov, T. Oba, J. R. Southon, and I. Koizumi (2002), Glacial Holocene environment of the southeastern Okhotsk Sea: Evidence from geochemical and palaeontological data, *Palaeogeogr. Palaeoclimatol. Palaeoecol.*, *177*(3–4), 237–263, doi:10.1016/S0031-0182(01)00335-2.

Gorbarenko, S. A., I. A. Basov, M. P. Chekhovskaya, J. Southon, T. A. Khusid, and A. Artemova (2005), Orbital and millennium scale environmental changes in the southern Bering Sea during the last glacial-Holocene: Geochemical and paleontological evidence, *Deep Sea Res., Part II*, *52*(16–18), 2174–2185, doi:10.1016/j.dsr2.2005.08.005.

Harada, N., K. H. Shin, A. Murata, M. Uchida, and T. Nakatani (2003), Characteristics of alkenones synthesized by a bloom of Emiliania huxleyi in the Bering Sea, *Geochim. Cosmochim. Acta*, *67*(8), 1507–1519, doi:10.1016/S0016-7037(02)01318-2.

Harada, N., M. Sato, A. Shiraishi, and M. C. Honda (2006a), Characteristics of alkenone distributions in suspended and sinking particles in the northwestern North Pacific, *Geochim. Cosmochim. Acta*, *70*(8), 2045–2062, doi:10.1016/j.gca.2006.01.024.

Harada, N., N. Ahagon, T. Sakamoto, M. Uchida, M. Ikehara, and Y. Shibata (2006b), Rapid fluctuation of alkenone temperature in the southwestern Okhotsk Sea during the past 120 ky, *Global Planet. Change*, *53*(1–2), 29–46, doi:10.1016/j.gloplacha.2006.01.010.

Harada, N., et al. (2012), Sea Surface temperature changes in the Okhotsk Sea and adjacent North Pacific during the last glacial maximum and deglaciation, *Deep Sea Res., Part II*, *61–64*, 93–105, doi:10.1016/j.dsr2.2011.12.007.

Honda, M. C., K. Imai, Y. Nojiri, F. Hoshi, T. Sugawara, and M. Kusakabe (2002), The biological pump in the northwestern North Pacific based on fluxes and major components of particulate matter obtained by sediment-trap experiments (1997–2000), *Deep Sea Res., Part II*, *49*(24–25), 5595–5625, doi:10.1016/S0967-0645(02)00201-1.

Hu, A. X., G. A. Meehl, B. L. Otto-Bliesner, C. Waelbroeck, W. Q. Han, M. F. Loutre, K. Lambeck, J. X. Mitrovica, and N. Rosenbloom (2010), Influence of Bering Strait flow and North Atlantic circulation on glacial sea-level changes, *Nat. Geosci.*, *3*(2), 118–121, doi:10.1038/ngeo729.

Huang, R. X., M. A. Cane, N. Naik, and P. Goodman (2000), Global adjustment of the thermocline in response to deepwater formation, *Geophys. Res. Lett.*, *27*(6), 759–762, doi:10.1029/1999GL002365.

Katsuki, K., and K. Takahashi (2005), Diatoms as paleoenvironmental proxies for seasonal productivity, sea-ice and surface circulation in the Bering Sea during the late Quaternary, *Deep Sea Res., Part II*, *52*(16–18), 2110–2130, doi:10.1016/j.dsr2.2005.07.001.

Katsuki, K., B. K. Khim, T. Itaki, N. Harada, H. Sakai, T. Ikeda, K. Takahashi, Y. Okazaki, and H. Asahi (2009), Land-sea linkage of Holocene paleoclimate on the Southern Bering Continental Shelf, *Holocene*, *19*(5), 747–756, doi:10.1177/0959683609105298.

Keigwin, L. D. (1998), Glacial-age hydrography of the far northwest Pacific Ocean, *Paleoceanography*, *13*(4), 323–339, doi:10.1029/98PA00874.

Keigwin, L. D., G. A. Jones, and P. N. Froelich (1992), A 15,000 year paleoenvironmental record from Meiji Seamount, far northwestern Pacific, *Earth Planet. Sci. Lett.*, *111*(2–4), 425–440, doi:10.1016/0012-821X(92)90194-Z.

Kiefer, T., and M. Kienast (2005), Patterns of deglacial warming in the Pacific Ocean: A review with emphasis on the time interval of Heinrich event 1, *Quat. Sci. Rev.*, *24*(7–9), 1063–1081, doi:10.1016/j.quascirev.2004.02.021.

Kiefer, T., M. Sarnthein, H. Erlenkeuser, P. M. Grootes, and A. P. Roberts (2001), North Pacific response to millennial-scale changes in ocean circulation over the last 60 kyr, *Paleoceanography*, *16*(2), 179–189, doi:10.1029/2000PA000545.

Kienast, S. S., and J. L. McKay (2001), Sea surface temperatures in the subarctic Northeast Pacific reflect millennial-scale climate oscillations during the last 16 kyrs, *Geophys. Res. Lett.*, *28*(8), 1563–1566, doi:10.1029/2000GL012543.

Kim, J. H., N. Rimbu, S. J. Lorenz, G. Lohmann, S. I. Nam, S. Schouten, C. Ruhlemann, and R. R. Schneider (2004), North Pacific and North Atlantic sea-surface temperature variability during the holocene, *Quat. Sci. Rev.*, *23*(20–22), 2141–2154, doi:10.1016/j.quascirev.2004.08.010.

Kohfeld, K. E., R. G. Fairbanks, S. L. Smith, and I. D. Walsh (1996), Neogloboquadrina pachyderma (sinistral coiling) as paleoceanographic tracers in polar oceans: Evidence from northeast water Polynya plankton tows, sediment traps, and surface sediments, *Paleoceanography*, *11*(6), 679–699, doi:10.1029/96PA02617.

Kuzmin, Y. V., G. S. Burr, and A. J. T. Jull (2001), Radiocarbon reservoir correction ages in the Peter the Great Gulf, Sea of Japan, and eastern coast of the Kunashir, southern Kuriles (northwestern Pacific), *Radiocarbon*, *43*(2A), 477–481.

Laskar, J., P. Robutel, F. Joutel, M. Gastineau, A. C. M. Correia, and B. Levrard (2004), A long-term numerical solution for the insolation quantities of the Earth, *Astron. Astrophys.*, *428*(1), 261–285, doi:10.1051/0004-6361:20041335.

Lund, D. C., A. C. Mix, and J. Southon (2011), Increased ventilation age of the deep northeast Pacific Ocean during the last deglaciation, *Nat. Geosci.*, *4*(11), 771–774, doi:10.1038/ngeo1272.

Manabe, S., and R. J. Stouffer (1988), Two stable equilibria of a coupled ocean-atmosphere model, *J. Clim.*, *1*, 841–866, doi:10.1175/1520-0442(1988)001<0841:TSEOAC>2.0.CO;2.

Mantua, N. J., S. R. Hare, Y. Zhang, J. M. Wallace, and R. C. Francis (1997), A Pacific interdecadal climate oscillation with impacts on salmon production, *Bull. Am. Meteorol. Soc.*, *78*(6), 1069–1079, doi:10.1175/1520-0477(1997)078<1069:APICOW>2.0.CO;2.

Marchal, O., et al. (2002), Apparent long-term cooling of the sea surface in the northeast Atlantic and Mediterranean during the Holocene, *Quat. Sci. Rev.*, *21*(4–6), 455–483, doi:10.1016/S0277-3791(01)00105-6.

McManus, J. F., R. Francois, J. M. Gherardi, L. D. Keigwin, and S. Brown-Leger (2004), Collapse and rapid resumption of Atlantic meridional circulation linked to deglacial climate changes, *Nature*, *428*(6985), 834–837, doi:10.1038/nature02494.

McNeely, R., A. S. Dyke, and J. R. Southon (2006), Canadian marine reservoir ages, preliminary data assessment, *Geol. Surv. Can.Open File Rep. 5049*, 3 pp., Geol. Surv. of Can., Ottawa.

Mikolajewicz, U., T. J. Crowley, A. Schiller, and R. Voss (1997), Modelling teleconnections between the North Atlantic and North Pacific during the Younger Dryas, *Nature*, *387*(6631), 384–387, doi:10.1038/387384a0.

Minoshima, K., H. Kawahata, and K. Ikehara (2007), Changes in biological production in the mixed water region (MWR) of the northwestern North Pacific during the last 27 kyr, *Palaeogeogr. Palaeoclimatol. Palaeoecol.*, *254*(3–4), 430–447, doi:10.1016/j.palaeo.2007.06.022.

Müller, P. J., and R. Schneider (1993), An automated leaching method for the determination of opal in sediments and particulate matter, *Deep Sea Res., Part I*, *40*(3), 425–444, doi:10.1016/0967-0637(93)90140-X.

Müller, P. J., G. Kirst, G. Ruhland, I. von Storch, and A. Rosell-Mele (1998), Calibration of the alkenone paleotemperature index $U^{K'}_{37}$ based on core-tops from the eastern South Atlantic and the global ocean (60°N–60°S), *Geochim. Cosmochim. Acta*, *62*(10), 1757–1772, doi:10.1016/S0016-7037(98)00097-0.

Müller, J., G. Masse, R. Stein, and S. T. Belt (2009), Variability of sea-ice conditions in the Fram Strait over the past 30,000 years, *Nat. Geosci.*, *2*(11), 772–776, doi:10.1038/ngeo665.

Müller, J., A. Wagner, K. Fahl, R. Stein, M. Prange, and G. Lohmann (2011), Towards quantitative sea ice reconstructions in the northern North Atlantic: A combined biomarker and numerical modelling approach, *Earth Planet. Sci. Lett.*, *306*(3–4), 137–148, doi:10.1016/j.epsl.2011.04.011.

Niebauer, H. J. (1988), Effect of El Nino Southern Oscillation and North Pacific weather patterns on interannual variability in the subarctic Bering Sea, *J. Geophys. Res.*, *93*(C5), 5051–5068, doi:10.1029/JC093iC05p05051.

Niebauer, H. J. (1998), Variability in Bering Sea ice cover as affected by a regime shift in the North Pacific in the period 1947–1996, *J. Geophys. Res.*, *103*(C12), 27,717–27,737, doi:10.1029/98JC02499.

Ohtani, K., Y. Akiba, and A. Y. Takenouti (1972), Formation of western subarctic water in the Bering Sea, in *Biological Oceanography of the Northern North Pacific Ocean*, edited by A. Y. Takenouti, pp. 32–44, Idemitsu Shoten, Tokyo.

Okazaki, Y., K. Takahashi, K. Katsuki, A. Ono, J. Hori, T. Sakamoto, M. Uchida, Y. Shibata, M. Ikehara, and K. Aoki (2005), Late Quaternary paleoceanographic changes in the southwestern Okhotsk Sea: Evidence from geochemical, radiolarian, and diatom records, *Deep Sea Res., Part II*, *52*(16–18), 2332–2350, doi:10.1016/j.dsr2.2005.07.007.

Okazaki, Y., A. Timmermann, L. Menviel, N. Harada, A. Abe-Ouchi, M. O. Chikamoto, A. Mouchet, and H. Asahi (2010), Deepwater formation in the North Pacific during the Last Glacial Termination, *Science*, *329*(5988), 200–204, doi:10.1126/science.1190612.

Okumura, Y. M., C. Deser, A. Hu, A. Timmermann, and S. P. Xie (2009), North Pacific climate response to freshwater forcing in the subarctic North Atlantic: Oceanic and atmospheric pathways, *J. Clim.*, *22*(6), 1424–1445, doi:10.1175/2008JCLI2511.1.

Overland, J. E., N. A. Bond, and J. M. Adams (2002), The relation of surface forcing of the Bering Sea to large-scale climate patterns, *Deep Sea Res., Part II*, *49*(26), 5855–5868, doi:10.1016/S0967-0645(02)00322-3.

Pisias, N. G., A. C. Mix, and L. Heusser (2001), Millennial scale climate variability of the northeast Pacific Ocean and northwest North America based on radiolaria and pollen, *Quat. Sci. Rev.*, *20*(14), 1561–1576, doi:10.1016/S0277-3791(01)00018-X.

Prahl, F. G., and S. G. Wakeham (1987), Calibration of unsaturation patterns in long-chain ketone compositions for paleotemperature assessment, *Nature*, *330*(6146), 367–369, doi:10.1038/330367a0.

Rahmstorf, S. (1995), Bifurcations of the atlantic thermohaline circulation in response to changes in the hydrological cycle, *Nature*, *378*(6553), 145–149, doi:10.1038/378145a0.

Rasmussen, S. O., et al. (2006), A new Greenland ice core chronology for the last glacial termination, *J. Geophys. Res.*, *111*, D06102, doi:10.1029/2005JD006079.

Reimer, P. J., et al. (2009), Intcal09 and Marine09 radiocarbon age calibration curves, 0–50,000 years cal BP, *Radiocarbon*, *51*(4), 1111–1150.

Saenko, O. A., A. Schmittner, and A. J. Weaver (2004), The Atlantic-Pacific seesaw, *J. Clim.*, *17*(11), 2033–2038, doi:10.1175/1520-0442(2004)017<2033:TAS>2.0.CO;2.

Sakamoto, T., et al. (2006), Millennial-scale variations of sea-ice expansion in the southwestern part of the Okhotsk Sea during the past 120 kyr: Age model and ice-rafted debris in IMAGES Core MD01–2412, *Global Planet. Change*, *53*(1–2), 58–77, doi:10.1016/j.gloplacha.2006.01.012.

Sancetta, C. (1983), Effect of Pleistocene glaciation upon oceanographic characteristics of the North Pacific Ocean and Bering Sea, *Deep Sea Res., Part A*, *30*(8), 851–869, doi:10.1016/0198-0149(83)90004-3.

Sancetta, C. (1992), Primary production in the glacial North Atlantic and North Pacific oceans, *Nature*, *360*(6401), 249–251, doi:10.1038/360249a0.

Sancetta, C., and S. W. Robinson (1983), Diatom evidence on Wisconsin and Holocene events in the Bering Sea, *Quat. Res.*, *20*(2), 232–245, doi:10.1016/0033-5894(83)90079-0.

Sarnthein, M., H. Gebhardt, T. Kiefer, M. Kucera, M. Cook, and H. Erlenkeuser (2004), Mid Holocene origin of the sea-surface salinity low in the subarctic North Pacific, *Quat. Sci. Rev.*, *23*(20–22), 2089–2099, doi:10.1016/j.quascirev.2004.08.008.

Sarnthein, M., T. Kiefer, P. M. Grootes, H. Elderfield, and H. Erlenkeuser (2006), Warmings in the far northwestern Pacific promoted pre-Clovis immigration to America during Heinrich event 1, *Geology*, *34*(3), 141–144, doi:10.1130/G22200.1.

Sarnthein, M., P. M. Grootes, J. P. Kennett, and M.-J. Nadeau (2007), ^{14}C reservoir ages show deglacial changes in ocean currents and carbon cycle, in *Ocean Circulation: Mechanisms and Impacts—Past and Future Changes of Meridional Overturning*, *Geophys. Monogr. Ser.*, vol. 173, edited by A. Schmittner, J. C. H. Chiang, and S. R. Hemming, pp. 175–196, AGU, Washington, D. C., doi:10.1029/173GM13.

Schmittner, A., E. D. Galbraith, S. W. Hostetler, T. F. Pedersen, and R. Zhang (2007), Large fluctuations of dissolved oxygen in the Indian and Pacific oceans during Dansgaard-Oeschger oscillations caused by variations of North Atlantic Deep Water subduction, *Paleoceanography*, *22*, PA3207, doi:10.1029/2006PA001384.

Seki, O., R. Ishiwatari, and K. Matsumoto (2002), Millennial climate oscillations in NE Pacific surface waters, *Geophys. Res. Lett.*, *29*(23), 2144, doi:10.1029/2002GL015200.

Seki, O., K. Kawamura, M. Ikehara, T. Nakatsuka, and T. Oba (2004a), Variation of alkenone sea surface temperature in the Sea of Okhotsk over the last 85 kyrs, *Org. Geochem.*, *35*(3), 347–354, doi:10.1016/j.orggeochem.2003.10.011.

Seki, O., M. Ikehara, K. Kawamura, T. Nakatsuka, K. Ohnishi, M. Wakatsuchi, H. Narita, and T. Sakamoto (2004b), Reconstruction of paleoproductivity in the Sea of Okhotsk over the last 30 kyr, *Paleoceanography*, *19*, PA1016, doi:10.1029/2002PA000808.

Seki, O., T. Nakatsuka, K. Kawamura, S. I. Saitoh, and M. Wakatsuchi (2007), Time-series sediment trap record of alkenones from the western Sea of Okhotsk, *Mar. Chem.*, *104*(3–4), 253–265, doi:10.1016/j.marchem.2006.12.002.

Seki, O., T. Sakamoto, S. Sakai, S. Schouten, E. C. Hopmans, J. S. Sinninghe Damste, and R. D. Pancost (2009), Large changes in seasonal sea ice distribution and productivity in the Sea of Okhotsk during the deglaciations, *Geochem. Geophys. Geosyst.*, *10*, Q10007, doi:10.1029/2009GC002613.

Sikes, E. L., J. K. Volkman, L. G. Robertson, and J. J. Pichon (1997), Alkenones and alkenes in surface waters and sediments of the Southern Ocean: Implications for paleotemperature estimation in polar regions, *Geochim. Cosmochim. Acta*, *61*(7), 1495–1505, doi:10.1016/S0016-7037(97)00017-3.

Southon, J. R., D. E. Nelson, and J. S. Vogel (1990), A record of past ocean-atmosphere radiocarbon differences from the Northeast Pacific, *Paleoceanography*, *5*(2), 197–206, doi:10.1029/PA005i002p00197.

Stabeno, P. J., J. D. Schumacher, and K. Ohtani (1999), The physical oceanography of the Bering Sea, in *Dynamics of the Bering Sea*, edited by T. R. Loughlin and K. Ohtani, pp. 1–28, Univ. of Alaska Sea Grant, Fairbanks.

Stuiver, M. (1980), Workshop on C-14 Data Reporting, *Radiocarbon*, *22*(3), 964–966.

Stuiver, M., and H. A. Polach (1977), Reporting of C-14 Data - Discussion, *Radiocarbon*, *19*(3), 355–363.

Stuiver, M., and P. J. Reimer (1993), Extended C-14 Data-Base and Revised Calib 3.0 C-14 Age Calibration Program, *Radiocarbon*, *35*(1), 215–230.

Ternois, Y., K. Kawamura, N. Ohkouchi, and L. Keigwin (2000), Alkenone sea surface temperature in the Okhotsk Sea for the last 15 kyr, *Geochem. J.*, *34*(4), 283–293, doi:10.2343/geochemj.34.283.

Timmermann, A., L. Menviel, Y. Okumura, A. Schilla, U. Merkel, O. Timm, A. X. Hu, B. Otto-Bliesner, and M. Schulz (2010), Towards a quantitative understanding of millennial-scale Antarctic warming events, *Quat. Sci. Rev.*, *29*(1–2), 74–85.

Vellinga, M., and R. A. Wood (2002), Global climatic impacts of a collapse of the Atlantic thermohaline circulation, *Clim. Change*, *54*(3), 251–267, doi:10.1023/A:1016168827653.

Yin, J. J., and R. J. Stouffer (2007), Comparison of the stability of the Atlantic thermohaline circulation in two coupled atmosphere-ocean

general circulation models, *J. Clim.*, *20*(17), 4293–4315, doi:10.1175/JCLI4256.1.

Yoneda, M., H. Uno, Y. Shibata, R. Suzuki, Y. Kumamoto, K. Yoshida, T. Sasaki, A. Suzuki, and H. Kawahata (2007), Radiocarbon marine reservoir ages in the western Pacific estimated by pre-bomb molluscan shells, *Nucl. Instrum. Methods Phys. Res., Sect. B*, *259*(1), 432–437, doi:10.1016/j.nimb.2007.01.184.

Zhang, J. L., R. Woodgate, and R. Moritz (2010), Sea ice response to atmospheric and oceanic forcing in the Bering Sea, *J. Phys. Oceanogr.*, *40*(8), 1729–1747, doi:10.1175/2010JPO4323.1.

10. Summary and Outlook

10.1. Summary

In this thesis I used stable isotope analyses, AMS ^{14}C analyses, a multi-proxy approach for biogenic productivity and terrigenous material transport, as well as sea surface and upper mixed layer temperature reconstructions to advance the understanding of North Pacific mid-depth water masses, in particular their ventilation and biogeochemical characteristics during the last glacial termination and the Holocene.

One focus was put on the reconstruction of past variations in Okhotsk Sea Intermediate Water (OSIW) ventilation and its influence on large-scale regional nutrient supply and biogeochemical cycles. I provided evidence for rapid and fundamental centennial- to millennial-scale changes in deglacial and Holocene ventilation. The achieved results help to establish a comprehensive picture of intermediate water in the North Pacific's marginal seas over the last 18,000 years before present. Integration of results from proxies for primary production, ventilation and terrigenous matter transport link changes in freshwater and detrital material supply from the hinterland to regional changes in intermediate water ventilation and export production. These changes and their biogeochemical imprint in turn precondition the nutrient characteristics of the water mass that is exported to the North Pacific. By analyzing records from the Okhotsk Sea and reference records from the open subarctic North Pacific, I hypothesized that the flow of intermediate water to the North Pacific did not collapse during the deglacial interstadial Bølling-Allerød and Preboreal phases. Instead, additional macro- (silicate) and micronutrients (iron) were entrained into Okhotsk Sea Intermediate Water and exported to the mid-depth North Pacific. This critically needed supply and supposed wintertime entrainment of usually limiting nutrients into the upper mixed layer supported a transient increase in both productivity and nutrient utilization in the North Pacific, analog to modern mechanisms. Characteristic ubiquitous deglacial productivity peaks had remained insufficiently explained previously and are thought to be connected with temporary modulations in the deglacial rise of CO_2 atmospheric concentrations.

Comparison between ventilation records from the Okhotsk and Bering Sea enabled the first synoptic reconstruction of deglacial intermediate water ventilation changes. These results show that existing hypotheses postulating a deepwater formation in the North Pacific during cold Heinrich Stadial 1 are unsubstantiated and cannot be reconciled with evidence from new deep records and intermediate water ventilation records. In addition, it could be shown that millennial-scale phases of increased (decreased) North Pacific Intermediate Water ventilation correspond to collapses (resumptions) of the Atlantic

Meridional Overturning Cell during Heinrich Stadial 1 (the Bølling-Allerød). This observation coupled with an in-phase development of alkenone-based sea surface temperature records between the North Atlantic and North Pacific calls for an atmospheric teleconnection pattern, likely transmitted via atmospheric modulations of the East Asian Monsoon systems. These largely determine in their winter expression strength and location of the Aleutian Low – Siberian High atmospheric action centers which in turn determine the prevalent temperature and sea ice patterns in the Bering and Okhotsk Sea. The observation that the deglacial Okhotsk Sea undergoes larger changes than the Bering Sea in intermediate water ventilation implies that forcing by the East Asian Summer Monsoon exerts additional low-latitude control on Okhotsk Sea mid-depth water formation via transfer of freshwater and latent heat to the northern shelf areas, where new Okhotsk Sea Intermediate Water is ventilated. Complementary reconstructions of sea surface and upper mixed layer temperatures revealed a complex oceanographic development of the subarctic North Pacific over the last glacial termination and early Holocene. Comparison of mixed layer stratification, temperature and sea ice changes between the Bering Sea, Okhotsk Sea and subarctic Northwest Pacific regions allowed for the first time to track spatially and temporally differing signals and assign minima in thermal stratification and seasonal contrasts with deglacial cold stadial phases.

Analyses of a suite of high-resolution sediment cores that cover the entire Holocene revealed that rapid millennial-scale changes in mid-depth ventilation are not solely restricted to glacial-interglacial transitions or glacial stages. I presented the first complete Holocene Okhotsk Sea Intermediate Water (OSIW) ventilation record based on epibenthic $\delta^{13}C$ time. This stacked record can be used to estimate past O_2 concentrations of OSIW. Results showed that the modern pattern of mid-depth North Pacific ventilation from the Okhotsk Sea has only been active since the middle Holocene around 6,000 years before present, and comparable levels of oxygenation were only reached during the last c. 2,000 years. Under naturally warmer-than-present early Holocene conditions, the Okhotsk Sea switched its role from a ventilation to an oxygen-consuming region, thereby enhancing mid-depth oxygen depletion in the North Pacific, with presumed repercussions for the utilization and provision of nutrients and impacts on regional biogeochemical cycles in the lower latitudes. The results also support the hypothesis that under future global warming scenarios, expansion of mid-depth lower latitude oxygen minimum zones and loss of high-latitude oxygenated waters in the North Pacific is likely to be supported by changes in the Okhotsk Sea, with consequences for marine ecosystems, natural CO2 balances and commercial exploitation of living resources.

The evidence presented in this thesis suggests that mid-depth ventilation in high latitudes like the Okhotsk Sea and Bering Sea is coupled with a high sensitivity to the regional (and ultimately global) development of sea surface temperatures and stratification. By comparing the modern mid-latitude

source region of intermediate water (Okhotsk Sea) with a potential additional source of well-ventilated intermediate water during the last glacial termination (Bering Sea), differences in the temporal development of the respective upper and deeper waters and their relations to major atmospheric and oceanic forcing factors could be identified. Further works, in particular combined model-data studies are needed to better track changes in the North Pacific surface and deep ocean and understand the underlying large-scale continent-ocean-atmosphere-sea ice interactions. To this extent, the differences between the data generated in this and complementary theses (Max, 2012; Riethdorf, 2012) and earlier modeling studies (Menviel et al., 2011; Okazaki et al., 2010a) underlines the necessity to further evolve both the spatial and temporal data coverage, as well as to increase the complexity of the used climate models.

The investigated regions, as areas of new water mass formation, represent particularly reactive and vulnerable components of the North Pacific's biogeochemical cycle. Changes in this biogeochemistry, together with the observed variations in nutrient delivery, stratification and oxygen supply in turn largely determine the efficiency of the high-latitude "biological pump" (CO_2 sink), as well as the nutrient provision to distal low-latitude regions of the Pacific that today are CO_2 sources to the atmosphere. Together, the components of this cycle studied here exert a significant control on the Pacific's role in the global oceanic carbon cycle.

10.2. Outlook: Hydrography and Ventilation of the Glacial North Pacific – A review and synopsis of German-Russian Studies in the Okhotsk Sea

The modern subarctic North Pacific is characterized in large by a permanent strong density stratification with a halocline, which also prevents the formation of new deepwater masses in today. Only mid-depth waters are ventilated by North Pacific Intermediate Water (NPIW) from water formed in the Okhotsk Sea. During the last glacial, the stratification and isolation of the deep North Pacific is thought to have been more pronounced, and a prominent hydrographic boundary at 2000 m water depth has been postulated based on stable carbon isotope results from depth transects in the subarctic Northwest Pacific (Keigwin, 1998a) and the Ontong Java Plateau (Herguera et al., 1992). The reconstructions postulated that NPIW was better ventilated than today between isolated abyssal and highly stratified surface North Pacific water masses. In contrast Cd/Ca-based evidence from off Japan does not show the development of the 2,000 m bathyal front in ventilation (Boyle, 1992; Ohkouchi et al., 1994).

Glacial deep to intermediate ventilation boundaries and carbon exchange in the Pacific have fundamental implications for the glacial global carbon budget and the storage of abyssal carbon in the deep ocean (Boyle, 1988b; Broecker, 1982; Broecker and Clark, 2010; Broecker et al., 2004). However, evidence from the North Pacific about past variations in glacial NPIW characteristics is sparse and has not much improved more than a decade after early seminal studies by Mix et al. (1991), Zahn et al. (1991) Keigwin (1998a) and Matsumoto et al. (2002a). Subsequent efforts have largely focused on single sites or the deglacial transition (Galbraith et al., 2007; Lund et al., 2011; Okazaki et al., 2012; Okazaki et al., 2010a). While these works showed dramatic short-term changes during the last deglaciation with transient phases of deep or intermediate water formation during the cold Heinrich-1 stadial, the glacial baseline from which these hypothesized deglacial transitions started remains as poorly understood as it was nearly a decade ago.

In this ongoing effort, I use the substantial collection of sediment cores obtained over the roughly ten years of German-Russian joint research efforts and re-sampled and -investigated those legacy cores as well as obtaining new stable isotope data from ten cores collected during the final phase of KOMEX and KOMEX-SONNE that fill major gaps in depth transects within the Okhotsk Sea. I carry out stable isotope analyses on diverse epibenthic *Cibicides* species from both the Holocene and Last Glacial maximum intervals and the deglacial transition. A first result of this work is an updated LGM time slice of North Pacific ventilation based on epibenthic $\delta^{13}C$ that can be integrated into earlier works (Herguera et al., 2010; Keigwin, 1998a; Matsumoto et al., 2002a) and provide a substantially updated comprehensive reconstruction of last glacial Pacific circulation and ventilation (Fig. 9-1).

Based on this collection of cores from intermediate (600-2200 m) water depths in the Okhotsk Sea, the hypothesis of an intermediate to deep hydrographic boundary during the last glacial in the northwest subarctic Pacific is reviewed. Evidence for a much weaker separation between intermediate and deep water than previously thought is found. Patterns more similar to the modern situation prevail in line with Cd/Ca-based early reconstructions. However, compared to modern profiles, the deep-intermediate Pacific between 600-2000 m is strikingly similar in ventilation characteristics to the deeper bathyal sites below 2000 m. Ongoing work on this dataset will complement this first analysis and add evidence for physical stratification based on oxygen the isotope datasets. Selected AMS ^{14}C paired planktic-benthic data shall complement the $\delta^{13}C$-based evidence and help better constrain water mass ages in the glacial North Pacific.

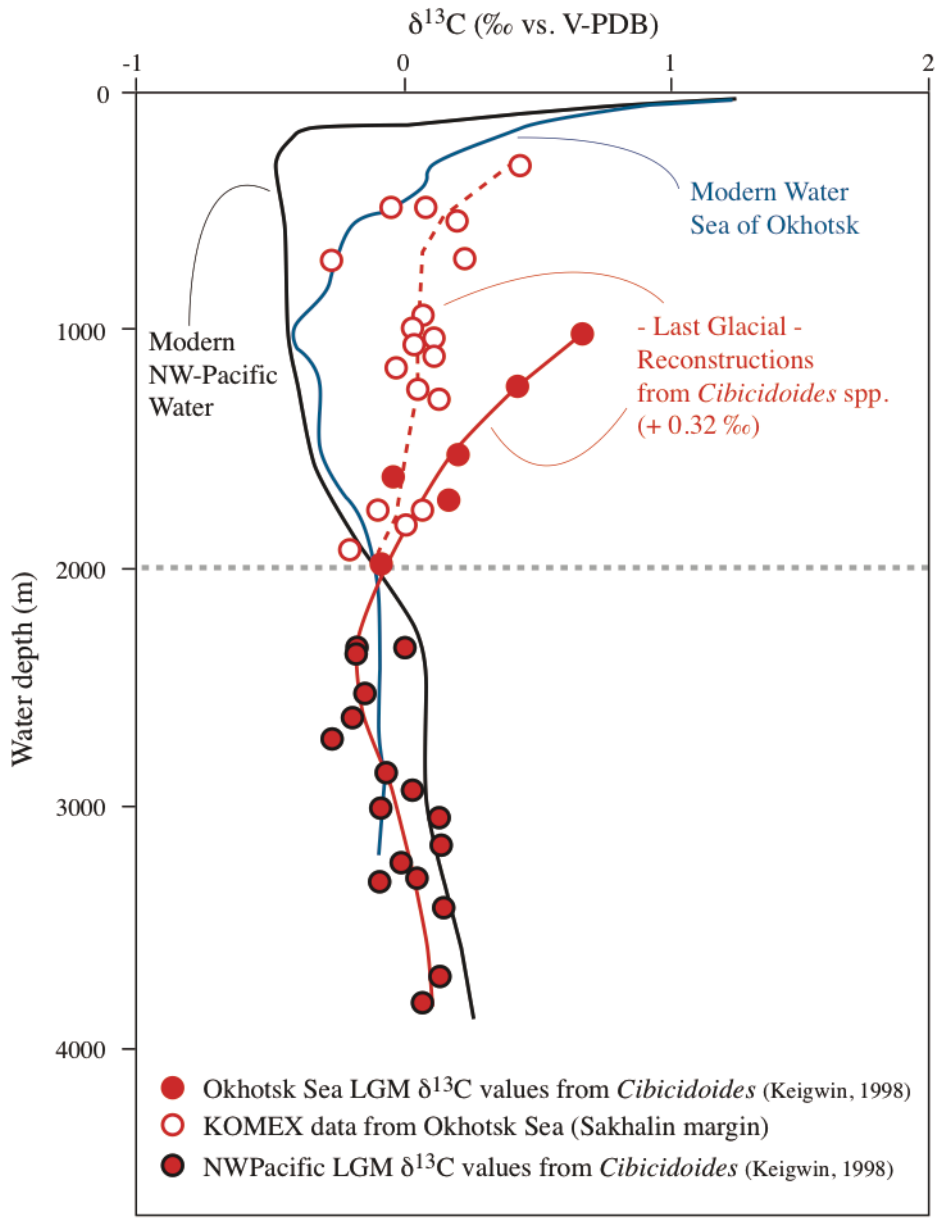

Figure 9.1: New Last Glacial Maximum $\delta^{13}C$-based North Pacific depth transect, based on measurements from KOMEX, KOMEX II and KOMEX-SONNE cores in comparison to existing data from the Okhotsk Sea and Northwest Pacific (Keigwin, 1998a).

11. References

Abelmann, A., Nimmergut, A., 2005. Radiolarians in the Sea of Okhotsk and their ecological implication for paleoenvironmental reconstructions. Deep Sea Research Part II: Topical Studies in Oceanography 52, 2302-2331.

Addison, J.A., Finney, B.P., Dean, W.E., Davies, M.H., Mix, A.C., Stoner, J.S., Jaeger, J.M., 2012. Productivity and sedimentary δ15N variability for the last 17,000 years along the northern Gulf of Alaska continental slope. Paleoceanography 27.

Adkins, J.F., Boyle, E.A., 1997. Changing atmospheric Delta C-14 and the record of deep water paleoventilation ages. Paleoceanography 12, 337-344.

Ahagon, N., Ohkushi, K., Uchida, M., Mishima, T., 2003b. Mid-depth circulation in the northwest Pacific during the last deglaciation: Evidence from foraminiferal radiocarbon ages. Geophysical Research Letters 30, 2097.

Ahagon, N., Uchida, M., 2004. Transient response of mid-depth circulation in the northwest Pacific around the Younger Dryas event inferred from AMS C-14 ages of foraminifera. Nuclear Instruments & Methods In Physics Research Section B-Beam Interactions With Materials And Atoms 223, 466-470.

Barash, M.S., Khusid, T.A., Matul, A.G., Chekhovskaya, M.P., Biebow, N., Nuernberg, D., Tiedemann, R., 2008. Distribution of benthic foraminifera in Upper Quaternary sediments of the Deryugin Basin (Sea of Okhotsk). Okeanologiya 48, 105-113.

Barker, S., Knorr, G., Vautravers, M.J., Diz, P., Skinner, L.C., 2010. Extreme deepening of the Atlantic overturning circulation during deglaciation. Nature Geoscience 3, 567.

Bauch, D., Erlenkeuser, H., Winckler, G., Pavlova, G., Thiede, J., 2002. Carbon isotopes and habitat of polar planktic foraminifera in the Okhotsk Sea: the 'carbonate ion effect' under natural conditions. Marine Micropaleontology 45, 83-99.

Bazarova, V.B., Klimin, M.A., Mokhova, L.M., Orlova, L.A., 2008. New pollen records of Late Pleistocene and Holocene changes of environment and climate in the Lower Amur River Basin, NE Eurasia, Quaternary International, pp. 9-19.

Beck, J.W., Richards, D., Edwards, R., Silverman, B., Smart, P., Donahue, D., Hererra-Osterheld, S., Burr, G., Calsoyas, L., Jull, A., Biddulph, D., 2001. Extremely large variations of atmospheric C-14 concentration during the last glacial period. Science (New York, NY) 292, 2453-2458.

Behl, R.J., Kennett, J.P., 1996. Brief interstadial events in the Santa Barbara basin, NE Pacific, during the past 60 kyr. Nature 379, 243-246.

Biebow, N., Hütten, E., 1999. Cruise Reports: KOMEX I and II: RV Professor Gagarinsky Cruise 22, RV Akademik M.A. Lavrentyev Cruise 28, GEOMAR Report. GEOMAR Research Centre for Marine Geosciences, Kiel, p. 188.

Biebow, N., Kulinich, R., Baranov, B., 2002a. Cruise Report R/V Akademik Lavrentiev Cruise LV29, GEOMAR Reports, 1 ed. GEOMAR Research Center for Marine Geosciences, Kiel, p. 190.

Biebow, N., Kulinich, R., Baranov, B., 2002b. KOMEX II, Kurile Okhotsk Sea Marine Experiment: Cruise report RV Akademik M.A.Lavrentyev cruise 29, Leg 1 and Leg 2 : Vladivostok - Pusan - Okhotsk Sea - Pusan - Okhotsk Sea - Pusan - Vladivostok ; May 25 - August 05,2002. GEOMAR Forschungszentrum für Marine Geowissenschaften, Kiel.

Biebow, N., Lüdmann, T., Karp, B.Y., Kulinich, R., 2000. Cruise Reports KOMEX V and VI: RV Professor Gagarinsky Cruise 26, MV Marshal Gelovany Cruise 1, GEOMAR Report. GEOMAR Research Centre for Marine Geosciences, Kiel, p. 296.

Blaauw, M., 2010. Methods and code for "classical" age-modelling of radiocarbon sequences. Quaternary Geochronology 5, 512-518.

Blaauw, M., 2012. Out of tune: the dangers of aligning proxy archives. Quaternary Science Reviews 36, 38-49.

Blaauw, M., Andres Christen, J., 2011. Flexible Paleoclimate Age-Depth Models Using an Autoregressive Gamma Process. Bayesian Analysis 6, 457-474.

Blaauw, M., Bennett, K.D., Christen, J.A., 2010. Random walk simulations of fossil proxy data. The Holocene 20, 645-649.

Blockley, S., Lane, C., Turney, C., Ramsey, C.B., 2012. The INTegration of Ice core, MArine and TErrestrial records (INTIMATE) group 8000 to 60,000 BP. Quaternary Science Reviews 36, 2-10.

Blockley, S.P.E., Blaauw, M., Ramsey, C.B., van der Plicht, J., 2007. Building and testing age models for radiocarbon dates in Lateglacial and Early Holocene sediments. Quaternary Science Reviews 26, 1915-1926.

Blockley, S.P.E., Lane, C.S., Hardiman, M., Rasmussen, S.O., Seierstad, I.K., Steffensen, J.P., Svensson, A., Lotter, A.F., Turney, C.S., Bronk Ramsey, C., 2011. Synchronisation of palaeoenvironmental records over the last 60,000 years, and an extended INTIMATE event stratigraphy to 48,000 b2k. Quaternary Science Reviews 36, 2-10.

Blunier, T., Brook, E., 2001. Timing of millennial-scale climate change in Antarctica and Greenland during the last glacial period. Science (New York, NY) 291, 109-112.

Bond, G., Showers, W., Cheseby, M., Lotti, R., Almasi, P., Demenocal, P., Priore, P., Cullen, H., Hajdas, I., Bonani, G., 1997. A pervasive millennial-scale cycle in North Atlantic Holocene and glacial climates. Science (New York, NY) 278, 1257-1266.

Botsul, A., Biebow, N., Lembke-Jene, L., 2002. Paleoceanography and Sedimentation in the Okhotsk Sea, In: Biebow, N., Kulinich, R., Baranov, B. (Eds.), KOMEX II, Kurile Okhotsk Sea Marine Experiment: Cruise report RV Akademik M.A.Lavrentyev cruise 29, Leg 1 and Leg 2 : Vladivostok - Pusan - Okhotsk Sea - Pusan - Okhotsk Sea - Pusan - Vladivostok ; May 25 - August 05,2002 ;. GEOMAR Forschungszentrum für Marine Geowissenschaften, Kiel.

Boyle, E., 1992. Cadmium and Delta-C-13 Paleochemical Ocean Distributions During the Stage-2 Glacial Maximum. Annual Review of Earth and Planetary Sciences 20, 245-287.

Boyle, E.A., 1988a. Vertical Oceanic Nutrient Fractionation and Glacial Interglacial Co2 Cycles. Nature 331, 55-56.

Broecker, W., 1982. Glacial to Interglacial Changes in Ocean Chemistry. Progress In Oceanography 11, 151-197.

Broecker, W., Clark, E., 2010. Search for a glacial-age C-14-depleted ocean reservoir. Geophysical Research Letters 37, -.

Broecker, W., Clark, E., Hajdas, I., Bonani, G., 2004. Glacial ventilation rates for the deep Pacific Ocean. Paleoceanography 19, PA2002.

Broecker, W.S., 1991. The great ocean conveyor. Oceanography 4, 79-89.

Broecker, W.S., Maier-Reimer, E., 1992. The influence of air and sea exchange on the carbon isotope distribution in the sea. Global Biogeochemical Cycles 6, 315.

Brunelle, B.G., Sigman, D.M., Cook, M.S., Keigwin, L.D., Haug, G.H., Plessen, B., Schettler, G., Jaccard, S.L., 2007. Evidence from diatom-bound nitrogen isotopes for subarctic Pacific stratification during the last ice age and a link to North Pacific denitrification changes. Paleoceanography 22, PA1215.

Brunelle, B.G., Sigman, D.M., Jaccard, S.L., Keigwin, L.D., Plessen, B., Schettler, G., Cook, M.S., Haug, G.H., 2010a. Glacial/interglacial changes in nutrient supply and stratification in the western subarctic North Pacific since the penultimate glacial maximum. Quaternary Sci Rev 29, 2579-2590.

Brzezinski, M.A., 2002. A switch from Si(OH) 4to NO 3− depletion in the glacial Southern Ocean. Geophysical Research Letters 29, 1564.

Bubenshchikova, N., Nuernberg, D., Lembke-Jene, L., Pavlova, G., 2008. Living benthic foraminifera of the Okhotsk Sea: Faunal composition, standing stocks and microhabitats. Marine Micropaleontology 69, 314-333.

Bubenshchikova, N.V., Nuernberg, D., Gorbarenko, S.A., Lembke-Jene, L., 2010. Variations of the Oxygen Minimum Zone of the Okhotsk Sea during the Last 50 ka as Indicated by Benthic Foraminiferal and Biogeochemical Data. Okeanologiya 50, 93-106.

Caissie, B.E., Brigham-Grette, J., Lawrence, K.T., Herbert, T.D., Cook, M.S., 2010. Last Glacial Maximum to Holocene sea surface conditions at Umnak Plateau, Bering Sea, as inferred from diatom, alkenone, and stable isotope records. Paleoceanography 25, PA1206-.

Cartapanis, O., Tachikawa, K., Bard, E., 2012. Latitudinal variations in intermediate depth ventilation and biological production over northeastern Pacific Oxygen Minimum Zones during the last 60 ka. Quaternary Science Reviews 53, 24-38.

Chikamoto, M.O., Menviel, L., Abe-Ouchi, A., Ohgaito, R., Timmermann, A., Okazaki, Y., Harada, N., Oka, A., Mouchet, A., 2012. Variability in North Pacific intermediate and deep water ventialtion during Heinrich events in two coupled climate models. Deep-Sea Res. Part II-Top. Stud. Oceanogr. 61-64, 114-126.

Chlachula, J., 2003. The Siberian loess record and its significance for reconstruction of Pleistocene climate change in north-central Asia. Quaternary Science Reviews 22, 1879-1906.

Cook, M.S., Keigwin, L.D., Sancetta, C.A., 2005a. The deglacial history of surface and intermediate water of the Bering Sea. Deep Sea Research Part II: Topical Studies in Oceanography 52, 2163-2173.

Craig, H., 1957. Isotopic standards for carbon and oxygen and correction factors for mass-spectrometric analysis of carbon dioxide. Geochimica Et Cosmochimica Acta 12, 133-149.

Croudace, I.W., Rindby, A., Rothwell, R.G., 2006. ITRAX: description and evaluation of a new multi-function X-ray core scanner. Geological Society, London, Special Publications 267, 51-63.

Crusius, J., Pedersen, T., Kienast, S., Keigwin, L., Labeyrie, L., 2004. Influence of northwest Pacific productivity on North Pacific Intermediate Water oxygen concentrations during the Boiling-Allerod interval (14.7-12.9 ka). Geology 32, 633-636.

Curry, W.B., Duplessy, J.C., Labeyrie, L.D., Shackleton, N.J., 1988. Changes in the distribution of delta C-13 of deep water TCO2 between the last glaciation and the Holocene. Paleoceanography 3, 317-341

Curry, W.B., Oppo, D.W., 2005. Glacial water mass geometry and the distribution of delta C-13 of Sigma CO2 in the western Atlantic Ocean. Paleoceanography 20, -.

Dadey, K.A., Janecek, T., Klaus, A., 1992. 37. Dry-Bulk Density: Its Use and Determination. Proceedings of the Ocean Drilling Program, Scientific Results: United States, College Station, TX, Texas A&M University, Ocean Drilling Program 126, 551-554.

Dansgaard, W., Johnsen, S., Clausen, H., DahlJensen, D., Gundestrup, N., Hammer, C., Hvidberg, C., Steffensen, J., Sveinbjornsdottir, A., Jouzel, J., Bond, G., 1993. Evidence for general instability of past climate from a 250 kyr ice-core recordEVIDENCE FOR GENERAL INSTABILITY OF PAST CLIMATE FROM A 250-KYR ICE-CORE RECORD. Nature 364, 218-220.

Davies, M.H., Mix, A.C., Stoner, J.S., Addison, J.A., Jaeger, J., Finney, B., Wiest, J., 2011. The deglacial transition on the southeastern Alaska Margin: Meltwater input, sea level rise, marine productivity, and sedimentary anoxia. Paleoceanography 26, PA2223-.

Dean, W.E., Zheng, Y., Ortiz, J.D., Van Geen, A., 2006. Sediment Cd and Mo accumulation in the oxygen-minimum zone off western Baja California linked to global climate over the past 52 kyr. Paleoceanography 21, PA4209.

Debret, M., Sebag, D., Crosta, X., Massei, N., Petit, J.R., Chapron, E., Bout-Roumazeilles, V., 2009. Evidence from wavelet analysis for a mid-Holocene transition in global climate forcing. Quaternary Science Reviews 28, 2675-2688.

del Giorgio, P., Duarte, C., 2002. Respiration in the open ocean. Nature 420, 379-384.

DeMaster, D.J., 1981. Measuring biogenic silica in marine sediments and suspended matter, In: Hurd, D.C., Spenser, D.W. (Eds.), Marine Particles: Analysis and Characterization. American Geophysical Union, Washington, D. C., pp. 363–368.

Derkachev, A.N., Nikolaeva, N.A., Gorbarenko, S.A., Harada, N., Sakamoto, T., Iijima, K., Sakhno, V.G., Hua Hua, L., Wang, K., 2012. Characteristics and ages of tephra layers in the central Okhotsk Sea over the last 350kyr. Deep Sea Research Part II: Topical Studies in Oceanography 61-64, 179-192.

Deutsch, C., Brix, H., Ito, T., Frenzel, H., Thompson, L., 2011. Climate-Forced Variability of Ocean Hypoxia. Science (New York, NY).

Deutsch, C., Emerson, S., Thompson, L., 2005. Fingerprints of climate change in North Pacific oxygen. Geophysical Research Letters 32, L16604.

Duce, R.A., Tindale, N.W., 1991. Atmospheric Transport of Iron and Its Deposition in the Ocean, Limnology and Oceanography, pp. 1715-1726.

Dugdale, R.C., Wilkerson, F.P., Minas, H.J., 1995. The role of a silicate pump in driving new production. Deep Sea Research Part I: Oceanographic Research Papers 42, 697-719.

Dullo, W., Biebow, N., 2004. SO178-KOMEX Cruise Report: Mass exchange processes and balances in the Okhotsk Sea, IFM-GEOMAR Report. IFM-GEOMAR, Kiel.

Dullo, W.-C., Baranov, B., van den Bogaard, C., 2009a. FS Sonne Fahrtbericht / Cruise Report SO201-2 KALMAR: Kurile-Kamchatka and ALeutian MARginal Sea-Island Arc Systems: Geodynamic and Climate Interaction in Space and Time, Busan/Korea - Tomakomai/Japan, 30.08. - 08.10.2009, IFM-GEOMAR Report. IFM-GEOMAR, Kiel.

Dullo, W.-C., Biebow, N., Georgeleit, K., 2005. SO178 KOMEX: Stoffaustauschprozesse und-bilanzen im Ochotskischen Meer: Hintergrund und erste Ergebnisse. IFM-GEOMAR, Leibniz-Institute for Marine Sciences, Kiel, p. 125.

Dullo, W.C., Baranov, B., van den Bogaard, C., 2009b. FS Sonne Fahrtbericht/ Cruise Report SO201-2 KALMAR, Busan/Korea-Tomakomai/Japan, 30.08-08.10.2009. IFM-GEOMAR Report 35, In: van den Bogaard, C. (Ed.), p. 233.

Duplessy, J.C., Arnold, M., Bard, E., Juilletleclerc, A., Kallel, N., Labeyrie, L., 1989b. Ams C-14 Study of Transient Events and of the Ventilation Rate of the Pacific Intermediate Water during the Last Deglaciation. Radiocarbon 31, 493-502.

Duplessy, J.C., Shackleton, N.J., Fairbanks, R.G., Labeyrie, L., Oppo, D., Kallel, N., 1988. Deepwater source variations during the last climatic cycle and their impact on the global deepwater circulation. Paleoceanography 3, 343.

Dykoski, C., Edwards, R., Cheng, H., Yuan, D., Cai, Y., Zhang, M., Lin, Y., Qing, J., An, Z., Revenaugh, J., 2005. A high-resolution, absolute-dated Holocene and deglacial Asian monsoon record from Dongge Cave, China. Earth And Planetary Science Letters 233, 71-86.

Emerson, S., Watanabe, Y.W., Ono, T., Mecking, S., 2004. Temporal trends in apparent oxygen utilization in the upper pycnocline of the North Pacific: 1980–2000. Journal Of Oceanography 60, 139-147.

Emile-Geay, J., Cane, M., Naik, N., Seager, R., Clement, A., Van Geen, A., 2003. Warren revisited: Atmospheric freshwater fluxes and "Why is no deep water formed in the North Pacific''. Journal Of Geophysical Research-Oceans 108, 3178.

Erlenkeuser, H., Party, T.I.S.S., 1995. Stable carbon isotope ratios in the waters of the Laptev Sea/Sept. 94, In: Kassens, H., Piepenburg, D., Thiede, J., Timokhov, L., Hubberten, H.-W., Priamikov, S.M. (Eds.), Russian-German Cooperation: Laptev Sea System, Bremerhaven, pp. 170-177.

Erlenkeuser, H., Spielhagen, R.F., Taldenkova, E., 1999. Stable isotopes in modern water and bivalve samples from the Kara Sea., In: Matthiessen, J., Stepanets, O.V., Stein, R., Fütterer, D.K., Galimov, E.M. (Eds.), The Kara Sea Expedition of RV Akademik Boris Petrov 1997: First Results of a Joint Russian-German Pilot Study. Alfred Wegener Institute, Bremerhaven, pp. 80-90.

Feely, R.A., Sabine, C.L., Schlitzer, R., Bullister, J.L., Mecking, S., Greeley, D., 2004. Oxygen utilization and organic carbon remineralization in the upper water column of the Pacific Ocean. Journal Of Oceanography 60, 45-52.

Fukamachi, Y., Mizuta, G., Ohshima, K., Talley, L., Riser, S., Wakatsuchi, M., 2004. Transport and modification processes of dense shelf water revealed by long-term moorings off Sakhalin in the Sea of Okhotsk. Journal Of Geophysical Research-Oceans 109, C09S10.

Fukamachi, Y., Shirasawa, K., Polomoshnov, A.M., Ohshima, K.I., Kalinin, E., Nihashi, S., Melling, H., Mizuta, G., Wakatsuchi, M., 2009. Direct observations of sea-ice thickness and brine rejection off Sakhalin in the Sea of Okhotsk. Continental Shelf Research 29, 1541-1548.

Galbraith, E., Kienast, M., Pedersen, T., Calvert, S., 2004. Glacial-interglacial modulation of the marine nitrogen cycle by high-latitude O-2 supply to the global thermocline. Paleoceanography 19, PA4007.

Galbraith, E.D., Jaccard, S.L., Pedersen, T.F., Sigman, D.M., Haug, G.H., Cook, M., Southon, J.R., Francois, R., 2007. Carbon dioxide release from the North Pacific abyss during the last deglaciation. Nature 449, 890-U899.

Galbraith, E.D., Kienast, M., Jaccard, S.L., Pedersen, T.F., Brunelle, B.G., Sigman, D.M., Kiefer, T., 2008. Consistent relationship between global climate and surface nitrate utilization in the western subarctic Pacific throughout the last 500 ka. Paleoceanography 23, PA2212.

Ganssen, G., 1981. Isotopic analysis of foraminifera shells: Interference from chemical treatment. Palaeogeography, Palaeoclimatology, Palaeoecology 33, 271-276.

Garcia, H.E., Locarnini, R.A., Boyer, T.P., Antonov, J.I., Baranova, O.K., Zweng, M.M., Johnson, D.R., 2010a. World Ocean Atlas 2009, Volume 3: Dissolved Oxygen, Apparent Oxygen Utilization, and Oxygen Saturation. U.S. Government Printing Office, Washington, D.C.

Garcia, H.E., Locarnini, R.A., Boyer, T.P., Antonov, J.I., Baranova, O.K., Zweng, M.M., Johnson, D.R., 2010b. World Ocean Atlas 2009, Volume 4: Nutrients (phosphate, nitrate, silicate). U.S. Government Printing Office, Washington, D.C.

Gebhardt, H., Sarnthein, M., Grootes, P.M., Kiefer, T., Kuehn, H., Schmieder, F., Röhl, U., 2008. Paleonutrient and productivity records from the subarctic North Pacific for Pleistocene glacial terminations I to V. Paleoceanography 23, PA4212-.

Gladyshev, S., Talley, L., Kantakov, G., Khen, G., Wakatsuchi, M., 2003. Distribution, formation, and seasonal variability of Okhotsk Sea Mode Water. Journal of Geophysical Research-Oceans 108.

Goes, J.I., Gomes, H.d.R., Limsakul, A., Saino, T., 2004. The influence of large-scale environmental changes on carbon export in the North Pacific Ocean using satellite and shipboard data. Deep Sea Research Part II: Topical Studies in Oceanography 51, 247-279.

Gong, D., Ho, C., 2002. The Siberian High and climate change over middle to high latitude Asia. Theoretical And Applied Climatology 72, 1-9.

Gorbarenko, S., Khusid, T.A., Basov, I., Oba, T., Southon, J., Koizumi, I., 2002a. Glacial Holocene environment of the southeastern Okhotsk Sea: evidence from geochemical and palaeontological data. Palaeogeography Palaeoclimatology Palaeoecology 177, 237-263.

Gorbarenko, S., Nürnberg, D., Derkachev, A., Astakhov, A., Southon, J., Kaiser, A., 2002b. Magnetostratigraphy and tephrochronology of the Upper Quaternary sediments in the Okhotsk Sea: implication of terrigenous, volcanogenic and biogenic matter supply. Marine Geology 183, 107-129.

Gorbarenko, S., Southon, J., Keigwin, L., Cherepanova, M., Gvozdeva, I., 2004. Late Pleistocene-Holocene oceanographic variability in the Okhotsk Sea: geochemical, lithological and paleontological evidence. Palaeogeography Palaeoclimatology Palaeoecology 209, 281-301.

Gorbarenko, S.A., Basov, I.A., Chekhovskaya, M.P., Southon, J., Khusid, T.A., Artemova, A.V., 2005b. Orbital and millennium scale environmental changes in the southern Bering Sea during the last glacial-Holocene: Geochemical and paleontological evidence. Deep Sea Research Part II: Topical Studies in Oceanography 52, 2174-2185.

Gorbarenko, S.A., Goldberg, E.L.a.v., Kashgarian, M., Velivetskaya, T.a.y.A., Zakharkov, S.P., Pechnikov, V.S., Bosin, A.A.a.e., Psheneva, O.Y.a.e., Ivanova, E.D., 2007a. Millennium scale environment changes of the Okhotsk sea during last 80 kyr and their phase relationship with global climate changes. Journal Of Oceanography 63, 609-623.

Gorbarenko, S.A., Harada, N., Malakhov, M.I., Vasilenko, Y.P., Bosin, A.A., Gol'dberg, E.L., 2008. Millennial-scale climatic and environmental oscillations in the Sea of Okhotsk in response to global changes during the last 190 Ka. Doklady Earth Sciences 423, 1410-1413.

Gorbarenko, S.A., Harada, N., Malakhov, M.I., Vasilenko, Y.P., Bosin, A.A., Goldberg, E.L., 2010a. Orbital and millennial-scale environmental and sedimentological changes in the Okhotsk Sea during the last 350kyr. Global And Planetary Change.

Gorbarenko, S.A., Harada, N., Malakhov, M.I., Velivetskaya, T.A., Vasilenko, Y.P., Bosin, A.A., Derkachev, A.N., Goldberg, E.L., d, A.V.I., 2012. Responses of the Okhotsk Sea environment and sedimentology to global climate changes at the orbital and millennial scale during the last 350 kyr. Deep-Sea Research II 61-64, 73-84.

Gorbarenko, S.A., Khusid, T.A., Basov, I.A., Oba, T., Southon, J.R., Koizumi, I., 2002c. Glacial Holocene environment of the southeastern Okhotsk Sea: evidence from geochemical and palaeontological data. Palaeogeogr Palaeocl 177, 237-263.

Gorbarenko, S.A., Psheneva, O.Y., Artemova, A.V., Matul, A.G., Tiedemann, R., Nuernberg, D., 2010b. Paleoenvironment changes in the NW Okhotsk Sea for the last 18 kyr determined with micropaleontological, geochemical, and lithological data. Deep Sea Research Part I: Oceanographic Research Papers 57, 797-811.

Gorbarenko, S.A., Tsoi, I.B., Astakhov, A.S., Artemova, A.V., Gvozdeva, I.G., Annin, V.K., 2007b. Paleoenvironmental changes in the northern shelf of the Sea of Okhotsk during the Holocene. Stratigraphy and Geological Correlation 15, 656-671.

Grootes, P.M., Nadeau, M.J., Rieck, A., 2004. 14C-AMS at the Leibniz-Labor: Radiometric dating and isotope research. Nuclear Instruments and Methods in Physics Research Section B 223-224, 55-61.

Grootes, P.M., Stuiver, M., White, J.W.C., Johnsen, S., Jouzel, J., 1993. Comparison of oxygen isotope records from the GISP2 and GRIP Greenland ice cores. Nature 366, 552-554.

Hansell, D.A., 2002. Dissolved organic carbon export with North Pacific Intermediate Water formation. Global Biogeochemical Cycles 16, 1007.

Harada, N., Ahagon, N., Sakamoto, T., Uchida, M., Ikehara, M., Shibata, Y., 2006. Rapid fluctuation of alkenone temperature in the southwestern Okhotsk Sea during the past 120 ky. Global And Planetary Change 53, 29-46.

Harada, N., Sato, M., Sakamoto, T., 2008. Freshwater impacts recorded in tetraunsaturated alkenones and alkenone sea surface temperatures from the Okhotsk Sea across millennial-scale cycles. Paleoceanography 23, PA3201.

Harada, N., Sato, M., Seki, O., Timmermann, A., 2012. Sea surface temperature changes in the Okhotsk Sea and adjacent North Pacific during the last glacial maximum and deglaciation. Deep-Sea Research Part II 61-64, 93-105.

Harris, P.G., Zhao, M., Rosell-Mele, A., Tiedemann, R., Sarnthein, M., Maxwell, J.R., 1996. Chlorin accumulation rate as a proxy for Quaternary marine primary productivity. Nature News 383, 63-65.

Harrison, P.J., Whitney, F.A., Tsuda, A., Saito, H., Tadokoro, K., 2004. Nutrient and Plankton Dynamics in the NE and NW Gyres of the Subarctic Pacific Ocean. Journal Of Oceanography 60, 93-117.

Hartin, C.A., Fine, R.A., Sloyan, B.M., Talley, L.D., Chereskin, T.K., Happell, J., 2011. Formation rates of Subantarctic mode water and Antarctic intermediate water within the South Pacific. Deep Sea Research Part I: Oceanographic Research Papers 58, 524-534.

Haug, G.H., Ganopolski, A., Sigman, D.M., Rosell-Mele, A., Swann, G.E.A., Tiedemann, R., Jaccard, S.L., Bollmann, J., Maslin, M.A., Leng, M.J., Eglinton, G., 2005. North Pacific seasonality and the glaciation of North America 2.7 million years ago. Nature 433, 821-825.

Haug, G.H., Sigman, D.M., Tiedemann, R., Pedersen, T.F., Sarnthein, M., 1999. Onset of permanent stratification in the subarctic Pacific Ocean. Nature 401, 779-782.

Hays, J., Morley, J., 2003. The Sea of Okhotsk: A window on the ice age ocean. Deep Sea Research Part I: Oceanographic Research Papers 50, 1481-1506.

Hendy, I., 2010. The paleoclimatic response of the Southern Californian Margin to the rapid climate change of the last 60ka: A regional overview. Quaternary International 215, 62-73.

Hendy, I., Kennett, J., 2003. Tropical forcing of North Pacific intermediate water distribution during Late Quaternary rapid climate change? Quaternary Science Reviews 22, 673-689.

Herguera, J., Jansen, E., BERGER, W., 1992. Evidence for a bathyal front at 2000 m depth in the glacial Pacific, based on a depth transect from Ontong Oava Plateau. Paleoceanography 7, 273-288.

Herguera, J., Peltzer, E., Brewer, P., 2009. Benthic foraminifera habitats and carbon isotopes: new perspective from thermodynamic constrains on intermediate waters respiration. Geophysical Research Abstracts, 2009 EGU General Assembly 2009 11, EGU2009-3831.

Herguera, J.C., Herbert, T., Kashgarian, M., Charles, C., 2010. Intermediate and deep water mass distribution in the Pacific during the Last Glacial Maximum inferred from oxygen and carbon stable isotopes. Quaternary Science Reviews 29, 1228-1245.

Hill, K., Weaver, A., Freeland, H., Bychkov, A., 2003. Evidence of change in the Sea of Okhotsk: Implications for the North Pacific. Atmosphere-Ocean 41, 49-63.

Hofmann, M., Broecker, W.S., Lynch-Stieglitz, J., 1999. Influence of a [CO 2(aq)] dependent biological C-isotope fractionation on glacial 13C/ 12C ratios in the ocean. Global Biogeochemical Cycles 13, 873.

Holbourn, A., Henderson, A.S., 2002. Re-Illustration and Revised Taxonomy for selected Deep-Sea Benthic Foraminifers. Palaeontologia Electronica 4, 43 pp.

Honda, M., Yamazaki, K., Tachibana, Y., Takeuchi, K., 1996. Influence of Okhotsk sea-ice extent on atmospheric circulation. Geophysical Research Letters 23, 3595-3598.

Honda, M.C., Imai, K., Nojiri, Y., Hoshi, F., Sugawara, T., Kusakabe, M., 2002. The biological pump in the northwestern North Pacific based on fluxes and major components of particulate matter obtained by sediment-trap experiments (1997-2000). Deep-Sea Res. Part II-Top. Stud. Oceanogr. 49, 5595-5625.

Hughen, K., Baillie, M., Bard, E., Beck, J., Bertrand, C., Blackwell, P., Buck, C., Burr, G., Cutler, K., Damon, P., Edwards, R., Fairbanks, R., Friedrich, M., Guilderson, T., Kromer, B., McCormac, G., Manning, S., Ramsey, C., Reimer, P., Reimer, R., Remmele, S., Southon, J., Stuiver, M., Talamo, S., Taylor, F., van der Plicht, J., Weyhenmeyer, C., 2004. Marine04 marine radiocarbon age calibration, 0-26 cal kyr BP. Radiocarbon 46, 1059-1086.

Hughen, K., Southon, J., Lehman, S., Bertrand, C., Turnbull, J., 2006. Marine-derived 14C calibration and activity record for the past 50,000 years updated from the Cariaco Basin. Quaternary Science Reviews 25, 3216-3227.

Huybers, P., Wunsch, C., 2010. Paleophysical Oceanography with an Emphasis on Transport Rates. Annual Review of Marine Science 2, 1-34.

Ikehara, K., Ohkushi, K.a.i., Shibahara, A., Hoshiba, M., 2006. Change of bottom water conditions at intermediate depths of the Oyashio region, NW Pacific over the past 20,000 yrs. Global And Planetary Change 53, 78-91.

Inagaki, M., Yamamoto, M., Igarashi, Y., Ikehara, K., 2009. Biomarker records from core GH02-1030 off Tokachi in the northwestern Pacific over the last 23,000 years: Environmental changes during the last deglaciation. Journal Of Oceanography 65, 847-858.

Isono, D., Yamamoto, M., Irino, T., Oba, T., Murayama, M., Nakamura, T., Kawahata, H., 2009. The 1500-year climate oscillation in the midlatitude North Pacific during the Holocene. Geology 37, 591-594.

Itaki, T., Ikehara, K., 2004. Middle to late Holocene changes of the Okhotsk Sea Intermediate Water and their relation to atmospheric circulation. Geophysical Research Letters 31, L24309.

Itaki, T., Khim, B.-K., Ikehara, K., 2008. Last glacial-Holocene water structure in the southwestern Okhotsk Sea inferred from radiolarian assemblages. Marine Micropaleontology 67, 191-215.

Itaki, T., Kim, S., Rella, S.F., Uchida, M., Tada, R., Khim, B.-K., 2012. Millennial-scale variations of late Pleistocene radiolarian assemblages in the Bering Sea related to environments in shallow and deep waters. Deep Sea Research Part II: Topical Studies in Oceanography 61-64, 127-144.

Itoh, M., Ohshima, K.I., Wakatsuchi, M., 2003. Distribution and formation of Okhotsk Sea Intermediate Water: An analysis of isopycnal climatological data. Journal of Geophysical Research 108, 3258-.

Itou, M., Ono, T., Noriki, S., 2003. Provenance of intermediate waters in the western North Pacific deduced from thermodynamic imprint on delta C-13 of DIC. Journal Of Geophysical Research-Oceans 108, 3347.

Jaccard, S., Haug, G.H., Sigman, D., Pedersen, T., Thierstein, H., Rohl, U., 2005. Glacial/interglacial changes in subarctic North Pacific stratification. Science (New York, NY) 308, 1003-1006.

Jaccard, S.L., Galbraith, E., 2013. Direct ventilation of the North Pacific did not reach the deep ocean during the last deglaciation. Geophysical Research Letters.

Jaccard, S.L., Galbraith, E.D., 2012. Large climate-driven changes of oceanic oxygen concentrations during the last deglaciation. Nature Geoscience 5, 151-156.

Jaccard, S.L., Galbraith, E.D., Sigman, D.M., Haug, G.H., 2010. A pervasive link between Antarctic ice core and subarctic Pacific sediment records over the past 800 kyrs. Quaternary Science Reviews 29, 206-212.

Jaccard, S.L., Galbraith, E.D., Sigman, D.M., Haug, G.H., Francois, R., Pedersen, T.F., Dulski, P., Thierstein, H.R., 2009. Subarctic Pacific evidence for a glacial deepening of the oceanic respired carbon pool. Earth And Planetary Science Letters 277, 156-165.

Jansen, J.H.F., Van der Gaast, S.J., Koster, B., Vaars, A.J., 1998. CORTEX, a shipboard XRF-scanner for element analyses in split sediment cores. Marine Geology 151, 143-153.

Kaiser, A., 2001. Ozeanographie, Produktivität und Meereisverbreitung im Ochotskischen Meer während der letzten ca. 350 ka, Dissertation Thesis, Supervisors: Thiede, J., Nuernberg, D., Tiedemann, R.. University of Kiel, p. 228.

Karstensen, J., Stramma, L., Visbeck, M., 2008. Oxygen minimum zones in the eastern tropical Atlantic and Pacific oceans. Progress In Oceanography 77, 331-350.

Katsuki, K., Khim, B.-K., Itaki, T., Okazaki, Y., Ikehara, K., Shin, Y., Yoon, H.I., Kang, C.Y., 2010. Sea-ice distribution and atmospheric pressure patterns in southwestern Okhotsk Sea since the Last Glacial Maximum. Global And Planetary Change 72, 99-107.

Katsumata, K., Ohshima, K.I., Kono, T., Itoh, M., Yasuda, I., Volkov, Y.N., Wakatsuchi, M., 2004. Water exchange and tidal currents through the Bussol' Strait revealed by direct current measurements. Journal of Geophysical Research-Oceans 109, C09S06, doi:10.1029/2003JC001864.

Keeling, R.F., Körtzinger, A., Gruber, N., 2010. Ocean Deoxygenation in a Warming World. Annual Review of Marine Science 2, 199-229.

Keigwin, L., 1998a. Glacial-age hydrography of the far northwest Pacific Ocean. Paleoceanography 13, 323-339.

Keigwin, L., 2002a. Late Pleistocene-Holocene paleoceanography and ventilation of the Gulf of California. Journal Of Oceanography 58, 421-432.

Keigwin, L., Jones, G., FROELICH, P., 1992a. A 15,000 Year Paleoenvironmental Record from Meiji Seamount, far Northwestern Pacific. Earth And Planetary Science Letters 111, 425-440.

Keigwin, L.D., 1998b. Glacial-age hydrography of the far northwest Pacific Ocean. Paleoceanography 13, 323-339.

Keigwin, L.D., 2002b. Late Pleistocene-Holocene paleoceanography and ventilation of the Gulf of California. Journal of Oceanography 58, 421-432.

Keigwin, L.D., Jones, G.A., Froelich, P.N., 1992b. A 15,000 Year Paleoenvironmental Record from Meiji Seamount, Far Northwestern Pacific. Earth and Planetary Science Letters 111, 425-440.

Khim, B., Sakamoto, T., 2012. Reconstruction of surface water conditions in the central region of the Okhotsk Sea during the last 180 kyrs. Deep Sea Research Part II: ….

Kienast, S., Hendy, I., Crusius, J., Pedersen, T., Calvert, S., 2004. Export production in the subarctic North Pacific over the last 800 kyrs: No evidence for iron fertilization? Journal Of Oceanography 60, 189-203.

Kim, S., Khim, B.K., Uchida, M., Itaki, T., Tada, R., 2011. Millenial-scale paleoceanographic events and implications for the intermediate-water ventilation in the northrn slope area of the Bering Sea during the last 71kyrs. Global and Planetary Change 79, 89-98.

Kimura, N., Wakatsuchi, M., 1999. Processes controlling the advance and retreat of sea ice in the Sea of Okhotsk. Journal of Geophysical Research 104, 11137-11150.

Kimura, N., Wakatsuchi, M., 2004. Increase and decrease of sea ice area in the Sea of Okhotsk: Ice production in coastal polynyas and dynamic thickening in convergence zones. Journal Of Geophysical Research-Oceans 109, C09S03.

Kitani, K., 1973. An oceanographic study of the Okhotsk Sea - particularly in regard to cold waters. Bull. Far Sear Fish. Res. Lab. 9, 45-76.

Klinkhammer, G.P., Mix, A.C., Haley, B.A., 2009. Increased dissolved terrestrial input to the coastal ocean during the last deglaciation. Geochemistry Geophysics Geosystems 10, -.

Kohfeld, K.E., Chase, Z., 2011. Controls on deglacial changes in biogenic fluxes in the North Pacific Ocean. Quaternary Science Reviews.

Kokfelt, U., 2003. An Analysis of Pollen, Spores and Chlorophycean Algae from the Sea of Okhotsk: Implications for Late Glacial and Holocene Climatic Change, Geomar & Geologisk Museum Copenhagen. Copenhagen, Kiel, p. 56.

Kozdon, R., 2002. Kurzfristige Änderungen im Sedimentationsgeschehen des westlichen Ochotskischen Meeres währedn des Holozäns - Implikationen für den NE-sibirischen Raum, Diploma Thesis, Mathematisch-Naturwissenschaftliche Fakultät. Christian-Albrechts-Universität zu Kiel, Kiel, p. 33.

Krebs, U., Timmermann, A., 2007. Tropical air-sea interactions accelerate the recovery of the Atlantic Meridional Overturning Circulation after a major shutdown. Journal of Climate 20, 4940-4956.

Kroopnick, P.M., 1985a. The distribution of ^{13}C of $\sum CO2$ in the world oceans. Deep Sea Research Part I: Oceanographic Research Papers 32, 57-84.

Kroopnick, P.M., 1985b. The Distribution of C-13 of Sigma-Co2 in the World Oceans. Deep-Sea Research Part a-Oceanographic Research Papers 32, 57-84.

Kuzmin, Y.V., Burr, G.S., Gorbunov, S.V., Rakov, V.A., Razjigaeva, N.G., 2007a. A tale of two seas: Reservoir age correction values (R, Delta R) for the Sakhalin Island (Sea of Japan and Okhotsk Sea). Nuclear Instruments & Methods In Physics Research Section B-Beam Interactions With Materials And Atoms 259, 460-462.

Kuzmin, Y.V., Burr, G.S., Jull, A.J.T., 2001. Radiocarbon reservoir correction ages in the Peter the Great Gulf, Sea of Japan, and eastern coast of the Kunashir, southern Kuriles (northwestern Pacific). Radiocarbon 43, 477-481.

Lam, P.J., Bishop, J.K.B., 2008. The continental margin is a key source of iron to the HNLC North Pacific Ocean. Geophysical Research Letters 35, L07608.

Lourantou, A., Lavric, J.V., Kohler, P., Barnola, J.M., Paillard, D., Michel, E., Raynaud, D., Chappellaz, J., 2010. Constraint of the CO2 rise by new atmospheric carbon isotopic measurements during the last deglaciation. Global Biogeochemical Cycles 24.

Löwemark, L., Hong, W.-L., Yui, T.-F., Hung, G.-W., 2005. A test of different factors influencing the isotopic signal of planktonic foraminifera in surface sediments from the northern South China Sea. Marine Micropaleontology 55, 49-62.

Lumpkin, R., Speer, K., 2007. Global Ocean Meridional Overturning. Journal Of Physical Oceanography 37, 2550-2562.

Lund, D.C., Mix, A.C., Southon, J., 2011. Increased ventilation age of the deep northeast Pacific Ocean during the last deglaciation. Nature Geoscience 4, 771-774.

Lutze, G.F., Thiel, H., 1989. Epibenthic Foraminifera from Elevated Microhabitats - Cibicidoides-Wuellerstorfi and Planulina-Ariminensis. J Foramin Res 19, 153-158.

Lynch-Stieglitz, J., Fairbanks, R.G., 1994. A conservative tracer for glacial ocean circulation from carbon isotope and palaeo-nutrient measurements in benthic foraminifera. Nature News 369, 308-310.

Lynch-Stieglitz, J., Stocker, T.F., Broecker, W.S., Fairbanks, R.G., 1995. The influence of air-sea exchange on the isotopic composition of oceanic carbon: Observations and modeling. Global Biogeochemical Cycles 9, 653.

Mackensen, A., Schumacher, S., Radke, J., Schmidt, D.N., 2000. Microhabitat preferences and stable carbon isotopes of endobenthic foraminifera: clue to quantitative reconstruction of oceanic new production? Marine Micropaleontology 40, 233-258.

Mahowald, N., Baker, A., Bergametti, G., Brooks, N., Duce, R., Jickells, T., Kubilay, N., Prospero, J., Tegen, I., 2005. Atmospheric global dust cycle and iron inputs to the ocean. Global Biogeochemical Cycles 19, -.

Marchitto, T.M., Lehman, S.J., Ortiz, J.D., Fluckiger, J., van Geen, A., 2007. Marine radiocarbon evidence for the mechanism of deglacial atmospheric CO(2) rise. Science 316, 1456-1459.

Marchitto, T.M., Lynch-Stieglitz, J., Hemming, S.R., 2005. Deep pacific CaCO3 compensation and glacial-interglacial atmosphericCO(2). Earth and Planetary Science Letters 231, 317-336.

Marcott, S.A., Shakun, J.D., Clark, P.U., Mix, A.C., 2013. A Reconstruction of Regional and Global Temperature for the Past 11,300 Years. Science (New York, NY) 339, 1198-1201.

Martin, S., Drucker, R., Yamashita, K., 1998. The production of ice and dense shelf water in the Okhotsk Sea polynyas. Journal Of Geophysical Research-Oceans 103, 27771-27782.

Masujima, M., Yasuda, I., 2009. Distribution and Modification of North Pacific Intermediate Water around the Subarctic Frontal Zone East of 150 degrees E. Journal Of Physical Oceanography 39, 1462-1474.

Matsumoto, K., Oba, T., Lynch-Stieglitz, J., Yamamoto, H., 2002a. Interior hydrography and circulation of the glacial Pacific Ocean. Quaternary Science Reviews 21, 1693-1704.

Matsumoto, K., Sarmiento, J., Brzezinski, M., 2002b. Silicic acid leakage from the Southern Ocean: A possible explanation for glacial atmospheric pCO(2). Global Biogeochemical Cycles 16, 1031.

Matul, A.G., Abelmann, A., Nuernberg, D., Tiedemann, R., 2009. Stratigraphy and Major Paleoenvironmental Changes in the Sea of Okhotsk during the Last Million Years Inferred from Radiolarian Data. Okeanologiya 49, 93-100.

Max, L., 2012. Millennial-scale changes in sea surface temperatures and intermediate water circulation in the northwest Pacific during the past 20,000 years, Fachbereich Geowissenschaften. University of Bremen, Bremen, p. 145.

Max, L., Lembke-Jene, L., Riethdorf, J.-R., Tiedemann, R., Nürnberg, D., submitted. Rapid changes in North Pacific Intermediate Water Formation during the Last Glacial Termination. manuscript for submssion to Earth And Planetary Science Letters. In this thesis: Chapter 7.

Max, L., Riethdorf, J.-R., Tiedemann, R., Smirnova, M., Lembke-Jene, L., Fahl, K., Nürnberg, D., Matul, A., Mollenhauer, G., 2012a. Sea surface temperature variability and sea-ice extent in the subarctic northwest Pacific during the past 15,000 years. Paleoceanography 27, PA3213.

McClymont, E.L., Martinez-Garcia, A., Rosell-Mele, A., 2007. Benefits of freeze-drying sediments for the analysis of total chlorins and alkenone concentrations in marine sediments. Organic Geochemistry 38, 1002-1007.

McCorkle, D., Corliss, B., Farnham, C., 1997. Vertical distributions and stable isotopic compositions of live (stained) benthic foraminifera from the North Carolina and California continental margins. Deep Sea Research Part I: Oceanographic Research Papers 44, 983-1024.

McCorkle, D.C., Keigwin, L.D., 1994. Depth profiles of δ 13C in bottom water and core top C. wuellerstorfi on the Ontong Java Plateau and Emperor Seamounts. Paleoceanography 9, 197.

McKay, J., Pedersen, T., Kienast, S., 2004. Organic carbon accumulation over the last 16 kyr off Vancouver Island, Canada: evidence for increased marine productivity during the deglacial. Quaternary Science Reviews 23, 261-281.

McKinney, C.R., McCrea, J.M., Epstein, S., Allen, H.A., Urey, H.C., 1950. Improvements in mass spectrometers for the measurement of small differences in isotope abundance ratios. Review of Scientific Instruments 21, 724.

McManus, J.F., Francois, R., Gherardi, J.-M., Keigwin, L.D., Brown-Leger, S., 2004a. Collapse and rapid resumption of Atlantic meridional circulation linked to deglacial climate changes. Nature 428, 834-837.

McManus, J.F., Francois, R., Gherardi, J.M., Keigwin, L.D., Brown-Leger, S., 2004b. Collapse and rapid resumption of Atlantic meridional circulation linked to deglacial climate changes. Nature 428, 834-837.

Menviel, L., Timmermann, A., Elison Timm, O., Mouchet, A., Abe-Ouchi, A., Chikamoto, M., Harada, N., Ohgaito, R., Okazaki, Y., 2011. Removing the North Pacific halocline: Effects on global climate, ocean circulation and the carbon cycle. Deep Sea Research Part II: Topical Studies in Oceanography.

Minoshima, K., Kawahata, H., Irino, T., Ikehara, K., Aoki, K., Uchida, M., Yoneda, M., Shibata, Y., 2007. Deep water ventilation in the northwestern North Pacific during the last deglaciation and the early Holocene (15-5 cal. kyr BP) based on AMS C-14 dating. Nuclear Instruments & Methods in Physics Research Section B-Beam Interactions with Materials and Atoms 259, 448-452.

Misumi, K., Tsumune, D., Yoshida, Y., Uchimoto, K., Nakamura, T., Nishioka, J., Mitsudera, H., Bryan, F.O., Lindsay, K., Moore, J.K., Doney, S.C., 2011. Mechanisms controlling dissolved iron distribution in the North Pacific: A model study. Journal of Geophysical Research 116.

Mix, A., Lund, D., Pisias, N., Boden, P., Bornmalm, L., Lyle, M., Pike, J., 1999. Rapid climate oscillations in the northeast Pacific during the last deglaciation reflect Northern and Southern Hemisphere sources. Mechanisms of Global Climate Change at Millennial Time Scales 112, 127–148.

Mix, A.C., Pisias, N.G., Zahn, R., Rugh, W., Lopez, C., Nelson, K., 1991. Carbon 13 in Pacific Deep and Intermediate Waters, 0-370 ka: Implications for Ocean Circulation and Pleistocene CO2. Paleoceanography 6, 205-226.

Mizuta, G., Ohshima, K., Fukamachi, Y., Itoh, M., Wakatsuchi, M., 2004. Winter mixed layer and its yearly variability under sea ice in the southwestern part of the Sea of Okhotsk. Continental Shelf Research 24, 643-657.

Monnin, E., Indermuhle, A., Dallenbach, A., Flueckiger, J., Stauffer, B., Stocker, T., Raynaud, D., Barnola, J.-M., 2001. Atmospheric CO2 concentrations over the last glacial termination. Science (New York, NY) 291, 112-114.

Monnin, E., Steig, E.J., Siegenthaler, U., Kawamura, K., Schwander, J., Stauffer, B., Stocker, T.F., Morse, D.L., Barnola, J.-M., Bellier, B., 2004. Evidence for substantial accumulation rate variability in Antarctica during the Holocene, through synchronization of CO2 in the Taylor Dome, Dome C and DML ice cores. Earth And Planetary Science Letters 224, 45-54.

Moore, P.G., 1985. Cibicides lobatulus(Protozoa: Foraminifera) epizoic on Astacilla longicornis(Crustacea: Isopoda) in the North Sea. Journal of Natural History 19, 129-133.

Morley, J., Heusser, L., Shackleton, N., 1991. Late Pleistocene/Holocene radiolarian and pollen records from sediments in the Sea of Okhotsk. Paleoceanography.

Müller, P.J., Schneider, R., 1993. An automated leaching method for the determination of opal in sediments and particulate matter. Deep Sea Research Part I: Oceanographic Research Papers 40, 425-444.

Murayama, M., Taira, A., Iwakura, H., Matsumoto, E., Nakamura, T., 1992. Northwest Pacific deep water ventilation rate during the past 35,000 years with the AMS 14C foraminifera ages, Summaries of Researchers Using AMS at Nagoya University (Nagoya University Center for Chronological Research), Nagoya, Japan (in Japanese with english abstract). 3, 114-121.

Nadeau, M.-J., Grootes, P.M., Schleicher, M., Hasselberg, P., Rieck, A., Bitterling, M., 1998. Sample throughput and data quality at the Leibniz-Labor AMS facility. Radiocarbon 40 (1), 239-245. 40, 239-245.

Nadeau, M.-J., Schleicher, M., Grootes, P.M., Erlenkeuser, H., Gottdang, A., Mous, D.J.W., Sarnthein, M., Willkomm, H., 1997. The Leibniz-Labor AMS facility at the Christian-Albrechts University, Kiel, Germany. Nuclear Instruments and Methods in Physics Research Section B 123, 22-30.

Nakamura, T., Awaji, T., 2004. Tidally induced diapycnal mixing in the Kuril Straits and its role in water transformation and transport: A three-dimensional nonhydrostatic model experiment. Journal Of Geophysical Research-Oceans 109, C09S07.

Nakamura, T., Toyoda, T., Ishikawa, Y., Awaji, T., 2004. Tidal mixing in the Kuril Straits and its impact on ventilation in the North Pacific Ocean. Journal Of Oceanography 60, 411-423.

Nakanowatari, T., Ohshima, K.I., Nagai, S., 2010. What determines the maximum sea ice extent in the Sea of Okhotsk? Importance of ocean thermal condition from the Pacific. Journal of Geophysical Research 115, C12031.

Nakanowatari, T., Ohshima, K.I., Wakatsuchi, M., 2007. Warming and oxygen decrease of intermediate water in the northwestern North Pacific, originating from the Sea of Okhotsk, 1955-2004. Geophysical Research Letters 34, L04602.

Nakatsuka, T., Fujimune, T., Yoshikawa, C., Noriki, S., Kawamura, K., Fukamachi, Y., Mizuta, G., Wakatsuchi, M., 2004a. Biogenic and lithogenic particle fluxes in the western region of the Sea of Okhotsk: Implications for lateral material transport and biological productivity. Journal Of Geophysical Research-Oceans 109, C09S13.

Nakatsuka, T., Handa, N., Harada, N., Sugimoto, T., Imaizumi, S., 1997. Origin and decomposition of sinking particulate organic matter in the deep water column inferred from the vertical distributions of its δ15N, δ13 and δ14. Deep Sea Research Part I: Oceanographic Research Papers 44, 1957-1979.

Nakatsuka, T., Nishioka, J., Shiraiwa, T., Project members, 2009. Biogeochemical linkage between Amur River basin and western subarctic Pacific by iron transport through Okhotsk Sea Intermediate Water: A new paradigm to explain changes in ocean primary productivity, PICES scientific report, p. 48.

Nakatsuka, T., Toda, M., Kawamura, K., Wakatsuchi, M., 2004b. Dissolved and particulate organic carbon in the Sea of Okhotsk: Transport from continental shelf to ocean interior. Journal Of Geophysical Research-Oceans 109, C09S14.

Nakatsuka, T., Yoshikawa, C., Toda, M., Kawamura, K., Wakatsuchi, M., 2002. An extremely turbid intermediate water in the Sea of Okhotsk: Implication for the transport of particulate organic matter in a seasonally ice-bound sea. Geophysical Research Letters 29, 1757.

Nimmergut, A., Abelmann, A., 2002. Spatial and seasonal changes of radiolarian standing stocks in the Sea of Okhotsk. Deep Sea Research Part I: Oceanographic Research Papers 49, 463-493.

Nishioka, J., Ono, T., Saito, H., Nakatsuka, T., Takeda, S., Yoshimura, T., Suzuki, K., Kuma, K., Nakabayashi, S., Tsumune, D., Mitsudera, H., Johnson, W.K., Tsuda, A., 2007. Iron supply to the western subarctic Pacific: Importance of iron export from the Sea of Okhotsk. Journal Of Geophysical Research-Oceans 112.

Nishioka, J., Ono, T., Saito, H., Sakaoka, K., Yoshimura, T., 2011. Oceanic iron supply mechanisms which support the spring diatom bloom in the Oyashio region, western subarctic Pacific. Journal Of Geophysical Research-Oceans 116, C02021.

Nishioka, J., Takeda, S., Kudo, I., Tsumune, D., Yoshimura, T., Kuma, K., Tsuda, A., 2003. Size-fractionated iron distributions and iron-limitation processes in the subarctic NW Pacific. Geophysical Research Letters 30, 14, 1730.

Nürnberg, D., Dethleff, D., Tiedemann, R., Kaiser, A., Gorbarenko, S.A., 2011. Okhotsk Sea ice coverage and Kamchatka glaciation over the last 350ka — Evidence from ice-rafted debris and planktonic δ18O. Palaeogeography Palaeoclimatology Palaeoecology 310, 191-205.

Nürnberg, D., Tiedemann, R., 2004. Environmental change in the Sea of Okhotsk during the last 1.1 million years. Paleoceanography 19, PA4011.

O' Brien, S.R., Mayewski, P.A., Meeker, L.D., Meese, D.A., Twickler, M.S., Whitlow, S.I., 1995. Complexity of Holocene Climate as Reconstructed from a Greenland Ice Core. Science (New York, NY) 270, 1962-1964.

Ogi, M., Tachibana, Y., 2006. Influence of the annual Arctic Oscillation on the negative correlation between Okhotsk Sea ice and Amur River discharge. Geophysical Research Letters 33, L08709.

Ogi, M., Tachibana, Y., Nishio, F., Danchenkov, M., 2001. Does the fresh water supply from the Amur river flowing into the sea of Okhotsk affect sea ice formation? Journal Of The Meteorological Society Of Japan 79, 123-129.

Ogi, M., Tachibana, Y., Yamazaki, K., 2004a. The connectivity of the winter North Atlantic Oscillation (NAO) and the summer Okhotsk High. Journal Of The Meteorological Society Of Japan 82, 905-913.

Ogi, M., Yamazaki, K., Tachibana, Y., 2004b. The summertime annular mode in the Northern Hemisphere and its linkage to the winter mode. Journal of Geophysical Research-Atmospheres 109, D20114.

Ohkouchi, N., Kawahata, H., Murayama, M., Okada, M., Nakamura, T., Taira, A., 1994. Was Deep-Water Formed in the North Pacific During The Late Quaternary - Cadmium Evidence From the Northwest Pacific. Earth And Planetary Science Letters 124, 185-194.

Ohkushi, K., 2004. Glacial intermediate water ventilation in the northwestern Pacific based on AMS radiocarbon dating. Nuclear Instruments & Methods In Physics Research Section B: Beam Interactions With Materials And Atoms 223-224, 460-465.

Ohkushi, K., Itaki, T., Nemoto, N., 2003. Last Glacial-Holocene change in intermediate-water ventilation in the Northwestern Pacific. Quaternary Science Reviews 22, 1477-1484.

Ohshima, K., Mizuta, G., Itoh, M., Fukamachi, Y., Watanabe, T., Nabae, Y., Suehiro, K., Wakatsuchi, M., 2001. Winter oceanographic conditions in the southwestern part of the Okhotsk Sea and their relation to sea ice. Journal Of Oceanography 57, 451-460.

Ohshima, K., Simizu, D., Itoh, M., Mizuta, G., Fukamachi, Y., Riser, S., Wakatsuchi, M., 2004. Sverdrup balance and the cyclonic gyre in the Sea of Okhotsk. Journal Of Physical Oceanography 34, 513-525.

Ohshima, K., Wakatsuchi, M., Fukamachi, Y., Mizuta, G., 2002. Near-surface circulation and tidal currents of the Okhotsk Sea observed with satellite-tracked drifters. Journal Of Geophysical Research-Oceans 107, 3195.

Ohshima, K.I., Nakanowatari, T., Riser, S., Wakatsuchi, M., 2010. Seasonal variation in the in- and outflow of the Okhotsk Sea with the North Pacific. Deep Sea Research Part II: Topical Studies in Oceanography 57, 1247-1256.

Okazaki, Y., Sagawa, T., Asahi, H., Horikawa, K., Onodera, J., 2012. Ventilation changes in the western North Pacific since the last glacial period. Climate Of The Past 8, 17-24.

Okazaki, Y., Seki, O., Nakatsuka, T., Sakamoto, T., Ikehara, M., Takahashi, K., 2006. Cycladophora davisiana (Radiolaria) in the Okhotsk Sea: A key for reconstructing glacial ocean conditions. Journal Of Oceanography 62, 639-648.

Okazaki, Y., Takahashi, K., Itaki, T., Kawasaki, Y., 2004. Comparison of radiolarian vertical distributions in the Okhotsk Sea near the Kuril islands and in the northwestern North Pacific off Hokkaido island. Marine Micropaleontology 51, 257-284.

Okazaki, Y., Takahashi, K., Nakatsuka, T., Honda, M.C., 2003. The production scheme of Cycladophora davisiana (Radiolaria) in the Okhotsk Sea and the northwestern North Pacific: implication for the paleoceanographic conditions during the glacials in the high latitude oceans. Geophysical Research Letters 30, 1939-.

Okazaki, Y., Timmermann, A., Menviel, L., Harada, N., Abe-Ouchi, A., Chikamoto, M.O., Mouchet, A., Asahi, H., 2010a. Deepwater formation in the North Pacific during the Last Glacial Termination. Science (New York, NY) 329, 200-204.

Overland, J., Adams, J., Bond, N., 1999. Decadal variability of the Aleutian low and its relation to high-latitude circulation. Journal Of Climate 12, 1542-1548.

Paillard, D., Labeyrie, L., Yiou, P., 1996. Macintosh program performs time-series analysis. Eos Transactions AGU 77, 379.

Pavlova, G.Y., Tishchenko, P.Y., Nedashkovskii, A.P., 2008. Distribution of alkalinity and dissolved calcium in the Sea of Okhotsk. Okeanologiya 48, 23-32.

Pena, L.D., 2005. Identification and removal of Mn-Mg-rich contaminant phases on foraminiferal tests: Implications for Mg/Ca past temperature reconstructions. Geochemistry Geophysics Geosystems 6, 25.

Pena, L.D., Cacho, I., Calvo, E., Pelejero, C., Eggins, S., Sadekov, A., 2008. Characterization of contaminant phases in foraminifera carbonates by electron microprobe mapping. Geochemistry Geophysics Geosystems 9, Q07012.

Peterse, F., Prins, M.A., Beets, C.J., Troelstra, S.R., Zheng, H., Gu, Z., Schouten, S., Damste, J.S.S., 2011. Decoupled warming and monsoon precipitation in East Asia over the last deglaciation. Earth And Planetary Science Letters 301, 256-264.

Petit, J., Jouzel, J., Raynaud, D., Barkov, N., Barnola, J.-M., Basile, I., Bender, M., Chappellaz, J., Davis, M., Delaygue, G., 1999. Climate and atmospheric history of the past 420,000 years from the Vostok ice core, Antarctica. Nature 399, 429-436.

Pickart, R.S., Moore, G.W.K., Macdonald, A.M., Renfrew, I.A., Walsh, J.E., Kessler, W.S., 2009. Seasonal Evolution of Aleutian Low Pressure Systems: Implications for the North Pacific Subpolar Circulation. Journal Of Physical Oceanography 39, 1317-1339.

Piotrowski, A.M., Goldstein, S.L., Hemming, S.R., Fairbanks, R.G., 2004. Intensification and variability of ocean thermohaline circulation through the last deglaciation. Earth And Planetary Science Letters 225, 205-220.

Rasmussen, S., Andersen, K., Svensson, A., Steffensen, J., Vinther, B., Clausen, H., Siggaard-Andersen, M., Johnsen, S., Larsen, L., Dahl-Jensen, D., Bigler, M., Rothlisberger, R., Fischer, H., Goto-Azuma, K., Hansson, M., Ruth, U., 2006a. A new Greenland ice core chronology for the last glacial termination. Journal of Geophysical Research - Atmospheres 111, D06102.

Rasmussen, S.O., Andersen, K.K., Svensson, A.M., Steffensen, J.P., Vinther, B.M., Clausen, H.B., Siggaard-Andersen, M.L., Johnsen, S.J., Larsen, L.B., Dahl-Jensen, D., Bigler, M., Rothlisberger, R., Fischer, H., Goto-Azuma, K., Hansson, M.E., Ruth, U., 2006b. A new Greenland ice core chronology for the last glacial termination. Journal of Geophysical Research-Atmospheres 111.

Rasmussen, S.O., Seierstad, I.K., Andersen, K.K., Bigler, M., Dahl-Jensen, D., Johnsen, S.J., 2008. Synchronization of the NGRIP, GRIP, and GISP2 ice cores across MIS 2 and palaeoclimatic implications. Quaternary Science Reviews 27, 18-28.

Reid, J.L., 1965. Intermediate Waters of the Pacific Ocean, The Johns Hopkins Oceanographic Studies. The Johns Hopkins Press, Baltimore, pp. 1-85.

Reimer, P.J., Baillie, M.G.L., Bard, E., Bayliss, A., Beck, J.W., Blackwell, P.G., Ramsey, C.B., Buck, C.E., Burr, G.S., Edwards, R.L., Friedrich, M., Grootes, P.M., Guilderson, T.P., Hajdas, I., Heaton, T.J., Hogg, A.G., Hughen, K.A., Kaiser, K.F., Kromer, B., McCormac, F.G., Manning, S.W., Reimer, R.W., Richards, D.A., Southon, J.R., Talamo, S., Turney, C.S.M., van der Plicht, J., Weyhenmeye, C.E., 2009a. INTCAL09 and MARINE09 Radiocarbon Age Calibration Curves , 0-50,000 Years cal. BP. Radiocarbon 51, 1111-1150.

Rella, S.F., Tada, R., Nagashima, K., Ikehara, M., Itaki, T., Ohkushi, K., Sakamoto, T., Harada, N., Uchida, M., 2012. Abrupt changes of intermediate water properties on the northeastern slope of the Bering Sea during the last glacial and deglacial period. Paleoceanography 27.

Richter, T.O., van der Gaast, S., Koster, B., Vaars, A., Gieles, R., de Stigter, H.C., De Haas, H., van Weering, T.C.E., 2006. The Avaatech XRF Core Scanner: technical description and applications to NE Atlantic sediments, In: Rothwell, R.G. (Ed.), New Techniques n Sediment Core Analysis. Geological Society, London, Special Publications. Geological Society, Special Publications, London, pp. 39-50.

Riethdorf, J.-R., Max, L., Nürnberg, D., Lembke-Jene, L., Tiedemann, R., 2013. Deglacial history of (sub) sea surface temperatures and salinity in the subarctic NW Pacific: Implications for upper-ocean stratification. Paleoceanography.

Riethdorf, J.R., 2012. Late Pleistocene to Holocene Changes in Upper-Ocean Stratification and its Impact on Marine Productivity, Sea Surface Temperatures, and Salinity in the Subarctic Northwest Pacific, Mathematisch-Naturwissenschaftliche Fakultät. Christian-Albrechts-Universität zu Kiel, Kiel, p. 181.

Rodionov, S.N., Bond, N.A., Overland, J.E., 2007. The Aleutian Low, storm tracks, and winter climate variability in the Bering Sea, Deep-Sea Research Part Ii-Topical Studies in Oceanography, pp. 2560-2577.

Rogachev, K., 2000. Recent variability in the Pacific western subarctic boundary currents and Sea of Okhotsk. Progress In Oceanography 47, 299-336.

Rogachev, K.A., C Carmack, E., Salomatin, A.S., Alexanina, M.G., 2001. Lunar fortnightly modulation of tidal mixing near Kashevarov Bank, Sea of Okhotsk, and its impacts on biota and sea ice. Progress In Oceanography 49, 373-390.

Röhl, U., Abrams, L.J., 2000. High-resolution, downhole, and nondestructive core measurements from Sites 999 and 1001 in the Caribbean Sea: application to the Late Paleocene Thermal Maximum, In: Leckie, R.M., Sigurdsson, H., Acton, G.D., Draper, G. (Eds.), Proceedings of the Ocean Drilling Program, Scientific Results, College Station, TX (Ocean Drilling Program). Ocean Drilling Program, College Station, TX.

Rohling, E.J., Grant, K., Bolshaw, M., Roberts, A.P., Siddall, M., Hemleben, C., Kucera, M., 2009. Antarctic temperature and global sea level closely coupled over the past five glacial cycles. Nature Geoscience 2, 500-504.

Rothwell, R.G., Rack, F.R., Rothwell, R.G., 2006. New techniques in sediment core analysis, Geological Society of London, Special Publications. The Geological Society of London, London, pp. 1-29.

Saenko, O.A., Schmittner, A., Weaver, A.J., 2004. The Atlantic-Pacific seesaw. Journal of Climate 17, 2033-2038.

Sagawa, T., Ikehara, K., 2008a. Intermediate water ventilation change in the subarctic northwest Pacific during the last deglaciation. Geophysical Research Letters 35, L24702.

Saito, H., Suga, T., Hanawa, K., Shikama, N., 2011. The Transition Region Mode Water of the North Pacific and Its Rapid Modification. Journal Of Physical Oceanography 41, 1639-1658.

Sakaguchi, Y., 1992. Cooling Around 9000 BP Caused by Permafrost Melt Water Burst. Bull. Dept. Geogr. Univ. Tokyo 24, 1-6.

Sakamoto, T., Ikehara, M., Aoki, K., Iijima, K., Kimura, N., Nakatsuka, T., Wakatsuchi, M., 2005. Ice-rafted debris (IRD)-based sea-ice expansion events during the past 100kyrs in the Okhotsk Sea. Deep Sea Research Part II: Topical Studies in Oceanography 52, 2275-2301.

Sakamoto, T., Ikehara, M., Uchida, M., Aoki, K., Shibata, Y., Kanamatsu, T., Harada, N., Iijima, K., Katsuki, K., Asahi, H., 2006. Millennial-scale variations of sea-ice expansion in the southwestern part of the Okhotsk Sea during the past 120 kyr: Age model and ice-rafted debris in IMAGES Core MD01-2412. Global And Planetary Change 53, 58-77.

Sarmiento, J.L., Gruber, N., Brzezinski, M.A., Dunne, J.P., 2004. High-latitude controls of thermocline nutrients and low latitude biological productivity. Nature 427, 56-60.

Sarnthein, M., Gebhardt, H., Kiefer, T., Kucera, M., Cook, M., Erlenkeuser, H., 2004. Mid Holocene origin of the sea-surface salinity low in the subarctic North Pacific. Quaternary Sci Rev 23, 2089-2099.

Sarnthein, M., Grootes, P.M., Kennett, J.P., Nadeau, M., Schmittner, A., Chiang, J., Hemming, S., 2007. 14C Reservoir Ages Show Deglacial Changes in Ocean Currents and Carbon Cycle, Ocean Circulation: Mechanisms and Impacts, AGU Geophysical Monograph Series. American Geophysical Union, pp. 175-196.

Sarnthein, M., Kiefer, T., Grootes, P., Elderfield, H., Erlenkeuser, H., 2006. Warmings in the far northwestern Pacific promoted pre-Clovis immigration to America during Heinrich event 1. Geology 34, 141-144.

Sarnthein, M., Schneider, B., Grootes, P.M., 2013. Peak Glacial C-14 Ventilation Ages Suggest Major Draw-Down of Carbon into the Abyssal Ocean. Climate of the Past Discussions 9, 925-965.

Sarnthein, M., Stattegger, K., Dreger, D., Erlenkeuser, H., Grootes, P., Haupt, B., Jung, S., Kiefer, T., Kuhnt, W., Pflaumann, U., Sarnthein, M., Stattegger, K., Dreger, D., Erlenkeuser, H., Grootes, P., Haupt, B., Jung, S., Kiefer, T., Kuhnt, W., Pflaumann, U., Schafer-Neth, C., Schulz, H., Schulz, M., Seidov, D., Simstich, J., van Kreveld, S., Vogelsang, E., Volker, A., Weinelt, M., 2000. Fundamental Modes and Abrupt Changes in North Atlantic Circulation and Climate over the last 60 ky – Concepts, Reconstruction and Numerical Modeling, In: Schäfer, P., Ritzrau, W., Schluter, M., Thiede, J. (Eds.), The Northern North Atlantic: A Changing Environment. Sringer, Berlin.

Sarnthein, M., Winn, K., Jung, S.J.A., Duplessy, J.-C., Labeyrie, L., Erlenkeuser, H., Ganssen, G., 1994. Changes in East Atlantic Deepwater Circulation over the last 30,000 years: Eight time slice reconstructions. Paleoceanography 9, 209-267.

Schlitzer, R., 2002. Interactive analysis and visualization of geoscience data with Ocean Data View. Computers & Geosciences 28, 1211-1218.

Schmittner, A., Galbraith, E.D., Hostetler, S.W., Pedersen, T.F., Zhang, R., 2007. Large fluctuations of dissolved oxygen in the Indian and Pacific oceans during Dansgaard-Oeschger oscillations caused by variations of North Atlantic Deep Water subduction. Paleoceanography 22.

Schmitz, W.J., 1996. On the World Ocean Circulation: Volume I, Some Global Features / North Atlantic Circulation, Woods Hole Oceanographic Institution, Technical Report. Woods Hole Oceanographic Institution, Woods Hole, MA, pp. WHOI-96-03, 148 pp.

Schubert, C., 2005. Chlorin Index: A new parameter for organic matter freshness in sediments. Geochemistry Geophysics Geosystems 6, -.

Schweizer, M., Pawlowski, J., Kouwenhoven, T., van der Zwaan, B., 2009. Molecular Phylogeny of Common Cibicidids and Related Rotaliida (Foraminifera) Based on Small Subunit Rdna Sequences. J Foramin Res 39, 300-315.

Scott, D.B., Takayanagi, Y., Hasegawa, S., Saito, T., 2000. Illustration and taxonomic reevaluation of Neogene foraminifera described from Japan. Palaeontologia Electronica 3, 41.

Seki, O., 2005. Decreased surface salinity in the Sea of Okhotsk during the last glacial period estimated from alkenones. Geophysical Research Letters 32, 4.

Seki, O., Harada, N., Sato, M., Kawamura, K., Ijiri, A., Nakatsuka, T., 2012. Assessment for paleoclimatic utility of terrestrial biomarker records in the Okhotsk Sea sediments. Deep Sea Research Part II: Topical Studies in Oceanography 61-64, 85-92.

Seki, O., Ikehara, M., Kawamura, K., Nakatsuka, T., Ohnishi, K., Wakatsuchi, M., Narita, H., Sakamoto, T., 2004. Reconstruction of paleoproductivity in the Sea of Okhotsk over the last 30 kyr. Paleoceanography 19, PA1016.

Seki, O., Kawamura, K., Nakatsuka, T., Ohnishi, K., Ikehara, M., Wakatsuchi, M., 2003. Sediment core profiles of long-chain n-alkanes in the Sea of Okhotsk: Enhanced transport of terrestrial organic matter from the last deglaciation to the early Holocene. Geophysical Research Letters 30, 1001.

Seki, O., Meyers, P.A., Kawamura, K., Zheng, Y., Zhou, W., 2009a. Hydrogen isotopic ratios of plant wax n-alkanes in a peat bog deposited in northeast China during the last 16 kyr. Organic Geochemistry 40, 671-677.

Seki, O., Sakamoto, T., Sakai, S., Schouten, S., Hopmans, E.C., Damste, J.S.S., Pancost, R.D., 2009b. Large changes in seasonal sea ice distribution and productivity in the Sea of Okhotsk during the deglaciations. Geochemistry Geophysics Geosystems 10, Q10007.

Seki, O., Yoshikawa, C., Nakatsuka, T., Kawamura, K., Wakatsuchi, M., 2006. Fluxes, source and transport of organic matter in the western Sea of Okhotsk: Stable carbon isotopic ratios of n-alkanes and total organic carbon. Deep Sea Research Part I: Oceanographic Research Papers 53, 253-270.

Shackleton, N., Fairbanks, R., Chiu, T., Parrenin, F., 2004. Absolute calibration of the Greenland time scale: implications for Antarctic time scales and for Delta C-14. Quaternary Science Reviews 23, 1513-1522.

Shcherbina, A., Talley, L., Rudnick, D., 2003. Direct observations of North Pacific ventilation: Brine rejection in the Okhotsk Sea. Science (New York, NY) 302, 1952-1955.

Shcherbina, A., Talley, L., Rudnick, D., 2004a. Dense water formation on the northwestern shelf of the Okhotsk Sea: 1. Direct observations of brine rejection. Journal Of Geophysical Research-Oceans 109, C09S08.

Shcherbina, A., Talley, L., Rudnick, D., 2004b. Dense water formation on the northwestern shelf of the Okhotsk Sea: 2. Quantifying the transports. Journal Of Geophysical Research-Oceans 109, C09S09.

Shcherbina, A.Y., Gregg, M.C., Alford, M.H., Harcourt, R.R., 2009. Characterizing Thermohaline Intrusions in the North Pacific Subtropical Frontal Zone. Journal Of Physical Oceanography 39, 2735-2756.

Shimizu, Y., IWAO, T., Yasuda, I., Ito, S., Watanabe, T., Uehara, K., Shikama, N., Nakano, T., 2004. Formation process of North Pacific intermediate water revealed by profiling floats set to drift on 26.7 sigma(theta) isopycnal surface. Journal Of Oceanography 60, 453-462.

Shirasawa, K., Lepparanta, M., Saloranta, T., Kawamura, T., Polomoshnov, A., Surkov, G., 2005. The thickness of coastal fast ice in the Sea of Okhotsk. Cold Regions Science And Technology 42, 25-40.

Sigman, D., Boyle, E., 2000. Glacial/interglacial variations in atmospheric carbon dioxide. Nature 407, 859-869.

Sigman, D.M., Hain, M.P., Haug, G.H., 2010. The polar ocean and glacial cycles in atmospheric CO(2) concentration. Nature 466, 47-55.

Skinner, L.C., 2008. Revisiting the absolute calibration of the Greenland ice-core age-scales*. Climate Of The Past 4, 295-302.

Sloyan, B.M., Talley, L.D., Chereskin, T.K., Fine, R., Holte, J., 2010. Antarctic Intermediate Water and Subantarctic Mode Water Formation in the Southeast Pacific: The Role of Turbulent Mixing. Journal Of Physical Oceanography 40, 1558-1574.

Sorokin, Y.I., Sorokin, P.Y., 1999. Production in the Sea of Okhotsk. Journal of Plankton Research 21, 201-230.

Southon, J., Noronha, A.L., Cheng, H., Edwards, R.L., Wang, Y., 2012. A high-resolution record of atmospheric 14C based on Hulu Cave speleothem H82, Quaternary Science Reviews, pp. 32-41.

Stommel, H., 1961. Thermohaline Convection with Two Stable Regimes of Flow. Tellus 13, 224-230.

Stuiver, M., 1980. Workshop on C-14 Data Reporting. Radiocarbon 22, 964-966.

Stuiver, M., Polach, H., 1977a. Discussion: Reporting of 14C Data. Radiocarbon 19, 355-363.

Stuiver, M., Polach, H.A., 1977b. Reporting of C-14 Data - Discussion. Radiocarbon 19, 355-363.

Stuiver, M., Reimer, P.J., 1993a Extended 14C database and revised CALIB radiocarbon calibration program. Radiocarbon 35, 215-230.

Svavarsson, J., Davidsdottir, B., 1995. Cibicides spp. (Protozoa, Foraminifera) as epizoites on the Arctic antenna-brooding Arcturus baffini (Crustacea, Isopoda, Valvifera). Polar Biology 15, 569-574.

Svensson, A., Andersen, K.K., Bigler, M., Clausen, H.B., Dahl-Jensen, D., Davies, S.M., Johnsen, S.J., Muscheler, R., Parrenin, F., Rasmussen, S.O., Roethlisberger, R., Seierstad, I., Steffensen, J.P., Vinther, B.M., 2008. A 60 000 year Greenland stratigraphic ice core chronology. Climate Of The Past 4, 47-57.

Tachibana, Y., Iwamoto, T., Ogi, M., Watanabe, Y., 2004. Abnormal meridional temperature gradient and its relation to the Okhotsk high. Journal Of The Meteorological Society Of Japan 82, 1399-1415.

Tachibana, Y., Oshima, K., Ogi, M., 2008. Seasonal and interannual variations of Amur River discharge and their relationships to large-scale atmospheric patterns and moisture fluxes. Journal of Geophysical Research-Atmospheres 113, D16102.

Tadokoro, K., Ono, T., Yasuda, I., Osafune, S., Shiomoto, A., Sugisaki, H., 2009. Possible mechanisms of decadal−scale variation in PO 4concentration in the western North Pacific. Geophysical Research Letters 36, L08606-.

Takahashi, K., 1998. The Bering and Okhotsk Seas: modern and past paleoceanographic changes and gateway impact. Journal of Asian Earth Sciences 16, 49-58.

Takahashi, T., Sutherland, S.C., Wanninkhof, R., Sweeney, C., Feely, R.A., Chipman, D.W., Hales, B., Friederich, G., Chavez, F., Sabine, C., Watson, A., Bakker, D.C.E., Schuster, U., Metzl, N., Yoshikawa-Inoue, H., Ishii, M., Midorikawa, T., Nojiri, Y., Körtzinger, A., Steinhoff, T., Hoppema, M., Olafsson, J., Arnarson, T.S., Tilbrook, B., Johannessen, T., Olsen, A., Bellerby, R., Wong, C.S., Delille, B., Bates, N.R., De Baar, H.J.W., 2009. Climatological mean and decadal change in surface ocean pCO2, and net sea–air CO2 flux over the global oceans. Deep Sea Research Part II: Topical Studies in Oceanography 56, 554-577.

Takeda, S., 2011. Iron and Phytoplankton Growth in the Subarctic North Pacific. Aqua-BioScience Monographs 4, 41-93.

Talley, L., Nagata, Y., Fujimura, M., Iwao, T., Kono, T., Inagake, D., Hirai, M., Okuda, K., 1995. North Pacific Intermediate Water in the Kuroshio-Oyashio Mixed Water Region. Journal Of Physical Oceanography 25, 475-501.

Talley, L.D., 1985. Ventilation of the Sub-Tropical North Pacific - the Shallow Salinity Minimum. Journal Of Physical Oceanography 15, 633-649.

Talley, L.D., 1993. Distribution and formation of North Pacific intermediate water. Journal Of Physical Oceanography 23, 517-537.

Talley, L.D., 2013. Closure of the global overturning circulation through the Indian, Pacific, and Southern Oceans: Schematics and transports. Oceanography 26, 80-97.

Talley, L.D., Roemmich, D., 1991. A TRIBUTE TO REID,JOSEPH,L. IN RECOGNITION OF 40 YEARS OF CONTRIBUTIONS TO OCEANOGRAPHY. Deep-Sea Research Part a-Oceanographic Research Papers 38, R7-R11.

Tanaka, S., Takahashi, K., 2005. Late Quaternary paleoceanographic changes in the Bering Sea and the western subarctic Pacific based on radiolarian assemblages. Deep-Sea Res. Part II-Top. Stud. Oceanogr. 52, 2131-2149.

Telford, R.J., Heegaard, E., Birks, H.J.B., 2004. All age—depth models are wrong: but how badly? Quaternary Science Reviews 23, 1-5.

Ternois, Y., Kawamura, K., Keigwin, L., Ohkouchi, N., Nakatsuka, T., 2001. A biomarker approach for assessing marine and terrigenous inputs to the sediments of Sea of Okhotsk for the last 27,000 years. Geochimica Et Cosmochimica Acta 65, 791-802.

Timmermann, A., Krebs, U., Justino, F., Goosse, H., Ivanochko, T., 2005. Mechanisms for millennial-scale global synchronization during the last glacial period. Paleoceanography 20.

Tjallingii, R., 2006. Application and quality of X-ray fluorescence core scanning in reconstructing late Pleistocene NW African continental margin sedimentation patterns and paleoclimate variations, In: Wefer, G., Stein, R. (Eds.), Fachbereich Geowissenschaften. Universität Bremen, Bremen, p. 114.

Tjallingii, R., Roehl, U., Kolling, M., Bickert, T., 2007. Influence of the water content on X-ray fluorescence core-scanning measurements in soft marine sediments. Geochem. Geophys. Geosyst. 8, Q02004.

Tomczak, M., Godfrey, J.S., 2003. Regional Oceanography: an Introduction, 2nd ed. Daya Publishing House, Delhi.

Toyama, K., Suga, T., 2010. Vertical structure of North Pacific mode waters. Deep Sea Research Part II: Topical Studies in Oceanography 57, 1152-1160.

Ueno, H., Yasuda, I., 2003. Intermediate water circulation in the North Pacific subarctic and northern subtropical regions. Journal Of Geophysical Research-Oceans 108, 3348.

Vaks, A., Gutareva, O.S., Breitenbach, S.F.M., Avirmed, E., Mason, A.J., Thomas, A.L., Osinzev, A.V., Kononov, A.M., Henderson, G.M., 2013. Speleothems Reveal 500,000-Year History of Siberian Permafrost. Science (New York, NY).

Van Geen, A., Zheng, Y., Bernhard, J., Cannariato, K., Carriquiry, J., Dean, W., Eakins, B., Ortiz, J., Pike, J., 2003. On the preservation of laminated sediments along the western margin of North America. Paleoceanography 18, 1098.

van Morkhoven, F.P.C.M., Berggren, W.A., Edwards, A.S., 1986. Cenozoic Cosmopolitan Dee-Water Benthic Foraminifera. Elf Aquitaine, Pau.

Van Scoy, K., Olson, D.B., Fine, R.A., 1991. Ventilation of North Pacific Intermediate Water: the role of the Alaskan Gyre. Journal of Geophysical Research 96, 16801-16810.

Verardo, D.J., Froelich, P.N., McIntyre, A., 1990. Determination of organic carbon and nitrogen in marine sediments using the Carlo Erba NA-1500 analyzer. Deep Sea Research Part A. Oceanographic Research Papers 37, 157-165.

Wang, Y., Cheng, H., Edwards, R., He, Y., Kong, X., An, Z., Wu, J., Kelly, M., Dykoski, C., Li, X., 2005. The Holocene Asian monsoon: Links to solar changes and North Atlantic climate. Science (New York, NY) 308, 854-857.

Wang, Y., Cheng, H., Edwards, R.L., Kong, X., Shao, X., Chen, S., Wu, J., Jiang, X., Wang, X., An, Z., 2008. Millennial- and orbital-scale changes in the East Asian monsoon over the past 224,000|[thinsp]|years. Nature 451, 1090-1093.

Warren, B., 1983. Why is no deep water formed in the North Pacific? Journal of Marine Research 41, 327-347.

Watanabe, T., Wakatsuchi, M., 1998. Formation of 26.8–26.9 σ θwater in the Kuril Basin of the Sea of Okhotsk as a possible origin of North Pacific Intermediate Water. Journal of Geophysical Research 103, 2849-2865.

Weltje, G.J., Tjallingii, R., 2008. Calibration of XRF core scanners for quantitative geochemical logging of sediment cores: Theory and application. Earth And Planetary Science Letters 274, 423-438.

Wong, C.S., Matear, R.J., Freeland, H.J., Whitney, F.A., Bychkov, A.S., 1998. WOCE line P1W in the Sea of Okhotsk 2. CFCs and the formation rate of intermediate water. Journal of Geophysical Research 103, 15625-15642.

Wu, B., Wang, J., 2002. Winter Arctic Oscillation, Siberian High and East Asian winter monsoon. Geophysical Research Letters 29, 1897.

Yagi, M., Yasuda, I., 2012. Deep intense vertical mixing in the Busso'l Strait. Geophysical Research Letters 39, L01602-.

Yamamoto, M., Suemune, R., Oba, T., 2005. Equatorward shift of the subarctic boundary in the northwestern Pacific during the last deglaciation. Geophysical Research Letters 32, L05609.

Yamamoto, M., Tanaka, N., Tsunogai, S., 2001. Okhotsk Sea intermediate water formation deduced from oxygen isotope systematics. Journal Of Geophysical Research-Oceans 106, 31075-31084.

Yamamoto, M., Watanabe, S., Tsunogai, S., Wakatsuchi, M., 2002. Effects of sea ice formation and diapycnal mixing on the Okhotsk Sea intermediate water clarified with oxygen isotopes. Deep Sea Research Part I: Oceanographic Research Papers 49, 1165-1174.

Yamashita, Y., Cory, R.M., Nishioka, J., Kuma, K., Tanoue, E., Jaffé, R., 2010. Fluorescence characteristics of dissolved organic matter in the deep waters of the Okhotsk Sea and the northwestern North Pacific Ocean. Deep Sea Research Part II: Topical Studies in Oceanography 57, 1478-1485.

Yasuda, I., 1997. The origin of the North Pacific Intermediate Water. Journal of Geophysical Research 102, 893-909.

Yasuda, I., Hiroe, Y., Komatsu, K., Kawasaki, K., Joyce, T., Bahr, F., Kawasaki, Y., 2001. Hydrographic structure and transport of the Oyashio south of Hokkaido and the formation of North Pacific Intermediate Water. Journal Of Geophysical Research-Oceans 106, 6931-6942.

Yasuda, I., OKUDA, K., Shimizu, Y., 1996. Distribution and modification of North Pacific Intermediate Water in the Kuroshio-Oyashio interfrontal zone. Journal Of Physical Oceanography 26, 448-465.

Yoshikawa, C., Nakatsuka, T., Wakatsuchi, M., 2006. Distribution of N* in the Sea of Okhotsk and its use as a biogeochemical tracer of the Okhotsk Sea Intermediate Water formation process. Journal Of Marine Systems 63, 49-62.

Zahn, R., Pedersen, T.F., Bornhold, B.D., Mix, A.C., 1991. Water Mass Conversion in the Glacial Subarctic Pacific (54ºN, 148ºW): Physical Constraints and the Benthic-Planktonic Stable Isotope Record. Paleoceanography 6, 543-560.

Zenk, W., Siedler, G., Ishida, A., Holfort, J., Kashino, Y., Kuroda, Y., Miyama, T., Muller, T., 2005. Pathways and variability of the Antarctic Intermediate Water in the western equatorial Pacific Ocean. Progress In Oceanography 67, 245-281.

Zheng, Y., Van Geen, A., Anderson, R., Gardner, J., Dean, W., 2000. Intensification of the northeast Pacific oxygen minimum zone during the Bolling-Allerod warm period. Paleoceanography 15, 528-536.

Appendix: Additional Publications Related to this Thesis

Additional co-authored publications in international peer-reviewed journals are listed here, which contain some of my data, analytical and interpretational work carried out within the framework of this thesis. These articles, however, are not listed as part of the results chapters due to my lesser involvement in the publications. Only bibliographical reference and the abstracts are thus here given for information; the reader is kindly referred to the original publications for further reading.

1. Living benthic foraminifera of the Okhotsk Sea: Faunal composition, standing stocks and microhabitats

Natalia Bubenshchikova [a,*], Dirk Nürnberg[b], Lester Lembke-Jene[c], Galina Pavlova[d]

a P.P.Shirshov Institute of Oceanology, Nakhimovski pr. 36, Moscow 117997, Russia

b Leibniz Institute for Marine Sciences, Wischhofstr. 1-3, Kiel 24148, Germany

c Alfred Wegener Institute for Polar and Marine Research, Am Alten Hafen 26, D-27568, Bremerhaven, Germany

d V.I.Il'ichev Pacific Oceanological Institute, 43 Baltiyskaya St., Vladivostok 690041, Russia

Published in: Marine Micropaleontology (2008) vol. 69, pp. 314-333.

Abstract

Live (Rose Bengal stained) benthic foraminifera were investigated in surface sediment samples from the Okhotsk Sea to reveal the relationship between faunal characteristics and environmental parameters. Live benthic foraminifera were quantified in the size fraction >125 μm in the upper 8 cm of replicate sediment cores, recovered with a multicorer at five stations along the Sakhalin margin, and at three stations on the southwestern Kamchatka slope. The stations are from water depths between 625 to 1752 m, located close or within the present Okhotsk Sea oxygen minimum zone, with oxygen levels between 0.3 and 1.5 ml l^{-1}. At the high-productivity and ice-free Kamchatka stations, live benthic foraminifera are characterized by maximal standing stocks (about 1700-3700 individuals per 50 cm^2), strong dominance of calcareous species (up to 87-91% of total live faunas), and maximal habitat depths (down to 5.2-6.7 cm depth). Vertical distributions of total faunal abundances exhibit a clear subsurface maximum in sediments. At the Sakhalin stations, which are seasonally ice-covered

and less productive, live benthic foraminifera show lower standing stocks (about 200-1100 individuals per 50 cm2), lower abundance of calcareous species (10-64% of total live faunas), and shallower habitat depths (down to 2.5-5.4 cm depth). Faunal vertical distributions are characterized by maximum in the uppermost surface sediments. It is suggested that 1) lower and strongly seasonal organic matter flux, caused by the seasonal sea ice cover and seasonal upwelling, 2) lower bottom water oxygenation (0.3-1.1 ml l^{-1}), and 3) more pronounced influence of carbonate-undersaturated bottom water along the Sakhalin margin are the main factors responsible for the observed faunal differences. According to species downcore distributions and average living depths, common calcareous species were identified as preferentially shallow, intermediate and deep infaunal. Foraminiferal microhabitat occupation correlates with the organic matter flux and the depth of the oxygenated layer in sediments.

2. Variations of the Oxygen Minimum Zone of the Okhotsk Sea during the Last 50 ka as Indicated by Benthic Foraminiferal and Biogeochemical Data

N. V. Bubenshchikova[a], D. Nürnberg[b], S. A. Gorbarenko[c], and L. Lembke-Jene[d]

a P.P. Shirshov Institute of Oceanology, Nakhimovski pr. 36, Moscow, 117997 Russia

b Leibniz Institute for Marine Sciences, Wischhofstr. 1 3, Kiel 24148, Germany

c V.I. Ilichev Pacific Oceanological Institute, RAS, 43 Baltiyskaya St., Vladivostok, 690041 Russia

d Alfred Wegener Institute for Polar and Marine Research, Columbusstrasse D 27568, Bremerhaven, Germany

Published in: Oceanology (2010) Vol. 50, No. 1, pp. 93–106.

Abstract

Benthic foraminiferal and sediment biogeochemical data (total organic carbon, calcium carbonate and biogenic opal contents) in two cores (1265 and 1312 m water depths) from the southeastern Sakhalin slope and one core (839 m water depth) from the southwestern Kamchatka slope were investigated to reconstruct variations of the oxygen minimum zone during the last 50 ka in the Okhotsk Sea. The oxygen minimum zone was less pronounced during the maximal cooling in the MIS 2 that is suggested to be caused by a maximal expansion of sea

ice cover, decrease of marine productivity and increase of production of the oxygenated Okhotsk Sea Intermediate Water (OSIW). A two-step-like strengthening of oxygen minimum zone during the warming in the Termination Ia and Ib was linked to (1) enhanced oxygen consumption due to degradation of large amount of organic matter in the water column and bottom sediments, originated from increased marine productivity and supply of terrigenous material from the submerged northern shelves; (2) sea ice cover retreat and reduction of OSIW production; (3) freely inflow of the oxygen-depleted deep intermediate water mass from the North Pacific.

3. Modern distribution of dinocysts from the North Pacific Ocean (37–64°N, 144°E–148°W) in relation to hydrographic conditions, sea-ice and productivity

Sophie Bonnet [a,*], Anne de Vernal [a], Rainer Gersonde [b], Lester Lembke-Jene [b]

a Centre de Recherche en Géochimie Isotopique et en Géochronologie (GEOTOP), Université du Québec à Montréal, Case postale 8888, Succursale Centre-Ville, Montréal, Québec, Canada H3C 3P8

b Alfred Wegener Institute for Polar and Marine Research (AWI), Am Alten Hafen 26, Bremerhaven, Germany

Published in: Marine Micropaleontology (2012) vol. 84-85, 87–113

Abstract

Palynological analyses were performed on 53 surface sediment samples from the North Pacific Ocean, including the Bering and Okhotsk Seas (37–64°N, 144°E–148°W), in order to document the relationships between the dino- cyst distribution and sea-surface conditions (temperatures, salinities, primary productivity and sea-ice cover). Samples are characterized by concentrations ranging from 18 to 143816 cysts/cm3 and the occurrence of 32 spe- cies. A canonical correspondence analysis (CCA) was carried out to determine the relationship between environ- mental variables and the distribution of dinocyst taxa. The first and second axes represent, respectively, 47% and 17.8% of the canonical variance. Axis 1 is positively correlated with all parameters except to the sea-ice and pri- mary productivity in August, which are on the negative side. Results indicate that the composition of dinocyst assemblages is mostly controlled by temperature and that all environmental variables are

correlated together. The CCA distinguishes 3 groups of dinocysts: the heterotrophic taxa, the genera Impagidinium and Spiniferites as well as the cyst of Pentapharsodinium dalei and Operculodinium centrocarpum. Five assemblage zones can be distinguished: 1) the Okhotsk Sea zone, which is associated to temperate and eutrophic conditions, seasonal up- wellings and Amur River discharges. It is characterized by the dominance of O. centrocarpum, Brigantedinium spp. and Islandinium minutum; 2) the Western Subarctic Gyre zone with subpolar and mesotrophic conditions due to the Kamchatka Current and Alaska Stream inflows. Assemblages are dominated by Nematosphaeropsis labyr- inthus, Pyxidinopsis reticulata and Brigantedinium spp.; 3) the Bering Sea zone, depicting a subpolar environment, influenced by seasonal upwellings and inputs from the Anadyr and Yukon Rivers. It is characterized by the dom- inance of I. minutum and Brigantedinium spp.; 4) the Alaska Gyre zone with temperate conditions and nutrient- enriched surface waters, which is dominated by N. labyrinthus and Brigantedinium spp. and 5) the Kuroshio Extension-North Pacific-Subarctic Current zone characterized by a subtropical and oligotrophic environment, which is dominated by O. centrocarpum, N. labyrinthus and warm taxa of the genus Impagidinium.

Transfer functions were tested using the modern analog technique (MAT) on the North Pacific Ocean (=359 sites) and the entire Northern Hemisphere databases (=1419 sites). Results confirm that the updated Northern Hemisphere database is suitable for further paleoenvironmental reconstructions, and the best results are obtained for temperatures with an accuracy of ±1.7 °C.

Appendix: Abbreviations used in the thesis

AAIW – Antarctic Intermediate Water

AMOC – Atlantic Meridional Overturning Circulation

B/A – Bølling-Allerød

cal. yr BP – calibrated years before present (BP = by convention AD1950)

cm b. sf. – centimeter below surface/seafloor

DOC – Dissolved Organic carbon

DOM – Dissolved organic matter

EDC – EPICA Dome Concordia

EKC – East Kamchatka Current

ENSO – El Niño – Southern Oscillation

EPICA – European Project for Ice Coring in Antarctica

ESC – East Sakhalin Current

Ka – „kilo-annum“, here equivalent to: calibrated yr before present x $1{,}000^{-1}$

MOC – Meridional Overturning Circulation

NGRIP – North Greenland Ice Core Project

NPIW – North Pacific Intermediate Water

OSIW – Okhotsk Sea Intermediate Water

PB – Preboreal

PDW – Pacific Deep Water

POC – Particulate Organic Carbon

POM – Particulate Organic Matter

SST – Sea Surface Temperature

V-PDB – Vienna – Pee Dee Belemnite

WSAG – Western Subarctic Gyre

WSAP – Western Subarctic Pacific

YD – Younger Dryas